Monitoring and investigating the process for cytosolic translocation after tau endocytosis

Samantha De La-Rocque

Institute of Neurology

Academic supervisors:

Giampietro Schiavo and Paul Whiting

A thesis submitted for the degree of

Doctor of Philosophy

University College London

September 2021

Declaration

I, Samantha De La-Rocque, confirm that the work presented in this thesis is my own. Where information has been derived from other sources, I confirm that this has been indicated in the work.

Abstract

Tau pathology is well documented in Alzheimer's disease and its build up follows a stereotypical spread correlating with disease severity. This reveals an apparent anatomically linked spread of tau, supporting the hypothesis that tau can propagate via cell-to-cell transfer. However, a direct visualisation of tau entering the cytosol of a recipient cell and a full understanding of the mechanism at the basis of this process are still lacking.

I have setup and optimised a strategy based on split-green fluorescent protein (GFP) to conclusively demonstrate cytosolic translocation of tau. Split-GFP is derived from the superfolder beta-barrel structure of GFPs truncated between 10th and 11th beta strands generating two non-fluorescent fragments named GFP1-10 and GFP11. In this project, the GFP11 is used to tag tau whereas the GFP1-10 is cytosolically expressed and acts as a sensor to detect the presence of tau in the cytoplasmic environment; only when the two GFP fragments associate will they reconstitute the fluorophore, thus maximising the signal to noise ratio. I have demonstrated the ability of the split-GFP assay to detect cellular uptake and release of tau into the cytosol in living cells. With this technique I have observed the real-time uptake dynamics of all six tau isoforms and the disease relevant P301S mutant and investigated potential mechanisms underpinning this process, including pH sensitivity and Rab GTPase activity. This assay has been tested both in cell-lines and primary neuronal cultures grown in custom-made microfluidic chambers, with the aim to improve the tools available to study tau propagation *in vitro* and *in vivo*.

Acknowledgements

Firstly I would like to thank Gipi my primary supervisor, whom without I would not have successfully completed my PhD. He is an inspiration to me not only as an incredible scientist with never-ending expertise, but as a person who has always provided me support, encouragement and pastoral care beyond his responsibilities; for this I will always be grateful.

To all the past and current members of the Schiavo lab I would like to say thank you for always offering your advice and being so willing to help right from the first day of my PhD until the very end, it was really appreciated. I have so many fun memories of Friday pubs, rock climbing and many more, all of which made these past four years an unforgettable experience. Having gone through my PhD with such an amazing lab, my best advice now would be; you can complete any PhD as long as you have the right group of people to support you.
A special mention goes to Ellie; we started our PhD on the same day and since then have gone through this journey together sharing all our lab successes, failures, joys and frustrations. I could not imagine this experience without her!
Finally, the biggest thank you goes to Eddi for being fundamental to my development as a scientist, no matter how busy he was he always found time to help me. I have found a friend for life and would not be here without him!
Thank you to my mum and dad who are my rock in life and were my biggest supporters during my PhD, always believing in my abilities, I could not have done it without them.

I wish everyone starting their PhD journey the best of luck!

Impact statement

Tau is a protein widely expressed in neurons and is responsible for a number of neurodegenerative diseases named tauopathies, including Alzheimer's disease and frontotemporal dementia. Under physiological conditions, soluble tau binds to microtubules and is part of the architectural network required for neuronal structure and function. However, under pathological conditions, tau displays reduced affinity to microtubules and is subject to aggregation; it is now hypothesized that pathological tau can undergo trans-synaptic spreading in all regions of the brain, which in turn is correlated with disease severity. Given the lack of effective aetiological treatment for tauopathies, mechanisms governing neuronal spread of tau are under active research in order to improve future therapeutic options. The prion-like theory of tau dictates that upon neuronal entry, pathological tau is able to evoke aggregation of soluble tau in a process known as seeded aggregation. Previous work has reported that tau is internalised in neurons via active endocytosis entering the endolysosomal pathway; from these membrane-bound compartments tau escapes to the cytosol where it seeds aggregation and continues spreading to neighbouring neurons.

The work presented here identifies a new method for observing the cytosolic translocation of tau in real-time via live fluorescence imaging. By using split-green fluorescent protein (GFP) technology, a single beta-strand fragment derived from GFP, GFP11, is used to tag tau, while the large GFP1-10 sensor fragment is expressed in the cytosolic environment. The reassembly of the two split-GFP domains gives rise to a reconstituted GFP signal used to confirm the

cytosolic entry of tau. We have demonstrated isoform-dependent differences in the cytosolic translocation of tau, and identified potential cellular mechanisms mediating this process, including pH maintenance via the vacuolar type H^+ ATPase and Rab GTPase activity.

These results demonstrate that this novel assay can be utilised to improve our understanding of this process and aid future work in this field. Furthermore, the GFP readout lends itself to high throughput analyses for testing promising pharmacological agents proposed to prevent pathological spread of tau. Moreover, this technology could be applied to other pathological proteins that are also predicted to spread in a prion-like manner, including β-amyloid and α-synuclein.

While there are multiple studies addressing tau uptake, further work is required to decipher how tau is able to gain access to the cytosol following endocytosis. The work presented here provides a complementary strategy to monitor tau internalisation in real-time and demonstrates how this methodology can be exploited to investigate biological mechanisms underpinning this process.

Table of contents

Contents

List of figures

Chapter 4: Investigating the process for cytosolic translocation of tau

Chapter 5: Evaluating the cytosolic translocation assay in primary neuronal cultures

Chapter 6: Conclusions and future perspectives

List of tables

Chapter 2: Materials and methods

Abbreviations

AAV – Adeno-associated virus
Aβ – Beta-amyloid
AD – Alzheimer's disease
ANOVA – Analysis of variance
ApoE – Apolipoprotein E
AU – Arbitrary units
BCA – Bicinchonicic acid
BiFC – Bimolecular fluorescence complementation
BP – Base pair
CFP – Cyan fluorescent protein
CHMP – Charged multivesicular body proteins
CIE – Clathrin independent endocytosis
CME – Clathrin mediated endocytosis
CRISPRi – Clustered Regularly Interspaced Short Palindromic Repeats interference
CSF – Cerebrospinal fluid
CTxB – Cholera toxin subunit B
CV – Column volume
DIV – Days *in vitro*
DMSO – Dimethyl sulfoxide
DN – Dominant negative
EEA1 – Early endosome antigen 1
ELISA – Enzyme-linked immunosorbent assay
ESCRT – Endosomal sorting complex required for transport
EV – Extracellular vesicle
FACS – Fluorescence activated cell sorting
FBS – Fetal bovine serum
FRET – Fluorescence resonance energy transfer
FTD – Frontotemporal dementia
FTDP – Frontotemporal dementia linked with Parkinsonism
GAP – GTPase activating protein
GFP – Green fluorescent protein
GDP – Guanosine diphosphate
GEF – GDP/GTP exchange factor
GTP – Guanosine triphosphate
HBSS – Hank's balanced salt solution
HEK – Human Embryonic Kidney 293 cells
HeLa – Henrietta Lacks cells
HRP – Horesradish peroxidase
HSPG – Heparan sulphate proteoglycans
iPSC – Induced pluripotent stem cells
LAMP – Lysosomal associated membrane protein
LB – Lysogeny broth
LDH – Lactate dehydrogenase assay
LMW – Low molecular weight
LRP1 – Low-density lipoprotein-receptor related protein 1
mAChR – Muscarinic acetylcholine receptor

MAPT – Microtubule associated protein tau
MFC – Microfluidic chambers
MTBR – Microtubule binding region
MTOC – Microtubule organising centre
MVB – Multivesicular bodies
NDP – Nuclear dot protein
NFT – Neurofibrillary tangles
N2a – Neuro-2a cells
OD – Optical density
RPM – Revolutions per minute
PBS – Phosphate-buffered saline
PCR – Polymerase chain reaction
PDMS – polydimethylsiloxane
Pit2B – Pitstop 2B
PET – Positron emission tomography
PHF – Paired helical filaments
PSP – Progressive supranuclear palsy
PTM – Post translation modification
PVDF – polyvinylidene difluoride
SDS PAGE – Sodium dodecyl sulphate polyacrylamide gel electrophoresis
SF – Straight filaments
siRNA – Small interfering RNA
SOC – Super optimal broth with catabolite repression
TAT – Transactivator of transcription
TEV – Tobacco Etch virus
TMB – 3,3',5,5'-tetramethylbenzidine
V-ATPase – vacuolar type H^+ ATPase
VPS – Vacuolar protein sorting
WT – Wild-type
YFP – Yellow fluorescent protein

Chapter 1: Introduction

The microtubule associated protein tau is a neuronal protein highly expressed throughout the human nervous system. Its discovery in 1975 was pivotal in understanding the assembly process of microtubules, a critical component for establishing cell shape and mediating cellular motion (Weingarten et al., 1975). Microtubules are a filamentous structure made of repeating polypeptide chains of α- and β-tubulin dimers creating a “tube-like” formation; in the absence of tau, this dimer is unable to polymerize into tubulin rings, the stable intermediate structure generated during the formation of microtubules (Weingarten et al., 1975). As such, tau became a well-established critical factor in neural physiology, and was later found to play a fundamental role in pathology.

At the beginning of the 20th century, Alois Alzheimer described a novel disease based from observations of a patient with severe cognitive impairment, associated with plaques and neurofibrillary tangles (NFT) detected in the brain post-mortem (Alzheimer, 1907) (Hippius and Neundörfer, 2003). However, not until 1985 was it shown that NFTs were made up of tau (Brion et al., 1985) (Grundke-Iqbal et al., 1986). The decades following saw an exponential growth in our understanding regarding the involvement of tau in pathology accompanied by an increased awareness of its physiological role (Iqbal et al., 2016). Despite this, there are still many unknowns relating to tau and its activity, which has broad clinical consequences; as such it remains an active field of research.

1.1 Tau activity in neuronal physiology

Tau is encoded by the microtubule associated protein tau (*MAPT*) gene on chromosome 17q21, which is made up of 16 exons, five of which are subject to alternative splicing. There are six isoforms of tau in the human brain which are generated by alterative splicing of exon 2, 3 and 10 (Fig 1.1) (Lee et al., 1988; Wang and Mandelkow, 2016).

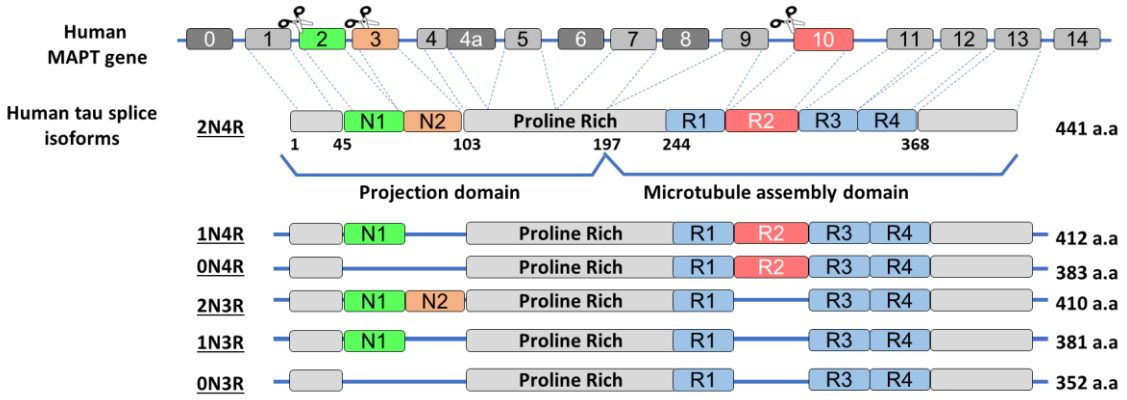

Figure 1.1 – Schematic of human *MAPT* gene and alternative splice isoforms. Microtubule associated protein tau (*MAPT*) gene is made up of 16 exons; exon 1, 4, 5, 7, 9, 11, 12 and 13 are constitutively expressed in the central nervous system. Scissors indicate alternative splicing, generating 6 tau isoforms. Exon 0 and 14 encode 5' and 3' untranslated sequence of *MAPT* mRNA respectively. Exons 4a, 6 and 8 are only transcribed in peripheral tissue.

Tau is highly expressed in all neuronal subtypes, yet has limited expression in glial cells (Binder et al., 1985; Shin et al., 1991). Under physiological conditions, tau is typically an unfolded protein with short/transient elements of secondary structure predominantly binding to microtubules in axons.

The microtubule binding region (MTBR) is the most studied region of tau. It is composed of repeats present in 3 or 4 copies (3R or 4R isoforms) depending on the alternative splicing of exon 10 which codes for the R2 region (Fig 1.1); it is

primarily responsible for the binding of tau to microtubules and stabilising the highly dynamic microtubule network (Lee et al., 1989). Interestingly, it has been found that 3R and 4R tau have differential abilities for stabilising microtubules; 4R tau is reported to promote microtubule polymerisation more readily (Goedert and Jakes, 1990) and more strongly stabilise microtubules (Panda et al., 2003) compared to 3R tau. Moreover, the activity of the MTBR appears to override the amino-terminal domain, since the behaviour of 0N-, 1N- and 2N- tau (4R) were all equivalent (Goedert and Jakes, 1990). Thus, any disturbance in the ratio of 3R or 4R tau could contribute to pathology seen in tauopathies, due to alterations of neuronal microtubule dynamics (Panda et al., 2003).

The role of the N-terminal projection domain is less clear, but it is thought to dictate spacing between microtubules, by projecting away from the microtubule when tau is bound (Méphon-Gaspard et al., 2016). Furthermore, it may interact with other intracellular components; recently, the phosphatase activating domain (PAD) present within the projection domain found between amino acids 2 and 18, was characterised and shown to be involved in the regulation of intracellular signalling cascades following phosphorylation by Fyn kinase at Tyr 18 (Kanaan et al., 2012).

Finally, the proline-rich region which spans across the projection and microtubule assembly domain, contains Thr-Pro and Ser-Pro motifs which are targeted by proline-specific kinases e.g. mitogen-activated protein kinase (MAPK), glycogen synthase kinase 3β (GSK3β) and JUN N-terminal kinase (JNK) (Wang and Mandelkow, 2016). Due to the mainly unfolded nature of tau, kinases have access to many potential phosphorylation sites, and this has

important implications for tau pathology. Tau is a highly modified protein, which undergoes extensive post-translation modifications (PTMs), which include phosphorylation, acetylation and proteolytic processing among others (Wang and Mandelkow, 2016).

To date, the main functional role of tau, as described, is stabilising microtubules and this has important consequences for processes including axonal transport and neurite outgrowth; in addition tau has been detected in the nucleus (Greenwood and Johnson, 1995; Thurston et al., 1996) with involvement in DNA repair (Sola et al., 2020). Tau is also reported to act as a post-synaptic scaffolding protein in dendrites (Mondragón-Rodríguez et al., 2012); for pathology this is also important as the redistribution of tau to the post-synaptic compartment triggered by phosphorylation of tau by Fyn kinase, is reported to be an early pathological event driven by tau (Briner et al., 2020). Nevertheless, the physiological role of tau, with exception to its binding to microtubules, is still poorly understood. Interestingly, under physiological conditions tau was found in the interstitial fluid of wild-type (WT) mice (Yamada et al., 2011), giving rise to the hypothesis that extracellular tau may have yet undetermined physiological roles.

1.2 Tau activity in neuronal pathology

The interest in the study of tau first peaked after identifying it as a key pathological marker of Alzheimer's disease (AD) (Grundke-Iqbal et al., 1986). However, it was not until the first *MAPT* mutation was found to cause frontotemporal dementia linked with parkinsonism-17 (FTDP-17) that it became clear that tau alone was sufficient to cause neurodegeneration and dementia.

Over time, many tau-mediated neurodegenerative diseases were identified including, progressive supranuclear palsy (PSP), frontotemporal dementia (FTD), Pick's disease and cortical basal degeneration; these examples are classified as primary tauopathies since deposits of tau pathology alone give rise to their diagnoses. In the case of AD, a secondary tauopathy, the presence of both beta-amyloid (Aβ) and tau are required for clinical diagnosis.

To date, AD remains the most studied tauopathy; however, in spite of this, there are still no successful therapeutic agents. The development of the Aβ hypothesis led the field to focus on Aβ as a clinical target. Briefly, it was proposed that by mutations of the amyloid precursor protein gene or clearance failures of Aβ, the rising levels of Aβ lead to the development of oligomers and diffuse Aβ plaques which in turn trigger an inflammatory response by glia and altered neuronal homeostasis. This will lead to tau pathology by aberrant phosphorylation due to dysfunction of kinases and phosphatases; in combination Aβ and tau lead to widespread neuronal dysfunction and eventual cell-death, causing AD-dementia (Selkoe and Hardy, 2016). Given multiple disappointing results from clinical trials aimed to treat AD by lowering Aβ levels, renewed interest has been taken in identifying tau-focused therapeutics.

Over 50 *MAPT* mutations have been identified predominantly clustering in the MTBR region, in particular within exon 10 (Strang et al., 2019); some of these are known to be causative for familial FTD including, P301L (Hutton et al., 1998), P301S (Bugiani et al., 1999) and V337M (Whitwell et al., 2009). Importantly, many of these mutations have been reported to influence microtubule binding and propensity for aggregation (Strang et al., 2019).

Interestingly, the alternative splicing of exon 10 has clinical importance as many tauopathies can be classified according to the absence or presence of R2 containing isoforms in pathological aggregates, for example 3R containing aggregates are found in Pick's disease, whereas 4R containing aggregates can be seen in PSP; in AD, both 3R and 4R tau is present. Within the MTBR, there are two short hexapeptide motifs present at the start of R2 and R3, named PHF6* and PHF6 respectively, which have a tendency to form β-sheets, a precursor step for tau aggregation (Li and Lee, 2006). These two motifs have also recently become targets for the development of therapeutic antibodies to prevent aggregation and halt the pathological spread of tau in AD (Roberts et al., 2020). Given the presence of all isoforms of tau in pathology, understanding their individual behaviour will be crucial in deciphering effective treatments for all tauopathies, including AD.

Under pathological conditions, tau typically reduces its affinity to microtubules and mis-localises to the cell soma; this may be as a result of mutation, hyperphosphorylation or other PTMs. An excess of soluble free tau in the cytoplasm is subject to oligomerization, forming intermediate structures including dimers and trimers. Further aggregated tau can form paired helical filaments (PHF) or straight filaments (SF), that finally develop into NFTs (Braak et al., 1994). These fibrous structures are seen across many tauopathies, yet the aetiology of this process is still unknown for many disease states. In familial tauopathies such as FTDP-17, it is believed that *MAPT* mutations contribute to this aggregation, however, in sporadic tauopathies, the causative factor(s) is unknown. In order to examine pathological tau aggregation, research groups have exploited the ability of the recombinant protein to aggregate *in vitro* and

form PHF-like structures (Crowther et al., 1992; Wille et al., 1992). Heparin is commonly used to trigger tau aggregation (Goedert et al., 1996), however it has been observed that *in vitro* formed aggregates do not accurately represent pathological aggregates obtained from human patients. Moreover, there appear to be disease-specific aggregate strains, which cannot be achieved from recombinant tau alone (Falcon et al., 2019, 2018b, 2018c; Fitzpatrick et al., 2017; Sanders et al., 2014; Zhang et al., 2019). This discovery was pivotal for the field, given that tau activity is largely dictated by its conformation and aggregation status. In addition, the notion of strain fidelity of tau aggregates between different tauopathies supports the growing theory that tau can behave in a prion-like manner.

1.2.1 Prion-like activity of tau

The term prion was first coined by Stanley Prusiner in 1982 to define a small proteinacious particle, containing no nucleic acids and highly resistant to degradation (Bolton et al., 1982). A number of neurodegenerative diseases were later found to mediated by the prion protein, including Creutzfeldt Jakob disease and fatal familial insomnia (Goldfarb et al., 1992). Several requirements need to be met for a neurodegenerative disease to be classified as a prionopathy. At the cellular level, there is recruitment and induction of misfolding of the native protein known as seeded aggregation, at the intercellular level, there is cell-to-cell propagation of the misfolded protein via a non-cell autonomous process, at the tissue level, there is protein induced cytotoxicity, which induces neurodegeneration, and finally at the organism level there is transmission of aggregated protein from host to recipient, meaning the protein is

infective and importantly there is strain specificity during transmission (Soto and Satani, 2011).

There are many debates as to whether tau is considered a true prion. It has been shown both *in vitro* and *in vivo* that seeded aggregation of tau can take place, following the cellular internalisation of tau aggregates (Clavaguera et al., 2009; Frost et al., 2009; Strang et al., 2019). It is also predicted that once mature tau aggregates are formed, they are subject to fragmentation into smaller seed-competent aggregates, forming a self-sustaining pathological process (Nizynski et al., 2017). To date, it is unknown which tau species forms the competent seed *in vivo.* The idea that tau could behave in a prion-like manner stem from pioneering work by Braak and Braak; in post-mortem AD samples, an anatomically-linked spreading of NFT of hyperphosphorylated tau was identified, commencing in the locus coeruleus in the brain stem (Braak and Braak, 1991) (Fig 1.2). There have now been several developments in our ability to trace tau pathology since Braak's proposal. Positron emission tomography (PET) tracer ligands are now available, which are able to track tau pathology more accurately in patients. As Braak had predicted for AD, PET studies have confirmed the anatomical spread of tau with pathology commencing in layer II of the entorhinal cortex propagating to the hippocampus with end stage pathology observed in the neocortex (Maass et al., 2017; Vogels et al., 2020); importantly, this progressive spread was shown to closely correlate with the severe decline in cognitive function seen in AD (Braak et al., 2006).

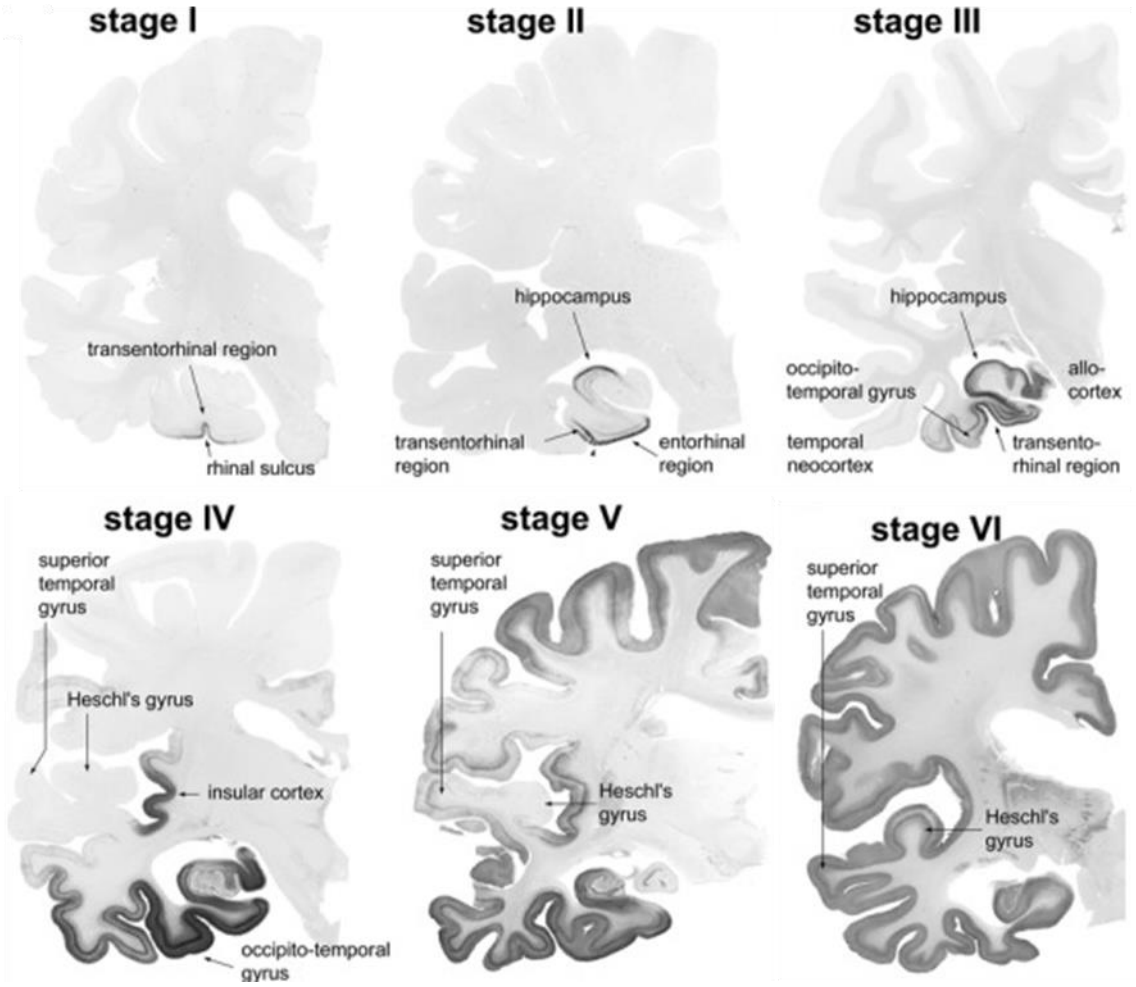

Figure 1.2 – Clinical pathological characteristics of Alzheimer's disease. Tau stained by AT8 antibody probing for phosphorylated tau in human patients with and without dementia demonstrating the spread of tau via anatomically linked pathways. *Stage I-II:* Pathological tau detected in the Transentorhinal cortex in superficial layers of entorhinal regions. Scattered pathology detected in the CA1 and presubiculum of the hippocampal circuit (Entorhinal stage). *Stage III-IV:* Tau pathology densely concentrated through trans entorhinal and entorhinal cortex. Consistent pathology detected in the hippocampus and within the insular cortex. Association areas of neocortex involved with higher executive functioning and language starting to become affected (limbic stage). *Stage V-VI*: All areas of neocortex affected, frontal lobe, parietal lobe, and occipital lobe including visual association area. Final disease stage pathology reached secondary neocortical areas (Isocortical stage). Information obtained from (Braak and Braak, 1991; Braak et al., 2006).

1.2.2 Extracellular pathological tau

Owing to the discovery of the prion protein which undergoes trans-synaptic cell-to-cell spread, tau is now being proposed to propagate in a similar manner (Holmes et al., 2014). The ability to undergo trans-synaptic spread relies on tau release from one neuron into the extracellular space or within the synaptic cleft, before being internalised into the recipient neuron. In support of this, tau has been detected in the extracellular medium and cerebrospinal fluid (CSF) of tauopathy transgenic mouse models as well as human patients (Guix et al., 2018; Pérez et al., 2016; Takeda et al., 2016; Wagshal et al., 2015). Importantly, tau detected in the CSF can be used to distinguish between healthy and AD cases according to their phosphorylation status (e.g. pT181); this would suggest that extracellular tau is playing a role in disease (Barthélemy et al., 2020; Cicognola et al., 2019). Tau truncation has also been found to influence secretion efficiency, with N-terminal fragments commonly detected in AD CSF and plasma samples (Quinn et al., 2018).

In addition, extracellular tau can exist either as free tau, or tau encapsulated in membrane-bound organelles, including exosomes (Howitt and Hill, 2016; Lee et al., 2019; Polanco et al., 2018; Wang et al., 2017) and ectosomes (Dujardin et al., 2014a); this distinction is important as it impacts the mode of cellular entry during transmission and affects propagation of pathology. When characterising endogenous tau secreted from WT cortical neurons, 90% was free tau, 7% was in ectosomes and 3% in exosomes (Dujardin et al., 2014a). Despite, the low percentage of extracellular vesicles (EVs) containing tau, if EVs contain seed competent tau, given the self-sustaining nature of seeding aggregation, EVs can still play a significant role in development of the pathology. In support of

this, EVs extracted from transgenic mouse models (Polanco et al., 2016) and human AD brains (Wang et al., 2017) were seed competent. Therefore, examining all forms of tau is needed to better understand pathology *in vivo.*

1.2.3 Cellular uptake of tau

Cellular uptake is a fundamental step for tau to transmit pathology as hypothesised by the prion-like theory. A landmark paper from Marc Diamond's laboratory observed for the first time intracellular transfer of recombinant tau fibrils in C17.2 cells (Frost et al., 2009). This group also observed preferential internalisation of aggregates compared to monomers, thus concluding that under physiological conditions, monomeric tau was unlikely to be internalised. This has since been debated, with multiple groups confirming the uptake of monomeric tau in cell lines (Michel et al., 2014) and human induced pluripotent stem cells (iPSCs) (Evans et al., 2018). In spite of this, it does seem that aggregated forms of tau are more readily internalised (Takeda et al., 2015; Wu et al., 2013), with one paper suggesting that trimeric tau is the minimal unit required for internalisation (Mirbaha et al., 2015).

Frost and colleagues investigated the mechanism of uptake of the MTBR of tau (Frost et al., 2009). MTBR fibrils were incubated with dextran (10 kDa) a marker for fluid phase endocytosis, or cholera toxin subunit B (CTxB), which binds to the ganglioside GM1 and is used as an indicator for cholesterol-enriched membrane microdomain trafficking (Aman et al., 2001). The data revealed negligible co-localisation between MTBR fibrils and CTxB, yet 24 % of MTBR fibrils co-localised with dextran (Frost et al., 2009). They proposed that tau aggregates were internalised by endocytosis and not via direct membrane

translocation. Further evidence has shown that uptake of tau at 4 °C was partially blocked (Frost et al., 2009), and once internalised co-localised with FM4-64, a well-established vesicular marker (Michel et al., 2014). Consequently, these data indicate that tau is actively endocytosed and is transported into the endo-lysosomal pathway (Mayor and Pagano, 2007).

1.2.3.1 Evidence for clathrin-mediated endocytosis of tau

Clathrin-mediated endocytosis (CME) has been observed for the internalisation of both monomeric (Falcon et al. 2018) and aggregated (Calafate et al. 2016) tau. It is a well-described mechanism for selective internalisation based on the formation of the curved clathrin lattice around the budding plasma membrane which forms a clathrin coated pit prior to its release into the cytosol as clathrin coated vesicles (Doherty and McMahon 2009).

Recent work showed that cell-secreted 2N4R-P301L aggregates co-localised with transferrin, a commonly used CME marker, upon incubation with rat hippocampal neurons for over four hours (Calafate et al. 2016). Uptake of recombinant monomeric 0N4R-P301S tau was also found to be mediated by CME; when supressing activity of CME components, including the nucleators of CME, FCHO and AP180, tau uptake was significantly reduced in human embryonic kidney (HEK) 293 and SH-SY5Y cells, comparable with transferrin (Falcon et al. 2018).

Receptor-mediated CME has also been observed for tau internalisation, including muscarinic acetylcholine receptor (mAChRs) subtypes 1 and 3 (Morozova et al., 2019) and most recently, low density lipoprotein-receptor

related protein 1 (LRP1) (Rauch et al., 2020). Many LRP1 ligands have been linked to AD pathology, including amyloid precursor protein and apolipoprotein E (ApoE) (Rebeck et al., 1993), the most statistically significant genetic locus associated with developing familial AD (Knauer et al., 1996; Kounnas et al., 1995). Experiments conducted in both H4 cells and human iPSCs confirmed that knockdown of LRP1 abolished endocytosis of recombinant WT tau monomers of all six isoforms. When testing aggregated forms of tau, oligomeric tau uptake was prevented, yet the uptake of sonicated fibrils was only reduced by 50%, thus inferring a structural difference influencing uptake via LRP1. These findings were confirmed *in vivo;* under baseline LRP1 expression, following adeno-associated virus (AAV) - mediated expression of tau, tau signal was detected throughout the contralateral hippocampus and cortex. However, upon shRNA-mediated LRP1 knockdown, human tau was only detected in neurons at the site of AAV injection, supporting the hypothesis that LRP1 dictates tau internalisation and spread.

1.2.3.2 Evidence for clathrin-independent endocytosis of tau

Despite the existing evidence for CME of tau, many groups have not observed clathrin involvement in this process. The use of Pitstop 2B (Pit2B), which inhibits clathrin function by binding its N-terminal domain to prevent access to accessory proteins and block CME (von Kleist et al., 2011), has been negligible in inhibiting the uptake of recombinant tau aggregates (Wu et al., 2013) and AD brain-derived tau oligomers (Puangmalai et al., 2020) in primary neurons. Thus, it has become apparent that clathrin-independent endocytosis (CIE) is also playing a role in tau uptake.

Macropinocytosis is a unique form of CIE, mediated by actin and the rearrangement of large areas of the plasma forming large membrane-bound vacuoles spanning 0.5-5 μm (Stillwell, 2016). Recombinant tau MTBR-fibrils were generated and applied to C17.2 cells (Holmes et al., 2013). Phalloidin, which is used to label filamentous actin, was found to encapsulate tau following uptake, forming vacuoles approximately 5 μm in diameter, hence considerably larger than typical endocytic vesicles (Holmes et al., 2013), suggesting macropinocytosis to be a form of endocytosis for tau.

Finally, another major area of investigation has been the analysis of the impact of heparan sulphate proteoglycans (HSPG) in tau uptake. HSPGs represent a wide range of different glycosaminoglycans exhibiting different compositions; however, their basic structure is made of a core protein covalently bound by one or more heparan sulphate chains. Crucially for tau, heparin, a densely sulphated form of heparan sulphate, has been described to induce its aggregation via multiple binding sites (Goedert et al., 1996). Given that it is not known which species of tau is being transmitted between neurons, it is important to assess the ability of different tau fragments to bind any potential receptor for tau uptake, including HSPGs. To investigate HSPG-mediated tau internalisation, Trans-Activator of Transcription (TAT), a marker of macropinocytosis mediated by HSPG, has been used. Upon co-incubation of recombinant TAT and tau MTBR-fibrils in C17.2 cells, a significant signal overlap was detected, with TAT signal appearing to encapsulate tau puncta (Holmes et al., 2013). These observations support the hypothesis that tau fibrils are internalised within macropinosomes upon interaction with HSPGs. The uptake of post-mortem human derived tau oligomers in primary cortical neurons

have also been affected by HSPG inhibition; by applying heparin as a competitive inhibitor, the uptake of AD tau oligomers was strongly inhibited (Puangmalai et al., 2020).

1.2.4 Trans-synaptic spread of tau

Many of the uptake mechanisms proposed for tau have been described at the synapse. CME is a well-established process that is widely observed in the post-synaptic area for neurotransmitter receptors upon stimulation (Jung and Haucke, 2007). For example, M1/M3-mAChRs have both been detected at both pre- and post-synaptic sites in the hippocampus (Levey, 1996; Rouse and Levey, 1997; Rouse et al., 1998; Yamasaki et al., 2010) and LRP1 has also been found to localise within the synapse at sites adjacent to the post-synaptic density, an area in which CME commonly takes place (Triller and Choquet, 2005). The clathrin-independent endocytic pathways reported for tau have also been shown to be present at the synapse, albeit they were not demonstrated in the context of tau uptake. HSPGs, for example, are present both at pre- and post-synaptic sites and have fundamental roles in synapse function (Condomitti and de Wit, 2018; Zhang et al., 2018), but further work is needed to elucidate this mechanism.

To obtain an understanding of tau propagation *in vivo*, transgenic mouse models have routinely been used to map pathology spread. Clavaguera and colleagues were the first to demonstrate tau spread in transgenic tau mouse models (Clavaguera et al., 2009). First, tau aggregates were extracted from aged mice expressing human 0N4R-P301S mutant tau, these aggregates were subsequently injected into young ALZ17 mice, a transgenic mouse line which

express WT 2N4R tau. Under baseline conditions ALZ17 mice do not form filamentous silver staining-positive tau pathology, however following intracerebral injection of tau aggregates into the hippocampus and overlying cortex, pathology was detected at 6, 12 and 15 months post injection. Crucially, pathology was detected not only within the injection site, but at synaptically connected regions including the entorhinal cortex, amygdala and thalamus (Clavaguera et al., 2009). These studies have since been advanced with transgenic mice expressing tau in restricted brain regions (de Calignon et al., 2012; Liu et al., 2012) or viral injections to restrict tau expression (Dujardin et al., 2014b; Wegmann et al., 2019). These studies confirmed that tau spread occurred with greater efficiency between areas that were functionally connected to site of tau expression.

In an attempt to confirm neuronal spread of tau experimentally, microfluidic chambers (MFCs) are commonly used to compartmentalise neurons and assess tau transmission. MFCs are composed of two or more chambers connected by narrow microgrooves, which only allow axons to grow through. Fluidic isolation can be achieved between the chambers by establishing a hydrostatic gradient. This ensures that there is no passive diffusion between compartments, but rather genuine cellular transmission of tau. MFCs can also be used to pinpoint the localisation of tau uptake and assess whether tau is capable of both anterograde and retrograde axonal transport.

Karen Duff's group explored the internalisation of a range of structural forms of tau, including monomeric tau, low molecular weight (LMW) tau aggregates defined as small spherical oligomers (10 – 30 nm) and fibrillar tau either straight

or helical twists of short (40 – 250 nm) or long (200 – 1600 nm) fibrils (Wu et al., 2013). A mixed culture of mouse cortical and hippocampal neurons were plated in a two-chamber MFC and exposed to all conformations of tau. Following a six-hour incubation period, only LMW aggregates and short fibrils were taken up at the somato-dendritic compartment and anterogradely transported along the axon. Under the same conditions, LMW aggregates were also confirmed to be internalised at axon terminals and retrogradely transported to the cell soma (Wu et al., 2013). It is important to note that this study was conducted with bacterially expressed recombinant tau, since it is known that *in vitro* produced tau may act differently to mammalian expressed tau (Falcon et al., 2018b; Fitzpatrick et al., 2017; Zhang et al., 2019), these results may not be translatable to more physiological species of tau, and therefore it is important to investigate multiple forms of tau.

The inter-cellular propagation of tau was investigated by Dujardin and colleagues using neuron secreted tau; in this setup, two neuronal populations were plated within a two-chamber MFC. By first overexpressing WT tau in 1st order neurons, after 48 h, tau was strongly detected within the infected neuron, and also in the 2nd order neurons, supporting the hypothesis that tau can spread within neuronal circuits (Dujardin et al., 2014b). Given that extracellular tau is also detected within EVs, it was important to assess specifically whether trans-synaptic spread could be observed with vesicular tau. Accordingly, exosomes extracted from Neuro-2a (N2a) cells expressing mutant tau harbouring the K280 deletion, were applied to primary neurons plated in a three-chamber MFC. These exosomes were shown to effectively internalise and anterogradely travel to axon terminals, where they were likely secreted into the extracellular space

before being internalised by 2nd order neurons (Wang et al., 2017). To date, there has not been a similar investigation conducted for ectosomes containing tau.

A large number of studies have been published confirming that tau can translocate from one neuron to another within MFCs (Calafate et al., 2015; Dujardin et al., 2014b; Hallinan et al., 2019; Nobuhara et al., 2017; Takeda et al., 2015; Wang et al., 2017). However, little work had been done to identify whether tau localises at synaptic terminals, prior to cellular transmission. A recent study using tau oligomers obtained from post-mortem human extracts from AD, PSP and dementia with Lewy bodies found that these oligomers were endocytosed by primary cortical neurons, and shown by confocal microscopy to co-localise with synapsin I and PSD-95, pre- and post-synaptic markers respectively (Puangmalai et al., 2020). This was an important finding as it confirmed that pathological tau are within the same compartment and co-localise with synaptic markers, which in turn, may be critical for its ability to propagate.

1.2.5 Cytosolic translocation of tau upon endocytosis

As described above, the prion-like theory for pathological tau predicts that upon uptake, seed-competent tau must be exposed to soluble tau to evoke aggregation and propagate pathology. Despite the acknowledgement of this critical step, very few studies have addressed this point; given that tau is suspected to enter the cell via active endocytosis, tau must escape this membrane-bound compartment to interact with tau in the recipient cell (Fig 1.3). This hypothesis has been supported by the observation from Wu and

colleagues. When incubating WT neurons with conditioned media taken from neurons cultured from the rTg4510 tauopathy mouse model expressing 0N4R-P301L tau, after two days there were discrete tau positive puncta, suggestive of its presence in vesicular compartments. Only after six days did the signal shift into a diffuse staining indicating its entry into the cytosol (Wu et al., 2016).

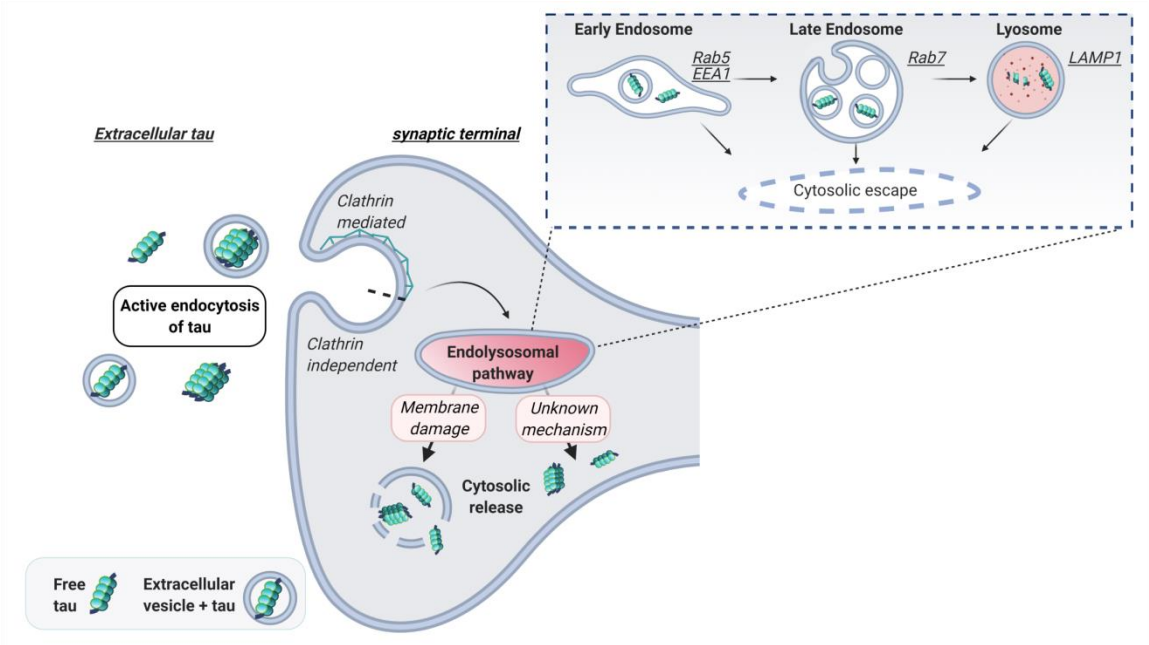

Figure 1.3 – Schematic of tau uptake and entry into the cytosol.
An example of a synaptic terminal with extracellular tau present either as free tau (left) or within extracellular vesicles (right). Active endocytosis of tau predicted to occur either by clathrin mediated or independent mechanisms. Upon endocytosis tau enters the endolysosomal pathway. Inset displays the progression of tau through the endolysosomal pathway passing through early endosomes, which mature into late endosome that can fuse with lysosomes (classic endolysosomal markers are indicated in the panel). Cytosolic escape hypothesised to occur from any stage within the pathway either via membrane damage of the organelles, or via unknown mechanisms. Adapted from (De La-Rocque et al., 2021)

Tau escape from intracellular vesicles and its precise kinetics are difficult to determine experimentally. Not only is this biological process important for neurodegenerative diseases, but also for viral (Helle and Dubuisson, 2008) or

bacterial (Ratts et al., 2003) entry into the cytosol, and for the intracellular delivery of therapeutic agents (Appelbaum et al., 2012; Gaston et al., 2019). As such, this remains an active area of research and in the context of tau, a highly understudied area within the field.

The endolysosomal pathway is difficult to experimentally characterise due to the progressive maturation occurring between early and late endosomes, and between the latter and lysosomes (Fig 1.3). Briefly, upon endocytosis, cargoes enter the cell within endocytic vesicles which then fuse into early endosomes. At the endosomal stage, cargo can either be returned back to the plasma membrane within recycling endosomes, directed to the trans-Golgi network, or continue through via late endosomes to lysosomes for degradation (Scott et al., 2014). The maturation phase between early endosomes to late endosomes/lysosomes involves extensive change both within the endosomal lumen including a drop in pH and remodelling of the membrane bilayer, leading to changes of proteins and lipids (Scott et al., 2014). From the early endosomes, there are also structural changes, including lipid bilayer invagination forming intraluminal vesicles, these endosomes are known as multivesicular bodies (MVB) and act as markers for the transition to late endosomes. At this stage, it is agreed that late endosomes and lysosomes fuse forming a hybrid organelle, that can transition fully into a lysosome (Russell et al., 2006) for cargo degradation.

This membrane remodelling of the endocytic pathway has routinely been used to discern the major endo-lysosomal compartments. Common markers of the early endosome are; early endosome antigen 1 (EEA1) and guanosine

triphosphate (GTPase) Rab5, late endosomes include Rab7 and finally lysosomes are routinely marked by lysosomal associated membrane protein 1 and 2 (LAMP1/2). However, it is important to note, that the molecular distinction between late endosomes and lysosomes is not clear, and to date, there is no unique lysosomal marker. Indeed, LAMP1 and 2 are also found in late endosomes (Chen et al., 2019); furthermore given there is a maturation phase between organelles, it is likely there will be endosomes positive for both Rab5 and Rab7 during this transition. Morphologically, however, these compartments can be identified via electron microscopy; historically late endosomes were referred to as light lysosomes, due to its stark difference in electron density compared to the classical lysosome (Neiss, 1983; Storrie, 1988).

Tau has been detected within these endolysosomal compartments in a wide range of studies, predominantly via co-localisation analyses shown with Rab5 (Calafate et al., 2016; Falcon et al., 2018a; Puangmalai et al., 2020; Wu et al., 2013), EEA1 (Ait-Bouziad et al., 2017), Rab7 (Chen et al., 2019; Falcon et al., 2018a) and LAMP1/2 (Chen et al., 2019; Puangmalai et al., 2020; Wu et al., 2013). This observation has been confirmed for many tau species including recombinant tau (monomeric and aggregated), cell-secreted tau and tau aggregates isolated from human patients; additionally, multiple cell-types tested have validated these findings, and significantly this was also observed in human iPSC-derived excitatory neurons (Evans et al., 2018), supporting the hypothesis that this mechanism does also occur in the human nervous system.

The most recent data published regarding cytosolic translocation of tau comes from Tuck and colleagues using a split-luciferase assay whereby, NanoLuc has

been divided into an 18 kDa subunit (LgBiT) that can be cytosolically expressed and an 11 amino acid peptide (HiBiT), which can be used to tag recombinant tau (Tuck et al., 2021). Using this setup, they have demonstrated in HEK293 cells that cytosolic entry of recombinant tau assemblies was dependent on clathrin mediated processes and upon siRNA knockdown of Rab7, halting the transition between late endosomes to lysosomes (Vanlandingham and Ceresa, 2009), there was an increase of cytosolic entry of tau (Tuck et al., 2021). Interestingly this was not seen following knockdown of Rab5, suggesting that the late endosomal compartment has a pronounced role in this process. In contrast, when testing primary neuronal cultures, cytosolic entry of tau was independent of clathrin and surprisingly was not altered following knockdown of Rab7 as seen in HEK293 cells. Further investigation revealed that reducing cellular levels of cholesterol by extraction with methyl-beta-cyclodextrin was an enhancer of cytosolic entry of tau assemblies in neurons and organotypic hippocampal slices. Moreover, this group examined the process for cytosolic tau entry with the use of an endosomal lysis assay in parallel with the split-luciferase assay; by adding a plasmid encoding luciferase to the extracellular space of HEK293, only following uptake and exit into the cytosol will expression of the luciferase plasmid take place. In the presence of Lipofectamine or AAV type 5, both known to trigger endosomal rupture for cellular entry, there was an increase in luciferase signal by 100 – 1000 fold, in contrast high concentrations of recombinant tau (1 µM) did not evoke a change in signal, and was comparable to control levels using 50 nM of tau, suggesting that tau entry into the cytosol is not a result of membrane damage/rupture.

The phenomenon of membrane damage by pathological tau was also investigated by Calafate and colleagues, by using a galectin-3 assay. Galectin-3 is a cytosolically expressed protein; its binding partner β-galactosides are carbohydrates that are found on extracellular cell membrane. Following internalisation, β-galactosides remain confined to the lumen of the endosomal compartment. In the event of endosomal leakiness, these sugars will be exposed to the cytosol where galectin-3 will be recruited. In this assay the investigators found that when treating primary hippocampal neurons with cell secreted 2N4R-P301L aggregates for 24 h, the mCherry-galectin-3 transitioned from a diffuse staining to distinct puncta in the cytosol, inferring that the endosomal membrane had developed holes and so galectin-3 could bind the intraluminal β-galactosides (Calafate et al., 2016). This method for detecting endomembrane damage has since been used by other groups with galectin-3 and -8, to assess the ability of tau to exit endolysosomal compartments (Chen et al., 2019; Falcon et al., 2018a).

However, galectins appear not only to signal membrane damage but also function as “danger receptors” for endolysosomal compartments (Thurston et al., 2012). The recruitment of galectins to β-galactosides triggers the activation of autophagy machinery, in particular nuclear dot protein 52 (NDP52). NDP52 can bind galectin-8 (Thurston et al., 2012), to trigger a cellular response, in the attempt of destroying the damaged organelle, thus preventing tau pathology propagation. This was confirmed by Falcon and colleagues: upon galectin-8 and NDP52 siRNA downregulation in HeLa cells, they found an increase in the extent of cytosolic tau release, which was indirectly measured by a boost of seeded aggregation. This was seen following the silencing of the autophagic

pathway, suggesting that galectin-8 recruits NDP52 to degrade potentially pathological tau aggregates.

The endosomal sorting complex required for transport (ESCRT) has also been shown to play a role in the cellular response to the endocytosis of tau aggregates (Chen et al., 2019). The ESCRT was historically considered a group of complexes (ESCRT- 0, -I, -II, -III and -IV) involved primarily in the sorting of ubiquitinated cargo within endosomes to MVB (Henne et al., 2011). The characterisation of the ESCRT machinery re-classified a subfamily of the vacuolar protein sorting (VPS) genes that previously were referred to as class E *VPS* genes in yeast. As such, the ESCRT complexes are largely made up of *VPS* proteins, many of which have been renamed to charged multivesicular body proteins (CHMPs).

To date, the ESCRT is known to be involved in exosome secretion, autophagy and membrane remodelling seen for both viral particle and vesicle budding in MVB (Henne et al., 2011). In the context of tau escape, ESCRT-III machinery, a complex made up of CHMP-2, -3, -4 and -6 (Henne et al., 2011), has been shown to mediate the repair of minor wounds at the plasma membrane (Jimenez et al., 2014). Following a CRISPRi silencing screening, knockdown of CHMP6 and VPS13D were identified to increase the rate of seeded aggregation evoked by recombinant 0N4R fibrils (Chen et al., 2019). These fibrils were incubated with HEK293 cells expressing two MTBR constructs with P301L and V337M mutations tagged with clover2 and mRuby2 respectively, competent for fluorescence resonance energy transfer (FRET) and flow cytometry analyses. This increase in aggregation was not due to increase in endocytosis, confirmed by measuring uptake levels of fluorescently tagged-0N4R fibrils, suggesting that

the observed effects are a result of intracellular processes (Chen et al., 2019). Under baseline conditions, tau fibrils co-localise with Rab7- and LAMP1-positive compartments, however following CHMP6 knockdown, there was a significant reduction in this co-localisation (Chen et al., 2019); this finding accompanied with increased seeding activity would suggest that seed competent tau has rapidly escaped into the cytosol.

To assess endosomal membrane integrity, Chen and colleagues utilised the galectin-3 assay following knockdown of ESCRT-III components. Interestingly, they observed that under control conditions incubation with tau fibrils did not lead to rapid endolysosomal membrane damage, only upon knockdown of CHMP6 or CHMP2 and -3, was there a change in the galectin-3 signal. This would suggest that the fibrils alone were not triggering membrane damage, but rather a defect in the ESCRT-III machinery, is leaving the endosomal membrane more susceptible to damage. In contrast, studies have shown that tau fibrils can initiate membrane damage and lead to vesicular rupture, albeit the mechanisms are not understood (Calafate et al., 2016; Flavin et al., 2017).

Consequently, it could be hypothesised that small lesions of the membrane trigger the recruitment of ESCRT-III complex leading to membrane repair; if this system fails under pathological conditions, tau could be released into the cytosol, now free to seed aggregation. This general process has been demonstrated (Skowyra et al., 2018), but not in the context of tau pathology.
Interestingly, the McEwan lab also identified the role of ESCRT pathway in cytosolic tau entry, in particular siRNA knockdown of VPS13D and VPS35, were both shown to trigger an increase in cytosolic tau entry, as measured with the

split-luciferase assay. This data lead the group to hypothesize that optimal functioning of endosomal sorting and membrane repair machinery are critical for cytosolic translocation of tau, albeit not being tau itself triggering membrane rupture (Tuck et al., 2021).

While the concept of membrane damage has been demonstrated with aggregated tau; it may be that this conformer of tau can induce membrane damage, however it has been shown that WT tau can also undergo physiological spread (Dujardin et al., 2018, 2014b) and since not all studies have observed tau-induced membrane damage, other mechanisms are likely to be involved.

An important factor to consider is how tau interacts with the lipid bilayer. Ait-Bouziad and colleagues investigated the ability of WT tau to interact with phosphatidylserine-containing liposomes generated using porcine brain lipids (Ait-Bouziad et al., 2017). Full-length tau was shown to bind these liposomes to a greater extent than MTBR alone; this was further investigated, when comparing 3R or 4R containing tau, the presence of R2 enhanced the ability of tau to bind vesicles and the stability of the interaction (Ait-Bouziad et al., 2017). This work observed that the two hexapeptide motifs, PHF6*(^{275}VQIINK^{280}) and PHF6 (^{306}VQIVYK^{311}), which both contain positive residues, were in-part mediating the strong interaction with the lipid bilayer. The mutation of these residues to the negatively charged glutamate reduced the extent of membrane binding. The authors hypothesized that the amphipathic nature of the residues within R2 and R3 can act as "molecular tweezers" which disrupt the membrane

by stripping the bilayer of negatively charged phospholipids (Ait-Bouziad et al., 2017).

If this process occurs on the extracellular surface, it could lead to rapid internalisation of tau or induce cytotoxic effects; alternatively if occurring within the endosomal lumen, it could facilitate the escape of tau into the cytosol. These findings offer a potential mechanism for how tau can interact at the lipid bilayer level and additionally, present isoform-dependent effects which can have implications for both uptake and cytosolic entry of tau.

The activity of tau at the endosomal membrane is important, since membrane damage is unlikely to be the only mediator of cytosolic escape. Although not observed for tau, it may be that chaperones are required to extract tau from the endolysosomal vesicle, as demonstrated for diphtheria toxin where a cytosolic translocation complex is required for cytosolic entry (Ratts et al., 2003). Furthermore, it has been shown that some proteins are retained within the endolysosomal pathway until later stages before cytosolic release, while others can be released from early endosomes (Appelbaum et al., 2012); in the context of tau, understanding how the cell controls translocation of endocytic cargo into the cytosol will be essential for developing novel therapeutics. Consequently, further research is needed to elucidate the precise mechanisms involved for the cytosolic entry of both pathological and physiological tau.

1.3 Experimental tools used for investigating tau endocytosis

To date, the experimental tools used to assess cellular entry of tau have rarely distinguished between uptake and cytosolic translocation of tau. Common techniques include fluorescent labelling of tau (Evans et al., 2018; Frost et al.,

2009; Holmes et al., 2013; Michel et al., 2014; Rauch et al., 2018), or post-fixation antibody probing (Calafate et al., 2016; Morozova et al., 2019; Wu et al., 2013). Additional approaches are used to confirm tau uptake, such as flow cytometry/ fluorescence-activated cell sorting (FACS) (Frost et al., 2009; Holmes et al., 2013; Rauch et al., 2020, 2018) or enzyme-linked immunosorbent assays (ELISA) used to quantify uptake in tau knockout neurons (Wu et al., 2016); while these assays have unique benefits for enhancing sensitivity and increasing quantification accuracy, they cannot distinguish between intracellular locations. In the case of fluorescent imaging, co-localisation analyses can be conducted at both the confocal and super-resolution level and the overlapping fluorescent signal will give information about the close proximity between two molecules. With regards to tau uptake, co-localisation between endolysosomal markers does not distinguish whether tau is on the luminal side, or cytosolic side. Electron microscopy has been used to observe tau internalisation by examining the extracellular surface (Hudák et al., 2019) and would provide high resolution images to examine intracellular interactions; however, this system is not compatible with live imaging under physiological conditions. This could be circumvented with the use of correlative light and electron microscopy, a technique that however is not suitable for high throughput analyses.

A unique system developed by Marc Diamond's group, cultured HEK293T cells expressing two MTBR-P301S constructs tagged with either CFP or YFP, referred to as "tau biosensor cells" (Holmes et al., 2014). Under baseline conditions these constructs are soluble, but when exposed to tau seeds including recombinant or human derived samples, this triggers aggregation of

the MTBR constructs generating a FRET signal. FACS can then be used to group FRET positive and negative cells in order to re-plate cells and confirm the accuracy of the FRET signal (Holmes et al., 2014). In this set up, tau amyloids are used to trigger intracellular aggregation, therefore it is assumed that the exogenous tau has been internalised and exposed to the soluble MTBR constructs. A recent controversial paper published by Eckhard Mandelkow's group suggested that exogenous tau aggregates were not directly triggering MTBR aggregation (Kaniyappan et al., 2020). It was argued that steric hindrances of the fluorescent tags attached to MTBR tau inhibited genuine seeded aggregation; this observation was made following *in vitro* aggregation of full-length and MTBR tau with and without green fluorescent protein (GFP) tags, to analyse kinetic and structural data and to compare with existing knowledge of PHF from AD patients. Interestingly, they found that aggregation of full-length tau was not impeded by the GFP tag. Nevertheless, this biosensor assay has provided a simple way to detect seeding competency, which is predicted to occur following internalisation of the tau seed.

In this regard, one could use this assay to detect cytosolic entry, however, firstly there is a delay in time following the seed exposure to the cytosol and the development of aggregates and secondly, it requires the use of pathological/seed competent tau to detect this entry. Therefore, a FRET negative signal does not necessarily mean there is no exogenous tau within the cytosol, but rather this tau has not triggered aggregation. This biosensor cell-line has been used to assess seeded aggregation in conjunction with galectin localisation following membrane damage, as previously described (Chen et al., 2019). However, should tau escape the endosomal lumen in the absence of

membrane damage, galectins would not be recruited; therefore, a novel assay is required to assess these factors.

A novel split-luciferase assay has been developed by the McEwan group, which has displayed high sensitivity for cytosolic entry of tau in both cell lines and primary neuronal cultures (Tuck et al., 2021), however this technique still lacks the component for subcellular visualisation of tau translocation.

1.4 The use of split-GFP technology in the study of tau

The assay I aim to develop will be based on the established concept of bimolecular fluorescence complementation (BiFC), split-GFP. In order to be an efficient “split” fluorescent protein, upon truncation the generated fragments need to be resistant to proteolysis, lack fluorescence in isolation, and finally, only reconstitute the fluorophore upon fragment complementation (Romei and Boxer, 2019).

GFPs have routinely been used as a method of tagging and visualising proteins, however the intrinsic size of GFP (~27 kDa) may confound experimental results and alter physiological protein activity. Split-GFP is derived from the super-folded GFP, a β-barrel with an internal α-helix structure, truncated to form two independently non-fluorescent fragments. Truncation points are generally inserted at junction points between β-strands and in the case of split-GFP, typically the truncation occurs between the 10^{th} and 11^{th} β-strands. The first 214 amino acids contain the first 10 β-strands (GFP1-10), while the remaining 215 – 230 amino acids make up the 11^{th} β-strand (GFP11, ~1.8 kDa) and is used to tag the protein of interest (Cabantous et al., 2005), which in this case will be tau (Fig 1.4C).

While the chromophore is contained within the internal α-helix, its formation and maturation which comprise cyclisation, oxidation and dehydration, require not only the critical internal residues S65, Y66 and G67, but also residues located on the external β-strands, including R96 and E222, both essential for dehydration and oxidation (Barondeau et al., 2003; Romei and Boxer, 2019) (Fig 1.4 A, B). E222 is located on the 11th β-strand; after truncation, E222 is lacking from GFP1-10, creating an incomplete core of the chromophore. Only upon re-association will there be reconstitution of the fluorophore (Fig 1.4C).

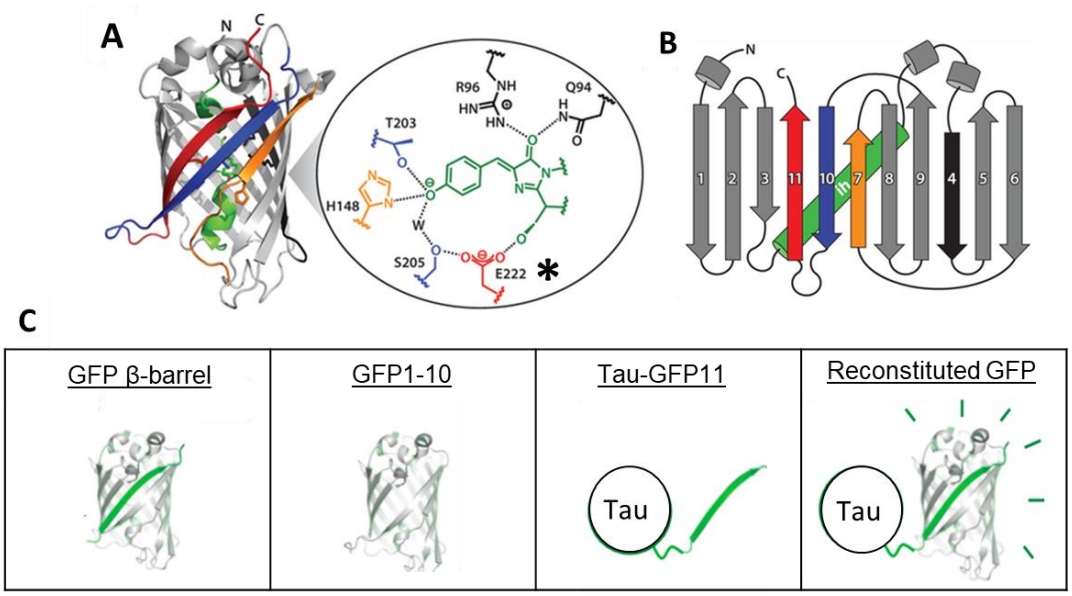

Figure 1.4 – Structure and topology of superfolder GFP used for split-GFP technology.

(A) β-barrel structure of GFP made up of 11 external β-strands and an internal α-helix (ih) forming the chromophore depicted in green ih– critical amino acids are shown and colour coded according to which β-strand they are located on (see B); E222 present on 11th β-strand highlighted with asterisks.

(B) Topology of 11 β-strands and ih. 11th β-strand 11 (red) forms the GFP11 fragment in split-GFP which contains E222. Amino acids present on 10th (blue), 7th (orange) and 4th (black) β-strands are depicted in (A) (Romei and Boxer, 2019).

(C) Split-GFP schematic; β-barrel GFP structure, GFP1-10 sensor fragment, tau tagged with single β-strand (tau-GFP11), reconstituted GFP with tau-GFP11 and GFP1-10. Adapted from (Leonetti et al., 2016).

Interestingly, the BiFC can detect weakly bound protein interactions (K_D in the μM-mM range) validating its highly sensitive nature (Magliery et al., 2005; Morell et al., 2007); furthermore, it has a sub-micromolar affinity for self-assembly *in vitro* (Cabantous et al., 2005). Once the functional GFP is formed, the interaction is virtually irreversible, generating a stable signal that can be used to monitor transient interactions (Cabantous et al., 2005; Magliery et al., 2005).

Split-GFP was first tested *in vitro* and developed in a bacterial system whereby BL21 (DE3) bacteria were co-expressing GFP11-tagged proteins with GFP1-10, in order to detect GFP signal. Interestingly, the fluorescent signal intensity was a linear function of protein concentration, enhancing the accuracy of the readout. This BiFC split-GFP tool has since been used for investigating a wide range of interactions, including inter-organelle contact sites between mitochondria and endoplasmic reticulum (Kakimoto et al., 2018) cellular localisation of either endogenous proteins e.g. protein kinase A (Kamiyama et al., 2016) or over-expressed proteins (Kaddoum et al., 2010) including disease relevant, Dj-1 (Calì et al., 2015) and TDP-43 (Foglieni et al., 2017). Split-GFP has also been utilised to monitor cytosolic delivery of recombinant cell-penetrating peptides tagged with GFP11, such as TAT and penetratin (Milech et al., 2015). However, this approach, to date, has not been applied to study the cellular entry of either recombinant or cell-secreted tau.

The first application of tau tagged with GFP11 in a mammalian setting was used to assess tau aggregation. Briefly, the aggregation-prone (K280 deletion) and aggregation-resistant (I277 and I308 substituted to proline) MTBR constructs were tagged with GFP11 and independently co-expressed with GFP1-10 (Chun

et al., 2007). The average fluorescence intensity was measured over five days; when compared to WT MTBR-GFP11, after three days the aggregation-prone construct had a significantly lower GFP signal. In contrast, the aggregation-resistant variant exhibited significantly higher fluorescent signal throughout the duration of the experiment (Chun et al., 2007). These data support the hypothesis, that upon aggregation of GFP11-tagged proteins, the small β-strand is sequestered and therefore hidden from the large GFP1-10 sensor. As such, it was predicted that tau aggregates were more readily formed by the aggregation prone MTBR construct compared to WT or aggregation resistant.

To directly assess self-assembly of tau, different approaches of BiFC have been taken. One group made use of the split-VENUS which in contrast to the already described split-GFP, is truncated to generate two similar sized non-fluorescent fragments containing either the amino- or carboxy-termini. These two fragments were used to individually tag full-length 2N4R tau forming two different constructs; the fluorescent signal detected from co-expression of tau-Venus (VN173) and tau-Venus (VC153) in HEK293 cells was compared with cells expressing tau-GFP. Here, the authors observed 19% reconstituted signal, compared to tau-GFP expressing cells, thus suggesting that under basal conditions tau exists predominantly as a monomer (Tak et al., 2013). After 24 h treatment with okadaic acid, an inhibitor of protein phosphatase 2A, there was a two-fold increase the BiFC signal, confirming the role of phosphorylation in tau self-assembly (Tak et al., 2013).

This work has been developed *in vivo* by the same group, to show longitudinal analysis of transgenic mice expressing 2N4R-P301L tau tagged with split-

VENUS fragments (Shin et al., 2020). Over 12 months BiFC signal could be detected with whole-brain imaging in the cortex, hippocampus and entorhinal cortex, in both the cell soma and axons. As expected, there was an age-dependent increase in the BiFC signal, particularly seen in the hippocampus. Interestingly, when brain sections were probed with phospho-tau antibodies over the same time period, AT8 positive signal (S202/T205) was only detected after nine months in the same areas that had BiFC signal at earlier time points (Shin et al., 2020). This observation generated the hypothesis that formation of oligomeric tau may precede and/or promote hyperphosphorylation at pathological sites. Future *in vivo* imaging of the BiFC may shed light on aggregation under physiological and pathological conditions.

BiFC has proved highly versatile and provided a novel approach to fluorescent imaging. This system offers an advantage over traditional methods for detecting protein interactions, such as the commonly used FRET, since the split-GFP system does not rely on multiple fluorescent signals. When using FRET, consideration must be taken when selecting the donor/acceptor fluorophore pair to ensure sufficient spectral overlap for efficient energy transfer, but minimizing the risk of exciting the acceptor molecule during direct donor fluorophore excitation. Given that neither GFP1-10 nor GFP11 is fluorescent on its own, there is no intrinsic risk of fluorescent emission upon excitation; therefore, it provides a simple ON/OFF system which can be easily quantified. In addition, the emitted BiFC signal has a linear relationship with protein concentration and so this tool can also be used to compare relative protein concentration between different conditions, without the technical complication of antibody binding affinity, which does not always follow a linear scale (Itagaki, 2000).

In this project I aim to develop an assay using the split-GFP to assess intracellular delivery of tau. A common reported problem of using split-GFP when studying protein-protein interactions is the potential self-dimerization between GFP1-10 and GFP11 fragments. While this is a caveat that needs to be considered, in this assay the two GFP fragments are first separated by a membrane barrier, therefore the risk of non-specific self-dimerization is negligible. In addition, upon expression of cytosolic GFP1-10, any interaction between tau-GFP11 will be a positive signal for entry of tau into the cytosol; if future work is conducted whereby GFP1-10 is co-expressed with potential binding partners of tau within the internalisation process, this issue will need to be addressed more closely. Although split-GFP is still a fluorescent tagging method for observing tau uptake, and will not be able to provide the resolution achieved with EM, this fundamental process of cytosolic entry does not require high resolution imaging, but rather a reliable way for visualising tau entry. If GFP1-10 were co-expressed with other proteins, then this work would have to be validated with higher-resolution imaging or other biochemical approaches, to confirm a molecular interaction. Nevertheless, when compared to alternative imaging strategies that could be used to investigate tau entry, split-GFP can be scaled-up for high throughput imaging with a simple readout measure. The ON/OFF nature of the GFP signal enables this system to be pharmacologically manipulated and therefore be a potential screening tool for assessing agents that promote or inhibit tau uptake on a large-scale.

1.5 Project aims

My project aims to develop a novel cytosolic translocation assay that can reliably detect the translocation of tau into the cytosol, whether it be directly across the plasma membrane, or from within the lumen of an endocytic vesicle. I will be first generating tau constructs with a GFP11 tag and then applying this modified tau protein extracellularly to cells expressing cytosolic GFP1-10. Only upon uptake and cytosolic entry will there be reconstitution of the GFP signal, directly confirming tau translocation across the lipid bilayer.

The specific aims of this thesis are as follows:

1. Develop and optimise the protocol for the cytosolic translocation assay based on split-GFP technology in cell-lines.
2. Investigate the cytosolic translocation propensity of all six WT tau isoforms, including 1N4R-P301S mutant tau.
3. Explore potential mechanisms mediating cytosolic translocation of tau.
4. Assess if cytosolic translocation assay based on split-GFP technology can be applied to primary cortical / hippocampal neurons.

First a proof of principle test will be conducted to ensure that in my hands co-expression of tau-GFP11 and GFP1-10 will give rise to reconstitution of the GFP signal from independent split-GFP domains. In addition, I will confirm that the individual GFP fragments are not fluorescent in the experimental conditions adopted in thesis.

Given the complex nature of tau in the extracellular space, bacterially expressed and mammalian cell-secreted tau will be tested for cytosolic translocation. Since all six tau isoforms are expressed throughout the CNS and

are well documented to play a role in tau-mediated pathology, I decided to investigate the cytosolic translocation propensity of each tau isoform to ascertain whether any isoform conferred an enhanced or reduced ability for cytosolic entry. To address pathological tau entry, the 1N4R-P301S mutant will also be introduced in addition to seeding aggregation with tau aggregates obtained from the tauopathy mouse model rTg4510.

Since there is very little mechanistic understanding regarding the process of cytosolic translocation of tau across lipid bilayers, this assay will be used to test the effect of manipulating specific intracellular pathways that may be involved. I will focus on whether the endocytic vesicles can influence the rate of release by altering the luminal pH with Bafilomycin A1, and Concanamycin A and by arresting the progression of the endolysosomal pathway via expression of specific Rab-GTPase dominant-negative mutants to assess whether localisation within these organelles are necessary for productive delivery of tau from their lumen into the cytosol.

Finally, I aim to test the cytosolic translocation assay in primary neurons; in parallel I will explore the use of novel MFCs to further investigate trans-synaptic tau spread.

Chapter 2: Materials and Methods

2.1 Reagents / media

Reagents used in this thesis were purchased from Sigma-Aldrich unless stated otherwise. Phosphate buffered saline (PBS) was made from 10 X PBS solution (GIBCO). All solutions were prepared with MiliQ water.

2.2 Chemical inhibitors and recombinant protein

All chemical compounds and recombinant proteins used within the project are listed in Table 2.1

Table 2.1 – Chemical compounds and recombinant proteins

Compound	Company	Working concentration	Description Mechanism
Bafilomycin A1	MP Biomedical	0.5 – 5 nM	Inhibitor of vacuolar H^+ ATPase
Concanamycin A	Millipore	0.5 – 10 nM	Inhibitor of vacuolar H^+ ATPase
MG-132	Merck	100 nM	Proteasome inhibitor
LysoTracker® Red DND-99	Invitrogen	50 nM	Probe for lysosomes, accumulates in acidic vesicles
Transferrin-conjugated to AlexaFluor 488	Thermo Fisher Scientific	50 µg/ml	Transferrin receptor ligand
10 kDa Dextran-conjugated to AlexaFluor 647	Thermo Fisher Scientific	100 µg/ml	Endocytic marker
4-aminopyridine (4-AP)	Sigma-Aldrich	2.5 mM	Voltage-gated potassium channel blocker
Bicuculline	Tocris	50 µM	Competitive $GABA_A$ receptor antagonist

2.3 Antibodies

All fluorescent secondary antibodies for immunofluorescence were purchased from Invitrogen (Host / Isotype; goat / IgG) and used at a 1:500 dilution. All other antibodies used are listed in Table 2.2.

Table 2.2 – Antibody list: All antibodies used in this study (with source and dilution factor)

Antibody	Species	Company	Western blot	Immunofluorescence
Primary antibodies				
Tau1 monoclonal (#MAB3420)	Mouse	Chemicon	1:5,000	1:1,000
AT8 monoclonal	Mouse	Eli Lilly	1:1,000	-
MC1 monoclonal	Mouse	Eli Lilly	1:1,000	1:500 (3 µg/ml)
Flag Monoclonal (#F1804)	Mouse	Sigma-Aldrich	1:1,000	1:1,000 (1 µg/ml)
GFP polyclonal (GFP-1020)	Chicken	Aves	-	1:1,000
HA (#11867423001)	Rat	Sigma/Roche	-	1:500 (100 ng/ml)
GAPDH (#2118)	Rabbit	Cell signalling	1:1,000	-
MAP2 polyconal (#188 004)	Guinea pig	Synaptic Systems	-	1:1,000
Antibody	**Species**	**Company**	**Western Blot**	**ELISA**
Primary antibodies				
Total tau (#A0024)	Rabbit	DAKO	-	1:3,600 (3 µg/ml)
Flag Monoclonal (#F3165)	Mouse	Sigma-Aldrich	-	1:500 (7.5 µg/ml)
Secondary antibodies				
Anti-mouse HRP (#P0217)	Swine	DAKO	1:2,000	
Anti-Rabbit HRP (#P0260)	Swine	DAKO	-	1:5,000
Anti-Rabbit HRP (#1858415)	Goat	Pierce	1:2,000	

2.4 Bacterial transformation

Approximately 50 ng of each DNA construct was mixed with 50 µl of chemically competent XL-10 Gold *E. coli* cells and incubated on ice for 30 min. For heat shock transformation, the DNA and XL-10 Gold mix was placed in a water bath at 42 °C for 45 s and immediately transferred to ice for two minutes. The bacteria were placed in a shaking incubator (225 RPM) for 1 h at 37 °C with 1 ml of Super optimal broth with catabolite repression (SOC), formulation/L: 20 g tryptone, 5 g yeast extract, 0.5 g NaCl, 5 g $MgSO_4$, $7H_2O$, 20 mM glucose. A final centrifugation step was conducted (4,000 RPM, 4 min) to pellet the bacteria and discard the supernatant leaving 50 – 100 µl for resuspension. Bacteria were plated on Lysogeny broth (LB) -agar dishes (formulation/L: 10 g tryptone 140, 5 g yeast extract, 5 g NaCl and 12 g agar) containing the appropriate antibiotic (1:1,000 ampicillin, 100 mg/ml) and grown at 37 °C overnight.

If DNA constructs were delivered as a bacterial stab a pipette tip was used to spread bacteria across an LB-agar plate; containing the appropriate antibiotic and grown overnight at 37 °C. The following day, single colonies were picked for recovery of plasmid DNA.

2.5 Isolation of plasmid DNA

Upon transformation, colonies were picked for overnight inoculation in LB medium (formulation/L: 10 g tryptone, 5 g yeast extract, 10 g of NaCl) containing appropriate antibiotic. Recovery of plasmid DNA was conducted

using QIAprep Spin Miniprep Kit (Qiagen) or Midi DNA purification was conducted (NucleoBond® Xtra Midi, Macherey Nagel), following manufacturer instructions.

2.6 Nucleic acid quantification

Isolated plasmid DNA pellet was diluted with 50 µl UltraPure™ DNase/RNase-free distilled water (Thermo Fisher Scientific) and the optical density (OD) was measured at 260 nm. DNA concentration was determined using a NanoDrop One spectrophotometer (Thermo Fisher Scientific), 1 unit of OD 260 corresponds to 50 mg/ml of double-stranded DNA.

2.7 Cloning and ligation

2.7.1 Plasmids

The pCDNA 2N4R-GFP11 plasmid was kindly donated by Dr. Tito Cali (University of Padova, Italy). The remaining tau isoforms (0N3R, 0N4R, 1N3R, 1N4R and 1N4R with P301S mutation) were kindly donated by Dr. Suchira Bose (Eli Lilly, Erl Wood UK) and Prof. Michel Goedert (2N3R). The pBi-TAT-86 plasmid was kindly provided by Dr. Bruno Beaumelle (Montpellier, France). The pHR-hSyn-EGFP was kindly donated by Dr. Dominic Aghaizu. All other plasmids were purchased on Addgene: pHR-SFFV-GFP1-10 (Addgene #80409); pET C-terminal TEV His-6 cloning vector (Addgene, #48285); DsRed-Rab5 N133I dsRed2 (#13051), DsRed-Rab7 T22N dsRed1 (#12662), DsRed-Rab11 S25N dsRed 1 (#12680).

2.7.2 Cloning – pCDNA 2N4R-GFP11

FastCloning was used to manipulate the mammalian expression vector pcDNA3-2N4R-GFP11 to insert both a restriction site at the C-terminal of 2N4R for sub-cloning of alternative tau isoforms and a FLAG-tag to facilitate detection in confocal microscopy (Li et al., 2011). To further this work, a bacterial expression vector was required for production of recombinant tau (pET C-terminal TEV His-6 cloning vector). When selecting the restriction site to be inserted, all restriction sites present in the pcDNA3 and pET vectors had to be considered. PmeI was selected for the C-terminal of 2N4R but due to its eight base pair (bp) recognition site, an additional base (A), was included to maintain the open reading frame. BamHI was already present at the N-terminal of 2N4R in the pcDNA-2N4R-GFP11 vector, so no additional restriction sites were added.

As described by Li et al (2011), FastCloning requires two polymerase chain reactions (PCR) for the vector and insert. Two sets of primers are designed for the vector and the desired insert. The insert forward primer contains the desired insert sequence and sections of the vector sequence both 5’ and 3’ to the desired location of insertion (Fig 2.1B). For pcDNA3-2N4R-GFP11, the generated insert sequence was: PmeI, a single nucleotide spacer and a FLAG tag. This sequence is only 108 bp therefore to aid the visualisation of the PCR product using agarose gel electrophoresis, the primer pair was designed to amplify a sequence of approximately 800 bp covering the vector sequence downstream of the insertion site.

The forward and reverse primers for the vector are designed to have an overlapping sequence with both forward and reverse insert primers (Fig 2.1).

The vector forward primer will have ~ 15 bp overlap with the insert reverse primer (Fig 2.1E, 2.1F), and the vector reverse primer will have ~ 15 bp overlap with the insert forward primer (Fig 2.1B, 2.1C).

A. **Original 2N4R-Linker-GFP11**

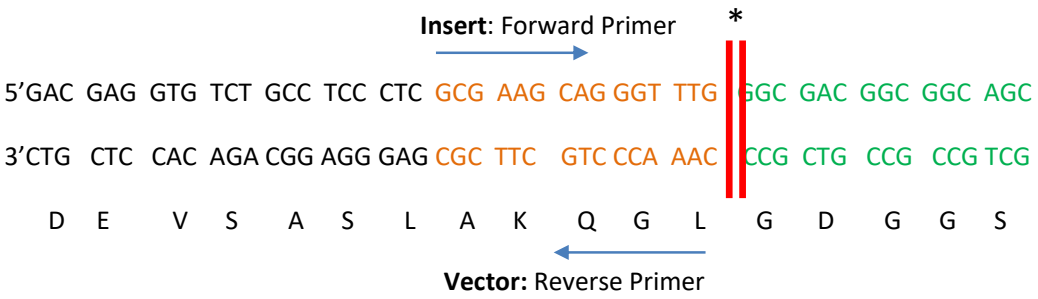

B. **Insert: Forward Primer**

*

5' GCG AAG CAG GGT TTG AGT TTA AAC GAC TAC AAA GAC GAT GAC GAT AAA GGC GAC GGC GGC AGC GGC GGC 3'

C. **Vector: Reverse Primer**

5' CAA ACC CTG CTT CGC GAG GGA GGC A 3'

D. **~800 bp downstream of GFP11 sequence**

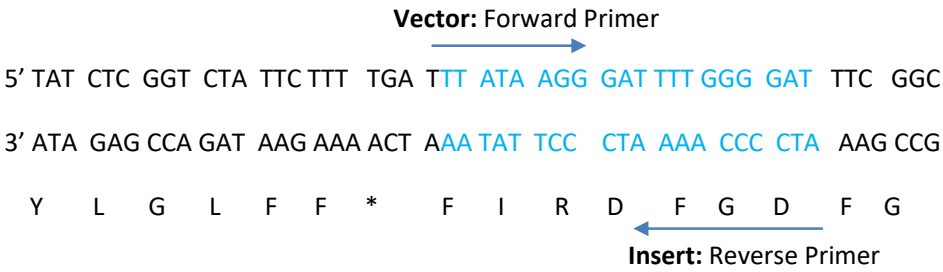

E. **Vector Forward Primer**

5' TT ATA AGG GAT TTT GGG GAT TTC GGC CTA TTG GTT 3'

F. **Insert Reverse Primer**

5' ATC CCC AAA ATC CCT TAT AA A TCA AAA GAA TAG ACC GAG ATA GGG T 3'

Figure 2.1 – FastCloning schematic for designing primers for pCDNA3-2N4R-GFP11. Double red line with asterisks (A) indicates the site of insertion of the new sequence. Single red lines with asterisks (B) are the borders for the new sequence: PmeI, A and FLAG tag. Matching colours indicate overlapping sequences.

The PCR parameters were optimised for the amplification of the pCDNA3 insert (Table 2.3), using the high fidelity Q5 polymerase (NEB). The PCR reaction and parameters were optimised for the amplification of the pcDNA3 vector. Table 2.3 displays the working parameters for the PCR, using the Expand Long Range Kit (Roche).

Table 2.3 – Optimised polymerase chain reaction conditions for pCDNA3 insert and vector amplicon.

PCR Cycling parameters pCDNA3 Insert			**PCR Cycling parameters pCDNA3 Vector**		
Temperature	*Time*	*No. of cycles*	*Temperature*	*Time*	*No. of cycles*
98 °C	2 min	1x	92 °C	2 min	1x
98 °C	10 s	35x	92 °C	10 s	10x
71 °C	30 s		55 °C	15 s	
72 °C	30 s (30 s/kb)		68 °C	6 min (60 s/kb)	
72 °C	2 min	1x	92 °C	10 s	25x
4 °C	∞		65 °C	15 s	
			68	6 min (60 s/kb)	
			68 °C	6 min	1x
			8 °C	∞	

Upon PCR amplification the vector and insert were analysed with 0.8 % agarose gel electrophoresis, to ensure the PCR products are of their predicted size using SYBR® Safe DNA gel stain (Invitrogen). Once confirmed, vector and insert were mixed at 3:5 ratio and digested with DpnI for 1 h at 37 °C; 5 µl of the mix was then transformed in Stratagene XL-10 Gold or NEB 10-beta *E. coli* cells. Upon transformation and recovery of plasmid DNA, positive colonies were confirmed by simultaneously digesting with BamHI (NEB) and PmeI (NEB). All plasmids (300 ng DNA) were double digested in a 10 µl reaction with 0.1 µl BamHI and 0.1 µl PmeI. Positive colonies were confirmed by DNA sequencing.

2.7.3 Cloning – pET 2N4R-GFP11

The FastCloning approach was applied to the pET C-terminal Tobacco etch virus (TEV) His-6 vector to insert BamHI-2N4R–PmeI-Flag-Linker-GFP11 upstream of the TEV, His6 site. When designing the vector and insert primer pairs, it was important to consider that the expression of the 2N4R-FLAG-GFP11 insert had to contain both the TEV site and the 6xHis tag. In the pcDNA3 vector, the sequence of tau contained a stop codon at the carboxy-terminus of GFP11. Therefore, the primer designed to amplify the BamHI-2N4R–PmeI-Flag-Linker-GFP11 had to replace the stop codon with an alternative amino acid used as a spacer. The choice of the amino acid was important as it should not disrupt the sequence for the TEV site. The canonical recognition site for TEV protease is Glu-Asn-Leu-Tyr-Phe-Gln-(Gly/Ser), where the protease cleaves between Gln and Gly/Ser. In the pET vector, the TEV sequence did not include the N-terminal glutamic acid. Therefore, in the reverse insert primer, the stop codon was substituted to glutamic acid to form part of the TEV sequence. The primer for the pET insert was now designed to produce a PCR product containing the BamHI-2N4R tau-PmeI-FLAG-linker-GFP11 (1446 bp) (Table 2.4). The optimised PCR parameters for pET vector and insert are displayed in Table 2.5

Table 2.4 – Primer pairs designed for FastCloning of pET and 2N4R tau

Insert: BamHI-2N4R-PmeI-Flag-GFP11 (5' – 3')	
Forward primer	ACTTTAAGAAGGAGATATAGTTGGATCCATGGCTGAGC
Reverse primer	GGATTGGAAGTAGAGGTTTTCTGTGATGCCGGCGGCGTT
Vector: pET c-terminal TEV His6 (5' – 3')	
Forward primer	AACCTCTACTTCCAATCCGGCTCT
Reverse primer	AACTATATCTCCTTCTTAAAGTTAAACAAAA

Table 2.5 – Optimised polymerase chain reaction conditions for pET insert and vectors amplicons

PCR Cycling parameters pET Insert			PCR Cycling parameters pET Vector		
Temperature	*Time*	*No. of cycles*	*Temperature*	*Time*	*No. of cycles*
98 °C	30 s	1x	98 °C	30 s	1x
98 °C	10 s	35x	98 °C	10 s	35x
72 °C	30 s		64.8 °C	30 s	
72 °C	90 s (30 s/kb)		72 °C	2 min 30 s (30 s/kb)	
72 °C	2 min	1x	72 °C	2 min	1x
4 °C	∞		4 °C	∞	

Once both pET vector and insert had been amplified, a 3:5 ratio of the PCR fragments was mixed for DpnI digestion, 5 µl; of the mix was transformed into *E. coli* XL-10 Gold, and DNA extracted from single colonies. DNA was simultaneously digested with BamHI and PmeI. Positive colonies were confirmed by DNA sequencing.

2.7.4 Subcloning and ligation of tau isoforms into GFP11 containing vector

To insert the alternative tau isoforms into the existing pcDNA3 and pET vectors containing the BamHI-tau-PmeI and Flag-tag and GFP11 sequence, additional primers were designed to carry out restriction enzyme/PCR cloning (Table 2.6). The forward primer included the BamHI sequence at the N-terminal of the protein sequence, and the reverse primer included the PmeI sequence at the Carboxy-terminal.

Table 2.6 – Primer pairs designed for polymerase chain reaction of inserts into GFP11 containing vector

Primer name	Primer description	Primer sequence (5' – 3')
0N3R, 1N3R, 2N3R, 0N4R, 1N4R, 1N4R-P301S	Forward primer	TAATA GGATCC ATGGCTGA GCCCCGC
	Reverse primer	TGATAA GTTTAAAC TCAAACCCTGCTTGGCCA
Tat	Forward primer	GTACAG GGATCC ATGGAGCCAGTAGATCCTAGACT
	Reverse Primer	TAGATG GTTTAAACT TTCCTTCGGGCCTGTCGGGTC

The newly constructed vector of pcDNA3 containing the BamHI-2N4R-PmeI-Flag-GFP11 was used as a template to generate all other Flag-GFP11 containing constructs. The NEB PCR Cloning Kit was used to introduce the generated PCR amplicon into an empty vector, pMiniT 2.0; ligation and transformation were conducted following manufacturer instructions. Positive colonies (300 ng DNA) were identified with a 10 µl double digest reaction with 0.1 µl BamHI and 0.1 µl PmeI. Positive colonies (2 µg DNA) were digested in a 50 µl reaction with 1 µl BamHI and 1 µl PmeI for 2 h at 37 °C. This digestion was then analysed with 0.8% agarose gel electrophoresis and the insert of the correct base pair dimension was extracted using the NucleoSpin Gel and PCR Clean-up kit (Macherey-Nagel).

To replace the alternative tau isoforms into the mammalian and bacterial expression vectors, both pcDNA3-2N4R-Flag-11 and pET-2N4R-Flag-11 were digested in a 50 µl reaction with 1 µl BamHI and 1 µl PmeI for 2 h at 37 °C followed by a 30 min incubation with 1 µl (0.2 U/µl) calf intestinal alkaline phosphatase (CIP) at 37 °C to avoid re-ligation of the linearized vector. Products were analysed on a 0.8 % agarose gel and extracted for purification. DNA concentration was determined using a NanoDrop One spectrophotometer.

All new inserts, including tat, were introduced into the pcDNA3 vector using the 5' BamHI and 3' PmeI sites (Table 2.6).

The amount of insert for T4 ligation reaction was determined with the relative length equation (Eq 1). The insert to vector ratio and the vector amount (ng) was predetermined as 1.2 and 30 ng respectively, following optimisation. The 20 µl ligation mix was prepared with vector, insert and nuclease free water added first and incubated at 37 °C for 5 min, followed by the addition 1 µl T4 DNA ligase (20 U/µl) and 2 µl 10x T4 buffer. Ligation mix was incubated at 16 °C overnight and stored at –20 °C before transformation. 10 µl of ligation reaction was added to chemically competent XL-10 Gold *E. coli* cells and transformed as previously described. Upon confirmation of positive colonies by double digestion with BamHI and PmeI, a Midi DNA purification was conducted (NucleoBond® Xtra Midi, Macherey Nagel)

Equation 1. Relative length calculation for T4 ligation reaction

$$Insert\ (ng) = \frac{ratio \times vector\ (ng) \times bp\ insert}{bp\ vector}$$

2.8 Protein extraction

2.8.1 Cell line and primary culture lysis

All cell cultures were lysed with chilled RIPA (50 mM trisaminomethane (Tris)-HCl pH 7.5, 150 mM NaCl, 1 mM EDTA, 1 % Triton-X 100, 1 % NP-40 plus 1x protease inhibitor cocktail, added fresh every time. Cell cultures were washed with chilled 1x PBS, scraped in RIPA buffer, and collected in Eppendorf tubes to

incubate on ice for 30 min. Lysates were spun at 14, 800x g for 15 min at 4 °C and pellet discarded. Lysates were either used for protein quantification, or added to 4x Laemlli buffer plus 10 % βME, added fresh, and denatured at 100 °C for 3 – 5 min.

2.8.2 Protein quantification

Bicinchoninic acid (BCA) quantification kit (Thermo Fisher Scientific) was used to quantify total protein concentration in lysates. Samples were incubated at 37 °C for 30 min with BCA reagents A and B as per manufacturer's instructions and analysed on a microplate reader (FLUOstar Omega, BMG Labtech), using bovine serum albumin (BSA) as protein standard.

2.8.3 Sodium dodecyl sulphate - polyacrylamide gel electrophoresis (SDS-PAGE)

Lysates were first mixed with 4x Laemlli sample buffer (250 mM Tris-HCl pH 6.8, 8 % SDS, 40 % glycerol, 0.02 % bromophenol blue) and 10 % fresh 2-mercaptoethanol (βME), then denatured at 100 °C for 3 min, loaded on 10 % SDS-PAGE gels (Bio-Rad) and electrophoresed with a constant voltage increasing from 60, 100 to 130 V for approximately 1 h.

2.8.4 Western blot

Proteins were transferred to polyvinylidene difluoride (PVDF) membranes via electrophoretic transfer with a Trans-Blot Turbo Transfer system (semi dry transfer, Bio Rad) run at 25 V, 1 A for 30 min with transfer buffer 10 x (25 mM Tris, 190 mM glycine), 20 % MeOH and 70 % H_2O. Membranes were blocked in 5 % BSA in Tris-buffered saline supplemented with 0.1 % Tween 20 (TBS-T) for 1 h at room temperature. Primary antibodies were incubated overnight at 4 °C

on a rocking shaker. This was followed by four 5 min washes with TBS-T and incubation with the appropriate secondary antibody conjugated with horseradish peroxidase (HRP) for 1 h at room temperature. Membranes were washed with TBS-T, as described and developed on the Amersham Imager (GE Healthcare) following the addition of Clarity ECL substrate (Bio Rad).

2.8.5 rTg4510 seed-competent tau aggregate extraction

Seed competent tau aggregates were extracted from 21-week rTg4510 mice forebrain expressing 0N4R-P301L tau, kindly donated by Dr. Suchira Bose (Eli Lilly, Erl Wood UK). Using a glass Dounce homogenizer (Scientific Laboratory Supplies), 1 ml of homogenisation buffer (50 mM Tris HCl pH 7.4, 150 mM NaCl, 1 mM EDTA protease and phosphatase inhibitor (Roche)) per 100 mg forebrain were mixed thoroughly until a homogenous mixture was formed. The homogenate was then centrifuged at 20,000x g for 20 min at 4 °C; supernatant was then incubated with 1 % sarkosyl (Sigma-Aldrich) and placed on a rotating shaker for 30 min at room temperature. The final centrifugation step was conducted with sarkosyl/brain extract at 100,000x g for 1 h at 20 °C. Supernatant was saved for testing and pellet was resuspended in 1x PBS with protease/phosphatase inhibitor – sample was passed through a 26 G needle to ensure efficient homogenisation. A sonicator probe (Qsonica) was used at 20 % AMP for 1 min at 4 °C. Samples were stored at -80 °C; before experimental use tau seeds were sonicated with 15 % AMP for 1 min at 4 °C, the concentrations used are stated in relevant results sections.

2.9 Enzyme-linked immunosorbent assay (ELISA)

The concentration of tau in conditioned cell-culture medium was determined

with a newly developed ELISA assay in partnership with Miss Chiara Panzi (Schiavo's laboratory). 96 well Nunc MaxiSorp™ flat-bottom plates (Thermo Fisher Scientific) were used for high protein binding capacity. 96 well plates were coated with capture antibody anti-Flag M2 (Sigma-Aldrich, mouse) diluted in 1x PBS (7.5 µg/ml, 50 µl per well) and placed on a microtitre plate shaker (750 RPM) overnight at 4 °C. The following day, the plate was rinsed once with wash buffer (1x PBS, Tween 20 0.05 % - PBST) 100 µl per well. To prevent any non-specific binding, a blocking solution was used made up of PBST with 1 % BSA, 100 µl per well was added to the plate and incubated at room temperature for 1.5 h on a rocking shaker (Quanterix, 500 RPM). A second wash step was conducted before adding the samples.

To establish a standard curve, recombinant human 1N4R tau-GFP11 was used at increasing concentrations, ranging from 0 to 250 ng/ml diluted in sample buffer. Conditioned tau medium was taken fresh or thawed from -80 °C and spun at 21,000x g for 5 min at 4 °C. To avoid saturation of signal, all conditioned tau media was diluted in fresh culture medium at a ratio of 3:2. All samples were added to the plate in triplicates (50 µl per well) and placed on rocking shaker for 1.5 h (500 RPM).

Following sample incubation, the plate was washed three times with wash buffer. The detection antibody total tau (DAKO, rabbit) was used at 3 µg/ml diluted in blocking solution, 50 µl per well and placed on rocking shaker for 1 h (500 RPM). A second wash step was conducted prior to adding the secondary antibody α-rabbit conjugated with HRP (swine) used at 1:5,000 diluted in blocking solution, 50 µl per well and placed on rocking shaker for 1 h (500

RPM); a final wash step was conducted.

In order to detect the signal with the ELISA, the chromogenic substrate 3,3',5,5'-tetramethylbenzidine (TMB, Thermo Fisher Scientific) was added to the wells. The interaction with the peroxidase triggers a colour change which allows the absorbance to be measured spectrophotometrically. 100 µl total per well of TMB was added to the plate and placed on the bench protected from the light, at room temperature for 15-30 min. As the reaction occurs the solution turns blue, therefore to avoid saturation of the signal 1 M sulphuric acid was added to stop the reaction (100 µl per well). This causes a colorimetric change from blue to yellow, which enables the absorbance peak to be measured at 450 nm. The microplate reader (FLUOstar Omega, BMG Labtech) was used.

2.10 Protein production and purification

2.10.1 Recombinant tau expression

Based on methods adapted from (KrishnaKumar and Gupta, 2017) the pET-2N4R-Flag-11-TEV-6xHis plasmid was transformed with BL21(DE3) competent cells (Novagen). A single colony was picked for overnight inoculation in 500 ml LB medium containing ampicillin 100 µg/ml (37 °C, 225 RPM). The OD of the bacteria was measured and when OD_{600} reached 0.6-0.7 isopropyl β-D-1-thiogalactopyranoside (IPTG) was added at a final concentration of 1 mM and incubated for a further 4 h at 37 °C at 225 RPM. Bacteria were centrifuged at 6,000x g for 15 min at 4 °C and the pellet was re-suspended in 20 ml lysis buffer (50 mM NaH_2PO_4, 0.3 M NaCl, 1 mM phenylmethylsulfonyl fluoride (PMSF) and 5 mM imidazole, pH 8), supplemented with protease inhibitor

cocktail (10x) in preparation for downstream purification method by Ni-NTA affinity chromatography (Fig 2.2A,B).

2.10.2 Bacterial cell lysis

The re-suspended pellet was directly boiled for 20 min with gentle agitation every 5 min and then incubated on ice for 10 min. The sample was centrifuged at 13,000x g for 20 min at 4 °C and the supernatant was filtered through a 0.22 µm filter and stored at -80 °C before further analysis (KrishnaKumar and Gupta, 2017) (Fig 2.2A,B).

2.10.3 Protein purification

Ni-NTA agarose (Qiagen) was used for purification. 250 µl of Ni-NTA beads (50 % slurry) was rinsed twice with lysis buffer prior to being incubated with 20 ml of bacterial lysate at 4 °C and placed on a rotating shaker overnight. The Ni-NTA resin was reconstituted in lysis buffer for gravity-based affinity purification; the final volume of Ni-NTA resin was 125 µl and this is considered the column volume (CV). To prepare the column for protein purification it is first equilibrated with equilibration buffer (50 mM NaH_2PO_4, 0.3 M NaCl, pH 8). The bacterial lysate and Ni-NTA was loaded onto the column and washed two times with five CVs of wash buffer: 1.25 ml (50 mM NaH_2PO_4, 0.3 M NaCl, 30 mM imidazole, pH 8), flow through was collected.

The resin bound by tau was then resuspended in 20 ml TEV cleavage buffer Z (50 mM Tris HCl pH8, 0.5 mM EDTA and 1 mM dithiothreitol (added fresh before use)), ensuring the approximate tau concentration did not exceed 0.5 mg/ml to avoid aggregation. Recombinant TEV and resin bound by tau was

mixed at a 1:50 ratio and placed on a rotating shaker for six hours at room temperature. The TEV and resin mix was then loaded onto the column and flow through containing recombinant tau was collected. These samples were concentrated using an ultra-0.5 mL centrifugal filter device with a 10 kDa cut off (Amicon ®); finally, a buffer exchange was conducted from buffer Z to 150 mM NaCl and 20 mM HEPES, pH 7.4. Samples were snap frozen in liquid nitrogen and stored at -80 °C until further use (Fig 2.2).

2.10.4 Tau protein analysis

The protein concentration of the purified protein samples were analysed by BCA quantification, SDS-PAGE and western blot as described above.

2.10.5 Coomassie staining

0.1 % Coomassie blue R250 (Thermo Fisher Scientific) dissolved in 45 % methanol, 45 % H_2O and 10 % acetic acid was used for gel staining. Following gel electrophoresis, the 10 % SDS-PAGE gels were incubated with warm staining solution for 15 min at room temperature on a rocking shaker. The de-staining buffer (40 % methanol, 50 % H_2O and 10 % acetic acid) was applied overnight at room temperature.

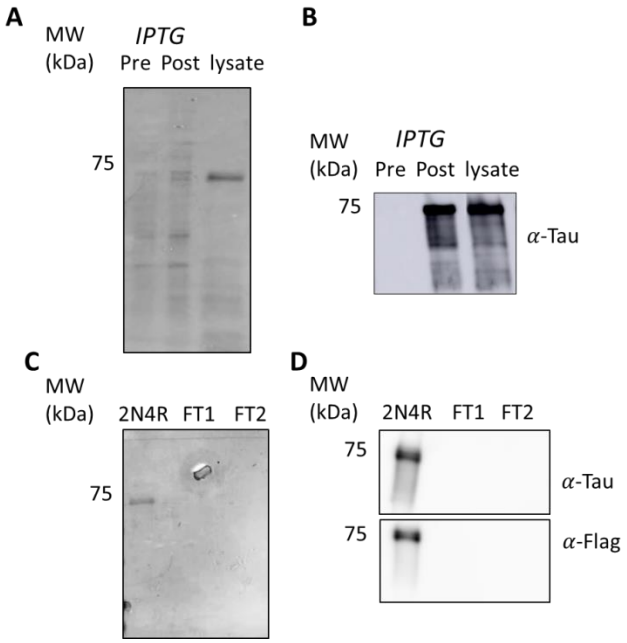

Figure 2.2 - 2N4R protein induction, extraction and affinity chromatography purification.

(A) Bacterial pellet loaded pre- and post-IPTG induction, in post-IPTG an additional band is present below 75 kDa indicating the expression of 2N4R tau. Post induction, bacteria was directly boiled for protein extraction (lysate); Coomassie staining.

(B) Western blot of samples from (A) probed with anti-tau antibody (Tau1).

(C) Coomassie staining of collected eluat of purified 2N4R by affinity chromatography with Ni-NTA beads. No protein lost in flow through wash samples (FT)

(D) Western blot of concentrated purified 2N4R tau, demonstrating positive reactivity to both α-Tau and α-Flag (mouse) antibody. No protein was lost in the flow through wash (FT) samples collected

2.11 Cell line culture methods

N2a and HEK293 cells were grown in T75 flasks (Thermo Fisher Scientific) with Dulbecco Modified Eagle Medium (DMEM, GIBCO), 10 % fetal bovine serum (FBS, Labtech international), 1 % Glutamax (ThermoFisher Scientific) and 50 µg/ml gentamicin at 37 °C, 5 % CO_2. HEK293 cells were first plated in 10 % FBS. FBS content was reduced sequentially from 10 % to 1 % after each passage number – cells remained at 1 % FBS throughout the duration of experiments. All dishes (Greiner) and coverslips (VWR) used for HEK293 cells

cultured in reduced FBS were coated with 20 µg/ml poly-D-lysine (Milipore) for 2 h at 37°C. All cells were plated as per stated in Table 2.7 and maintained at 37 °C, 5 % CO_2.

Table 2.7 – Plating density for cell-line cultures

Culturing conditions	
Cell plate	*Cell count*
6 well dish	600,000
12 well dish	250,000
24 well dish	175,000

2.12 Primary neuronal culture methods

2.12.1 Dissection of mice embryos

Primary cortical and hippocampal cultures were isolated from E16-17 WT mice embryos. Pregnant female C57BL/6J inbred mice were euthanized by cervical dislocation and confirmation by decapitation, in accordance with animals (Scientific Procedures) Act 1986.

The embryos were removed; their heads severed using appropriate surgical tools and placed in ice cold Hank's Balanced Salt Solution (HBSS, Gibco) for dissection. Brains were extracted using two straight-end forceps to cut caudally along the centre of the skull. To first expose the hippocampus, the cerebral hemispheres were separated and the midbrain removed. Finally, the meninges were detached and the hippocampus carefully dissected out followed by the cortex, both independently incubated in ice-chilled HBSS and maintained

separate for culturing and plating (Banker and Cowan, 1977).

2.12.2 Culturing and plating

HBSS was aspirated after the hippocampi and cortices collected at the bottom of their respective tubes. The tissue was washed 3x with 10 ml cold HBSS and incubated with 50 % Accutase and 50 % HBSS at 37 °C for 8 min with gentle agitation every 2 min. The tissue was washed 5x with 10 ml warm HBSS and finally left in 1.5 ml HBSS. Both hippocampi and cortices were triturated with a 5 ml stripette, a glass Pasteur pipette and left to settle for 5 min. The supernatant was transferred to a fresh eppendorf tube for cell counting. The cell density was determined using countess II FL automated cell counter (Thermo Fisher Scientific) mixed 1:1 ratio (5 µl) with Trypan Blue Stain 0.4% (Thermo Fisher Scientific). Neurons were plated as per stated in Table 2.8 and maintained at 37 °C, 5 % CO_2.

Table 2.8 – Plating density for neuronal cultures

Culturing conditions	
Cell plate	*Cell count*
6 well dish	200,000
12 well dish	100,000
24 well dish	75,000
Mattek	60,000
MFCs	100,000

All coverslips were NOCHROMIX treated, as per manufacture's protocol before culturing. Culture dishes with and without coverslips were coated overnight prior to plating. 0.4 M borate buffer (0.4 M sodium tetraborate decahydrate and 0.4 M boric acid, Sigma-Aldrich, pH 8.5,) was used for mixing poly-L-lysine (PLL,

Sigma-Aldrich) in a 1:100 dilution for a final PLL concentration of 50 µg/ml; Glass bottom dishes (matTeks and MFCs) were coated with a final PLL concentration of 100 µg/ml.

On the morning of dissection, culture dishes were washed 3x with autoclaved H_2O and left to dry before adding primary hippocampal/cortical media (1 % glucose, 1x Glutamax, 1 % penicillin/streptomycin, 1x B27, Neurobasal).

2.13 Fabrication of microfluidic chambers (MFCs)

MFCs were assembled based on designs made in collaboration with Dr. Andrea Serio, The Francis Crick Institute, London. Epoxy resin masters (EPON) were made by mixing all ingredients stated in Table 2.9, and placed in a vacuum desiccator for 60 min to remove air bubbles. The mixture was poured into a tin cup and a polydimethylsiloxane (PDMS) master, donated by Dr. Serio, was used as a mould. The PDMS copy was placed onto the epoxy resin with the design facing downwards and incubated overnight at 65 °C for polymerisation. The PDMS mould was carefully removed from the resin with bent tip forceps.

Table 2.9 – Ingredients for EPON resin preparation – Final weight 20 g per epoxy master mould.

Components	Required weight (g)
Taab 812 resin	9.6
Methyl nadic anhydride (MNA)	6.6
Dodecenyl succinic anhydride (DDSA)	3.8
2, 4, 6-tri (diamethylaminomethyl) phenol (DMP-30)	0.4

New PDMS devices were produced by replica moulding. A 10:1 ratio of PDMS: curing agent (Dow Corning; VWR) was mixed vigorously and placed in a vacuum desiccator for 40 min to remove air bubbles. ~4 ml was poured into each resin master and incubated 1 h at 65 °C for polymerisation. The PDMS device was carefully removed and cut to shape with a 28 mm round punch; a further four wells were cut out with a 5 mm punch (Fig 2.3). The PDMS device was cleaned with tape before being placed in a plasma cleaner (Diener) together with a 50 mm glass-bottomed dish (Fig 2.3). The plasma treatment of the glass and PDMS alters their surface properties to allow a permanent bond to develop upon contact. The PDMS bonded to the glass-dish were incubated at 65 °C for 5 min before coating with 100 µg/ml PLL overnight prior to culturing. Fluidic isolation was maintained by keeping the difference in volume between somatic and axonal compartments greater than 50-150 µl (discussed further in Results) (Fig 2.3A).

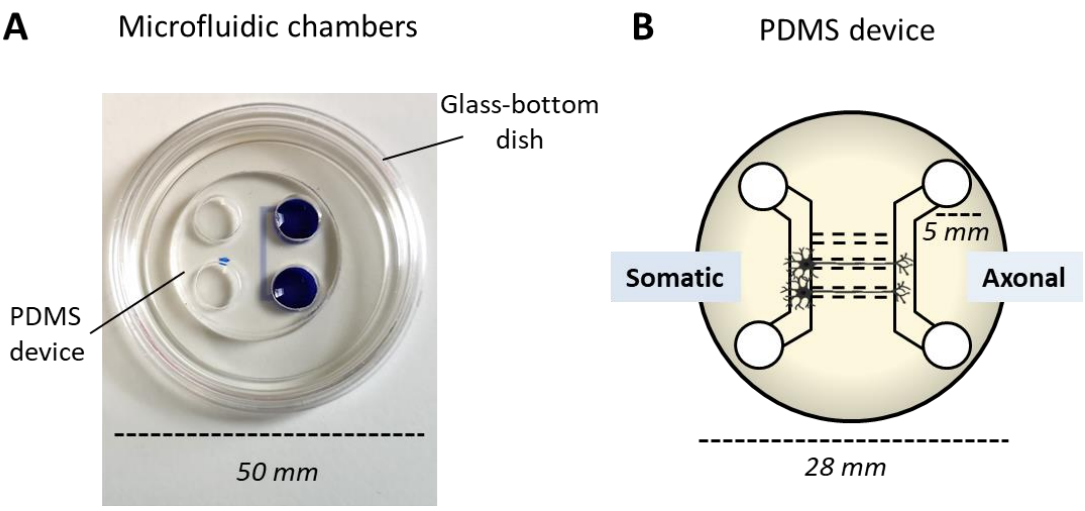

Figure 2.3 – Schematic of microfluidic chambers.

(A) Example of PDMS device bound with glass-bottom dish (50 mm diameter). Dot on left side of PDMS device marks "somatic compartment", thus right side is "axonal compartment". Fluidic isolation demonstrated by the addition of water and Coomassie Blue R250 in somatic and axonal compartment respectively with a volume difference greater than 50 – 150 µl.

(B) Schematic of PDMS device, highlighting somatic and axonal compartment with neuronal axons crossing the microgrooves. Dimensions of PDMS device are displayed.

2.14 Genetic manipulation of cell lines

2.14.1 Transfection

Lipofectamine 3000 and P3000TM Enhancer (Thermo Fisher Scientific) were used to prepare transfection reaction and this differed according to the type of cell culture vessel as described (Table 10). Two transfection reactions were prepared, (A); DNA, Lipofectamine P3000TM enhancer and Optimem and (B); Lipofectamine 3000 and Optimem, which was briefly vortexed. Reactions A and B were mixed thoroughly at a 1:1 ratio and incubated at room temperature for 15 min; transfection mix was added drop by drop to each cell plate well.

Table 2.10 – Lipofectamine 3000 Transfection protocol used for cell-line cultures

Cell plate	DNA (µg)	Lipofectamine 3000 (µl) 2 µl/µg	Lipofectamine P3000TM Enhancer (µl) - 2µL/µg	Optimem (µl)	Total reaction volume (µl)
6 well dish	1.5-2	3-4	4	2 x 125	250
12 well dish	1	2	2	2 x 50	100
24 well dish	0.5	1	1	2x 25	50

2.14.2 Lentiviral production

Lentiviral expression vectors were produced with pLenti HEK cells (TAKARA). The HEK cells were grown in T75 flasks with DMEM, (GIBCO), 10 % FBS (Labtech international) and 1:100 Glutamax (Thermo Fisher Scientific) at 37 °C, 5 % CO_2. The cells were split 2x and transferred onto T175 flasks for transfection. Briefly, per T175 flask of pLenti HEK cells 11.75 µg of PAX (packaging vector), 7.8 µg of VSV-G (enveloping vector) and 11.75 µg of the plasmid of interest was transfected using 50 µl Lipofectamine 3000 Reagent and 62.5 µl P3000TM Enhancer Reagent (Thermo Fisher Scientific). 48 h post transfection, media were collected and stored at 4 °C and 30 ml of was added to the cells for a further 24 h. All media collected were combined and centrifuged at 1,500 RPM at 4 °C for 10 min to remove cell debris. Lenti-X concentrator (Clontech) was added at a 1:3 ratio to the supernatant and incubated for 72 h at 4 °C. The mix was centrifuged at 3,000 RPM at 4 °C for 45 min, the majority of media was discarded for the final centrifugation at 3,000 RPM at 4 °C for 10 min. After gently removing all the media, pellets were combined and re-suspended with a total of 400 µL Optimem

(Thermo Fisher Scientific) per virus. Two T175 flasks were used per production. Aliquots were made, snap frozen in liquid nitrogen and stored at -80 °C until further use.

2.15 Genetic manipulation of primary neuronal cultures

2.15.1 Transfection

Primary cortical / hippocampal cultures were transfected with Lipofectamine 2000 (ThermoFisher Scientific) between DIV 5-7. Preparation of transfection reaction and media differed according to cell culture vessel as described in Table 2.11. For the transfection reaction; the neurobasal was mixed thoroughly with DNA and Lipofectamine and incubated for 15 min at 37 °C. In the final five minutes of DNA-Lipofectamine incubation, the transfection media was prepared; all residual conditioned media from the cell plate was saved for post-transfection.

Gently, the transfection media was added to the neurons, followed by drop by drop addition of transfection reaction; this was incubated at 37 °C for 30 min. Finally, all media was replaced with post-transfection media made up of 50 % conditioned media and 50 % freshly made media.

Table 2.11 – Lipofectamine 2000 Transfection protocol used for primary neuronal cultures

Culturing conditions	**Transfection reaction**			**Transfection media**	
Cell plate	*DNA (µg)*	*Lipofectamine 2000*	*Neurobasal (µl)*	*Neurobasal (µl)*	*Conditioned media (µl)*
12 well dish	1.5	2	200	800	200
24 well dish	1	1	100	400	100

2.15.2 Lentiviral transduction

All lentiviral transductions were conducted between DIV 4 – 6. Lentiviral particles were added to conditioned media from neuronal cultures. No media change took place, unless stated otherwise. Volume of lentivirus used according to cell culture dish is listed in Table 2.12. Cultures were assayed either via immunocytochemistry or live imaging.

Table 2.12 – Lentiviral particle volume used in primary neuronal cultures

Cell plate	Lentivirus volume (µl)
24 well dish	1
12 well dish	2
6 well dish	2.5
MFC	0.5
Mattek	0.5

2.16 Immunocytochemistry and microscopy

All cells and neurons were fixed with 4 % paraformaldehyde (PFA, Thermo Fisher Scientific) and 4 % sucrose in phosphate-buffered saline (PBS), incubated for 15 min at room temperature and then washed 3x with 1x PBS. Cells were permeabilised with 0.5 % BSA, 0.2 % Triton-X 100, 10 % goat serum and 1x PBS for 15 min at room temperature. Primary antibodies were diluted in "blocking solution" 0.5 % BSA, 10 % goat serum and 1x PBS and incubated for 1 h at room temperature in the dark. Coverslips were washed 3x every 10 min with high salt buffer – 500 mM NaCl and 20 mM NaH_2PO_4 in H_2O, pH 7.4. Secondary antibodies were diluted in blocking solution and incubated for 1 h at room temperature in the dark. Coverslips were washed again 3x every 10 min

with high salt buffer, and finally washed in H_2O prior to being mounted on slides with Mowiol 4-88 (Sigma-Aldrich). Cells were imaged with an inverted Zeiss confocal laser scanning microscope (LSM) 880, images were processed using Image J.

2.17 Live imaging

Live imaging with the LSM 880 confocal microscope of primary neuronal cultures were conducted with Tyrode's buffer (15 mM D-glucose, 108 mM NaCl, 5 mM KCl, 2 mM $MgCl_2$, 2 mM $CaCl_2$ and 25 mM HEPES-NaOH, pH 7.4). Cell media was swapped with Tyrode's buffer 20 min prior to live imaging to allow cells to acclimatise.

Live imaging with the widefield Incucyte® (Sartorius) microscope; cell culture dishes/plates were placed in the Incucyte® approximately 20 min prior to start of the programmed imaging cycle. Images collated from the Incucyte® software were analysed with Image J.

2.18 *In vitro* cell-line experimental methods

In vitro GFP complementation assay were conducted with HEK293 cell lysate and recombinant tau-GFP11. HEK293 lysate was estimated to have 2.5 µg protein per microliter of lysate based on BCA quantifications; up to 40 µl of lysate was mixed with recombinant tau-GFP11. Concentration of recombinant tau-GFP11 used between 0 - 2 µM. Total reaction volume was 100 µl made up with 1x PBS. GFP reconstitution reaction was conducted in a 96 well plate (Corning) over 4 h at room temperature in the dark. The microplate reader (FLUOstar Omega, BMG Labtech) was used for GFP detection (488 nm

excitation).

2.19 Cell line lactate dehydrogenase (LDH) assay

To test for cell death, LDH assay (Roche) was conducted on the conditioned cell media of HEK293 cells transiently transfected with human tau constructs. High LDH samples were taken from non-transfected cells treated with lysis solution, as per the manufacturer's protocol and assigned as 100 % cytotoxicity. Background control was taken from both fresh media and conditioned media from non-transfected cells.

2.20 Cell line bimolecular fluorescence complementation (BiFC) assay

HEK293 cells cultured in 1 % FBS medium were plated in a 6 well plate (Nunc). 18 h post plating cells were transiently transfected with Lipofectamine-3000 using pcDNA3.1 constructs encoding human tau-GFP11. Fresh cell medium was added six hours post transfection to avoid downstream Lipofectamine interference. The conditioned tau medium was collected 48 h post transfection and centrifuged at 2,000x g for five minutes prior to use to pellet any dead cells or cellular debris and either used experimentally or stored at -80 °C. In parallel, HEK293 cells were plated in a 24 well plate (Cell star, Greiner). The next day cells were transiently transfected with constructs encoding GFP1-10 (or co-transfected with Rab GTPase constructs) using Lipofectamine-3000. Six to eight hours post transfection 80% of the conditioned media was removed and replaced with fresh tau-GFP11 containing medium.

For live imaging, the 24 well plate was placed in the Incucyte® with phase and green channels selected for detection of the reconstituted GFP using a 20x

objective with 300 ms set acquisition time. Cells were monitored every 4 h over a 60 h period.

2.20.1 BiFC - Time pulse experiment with tau-GFP11 media

HEK293 cells were cultured in 24 well dish; 18 h post plating cells were transiently transfected with constructs encoding GFP1-10 using Lipofectamine-3000. Six to eight hours post transfection 80% of the conditioned media was removed and replaced with fresh tau-GFP11 containing medium for 30 min, 60 min and 24 h. Conditioned media swapped with fresh media not containing tau-GFP11 and cells were monitored every 4 h over a 60 h period.

2.20.2 BiFC – Incubation with recombinant tau-GFP11

HEK293 cells were cultured in 24 well dish; 18 h post plating cells were transiently transfected with constructs encoding GFP1-10 using Lipofectamine-3000. Six to eight hours post transfection, 80 % of the conditioned media was removed and replaced with fresh media containing 4 – 800 nM of recombinant tau-GFP11, produced as stated above (2.10). Cells were monitored every 4 h over a 60 h period.

2.20.3 BiFC assay - rTg4510 seed competent tau aggregates

rTg4510 seed competent tau aggregates (500 ng/ml) produced as stated above (2.8.5) were sonicated with 15 % AMP for 1 min at 4°C, prior to being mixed with conditioned tau-GFP11 media and incubated with GFP1-10 expressing cells. Monitoring of GFP was performed in the Incucyte® as previously described.

2.21 Effect of vacuolar type H^+ATPase inhibition on tau trafficking

Bafilomycin A1 (BafA1, MP Biomedical) and Concanamycin A (ConA, Millipore) were used for alkalinising organelles from the endolysosomal pathway by specific inhibition of the vacuolar type H^+ ATPase (V-ATPase).

2.21.1 Lysosomes

HEK293 cells were cultured in 24 well dish, 18 h post plating 5 nM BafA1 or 10 nM ConA were used for 5 min treatment. Conditioned media was replaced with fresh media containing LysoTracker® Red DND-99 (50 nM) (Invitrogen) and 0.5 nM BafA1/ConA to maintain V-ATPase inhibition. This treatment was left for 30 min at 37 °C prior to live imaging on the Incucyte®. DMSO (Dimethyl sulfoxide, Sigma-Aldrich) was used as vehicle control.

2.21.2 Endocytic markers

HEK293 cells were cultured in 24 well dish, 18 h post plating 10 nM ConA were used for five minute treatment. Conditioned media was replaced with fresh media containing fluorescently labelled Transferrin-488 (50 µg/ml, Thermo Fisher Scientific) or Dextran-647 (100 µg/ml, Thermo Fisher Scientific) with 0.5 nM ConA to maintain V-ATPase inhibition. This treatment was left for 3 h at 37 °C prior to fixing and imaging with either Zeiss fluorescent microscope or inverted Zeiss LSM 880 confocal microscope.

2.21.3 Secreted-tau-GFP11

HEK293 cells were cultured in 24 well dish, 18 h post plating cells were transfected with GFP1-10. Six to eight hours post transfection, cells were pre-

treated with 5 nM BafA1 or 10 nM ConA for 5 min, conditioned media was replaced with fresh media containing tau-GFP11 with either 0.5 nM BafA1 or 0.5 nM ConA. Cells were monitored every 4 h over a 60 h period.

Alternatively, six to eight hours post GFP1-10 transfection, conditioned media was removed and fresh media containing tau-GFP11 was added for varying time periods (5 – 240 min). Conditioned tau media was then removed and saved during a 5 min treatment of either 5 nM BafA1 or 10 nM ConA; the saved tau media was supplemented with 0.5 nM BafA1 or 0.5 nM ConA and incubated with GFP1-10 cells to be monitored every 4 h over a 60 h period.

2.22 Primary neuronal culture experimental methods

2.22.1 BiFC- Recombinant tau-GFP11

Neurons were either transfected or transduced with GFP1-10 between DIV 4-6. At DIV 8-10 purified recombinant tau-GFP11 or vehicle control was incubated with neurons for 1 – 24 h at 37 °C. Final concentration of recombinant tau-GFP11 stated in relevant result section (range 0.5 – 2 µM). Neurons were assayed via live imaging either in the Incucyte or with an inverted Zeiss LSM 880 confocal microscope before fixation and immunocytochemistry.

2.22.2 BiFC- Neuron secreted tau-GFP11

To test split-GFP assay in primary neurons, cortical / hippocampal neurons were plated in both 6 and 24 well dish for tau-GFP11 and GFP1-10 transduction respectively. At DIV 5 neurons were transduced with lentiviral particles, 24 h

later 50 % media was changed for fresh media. DIV 8-10 tau-GFP11 containing media was transferred to GFP1-10 expressing neurons. Neurons were assayed over 6 to 7 days, via live imaging either in the Incucyte or with an inverted Zeiss LSM 880 confocal microscope before fixation and immunocytochemistry.

2.22.3 BiFC - HEK293 cell secreted tau-GFP11

Primary cortical / hippocampal neurons were plated in a 24 well dish. At DIV 5 neurons were transduced with lentiviral particles carrying GFP1-10 cDNA. In parallel HEK293 cells were plated in a 6 well dish in regular HEK293 media (1% Glutamax, 50 µg/ml Gentamicin, 1% FBS, DMEM). 18 h post plating cells were transfected with tau-GFP11. Six hour post transfection conditioned media was replaced with primary culture media (1% glucose, 1x Glutamax, 1% penicillin/streptomycin, 1x B27, Neurobasal). HEK293 cell secreted tau-GPF11 was transferred to primary neuronal cultures (DIV 7-8) for longitudinal live imaging or immunocytochemistry over 6 to 7 days. Variations of the described experiment were conducted and described below.

2.22.4 BiFC - Neuronal stimulation

In attempts to improve neuronal uptake of tau-GFP11, 4-AP (2.5 mM) and Bicuculline (50 µM) were mixed with HEK293-cell secreted tau-GFP11 and incubated with GFP1-10 expressing primary neuronal cultures for 1 h at 37 °C. Conditioned media was then replaced with fresh neuronal media, unless stated otherwise. Chronic stimulation was also conducted with 2.5 mM 4-AP and HEK293-cell secreted tau-GFP11, where conditioned media was not replaced. Neurons were assayed via live imaging either in the Incucyte or with an inverted Zeiss LSM 880 confocal microscope before fixation and immunocytochemistry.

2.22.5 BiFC - Proteasome degradation inhibition

To test whether tau degradation was impacting the reconstitution of GFP tau signal, the cell-permeable proteasome inhibitor MG-132 (100 nM) was applied with HEK293 cell-secreted tau-GFP11 to GFP1-10 expressing neurons with and without neuronal stimulation by 4-AP (2.5 mM) for 4 h. Neurons were assayed via live imaging with an inverted Zeiss LSM 880 confocal microscope.

2.22.6 BiFC – trans-synaptic spread of tau-GFP11

Primary cortical neurons were plated in somatic and axonal compartment of MFCs; at DIV 4 neurons in axonal compartment were transduced with lentiviral particles encoding GFP1-10, at DIV 6 neurons in the somatic compartment were transduced with lentiviral particles encoding tau-GFP11. Neurons were assayed over 6 to 7 days, via live imaging with an inverted Zeiss LSM 880 confocal microscope before fixation and immunocytochemistry.

2.22.7 Co-culture of primary cortical neurons and HEK293 cells

Primary cortical neurons were plated in somatic compartment of MFCs; at DIV 5 neurons were transduced with lentiviral particles, 24 h later 50% media was changed for fresh media. At DIV 8-10, tau-GFP11 expressing HEK293 cells were transferred and seeded in axonal compartment of MFC, with direction of fluidity from axonal to somatic compartment. Neurons were assayed over 6 to 7 days, via live imaging with an inverted Zeiss LSM 880 confocal microscope.

2.23 Statistics

All statistical analysis was performed using GraphPad Prism. Data were confirmed to be normally distributed with the Shapiro-Wilk test. When

comparing the difference between two groups either unpaired Student's t-test with or without Welch's correction were used, or paired t-test. If there were multiple groups, a one-way analysis of variance (ANOVA) was used followed by either Tukey's or Dunnett's multiple comparison test. All statistical tests used, along with associated p-values are stated in figure legends. Statistical significance noted is as follows: *, $P \leq 0.05$, **, $P \leq 0.01$, ***, $P \leq 0.001$.

Chapter 3 - Development and optimisation of cytosolic translocation assay for tau

3.1 Introduction

To date, split-GFP components have routinely been used for determining protein localisation (Foglieni et al., 2017; Kaddoum et al., 2010; Kamiyama et al., 2016) and inter-organelle interactions (Kakimoto et al., 2018). In parallel, this tool has been used to understand the mechanism of cytosolic delivery, in particular of cargoes that have been tagged with cell penetrating peptides (Milech et al., 2015).

As described in the introduction, with regards to tau, split-fluorescent proteins have been used to investigate self-assembly of tau both in cellular systems (Chun et al., 2007; Tak et al., 2013) and *in vivo* (Shin et al., 2020) yet, split-GFP complementation has not been used to directly address the cytosolic delivery of tau following endocytosis, a mechanism that is still poorly understood. One reason for this is the difficulty in accurately observing, with standard imaging methods, when tau has escaped the endocytic / endolysosomal pathway to enter the cytosol. This is an important process since it is reported to occur both in physiology (Chen et al., 2019; Dujardin et al., 2018) and pathology in which it constitutes a fundamental step in the prion like spreading of pathological tau (Chen et al., 2019; Dujardin et al., 2018). Therefore, analysis of its mechanism is a priority for the field and requires a reliable way of being monitored. Given that most existing methods rely on either seeding aggregation (Holmes et al., 2014), or monitoring galectin mislocalisation as membrane damage reporters

(Chen et al., 2019). Recent work conducted by the McEwan lab generated a novel split-luciferase assay to investigate cytosolic entry of tau by measuring the luciferase signal. I aim to develop a new complementary tool to aid this investigation to provide direct visualisation of cytosolic tau entry, which is not achieved with existing methods.

In the following Chapter I will describe optimisation experiments to develop a system that can reliably detect the time point of tau entry into the cytosol by monitoring the green fluorescent signal generated by the complementation between the GFP11 tagged to tau and the acceptor GFP1-10 protein expressed in the cytosol of the recipient cell. In the field of tau research, recombinant tau has predominately been used to study cellular uptake (Frost et al., 2009; Rauch et al., 2020) and cytosolic entry (Chen et al., 2019; Falcon et al., 2018a), with some groups also utilising cell-secreted (Calafate et al., 2016, 2015) or human derived tau samples (Puangmalai et al., 2020). Consequently, I will test both recombinant and cell-secreted tau to identify the best experimental setup.

3.2 Results

3.2.1 Testing the functionality of mammalian expressed tau-GFP11

To start developing the cytosolic translocation assay I wanted to first test the functionality of both the GFP1-10 and tau-GFP11 constructs. Both mammalian expression vectors were transfected into HEK293 cells; positive transfection of both GFP1-10 and tau-GFP11 can be seen in Figure 3.1. By immunocytochemistry a polyclonal α-GFP antibody (Chicken, Aves) was used

to detect the GFP1-10 and a monoclonal α-Flag (Mouse, Sigma-Aldrich) antibody was used to detect the tau-GFP11 construct which contains a Flag tag. In Figure 3.1A it is possible to observe that a cell in which there is co-expression of the two split-GFP domains there is convincing reconstitution of the GFP signal. Figure 3.1A also contains highlighted regions which demonstrate examples of when either the GFP1-10 or tau-GFP11 is expressed in isolation, and subsequently do not yield any detectable GFP signal, confirming that the fragments alone are not auto fluorescent. Importantly, from this representative image it can be seen that there is no apparent aggregation of tau with the addition of the GFP11 tag and the cell morphology look healthy.

In Figure 3.1B there is a representative image of GFP1-10 expressing cells to demonstrate the GFP signal profile with a higher 488 nm laser power; low and high exposure examples have been shown in order to compare genuine GFP reconstitution (highlighted in Fig 3.1B) versus background signal. From this image it is clear that even when the GFP signal is boosted, the reconstituted GFP signal is considerably stronger compared to the background, confirming the functionality of the split-GFP domains.

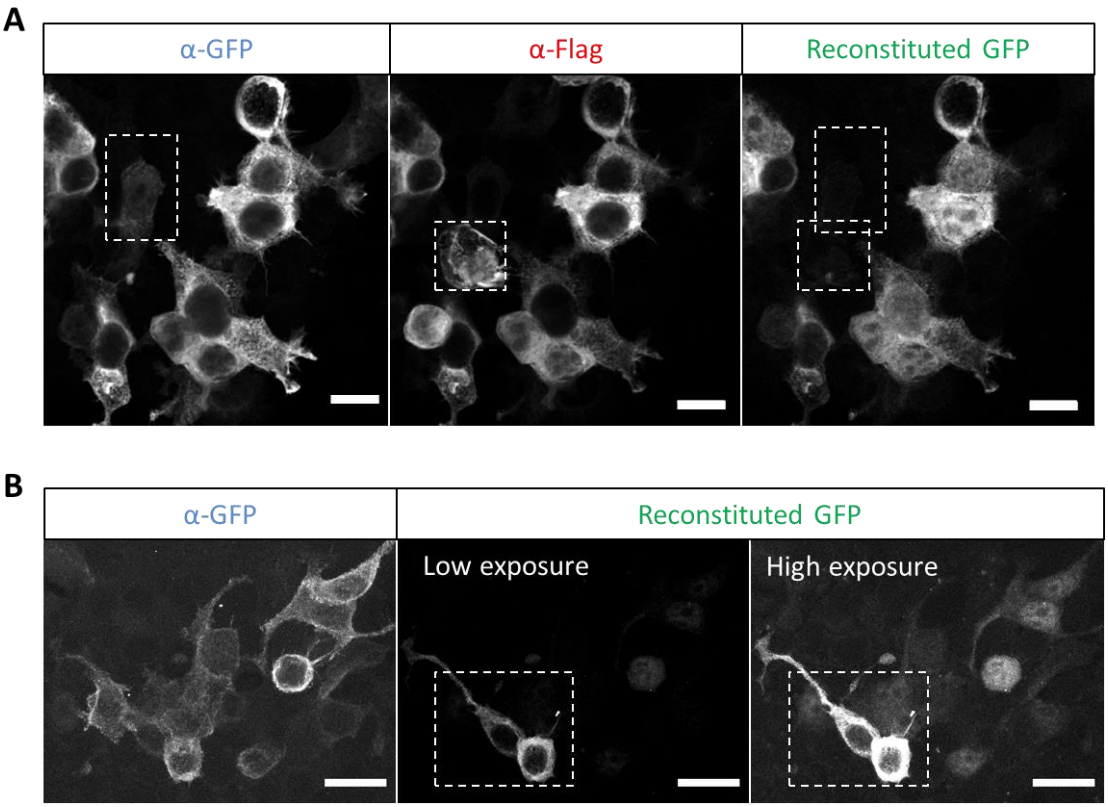

Figure 3.1 – Co-expression of GFP1-10 and tau-GFP11 in HEK293 cells.
GFP1-10 and 2N4R tau-GFP11 co-expressed for 24 h prior to fixation and immunocytochemistry for confocal imaging. α-GFP (Chicken) (Alexa Fluor 647) and α-Flag (Mouse) (Alexa Fluor 555) antibodies were used to probe for GFP1-10 and tau-GFP11 respectively.

(A) Representative images show that the reconstituted GFP signal is visible only in cells co-expressing both GFP1-10 and tau-GFP11 (488 nm channel). Single expression of GFP1-10 and tau-GFP11 has been highlighted and demonstrates no detectable GFP signal. Scale bar, 15 µm.

(B) Representative image displaying higher 488 nm laser power with a low and high exposure example to demonstrate the background fluorescence generated by GFP1-10. Genuine reconstruction of GFP has been highlighted. Scale bar, 25 µm.

Experiment repeated with 3 biological replicates, achieving similar results.

3.2.2 Testing the functionality of recombinant tau-GFP11

Having confirmed GFP reconstitution of tau-GFP11 by co-expression of the mammalian vector with GFP1-10, I also wanted to have a simple test to confirm functionality of the *E.coli* produced recombinant tau-GFP11, prior to testing

cytosolic translocation. I decided to test the activity of recombinant tau-GFP11 in an *in vitro* set up.

Briefly, HEK293 cells were transfected with GFP1-10 and lysed 24 h post transfection. The lysate was then collected and incubated with purified monomeric recombinant tau-GFP11 at room temperature over four hours prior to measuring the fluorescence with a spectrofluorometer.

A similar experimental design has been conducted by Kaddoum and colleagues, but instead, permeabilised HEK293 or N2a cells expressing GFP11 tagged protein were incubated with a solution containing recombinant GFP1-10 protein and the fluorescence was measured by FACS flow cytometry (Kaddoum et al., 2010). My experiment was designed to test the activity of the free exogenous recombinant tau, rather than recombinant GFP1-10.

In this set up I examined whether recombinant tau-GFP11 could produce fluorescence when in contact with mammalian expressed GFP1-10, without the need to cross a physical barrier. By lysing and centrifuging the GFP1-10 expressing cells, this exposed the intracellular protein contents by removing the cellular membrane and unlysed cells, and so the two split-GFP domains will have direct access to each other. Based on previous BCA quantifications of HEK293 lysates, it was estimated that in 1 µl of lysate there was 2.5 µg of total protein (data not shown). From this I decided to test samples containing 50 – 100 µg total protein.

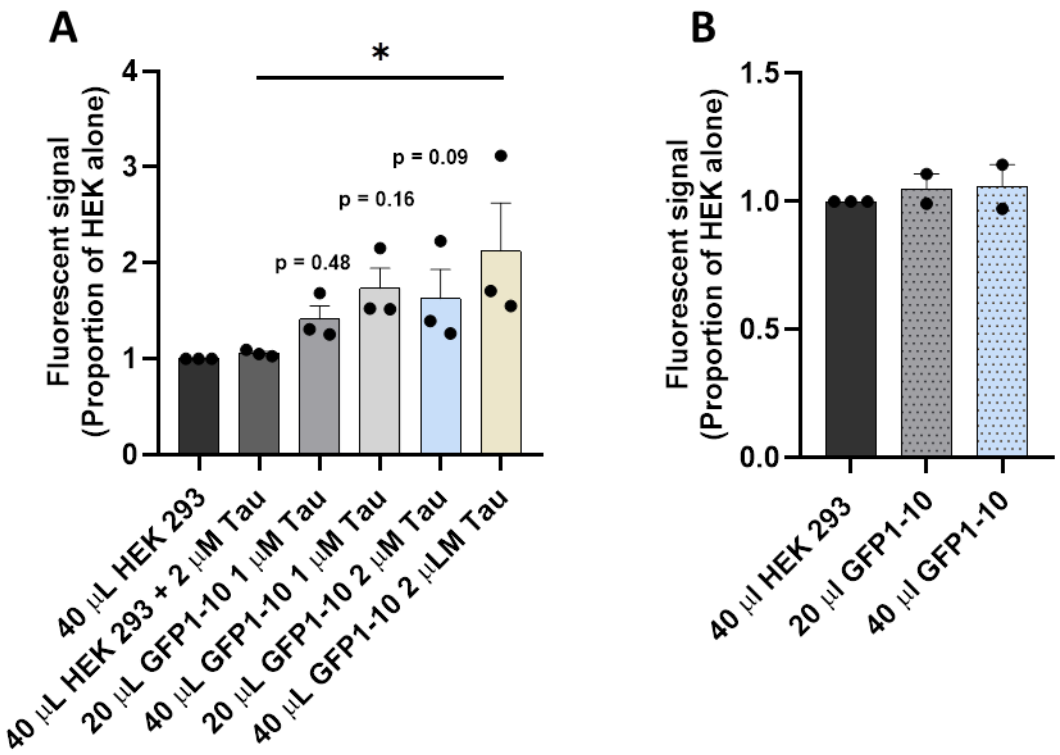

Figure 3.2 – *In vitro* GFP reconstitution of recombinant tau-GFP11 and mammalian expressed GFP1-10.
Bar charts displaying the GFP fluorescent signal generated by either 20 or 40 µl of GFP1-10 lysate in the presence of 0, 1 or 2 µM of recombinant tau-GFP11 as a percentage of the signal generated by non-transfected HEK lysate (40 µl HEK 293). Signal measured with spectrofluorometer.

(A) Lysates with or without GFP1-10 incubated with recombinant tau-GFP11 for 4 h at room temperature. A significant difference was identified between *40 µl HEK 293 + 2 µM tau* and *40 µl GFP1-10 + 2 µM tau* , * $p < 0.05$ one-way ANOVA, followed by Dunnett's multiple comparison conducted (n = 3, biological replicates). All other comparisons to *40 µl HEK 293 + 2 µM tau* were not significant. Bar graph represent mean ± S.E.M

(B) Lysates with or without GFP1-10 were measured for auto fluorescent signal (n = 2, biological replicates). Bar graph represent mean ± standard deviation.

I have shown that this *in vitro* set up can detect GFP reconstitution; in Figure 3.2A there is a significant difference between fluorescent signal detected when 2 µM tau-GFP11 is incubated with either HEK293 lysate or 40 µl GFP1-10 lysate. Whilst all remaining comparisons to HEK293 lysate plus 2 µM tau-

GFP11 are not significant, there is a clear dose-dependent relationship both with respect to the availability of GFP1-10 protein and the amount of recombinant tau present. In the presence of 20 µl GFP1-10 lysate, when doubling the amount of tau from 1 to 2 µM there is a small increase in the fluorescent signal. Yet, when the lysate volume increased to 40 µl, still in the presence of 2 µM tau-GFP11, the signal increased approximately 30 %, suggesting that the availability of GFP1-10 was the limiting factor.

Importantly, from Figure 3.2 it has been confirmed, that neither recombinant tau-GFP11 (Fig 3.2A - *40 µl HEK 293 + 2 µM tau*) nor lysates containing GFP1-10 (Fig 3.2B) exhibit higher levels of auto-fluorescence when compared to HEK293 lysates. Furthermore, in Figure 3.2B I have shown that there is no change in the background fluorescence when increasing the volume of GFP1-10 lysate. As such, this test confirmed the functionality of recombinant tau-GFP11 *in vitro*.

3.2.3 Testing the functionality of secreted tau-GFP11

Having confirmed the activity of mammalian expressed tau-GFP11 and of recombinant tau-GFP11 to produce reliable fluorescent signal when mixed with the GFP1-10, I wanted to test the functionality of secreted tau. When compared to recombinant tau, tau-GFP11 produced by mammalian cells would be more physiologically relevant and include PTMs not present in tau expressed by bacteria. To do this I used the HEK293 cell line to express and secrete tau (as previously reported by, (Chai et al., 2012; Houck et al., 2016); the conditioned media would then be transferred to HEK293 cells expressing soluble GFP1-10. The aim of this experiment was to assess whether secreted tau was compatible

with the assay to test translocation of tau across cellular and endosomal membrane into the cytosol.

First, I wanted to ensure that prolonged expression of tau isoforms would not cause a dramatic increase in cell death. This was considered, since a disruption of the cell membrane integrity could suggest that tau is not being secreted but rather is set free in the extracellular media after cell death and so not representing the physiologically secreted species. Furthermore, if there are high levels of cytotoxic agents within the media as a result of cell death, this would in turn affect the health of recipient GFP1-10 cells. By utilising a well-established LDH assay (Roche), I determined that there was no heightened cell death following transfection with all six tau isoforms tagged with GFP11 compared with non-transfected cell culture media (Fig 3.3).

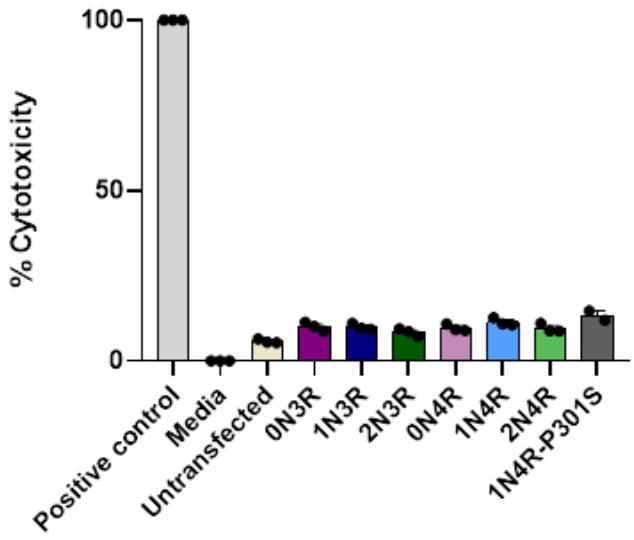

Figure 3.3 – Lactate dehydrogenase (LDH) assay for transfection of tau isoforms in HEK293 cells. Bar chart to represent the cytotoxicity generated 30 h post-transfection of all WT tau isoforms and 1N4R-P301S mutant. Percentage of cytotoxicity calculated as: *% Cytotoxicity = (experimental value – media background) / (positive control – media background) multiplied by 100*. High LDH samples, named positive control, were taken from non-transfected cells treated with lysis solution and assigned as 100 % cytotoxicity. (2-3, technical replicates, n = 1, biological replicate). Bar graph represent mean ± S.E.M.

Next I sought to determine the optimal time period for tau expression in HEK293 cells, to ensure there were sufficient tau levels in the conditioned media that would enable successful detection within the system. In this model, Lipofectamine 3000 is being used for transient expression of human tau-GFP11. To compare the kinetics of tau secretion, I collected media after one and two day/s of expression and incubated with GFP1-10 expressing cells.

Considering Figure 3.4 shows that the conditioned media collected after one day of expression generated a higher level of reconstituted GFP signal compared to that of two days, this was an intriguing result, since one would expect there to be greater levels of tau in the media when allowing the cells to secrete over a longer period of time and consequently higher number of GFP positive cells.

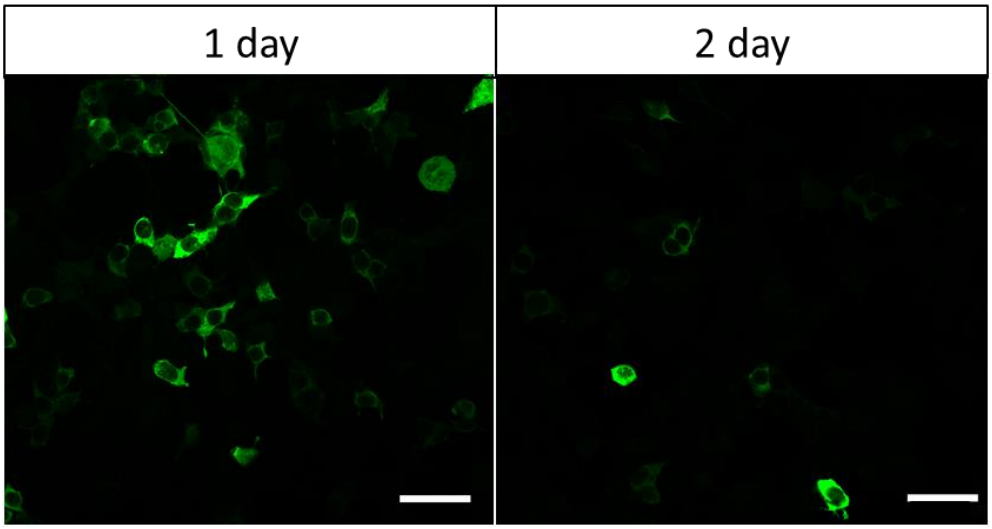

Figure 3.4 – Potential effect of Lipofectamine 3000 on cytosolic translocation assay. After transfecting HEK293 cells with tau-GFP11, conditioned media containing tau was collected and incubated with GFP1-10 expressing cells. Residual DNA-Lipofectamine 3000 complex present in the conditioned media may have caused co-expression of tau-GFP11 and GFP1-10. This was a time-dependent effect; collecting conditioned media 1 day after transfection led to high levels of co-expression, whereas after 2 days there were lower levels of co-expression. Scale bar, 50 μm. Experiment repeated with 2 biological replicates, achieving similar results.

I investigated potential reasons behind this finding; I hypothesized that there was residual DNA-Lipofectamine complex remaining in the media that had not been internalised by tau expressing cells, therefore upon incubation with GFP1-10 expressing cells, the DNA-Lipofectamine complex would be internalised leading to the co-expression of GFP11 and GFP1-10 fragments in the same cell, thus generating reconstituted GFP. This hypothesis also addresses why there were fewer GFP positive cells in recipient GFP1-10 expressing cells after allowing two days for tau secretion compared with one day. Over two days the residual DNA-Lipofectamine complex present in the conditioned media of tau secreting cells will either be internalised or degraded, consequently, when transferring the media there is less chance of co-expression of GFP11 and GFP1-10.

To test this hypothesis, I simply replaced the media containing the transfection mix six hours post-transfection with fresh culture media, in this way there is enough time for the DNA-Lipofectamine complex to be internalised, while avoiding any residual DNA-Lipofectamine complex contaminant. When using this methodology, conditioned media taken one day post tau transfection did not generate GFP positive cells, strongly suggesting that components from the transfection mix were causing this time-dependent effect. In order to provide an independent confirmation of this effect, tau-GFP11 could be co-transfected with an additional fluorescent protein e.g. mCherry, if mCherry positive cells were detected after the transfer of the conditioned medium, this would confirm the above discussed Lipofectamine-dependent mechanism, as mCherry should not be secreted nor endocytosed.

In addition, it became clear that the amount of secreted tau after only one day of expression did not surpass the threshold of detection by the assay (data not shown). Consequently, I allowed two days for tau expression in order to obtain a higher concentration of cell-secreted tau-GFP11. When conducting the cytosolic translocation assay and allowing two days for tau secretion, I detected positive GFP reconstitution (Fig 3.5); the following experiments presented in this thesis are conducted using this timeframe.

Importantly, I have shown that HEK293 cell-secreted tau-GFP11 is also capable of GFP reconstitution when incubated with mammalian expressed GFP1-10. At this stage both bacterially expressed and cell-secreted tau were tested, to determine which source of tau will be used for further experiments and establish the optimal protocol for the assay.

3.2.4 Visualising the reconstituted GFP signal from secreted tau-GFP11

Next, I wanted to compare different imaging techniques to determine the best method for detection of the reconstituted GFP signal. Figure 3.5 demonstrates the difference in sensitivity when the cells are imaged live either with a standard fluorescent microscope or the Incucyte®, or have been fixed and stained (Fig 3.5). Given I was interested in conducting time course experiments, I decided that live imaging in the Incucyte® would be the best option both for longitudinal imaging and the sensitivity of detection to avoid fixation artefacts.

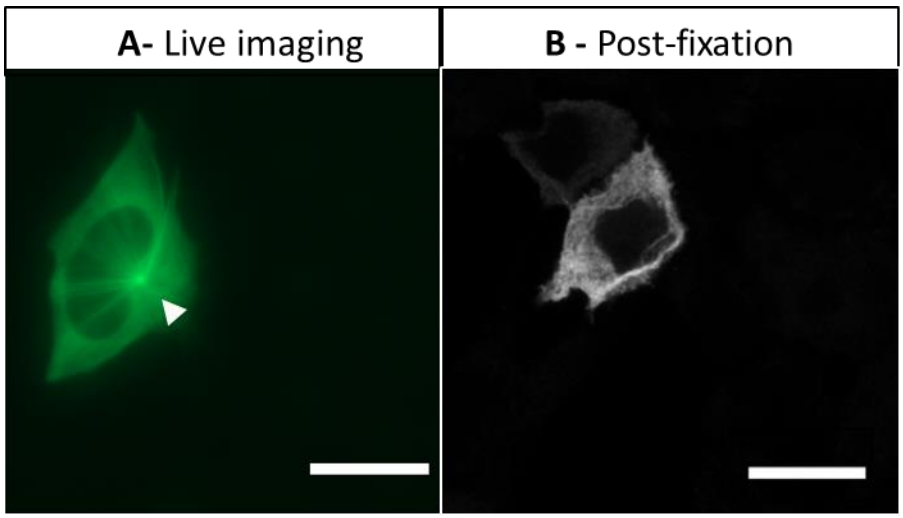

Figure 3.5 – Comparison of live and fixed cell imaging of reconstituted tau GFP signal. Cytosolic translocation of 1N4R-GFP11 into cytosol of GFP1-10 expressing cells. Two cells representative of two imaging conditions.

(A) Live imaging conducted on bench top fluorescent microscope with a green LED. White triangle pointing to predicted microtubule organising centre. Scale bar, 15 μm.

(B) Cells were fixed and immunocytochemistry conducted; confocal microscopy imaging used with the 488 nm laser to detect positive GFP cell. Scale bar, 15 μm.

Experiment repeated with 3 biological replicates, achieving similar results.

Interestingly, following cytosolic translocation of tau I repeatedly observed an intense GFP hotspot likely to represent the microtubule organising centre (MTOC) accompanied with astral microtubules, both bound by tau (Fig 3.5A). This was only observed with live imaging, suggesting that during fixation, the integrity of this structure was lost, thus validating the choice for live imaging when observing cytosolic translocation. To further investigate this observation, an anti γ-tubulin antibody could be used to probe for the MTOC and astral microtubules.

I also included an empty GFP11 control, to ensure that the secretion and/or cytosolic translocation results I had observed were due to the function of tau, rather than the GFP11 tag. As anticipated, there was no reconstituted GFP

signal, when incubating GFP1-10 expressing cells with conditioned media from cells expressing the empty GFP11 protein (data not shown).

To confirm the reconstituted GFP signal was specific to tau and not representing a general protein response, I introduced the HIV TAT-86 peptide sequence into a GFP11 containing mammalian expression vector. According to its reported role in modulating viral transcription, TAT-86 has been shown to have strong nuclear localisation (Hauber et al., 1987), moreover it has been shown that extracellular TAT is capable of being endocytosed (Yezid et al., 2009). Therefore, upon cellular entry, I expected the reconstituted GFP signal generated by TAT-86 to be localised in the nucleus. Since GFP1-10 is expressed in the cytosol, upon binding with TAT-GFP11, the reconstituted TAT-GFP chimera should be targeted to the cellular location of the untagged protein.

Briefly, TAT-GFP11 was expressed in HEK293 cells, six hours post-transfection fresh medium was added; conditioned medium was collected two day post-expression and transferred to GFP1-10 expressing HEK293 cells, to be monitored by live imaging. As shown in Figure 3.6, GFP reconstitution can be easily detected, in addition, this fluorescent signal is localised to the nucleus, and as expected for the TAT peptide, there is a brighter signal within sub-nuclear structures that are likely to be nucleoli (Fig 3.6).

From this control experiment, I concluded that the reconstituted GFP signal was representative of endogenous protein localisation, since TAT-GFP11 and tau-GFP11 display distinct cellular distribution patterns. As such, I ascertained that GFP1-10 expressing HEK293 cells could reliably detect tau-GFP11 cytosolic

translocation; furthermore the assay is able to detect tau fate and potentially tau mislocalisation under live imaging conditions.

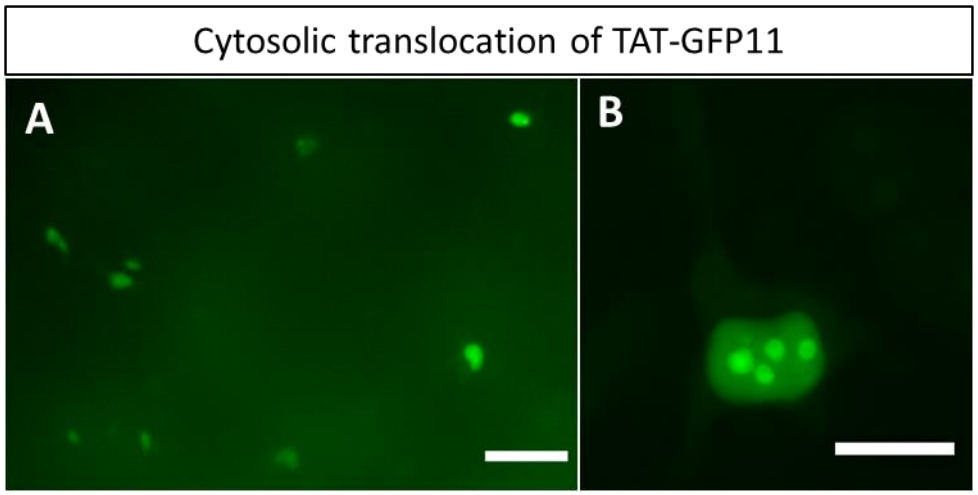

Figure 3.6 – Cytosolic translocation of cell-secreted TAT-GFP11.
Conditioned media containing TAT-GFP11 was incubated with HEK293 cells expressing GFP1-10 and monitored live on the Incucyte®.

(A) Representative image demonstrating positive GFP reconstitution of TAT-GFP11. Scale bar, 50 µm.
(B) Example of specific nuclear GFP signal following cytosolic translocation of TAT-GFP11. Scale bar, 25µm.

Experiment repeated with 2 biological replicates, achieving similar results.

3.2.5 Establishing the timescale for the cytosolic translocation assay

The methodology of the assay was established after a preliminary test to determine the timescale of the experiment; briefly, tau-GFP11 constructs are transfected in HEK293 cells, six hours post-transfection culture media is replaced with fresh media. Two days post-expression, conditioned media containing tau is collected and incubated with HEK293 cells expressing cytosolic GFP1-10, which is monitored every four hours by live imaging using the Incucyte® over 60 h (Fig 3.7A).

The kinetic of the process for cellular tau internalisation was determined by observing when the cell count of GFP-positive cells had plateaued. By conducting the experiment with cell-secreted 1N4R tau-GFP11, I detected the reconstituted GFP signal after approximately 10 h of incubation which peaked by 40 - 50 h (Fig 3.7B-C). As such, I decided to monitor the experiment over a 60 h period (Fig 3.7C). Important controls included were HEK293 cells expressing GFP1-10 alone and non-transfected cells incubated with 1N4R-GFP11; as predicted, neither condition yielded detectable GFP signal over the 60 h time period (Fig 3.7C).

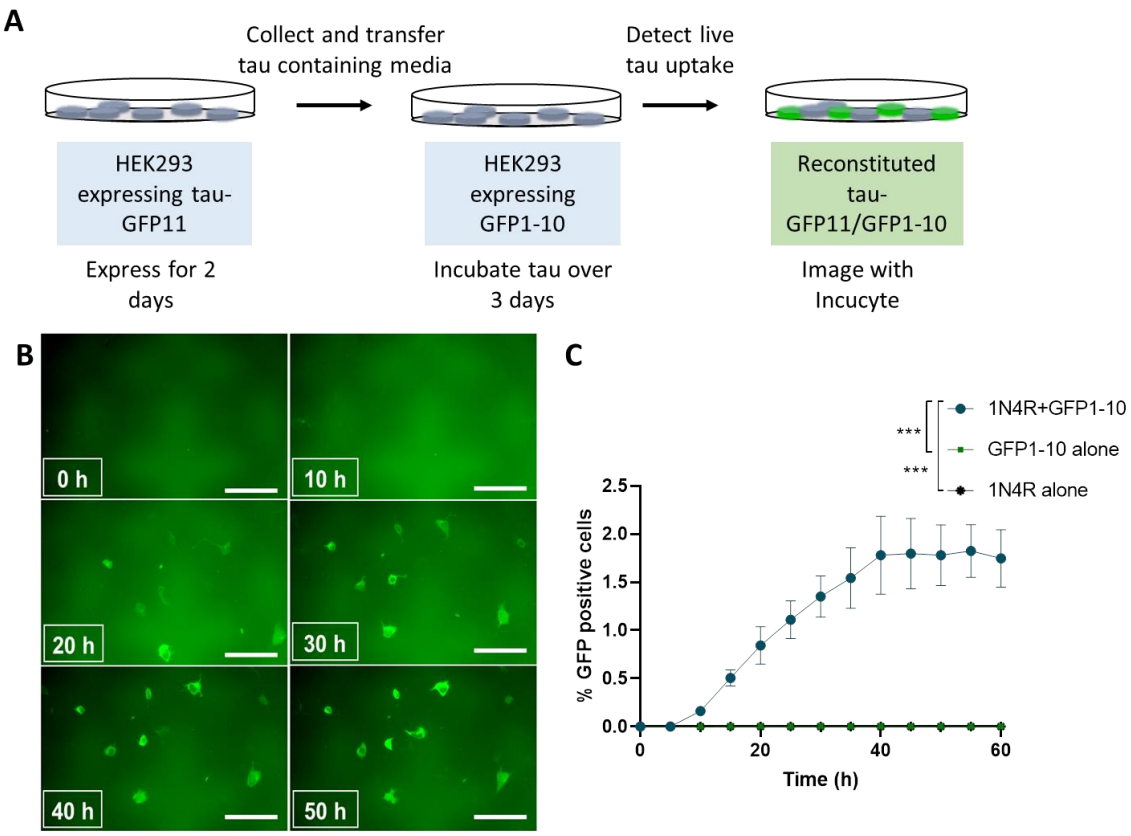

Figure 3.7 – Tau-GFP11 cytosolic translocation and GFP reconstitution.

(A) Schematic representation of the cytosolic translocation assay. HEK293 cells were transfected with either tau-GFP11 or GFP1-10 constructs. Conditioned media containing tau-GFP11 was transferred to GFP1-10 expressing cells for detection of reconstituted GFP.
(B) Live imaging of HEK293 cells expressing GFP1-10 incubated with 1N4R-GFP11 media, fluorescence monitored in the Incucyte®. Scale bar, 100 µm.
(C) Quantification of percentage of GFP positive cells over time (*** $p < 0.0001$, one-way ANOVA, followed by Dunnett's multiple comparison) ($n = 3$, biological replicates). Data points represent mean ± SEM.

An additional speculative experiment was conducted to evaluate whether there was a minimum time needed for tau-GFP11 to be incubated with GFP1-10 cells before the system reaches saturation and if the number of GFP positive cells are equivalent to those seen following 60 h tau-GFP11 incubation. I decided to test different incubation times for tau-GFP11 including 0.5, 1 and 24 h.

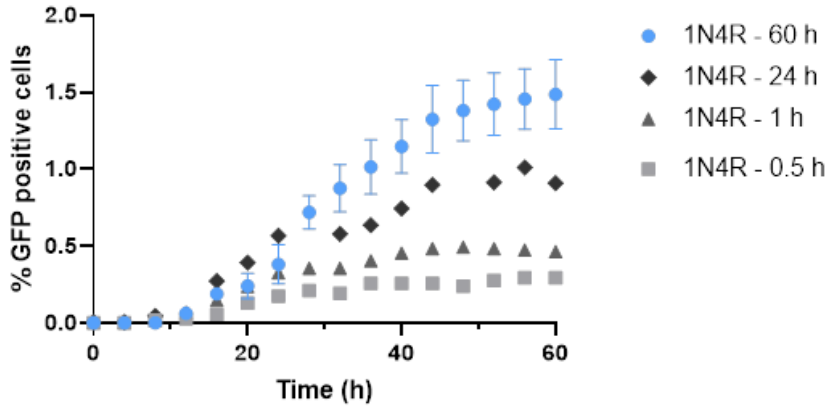

Figure 3.8 – Evaluating different tau-GFP11 incubation times for cytosolic translocation. Conditioned media containing 1N4R-GFP11 was transferred to GFP1-10 expressing cells and incubated for, 0.5, 1, 24 or 60 h. Upon tau-GFP11 incubation, conditioned cell media, free of tau, was replaced for monitoring of GFP signal in the Incucyte®. Quantification of the percentage of GFP positive cells over time between 60 h incubation (n = 3) versus 0.5, 1 and 24 h (n = 1, biological replicates). Data points represent mean ± SEM

This simple experiment demonstrated that with short incubation periods of 30 and 60 min, the percentage of GFP positive cells reached approximately 0.5 % compared with a mean of 1.5 % seen with 60 h incubation. Even after 24 h of incubation, it appears that the system is not yet saturated to the degree seen after 60 h. From these data, it would seem that there is a percentage of cells that translocate tau rapidly i.e. in the first 24 – 30 h, suggesting that the cells may need to be in a certain physiological state in order for tau to be effectively translocated into the cytosol. The shorter the incubation time of tau-GFP11, the less likely tau is to come into contact with GFP1-10 expressing cells that are in the right state for internalisation. However, this was an exploratory experiment, therefore additional biological replicates are required for a more conclusive interpretation.

At this stage it was important to consider the maturation time of the GFP signal in this system. From these data, there is an apparent delay of eight hours where there is no detectable GFP (Fig 3.7C and 3.8).

According to the literature full-length superfolded GFP, which was used to develop the split-GFP, has a maturation time of 13.6 min whereby 50 % of proteins have undergone chromophore maturation (Balleza et al., 2018). However, this phenomenon has been investigated with split fluorescent proteins and has shown that although the binding *in vitro* between the GFP11 and GFP1-10 can occur within minutes, the process of fluorophore formation occurs over five hours before stabilising, with the peak occurring by approximately three hours (Cabantous et al., 2005). In contrast, recent *in vitro* work determined that the maturation rate between full-length and split-GFP were roughly equal at, 0.018 and 0.016 min^{-1} respectively (measuring fluorescence intensity over time) (Köker et al., 2018). This would suggest that any disparity in the time for fluorescence detection could be due to the concentration of each GFP moiety. In a cell model, the absence of GFP signal could be due to tau-GFP11 being trapped within a membrane-bound compartment preventing the GFP11 tag from coming into contact with the GFP1-10 expressed in the cytosol.

When using the split-GFP system to investigate cellular entry of tau, the focus was not to identify kinetics but rather have a system which enables a visual detection of the point of entry in the cytoplasm and therefore investigate mechanistic pathways that may play a role in this process. Consequently, these results provide the proof of principle that the system is sensitive enough to detect the cellular entry of tau from an endosomal compartment and/or the

plasma membrane; with this knowledge we can use the assay to investigate the entry dynamics of all six tau isoforms.

3.2.6 Development of an ELISA to quantify amount of cell-secreted tau

Having conducted the initial experiment with one tau isoform, it was critical to develop a method to accurately detect the amount of tau present within the culture media samples when expressing different tau isoforms. Being able to measure the tau concentration and normalise across the isoforms will ensure that any isoform-dependent difference detected in cytosolic translocation is not due to varying tau levels in the media, but rather is an intrinsic feature of the isoform.

I developed a novel ELISA system for tau in partnership with Miss Chiara Panzi (Queen Square Institute of Neurology) from the Schiavo laboratory. This ELISA was specifically developed to measure the concentration of tau within the conditioned media samples. Given the C-terminal Flag-tag present on the human tau construct, we decided to use an α-Flag M2 (mouse, Sigma-Aldrich) as the capture antibody to improve signal specificity and avoid non-specific binding. The detection antibody selected was a polyclonal total tau antibody (Rabbit, DAKO), developed to target amino acids 243 – 441, and therefore able to detect all six isoforms of tau. This ELISA was a colorimetric-based assay and so the secondary antibody used was an α-rabbit conjugated to HRP (swine, DAKO). In the presence of the TMB substrate and HRP peroxidase, an enzymatic reaction is triggered which causes a colorimetric change. This reaction is then stopped prior to saturation with the addition of sulphuric acid

before being placed in a microplate reader. The absorbance values can then be used to measure and quantify the concentration of tau within a sample.

A standard curve was established with recombinant 1N4R tau-GFP11 protein produced from *E. Coli*. By using concentrations ranging from 0 – 250 ng/ml, I determined a robust relationship between absorbance and the concentration of recombinant tau (Fig 3.9A, B). By graphing these data, one could run a regression analysis through the experimental points, thus obtaining the best fit equation and from this calculate the amount of tau within the conditioned tau media samples. Figure 3.9B is displaying an example of the concentration values (ng/ml) obtained for each tau isoform.

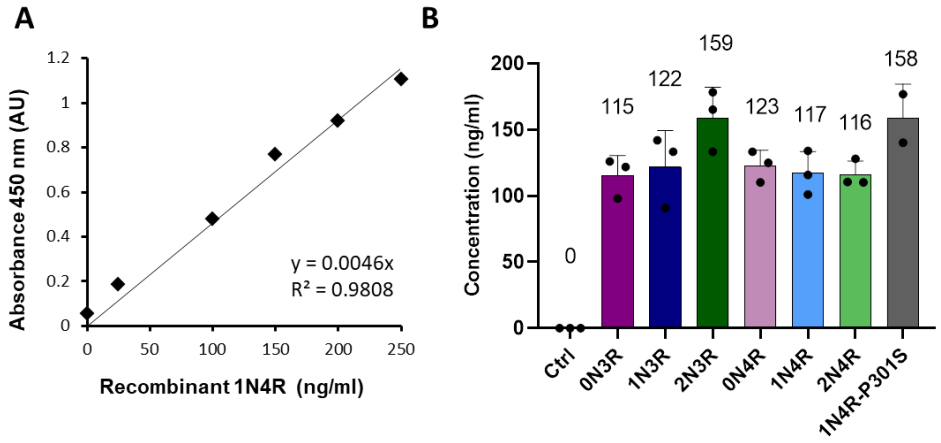

Figure 3.9 – Application of ELISA to determine tau concentration secreted from HEK293 cells. The α-Flag M2 (mouse, Sigma-Aldrich) antibody was used for capturing tau-GFP11 and total tau (Rabbit, DAKO) used as a detection antibody. Secondary α-Rabbit HRP (Swine, DAKO) antibody was used prior to addition of TMB substrate to enable absorbance to be measured at 450 nm.

(A) Scatter plot of data displaying absorbance values at 450 nm for each known concentration of recombinant 1N4R tau-GFP11. Values are displayed with the best fitting regression line, equation of line and the correlation coefficient R^2.

(B) An example of concentrations obtained for each tau isoform using the standard curve shown in B

Bar and data points represent mean ± SD. AU, Arbitrary units.

3.2.7 Evaluating recombinant and cell-secreted tau-GPF11 in cytosolic translocation assay

Using this newly developed ELISA, I was able to determine the concentration of tau-GFP11 present in the conditioned media that was producing reliable GFP reconstitution following cytosolic translocation. In Figure 3.9 an example is shown of the range of tau concentrations that is present in the conditioned media. Since this has been calculated from the known amount of recombinant tau, I wanted to test this equivalent amount of recombinant tau in the cellular assay, given that the functionality of recombinant tau-GFP11 had already been confirmed *in vitro*, albeit with higher concentrations (1- 2 µM, Fig 3.2A) to ascertain the ability to tau to be endocytosed and enter the cytosol.

A range from 50 – 200 ng/ml of recombinant 1N4R tau-GFP11 was applied to GFP1-10 expressing HEK293 cells (data not shown). The final concentrations achieved were 1, 2 and 4 nM of tau-GFP11. Following the same protocol as established for secreted tau, recombinant 1N4R-GFP11 was incubated with GFP1-10 expressing cells over a 60 h period and imaged with the Incucyte®. As seen from Figure 3.10, 200 ng/ml (4 nM) of recombinant tau-GFP11 did not lead to GFP reconstitution, as seen with ~ 200 ng/ml of cell-secreted tau (Fig 3.10). From this result it appears that the efficiency of uptake and/or cytosolic translocation of recombinant tau is different to that of mammalian tau.

In the majority of the published work, the concentration of recombinant tau ranges between 5 – 500 nM (Falcon et al., 2015; Frost et al., 2009; Morozova et al., 2019; Rauch et al., 2020). Therefore, in attempts to test the lower limit of sensitivity of the split-GFP system, I increased the amount of recombinant

1N4R tau-GFP11 100 – 200 fold, applying either 400 or 800 nM of recombinant 1N4R tau-GFP11 to GFP1-10 expressing cells. From this experiment, only three GFP positive cells were identified with a similar intensity and localisation of the signal seen with HEK293 cell secreted 1N4R; including the appearance of a tau-decorated MTOC (Fig 3.10).

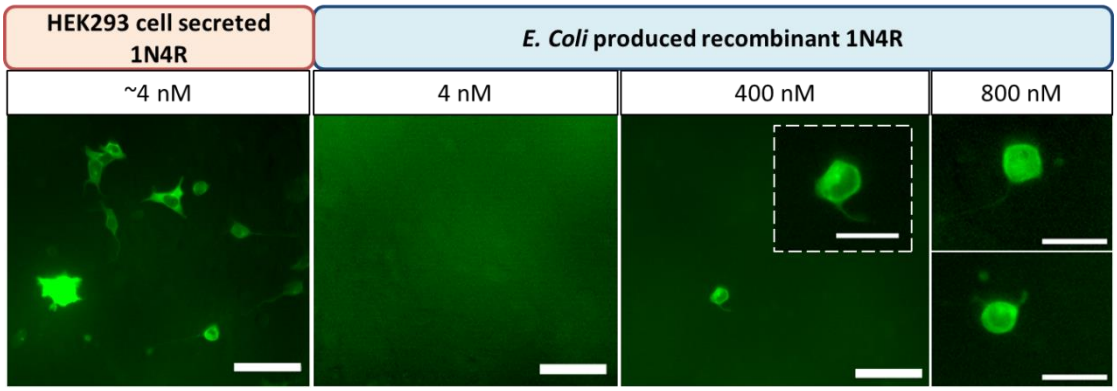

Figure 3.10 – Comparison of cytosolic entry between cell secreted and recombinant 1N4R tau. Representative images of GFP1-10 expressing cells incubated for 60 h with either; HEK293 cell secreted 1N4R tau-GFP11 (4 nM) (n = 3), or recombinant 1N4R tau-GFP11 (4 nM, 400 nM and 800 nM) (n = 2). HEK293 cell secreted 1N4R tau is more efficiently translocated into the cytosol compared to recombinant 1N4R tau. 4 nM of recombinant tau did not generate any GFP positive cells; only 1 and 2 GFP positive cells were identified for 400 nM and 800 nM tau respectively. Scale bar, 50 µm. Magnified inset scale bar, 25 µm.

Taking into consideration the efficiency of both recombinant and mammalian produced tau, and the physiological nature of secreted tau, it was decided that all further experiments conducted in cell lines would be done using HEK293 cell secreted tau-GFP11, using the protocol established in Fig 3.7A.

3.3 Discussion

The aim of this chapter was to set up and optimise an endocytosis and cytosolic translocation assay for tau based on the split-GFP complementation system. From these data, I have shown that this assay can effectively monitor protein translocation across the membrane and into the cytosol. Given the existing evidence regarding the endocytosis of tau and its translocation through the endolysosomal pathway before exiting into the cytosol (De La-Rocque et al., 2021) we have utilised a simple tool that provides a quantifiable ON/OFF system for detecting the moment of tau entry into the cytosol.

First I confirmed the activity of the GFP11 and GFP1-10 fragments with co-expression of both split-GFP domains; from the immunocytochemistry data, I also confirmed that the GFP11 tag did not induce aberrant mislocalisation or aggregation of tau, as this could influence the uptake behaviour of tau and compromise the physiological relevance of the results (Fig 3.1). This could also be tested by staining with Thioflavin S or using antibodies targeting aggregated species of tau (e.g. MC1 or PHF-1) to confirm there are no tau aggregates. Many studies have shown that different structural forms of tau can impact its internalisation mechanism; for the development and optimisation of the assay I decided to focus on the soluble form of tau.

As previously described, the research on the mechanisms of tau internalisation heavily relies on recombinant tau uptake (Chen et al., 2019; Falcon et al., 2018a; Frost et al., 2009; Rauch et al., 2020), this prompted me to test the functionality of recombinant monomeric tau-GFP11. I have shown that recombinant tau-GFP11 is capable of engaging in GFP complementation when

exposed to GFP1-10 in an *in vitro* set up (Fig 3.2). However when in cellular conditions, recombinant tau-GFP11 produced a very low level of effective GFP reconstitution with cytosolic GFP1-10 (Fig 3.9).

One reason may be that I have been applying WT recombinant tau, in the absence of any *in vitro* aggregation; as such it is likely to be monomeric tau (or LMW oligomeric forms). Monomeric tau has been reported to be the least effective at being internalised amongst the different tau species both in cell lines (Frost et al., 2009) and in primary neuronal cultures (Wu et al., 2013). As such, the low level of internalisation may be a result of tau conformation. However, other groups have reported significant levels of internalisation of monomeric recombinant tau (Evans et al., 2018; Michel et al., 2014), therefore this is unlikely to be the only reason for the lack of reconstituted GFP signal within HEK293 cells. In the live cellular system the maximum concentration of recombinant tau tested was 800 nM. However, when tested *in vitro* up to 2 µM of recombinant tau-GFP11 was used (Fig 3.2). Crucially, the *in vitro* and live cellular systems cannot be directly compared, given the difference in GFP1-10 availability in both systems. *In vitro,* the GFP1-10 protein had been released and concentrated into 100 µl total volume, whereas in living cells, GFP1-10 expressing cells were cultured with 400 µl of media upon incubation with recombinant tau-GFP11, moreover, the plasma membrane is fully intact effectively enclosing the GFP1-10 protein. These factors in combination are likely to reduce the chance of lower concentrations of recombinant tau-GFP11 generating reconstituted GFP signal.

When testing secreted tau-GFP11, I found that much lower concentrations, compared to recombinant tau, were effective at cytosolic translocation and provided a high level of GFP reconstitution (Fig 3.10). Having developed an ELISA-based approach capable of accurately measuring tau levels within the conditioned media, I was able to compare equivalent levels of cell-secreted and recombinant tau. This direct comparison demonstrated that the recombinant tau and the tau secreted from HEK293 cells did not have equivalent internalisation abilities.

A current limitation of this system is the lack of characterisation of the tau secreted from HEK293 cells. It is not known whether such tau has been secreted in free form, or within a membrane-bound vesicle. One way to overcome this would be to perform serial ultracentrifugation steps with the conditioned tau media and collect both supernatant and pellet. In this way, one could probe for tau and EV markers including Alix and TSG101, cytosolic proteins recovered in endolysosomes as part of the ESCRT pathway, and CD63, part of the tetraspanin family that is a transmembrane protein found on the surface of endosomes as well as the plasma membrane, (Kowal et al., 2016; Théry et al., 2018). This characterisation would allow the separation of free tau and EV-containing tau to test them independently for endocytosis and cytosolic translocation. A recent study has shown that tau contained within EVs was more efficient at spreading within the brain of WT mice, compared to free tau aggregates (Ruan et al., 2021). This could also provide a potential explanation for the differing efficiencies for cellular internalisation of free recombinant versus cell-secreted tau-GFP11. Furthermore, if there is tau contained within EVs this may be escaping the detection of the ELISA, since the

tau-GFP11 would be enclosed, therefore permeabilizing the sample prior to starting the ELISA may be one option for bypassing this problem.

Having selected cell-secreted tau-GFP11 as the basis for the assay, I also decided that longitudinal live imaging would be the most effective way to monitor cytosolic translocation. Furthermore, in the absence of fixation I would avoid any quenching of the GFP signal and any morphological artefact due to chemical fixation. With the Incucyte® I selected 60 h as the final time point for longitudinal imaging, as this was when the number of GFP positive cells had already plateaued (Fig 3.7).

As previously discussed, the kinetics relating to the time taken for the GFP signal to develop and the likely delay in chromophore maturation, limits its interpretation and therefore has not been used to determine any biological mechanism. The time lag from when tau is applied at time zero, to when fluorescent signal is first detected is a limitation in the system. A future set of experiments to address this would be to stain the cells for tau without cell permeabilisation at different time points. In this way one could examine whether there is still tau bound to the extracellular membrane, when GFP is first detected and whether the level of extracellular tau continues to decrease as the number of GFP positive cells increase.

Given how rapidly endocytosis occurs (second to minutes) and the knowledge that proteins can travel through the endolysosomal pathway over a one hour period (Huotari and Helenius, 2011), the time taken for GFP signal to be detected will incorporate both the time taken for tau to reach the cytosol, and

the GFP maturation time. In addition, it is likely that the GFP1-10 expressing cells also need to be in a particular “ON” state, whereby the cells are receptive for tau internalisation. From Figure 3.8 one can observe the difference in percentage of GFP positive cells according to the different incubation times of tau-GFP11. Despite endocytosis being a rapid process, it would seem that not all tau-GFP11 within the media is internalised within that short time period, otherwise one would expect the number of GFP positive cells to be equivalent of that seen after a 60 h incubation of tau-GFP11. It can be hypothesized that all the cells in culture are not in an equivalent state, therefore the longer tau is present, the more likely the cells will enter this “ON” state to enable successful internalisation.

It is reported that during a cell cycle, rates of endocytosis can differ (Santos and Boucrot, 2018). Regional cell-to-cell contact within a culture, leading to contact inhibition will also arrest the cell cycle, which in turn will differentially affect endocytosis rates of cells within a single experiment (Santos and Boucrot, 2018). Furthermore, if within a culture, cells are in slightly different phases of mitosis, this may in part determine whether cells are in the “ON” state for tau internalisation. This could potentially be tested by chemically halting all the cells in culture at different points within the cell cycle to assess if better synchronisation of the emergence of GFP-positive cells can be achieved.

An additional element can be the expression level of GFP1-10 which may not be equal amongst different cells in culture, therefore the concentration of tau required in each cell to surpass the threshold for GFP detection by the Incucyte® could differ. A possible way to bypass this would be in future

experiments to isolate GFP1-10 expressing cells and generate a stable cell line to avoid any possible artefact due to the use of Lipofectamine when expressing GFP1-10.

Nevertheless, the assay provides a visual readout for when and where tau has definitively entered the cytosol, since the GFP11 tag will not be in contact with the cytosolic GFP1-10 when enclosed by endocytic and endolysosomal vesicles. A surprising observation was the distinct signal localisation achieved with the reconstituted GFP upon tau entry, appearing to bind or co-localise with microtubules. This was confirmed to be specific for tau, since when testing the cytosolic entry of TAT-GFP11 the expected nuclear localisation was achieved (Fig 3.6).

In summary, I have established and optimised an assay that can reliably detect tau-GFP11 entry into the cytosol following endocytosis. This assay will now be used in order to compare cytosolic translocation activity of the six human tau isoforms and tested to address biological questions relating to the mechanisms involved in the cytosolic entry of tau.

Chapter 4: Investigating the process for cytosolic translocation of tau

4.1 Introduction

As demonstrated in chapter 3, I optimised the split-GFP system to reliably monitor the live cytosolic translocation of tau in living cells. With this system in place, I sought to compare the dynamics between all six WT tau isoforms and of the FTD-linked 1N4R-P301S mutant.

Thus far, few studies have reported the uptake dynamics of individual tau isoforms; recent work published by Rauch and colleagues identified LRP1 as a mediator of tau endocytosis and importantly this was confirmed for all six tau isoforms in the H4 cell line (Rauch et al. 2020). This study was conducted with fluorescently labelled recombinant tau, measuring uptake by flow cytometry, therefore there was no distinction of whether tau was present in intracellular vesicles, or within the cytosol. Furthermore, there was no comparison between isoforms to determine to what extent LRP1 mediated the endocytosis of each individual isoform.

Once any tau species is endocytosed it is important to understand the cytosolic entry of each individual isoform, and whether there are biological differences in this entry, considering that in many tauopathies, multiple tau isoforms are present in pathology, e.g. AD contains all 6 isoforms and Pick's disease contains all 3R tau. To my knowledge there has not been a comprehensive investigation of all six tau isoforms to compare their cytosolic entry.

As discussed in the introduction, the mechanisms of tau uptake are still actively being investigated. However, there is a consensus that tau is unlikely to directly cross the plasma membrane (Frost et al., 2009; Michel et al., 2014), but rather be internalised into endocytic vesicles via clathrin dependent (Calafate et al., 2016; Falcon et al., 2018a) or independent endocytosis (Holmes et al., 2013) and traffic through the endolysosomal pathway, before being released into the cytosol (Chen et al., 2019; Wu et al., 2013).

The endolysosomal pathway forms a network whereby cargoes travel through different intracellular membrane-bound organelles comprised of early endosomes, recycling endosomes, late endosomes and lysosomes (Russell et al., 2006; Scott et al., 2014). There are many biological functions for the endocytic pathway, including protein sorting and recycling, targeted degradation and signalling. From existing literature, it seems that tau should escape into the cytosol from the endolysosomes, however the mechanism is still unknown (Chen et al., 2019; Falcon et al., 2018a).

Due to the action of the V-ATPase an acidic environment characterises the lumen of these organelles, compared with the neutral pH of the cytosol. This ranges from pH 6.5 to 4.5 seen in the early endosome and lysosome respectively. In the lysosome, the acidic pH is required for the activity of hydrolases (Hu et al., 2015). As such, the role of pH has become an important factor to investigate when assessing the functionality of these organelles in relation to cargo trafficking. Changing of pH levels by inhibiting the V-ATPase has also been shown to alter cytosolic translocation of bacterial protein toxins e.g. diphtheria toxin (Umata et al., 1990). Interestingly, tau conformers have

been shown to be resistant to lysosomal enzymes (Novak et al., 1993; Polanco et al., 2021), so one could assume that when tau is in an acidic environment it would not be rapidly degraded, therefore if tau can escape the endolysosomal pathway into the cytosol, it will do so retaining its physiological activity.

Distinct molecular fingerprinting of the organelles within the endolysosomal pathway is still actively being investigated due to the nature of gradual maturation of early to late endosomes and finally to lysosomes, therefore drawing accurate conclusions of protein trafficking through the endolysosomal pathway is still difficult (Russell et al., 2006; Scott et al., 2014). A group of small GTPases known as Rabs (Ras-related in brain) are key regulators of the endocytic pathway; Rabs are soluble proteins that work by alternating between active or inactive conformations that are either GTP or GDP bound respectively (Stenmark and Olkkonen, 2001). In the presence of a GDP/GTP exchange factor (GEF) GDP bound to Rabs will be converted by nucleotide exchange to GTP; in contrast, when bound by GTP, a GTPase activating protein (GAP) will hydrolyse GTP by removing an inorganic phosphate (Stenmark and Olkkonen, 2001). This cycle enables active Rabs to interact with effector proteins and be reversibly targeted to intracellular membranes i.e. endocytic vesicles. Over time, specific Rab GTPases have been characterised and found to associate with different endosomal compartments, and so are used as endolysosomal markers (Hu et al., 2015). Tau has been shown to co-localise with different Rabs including Rab5 (Calafate et al., 2016; Falcon et al., 2018a; Puangmalai et al., 2020; Wu et al., 2013) and Rab7 (Chen et al., 2019; Falcon et al., 2018a) markers for early and late endosomes respectively. Expression of mutant Rab-GTPases is a common tool to study protein trafficking following endocytosis. By

halting the transition of cargo one can investigate the involvement of particular organelles of the endolysosomal pathway.

In this chapter I will apply the cytosolic translocation assay to investigate baseline differences between tau isoforms in their efficiency of internalisation. I will also explore potential biological mechanisms that mediate the cytosolic entry of tau, such as modulating the pH within the endocytic pathway and investigate loss of function mutations of different Rabs to decipher further biological mechanisms.

4.2 Results

4.2.1 Investigating cytosolic translocation of tau isoforms

4.2.1.1 Comparing cytosolic translocation of 1N4R and 1N4R-P301S mutant tau

First I wanted to assess the difference in activity between the WT 1N4R and the 1N4R-P301S tau mutant, which is causative for familial FTD (Bugiani et al., 1999). This mutation has been shown to increase the propensity for aggregation and influence microtubule dynamics (Strang et al., 2019). Therefore, the spread of this mutant is likely to accelerate the development of pathology; I wanted to investigate if this mutant tagged with GFP11 had an enhanced ability to be internalised, compared to the WT protein, as measured by GFP reconstitution with GFP1-10.

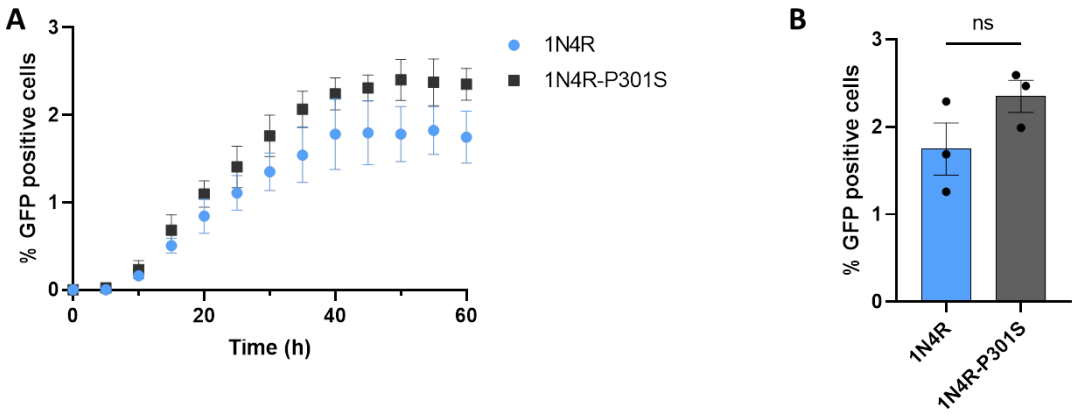

Figure 4.1 – Cytosolic translocation of 1N4R and 1N4R-P301S in HEK293 cells.

(A) Quantification of the percentage of reconstituted-GFP positive cells over time from both 1N4R and 1N4R-P301S tagged with GFP11 incubated with GFP1-10 expressing HEK293 cells.

(B) Quantification of the percentage of reconstituted-GFP positive cells taken from A, t= 60 h, of both 1N4R and 1N4R-P301S. No significant difference observed (p = 0.1748, unpaired Student's t-test with Welch's correction).

Bar and data points represent mean ± SEM. (n = 3 biological replicates).

By expressing either the 1N4R or the 1N4R-P301S human tau tagged with GFP11 I was able to collect the conditioned media and incubate it with HEK293 cells expressing GFP1-10 to be observed periodically by live imaging using the Incucyte® longitudinal microscope. In Figure 4.1A, the number of cells positive for reconstituted GFP signal first becomes visible approximately 10 h post tau incubation and reaches a plateau by 50 h for both 1N4R and 1N4R-P301S tau. As described, GFP reconstitution confirms the entry of tau into the cytosol following endocytosis. When quantifying the absolute number of GFP positive cells as a percentage of total cells there was no significant difference between the WT and mutant tau by 60 h (Fig 4.1B), only an apparent trend for enhanced uptake of 1N4R-P301S tau (Fig 4.1).

However, the data presented in Figure 4.1 has not been normalised to tau levels, and so the trend observed may be due to differences in tau levels in the media between WT and mutant tau, rather than a direct effect of the mutation. With the newly developed ELISA described in Chapter 3 (3.2.6), I could reliably measure tau levels in the conditioned media and therefore directly compare the levels of each isoform. By measuring the levels of 1N4R and 1N4R-P301S tau, the concentration of 1N4R tau was taken as baseline to calculate the relative amount of 1N4R-P301S tau, generating a concentration ratio (1N4R-P301S concentration value, divided by 1N4R value). After calculating the percentage of reconstituted GFP cells, this value was divided by the concentration ratio to normalise the cytosolic translocation to the differences in tau levels, termed *normalised internalisation.*

To confirm this normalisation was appropriate, I first checked whether the internalisation of tau-GFP11 was concentration dependent and the system was not already at saturation. This was important to ensure that this normalisation was not creating artefacts. In Figure 4.2 I have verified the linearity of the dose-effect relationship with two concentrations of 1N4R and 1N4R-P301S; with this result I was confident that the current normalisation strategy was appropriate for my assay.

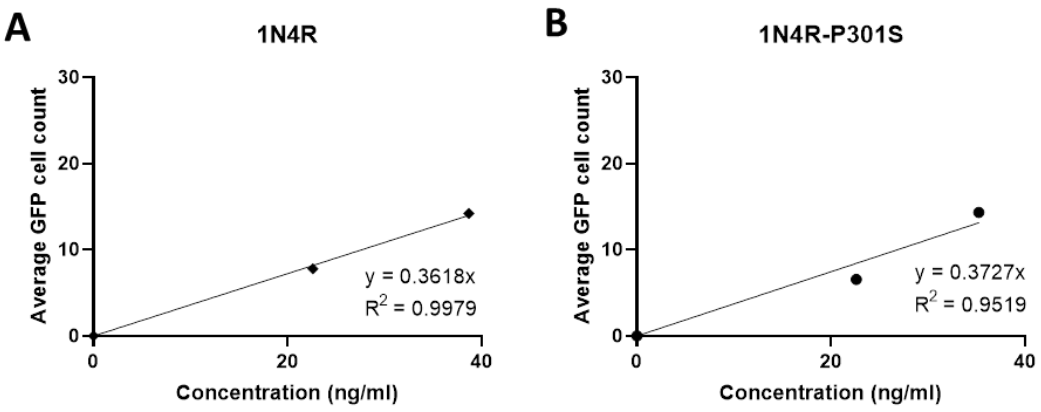

Figure 4.2 - 1N4R and1N4R-P301S undergo cytosolic translocation in a dose dependent manner. GFP1-10 expressing HEK293 cells were incubated with different concentrations of 1N4R or 1N4R-P301S tau and the number of GFP positive cells were counted.

(A, B) Scatter plot of average GFP positive cell count for 1N4R and 1N4R-P301S tau with best fitting regression line, equation of line and correlation coefficient R^2.

Data points represent mean (n = 1, biological replicates).

With the ELISA established and a dose-dependent effect for cytosolic translocation confirmed, I repeated the experiment comparing the normalised internalisation between 1N4R and 1N4R-P301S tau. In Figure 4.3, there is a divergence between the two isoforms, with WT 1N4R exhibiting an enhanced ability for cytosolic entry compared with the mutant. This is apparent after 24 h and remains constant throughout the duration of the experiment (Fig 4.3A-B). It appears that the P301S mutation confers a disadvantage for tau to enter the cytosol, either due to reduced levels of endocytosis, or via a cellular mechanism which prevents the exit of 1N4R-P301S tau from the endocytic / endolysosomal vesicles. However, reports have found tau levels in FTD and AD patients to be significantly higher compared to healthy controls (Green et al., 1999). Therefore, in the case of 1N4R-P301S, an FTD-linked mutation, while the cytosolic translocation activity may be less than of WT tau, if the extracellular

levels are higher, the overall amount of 1N4R-P301S entering the cell may be the same, or higher.

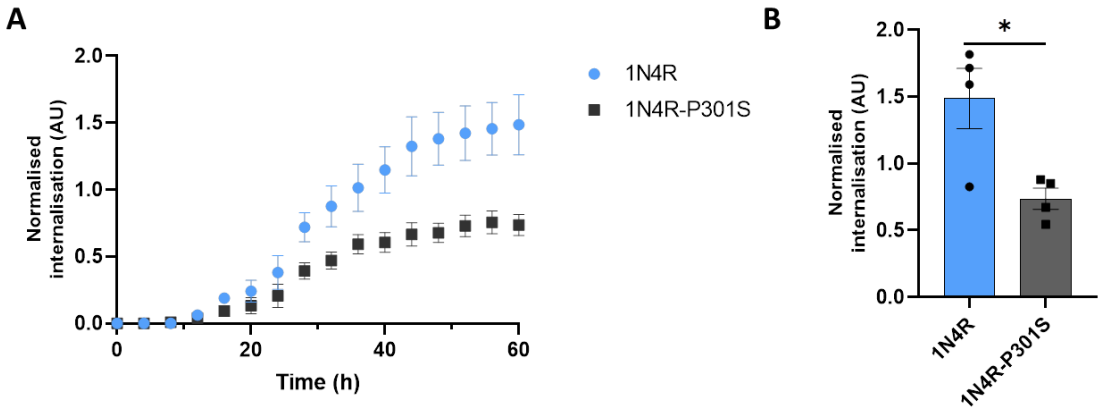

Figure 4.3 – 1N4R displays enhanced cytosolic translocation compared with 1N4R-P301S in GFP1-10 expressing HEK293 cells.

(A) Normalised internalisation calculated with percentage of GFP positive cells, normalised to 1N4R tau-GFP11 concentration in extracellular media between 1N4R vs 1N4R-P301S condition.

(B) Quantification of the values taken from A, t= 60 h, of both 1N4R (blue bar) and 1N4R-P301S (grey bar). A significant difference was observed ($p = 0.0383$, unpaired Student's t-test with Welch's correction).

Bar and data points represent mean ± SEM. (n = 4, biological replicates). AU, arbitrary units.

4.2.1.2 Comparing cytosolic translocation of all six tau isoforms

This assay was then used to compare the efficiency for cytosolic transfer between all six tau isoforms. In all experiments discussed in this section, the normalised internalisation has been quantified using 2N4R tau as the standard isoform to calculate the concentration ratio; this was decided since 2N4R tau is the largest size tau protein containing both projection domains at the N-terminal and all four domains of the MTBR, therefore it was chosen as the "baseline" isoform. Consequently, I first wanted to check the dose-dependent effect for the remaining tau isoforms that were not being used as baseline.

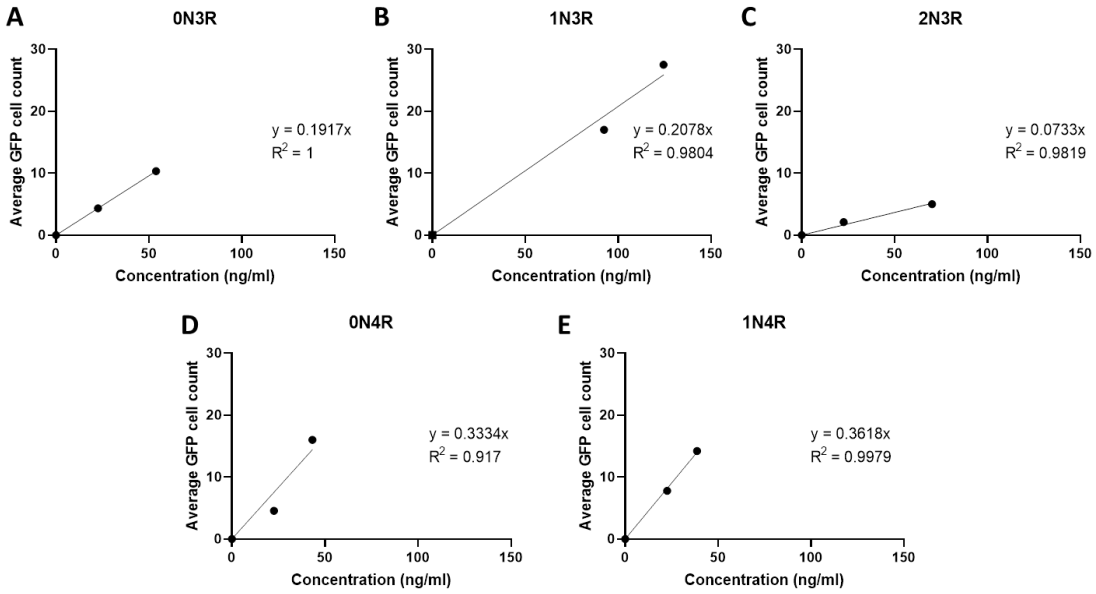

Figure 4.4 – Wild-type tau isoforms undergo cytosolic translocation in a dose-dependent manner. Graphs A-E are scatter plots of average GFP positive cell count for tau isoforms (labelled in figure) with best fitting regression line, equation of line and correlation coefficient R^2.
Data points represent mean (n = 1, biological replicates).

For all isoforms tested, there was a clear dose-dependent effect in the extent of cytosolic translocation of tau confirmed by the value of the correlation coefficient R^2 (Fig 4.4 A-E). Moreover, in this figure there are differences in the slope value of the best fitting regression line between isoforms, indicating a difference in the amount of tau needed to generate the same number of GFP-positive cells, suggesting that the isoforms have a different inherent ability for cytosolic entry; however, this observation comes from a single experiment. To enhance the reliability of these findings, additional biological replicates are needed; furthermore the baseline 2N4R tau isoform should also be included in the dose-dependent test. Importantly, dose-dependent tau uptake (Takeda et al., 2015) and cytosolic entry (Tuck et al., 2021) has been confirmed in the literature. As

such, for the purpose of my analysis the data obtained in this experiment, alongside those already published validated my normalisation method.

As stated above, 2N4R tau was used as the baseline isoform to calculate the concentration ratio for all isoforms. The MTBR is the most studied region of tau, given its involvement in both physiology and pathology. Therefore, first I wanted to assess whether a change of the MTBR would influence internalisation, whilst keeping the number of projection domains located at the N-terminus the same.

When comparing the 0N isoforms, there was a slight trend towards enhanced uptake for 0N4R compared to 0N3R, however this was not statistically significant (at t = 60 h, P = 0.1944) (Fig 4.5A). Yet when comparing 1N3R and 1N4R tau there was no significant difference between the isoforms (at t = 60 h, P = 0.8403) (Fig 4.5B). Interestingly, I observed a significant difference between 2N3R and 2N4R (at t = 60 h, P = 0.0268), with 2N4R exhibiting a greater ability for translocation to cytosol compared with 2N3R (Fig 4.5C).

Next I compared the isoforms according to the N-terminal projection domain. When grouping the data from 2N-, 1N- and 0N- tau isoforms, I observed an enhanced ability of 1N tau to be internalised compared with the remaining isoforms (Fig 4.5D). While there was only a significant difference between 0N- and 1N- tau, this is because the 2N3R and 2N4R tau values have high variability, therefore, the difference between 1N and 2N does not reach significance (albeit close, p = 0.0627). Despite this, it does appear that the 1N isoforms have an enhanced propensity for cytosolic translocation.

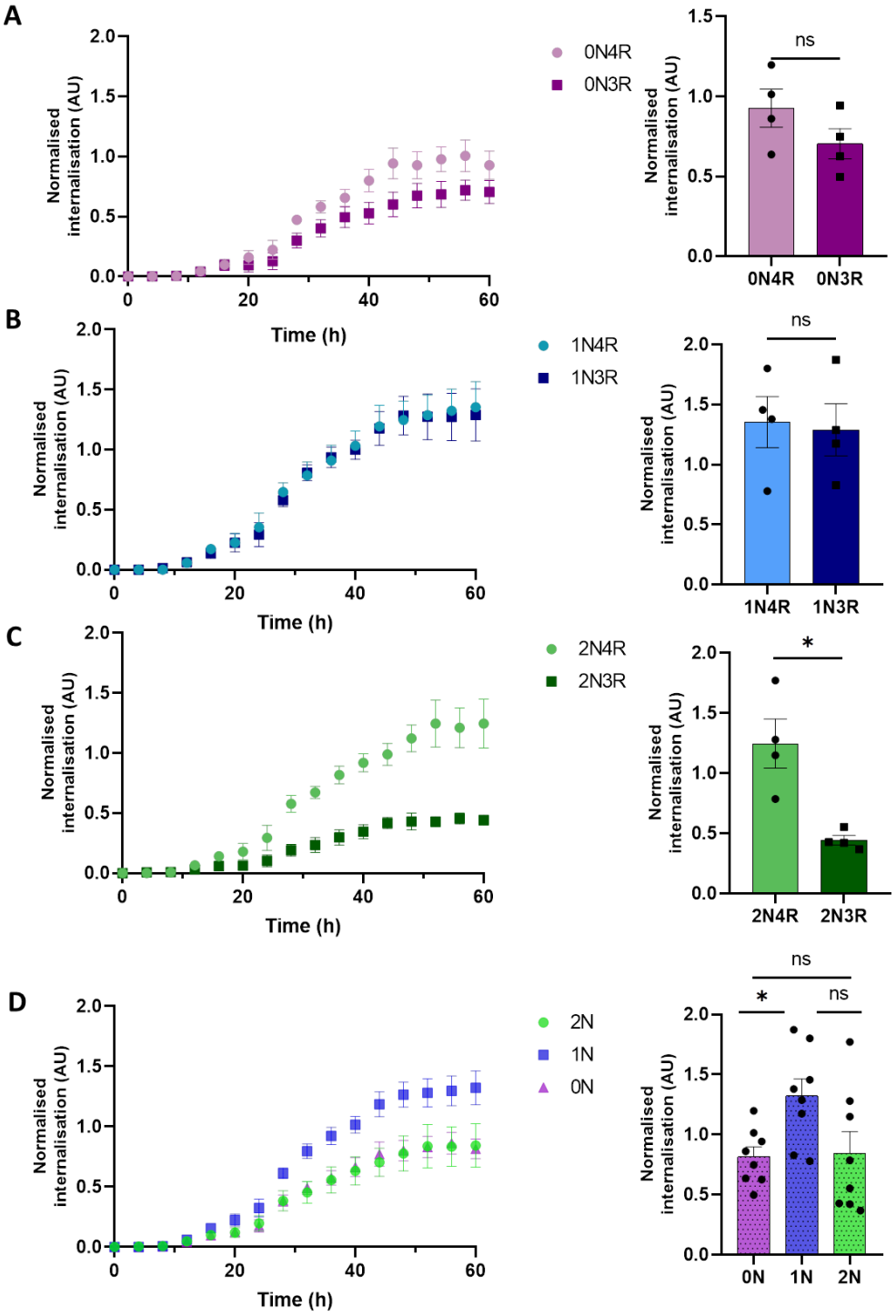

See figure legend on page below.

Figure 4.5 – Investigating the effect of MTBR and projection domain of tau on cytosolic translocation in GFP1-10 expressing HEK293 cells. Normalised internalisation calculated with percentage of GFP positive cells over time (hours). Tau-GFP11 concentration normalised to 2N4R tau isoform.

(A) Normalised internalisation quantified for 0N4R and 0N3R tau. Quantification of values taken from A t = 60 h, of both 0N4R and 0N3R. No significant difference was observed (p = 0.1944, unpaired Student's t-test with Welch's correction).

(B) Normalised internalisation quantified for 1N4R and 1N3R tau. Quantification of values taken from B t = 60 h, of both 1N4R and 1N3R. No significant difference was observed (p = 0.8403, unpaired Student's t-test, with Welch's correction).

(C) Normalised internalisation quantified for 2N4R and 2N3R tau. Quantification of values taken from C t = 60 h, of both 2N4R and 2N3R. A significant difference was observed (* p = 0.0268, unpaired Student's t-test, with Welch's correction).

(D) Normalised internalisation quantified for 2N-, 1N- and 0N- tau isoforms. Quantification of values taken from D t = 60 h of 2N-, 1N- and 0N- tau. A significant difference was observed between 1N and 0N (* p = 0.0466); a strong trend was identified between 2N and 1N groups albeit not significant (p = 0.0627); No significant difference was found between 0N and 2N (p = 0.9884) – A one-way ANOVA followed by Tukey's multiple comparisons test was conducted.

Bar and data points represent mean ± SEM. (n = 4, biological replicates). AU, arbitrary units.

Next, I wanted to look individually at the isoforms and the effect of 2N, 1N or 0N tau; for clarity the 3R and 4R isoforms have been separated in Figure 4.6A and B respectively. From Figure 4.6A it can be seen that in the absence of the R2 region (3R tau), the 0N- and 2N- isoforms have a reduced efficiency for internalisation compared with the 1N- isoform (Fig 4.6A). Whilst in the presence of the R2 region, the change of N-terminal domain number does not heavily influence internalisation activity; although we have detected a trend for reduced internalisation of 0N4R tau compared with 1N4R and 2N4R (Fig 4.6B).

An interesting observation emerged when comparing all six isoforms; 2N3R tau was found to have the lowest capability for cytosolic translocation of all the WT isoforms (Fig 4.6 C). As previously described there was a significant difference

between 2N3R and 2N4R, yet when comparing 1N3R and 2N4R, there was no significant difference (Fig 4.6C). This suggests that what is driving the different internalisation activities is not the protein sequence of either the 2N or the 3R region, but rather a difference in protein folding or a PTM unique to 2N3R tau. In addition, when looking solely at the 3R isoforms there is a clear reduction of internalisation of 0N3R compared 1N3R, albeit not significant (at t = 60 h, P = 0.161, one-way ANOVA, followed by Tukey's multiple comparison) (Fig 4.6C). If the sequence of the N-projection domain was driving the internalisation activity of the 1N3R over 0N3R one may expect that 2N3R tau would have the greatest ability to internalise within the 3R group. However, the data shows that 2N3R has a significantly weaker internalisation activity compared with 1N3R (p = 0.0177, one-way ANOVA, followed by Tukey's multiple comparison) and a consistent trend seen with 0N3R (not significant) (Fig 4.6C). Further evidence that this heterogeneity is not sequence-driven comes from the significant difference observed between 1N4R and 2N3R (at t = 60 h, p = 0.0099, one-way ANOVA, followed by Tukey's multiple comparison), but as already described there is no difference between 1N4R and 1N3R (at t = 60 h, p = 0.9997, one-way ANOVA, followed by Tukey's multiple comparison) or 1N4R and 2N4R (at t = 60 h, p = 0.9967 one-way ANOVA, followed by Tukey's multiple comparison (Fig 4.3.5c). So alone, the projection domain or the MTBR does not seem to influence the internalisation, but rather their combined presence which may lead to unique post-translational changes or differences in conformation that in turn can alter cytosolic entry dynamics. It appears that the 4th MTBR confers higher efficiency for the internalisation and cytosolic translocation of tau, with 1N3R being a special case.

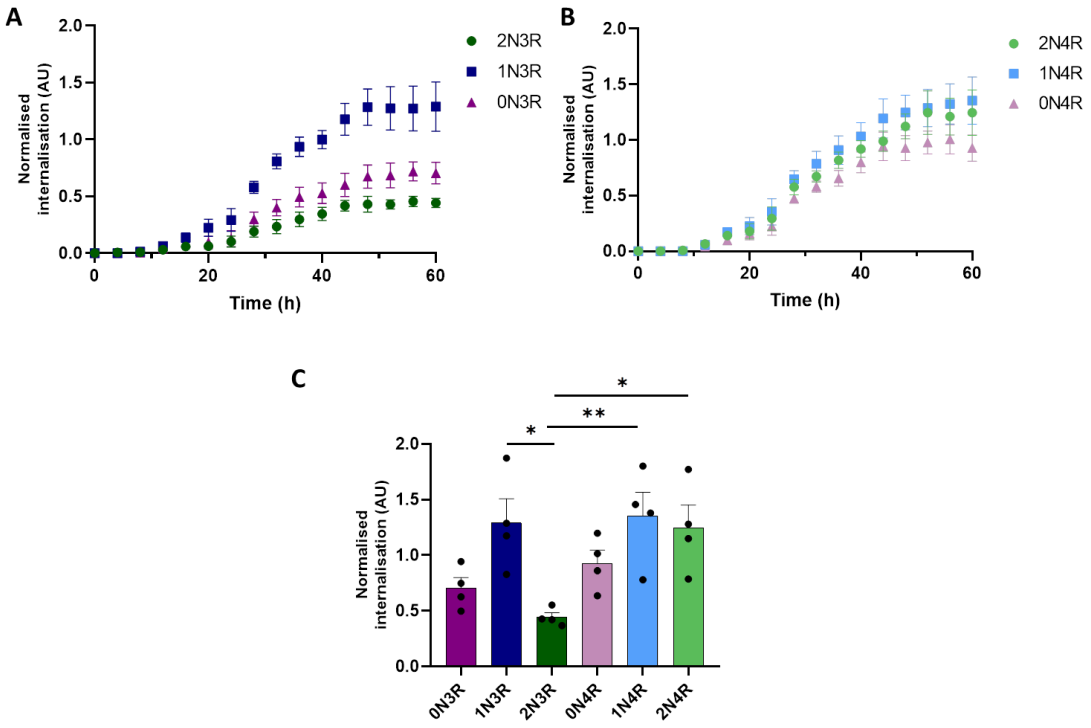

Figure 4.6 – Comparison of all six tau isoforms for cytosolic translocation. Normalised internalisation calculated with percentage GFP positive cells, with all tau-GFP11 levels normalised to concentration of 2N4R tau concentration.

(A) Normalised internalisation quantified over time of 3R isoform groups (0N3R, 1N3R and 2N3R).

(B) Normalised internalisation quantified over time of 4R isoform groups (0N4R, 1N4R and 2N4R).

(C) Quantification of values taken from A t= 60 h, of all tau isoforms. A significant difference was observed between 2N4R and 2N3R (* p = 0.0262); 1N4R and 2N3R (** p = 0.0099); 2N3R and 1N3R (* p = 0.0177) A one-way ANOVA, followed by Tukey's multiple comparison was conducted. All other comparisons were not significant p > 0.05.

Bar and data points represent mean ± SEM. (n = 4, biological replicates). AU, arbitrary units.

4.2.2 Investigating cytosolic tau accumulation in HEK293 cells

Having compared the number of GFP positive cells per isoform, I sought to measure the intensity of the reconstituted GFP signal as, it has been reported that the emitted BiFC signal follows a linear relationship with protein concentration (Itagaki 2000). Therefore, the signal intensity can be used as a proxy to measure the amount of tau present within the cytosol. I wanted to

investigate whether the signal intensity would change over time and whether there was an isoform-dependent effect.

For this analysis, I randomly selected GFP-positive cells to track signal intensity over a set time period. To ensure there were no inherent differences in the GFP signal between isoforms, including the 1N4R-P301S mutant, I measured the signal intensity when GFP cells were first detected on the Incucyte®, labelled time zero. The raw intensity values displayed in Figure 4.7 demonstrate no significant difference amongst all isoforms of tau ($p > 0.05$, one-way ANOVA, followed by Tukey's multiple comparison), suggesting that when the initial cytosolic entry of tau occurs there is an equivalent protein amount within the cytosol across all isoforms.

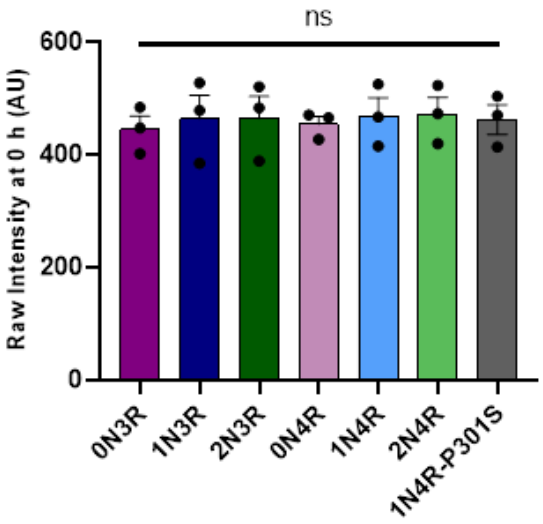

Figure 4.7 – Measuring reconstituted GFP signal intensity following cytosolic translocation of tau.
Cytosolic translocation assay conducted and cells monitored with the Incucyte®. When GFP-positive cells were first detected, their raw signal intensity was measured. No significant difference was identified between isoforms ($p > 0.05$, one-way ANOVA, followed by Tukey's multiple comparison was conducted).
Bar and data points represent mean ± SEM. (n = 3, biological replicates, total of 44 – 59 cells measured per isoform). AU, arbitrary units.

Having measured the initial GFP intensity, I wanted to assess whether the signal intensity would change over time. Unfortunately, monitoring the same cell over 60 h to capture the entire experiment timeline was difficult due to

technical issues. When using the Incucyte®, the position of imaging is not reliably fixed therefore, the same field of view is unlikely to be captured for every imaging session. Nevertheless, as described previously in this chapter, the number of GFP-positive cells starts to notably rise from 20 h before levelling off after 40 h. Having examined multiple data sets, I found that over 40 h I could reliably capture the same cell for quantification. Importantly, to ensure that the dynamics of tau translocation were comparable between cells, the time point when a GFP positive cell was first detected was set to time 0, in this way the GFP signal represented the same time point in the cytosolic translocation process, irrespective of when the process began.

For clarity in the data presentation and quantification, all cells included in the analysis were measured for a 20 h period from the initial detection. It is important to remember that image acquisition occurs every four hours, therefore time 0 does not represent an exact alignment in the cytosolic translocation process between cells, but rather an approximation that will be used in this analysis. Figure 4.8A displays a representative time lapse of newly detected GFP-positive cells that are being tracked over time, following tau-GFP11 translocation. By creating a region of interest around each cell, the GFP signal intensity was measured to gain insight on the process of tau translocation and whether there is a continuous cytosolic entry of tau over time or one entry event.

4.2.2.1 Comparing cytosolic tau accumulation between 1N4R vs 1N4R-P301S tau

I first wanted to focus on the changes of GFP signal intensity of 1N4R WT and 1N4R-P301S mutant. By normalising the intensity all GFP positive cells at time 0 h to one, it can be seen that there is no significant increase or decrease in the signal intensity from time 0 to 20 h, although there does seem to be a trend towards a small increase over time. With both 1N4R and 1N4R-P301S there are examples of individual cells that display > 2 fold increase of GFP intensity over time, suggesting that tau is continuing to enter the cytosol during this period. From these data, it appears that when tau undergoes cytosolic translocation, the P301S mutation does not confer any changes to the extent of tau accumulation within the cytosol. Overall, for both WT and mutant, it seems that the steady state concentration of reconstituted tau in the cytosol does not change over time.

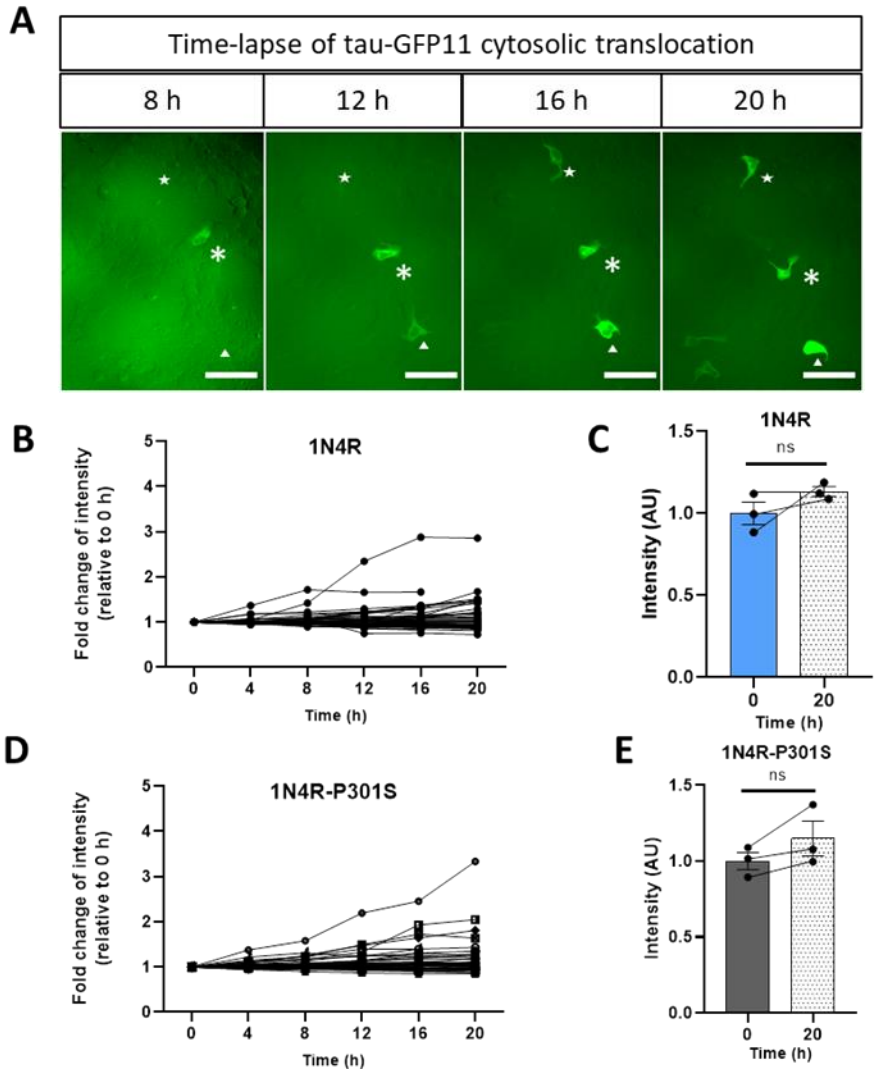

Figure 4.8 – Measuring reconstituted GFP signal intensity following cytosolic translocation of 1N4R and 1N4R-P301S tau over time.

(A) Representative image of longitudinal imaging of cytosolic translocation of tau-GFP11 in GFP1-10 expressing HEK293 cells generating GFP reconstitution from 8 to 20 h. Scale bar, 50 µm.

(B) Reconstituted GFP intensity measured over time for 1N4R tau. Data displays fold change of GFP signal intensity that has been set to 1 at time of initial detection (51 cells monitored).

(C) Reconstituted GFP signal intensity values measured at time 0 and 20 h for 1N4R tau. No significant difference was observed ($p = 0.2772$, paired Student's t-test).

(D) Reconstituted GFP intensity measured over time for 1N4R-P301S tau. Data displays fold change of GFP signal intensity that has been set to 1 at time of initial detection (50 cells monitored).

(E) Reconstituted GFP signal intensity values measured at time 0 and 20 h for 1N4R-P301S tau. No significant difference was observed ($p = 0.1609$, paired Student's t-test).

Average pixel intensity was measured for each cell positive for GFP signal. Scatter plot data points represent individual cell measurements. Bar graphs present reconstituted GFP intensity values measured at time 0 and 20h. Bar and data points represent mean ± SEM (n = 3, biological replicates). AU, arbitrary units.

4.2.2.2 Comparing cytosolic tau accumulation between all six tau isoforms

When analysing all six isoforms of WT tau, the predominant trend was that once tau had entered the cytosol, it reached an equilibrium whereby there is no overall change in the protein concentration over time.

In the 3R tau group, there was no significant difference over 20 h for 0N3R and 2N3R tau, yet interestingly, 1N3R tau gave rise to a significant increase in signal intensity from 0 to 20 h ($p = 0.0474$, paired Student's t-test). Given the small extent of significance one could argue that only a small sub-population of cells gives rise to this trend, and that this population is more evident for 1N3R tau. While there were two cells in the 0N3R group that had increasing GFP intensity over time, the remaining cells analysed did not follow this trend. In the 4R tau group, there was no significant change over 20 h; as described above, 1N4R tau displayed an apparent trend for a small increase in intensity albeit not significant ($p = 0.2772$, paired Student's t-test).

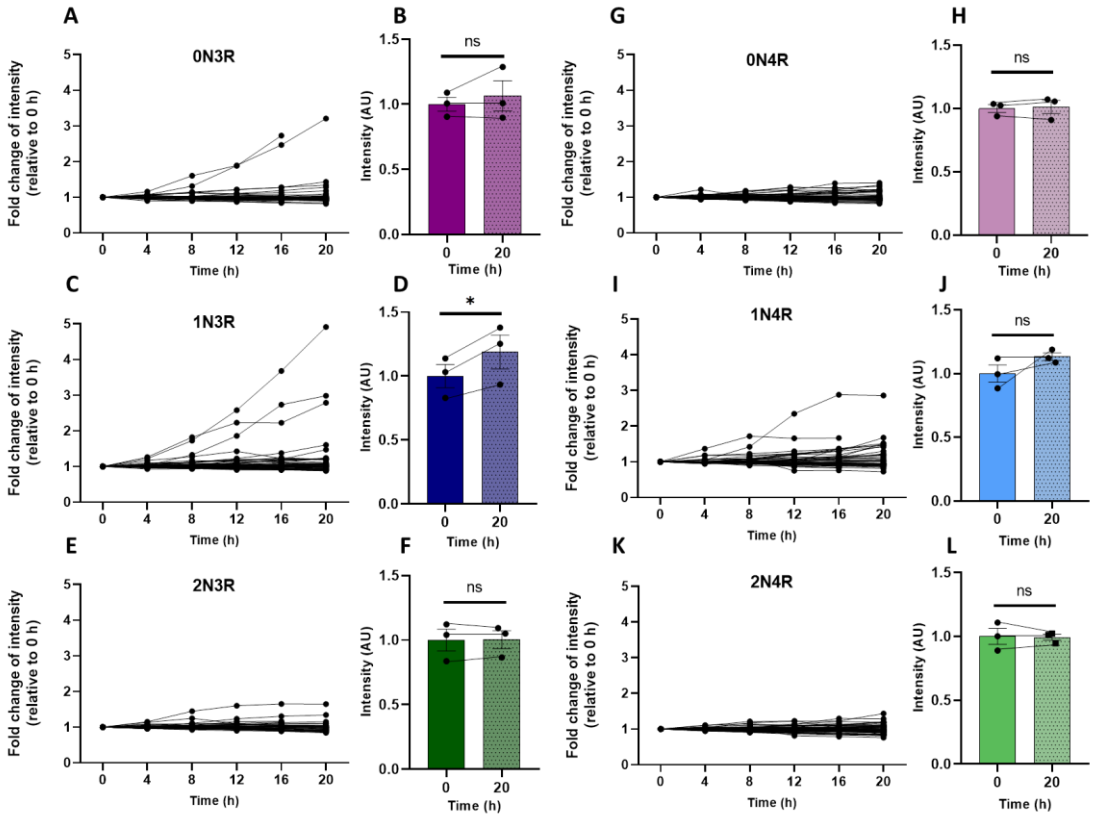

Figure 4.9 – Measuring reconstituted GFP signal intensity following cytosolic translocation of 6 tau isoforms over time.

Average pixel intensity was measured for each cell positive for GFP signal. Scatter plots display fold change of reconstituted GFP signal intensity from initial detection over 20 h. Data points represent individual cell measurements. Bar graphs present reconstituted GFP intensity values measured at time 0 and 20h.

(A) Fold change of signal intensity for 0N3R tau. (52 cells monitored).
(B) Signal intensity measured at time 0 and 20 h for 0N3R tau. No significant difference was observed (p = 0.4378).
(C) Fold change of signal intensity for 1N3R tau. (54 cells monitored).
(D) Signal intensity measured at time 0 and 20 h for 1N3R tau. A significant difference was observed (p = 0.0474).
(E) Fold change of signal intensity for 2N3R tau. (44 cells monitored).
(F) Signal intensity measured at time 0 and 20 h for 2N3R tau. No significant difference was observed (p = 0.8695).
(G) Fold change of signal intensity for 0N4R tau. (55 cells monitored).
(H) Signal intensity measured at time 0 and 20 h for 0N4R tau. No significant difference was observed (p = 0.6261).
(I) Fold change of signal intensity for 1N4R tau. (51 cells monitored).
(J) Signal intensity measured at time 0 and 20 h for 1N4R tau. No significant difference was observed (p = 0.2772).
(K) Fold change of signal intensity for 2N4R tau. (59 cells monitored).
(L) Signal intensity measured at time 0 and 20 h for 2N4R tau. No significant difference was observed (p = 0.9030).

Bar and data points represent mean ± SEM (n = 3, biological replicates). Paired Student's t-test was used for all statistics. AU, arbitrary units.

Having measured and quantified the intensity over time for each individual isoform, I wanted to check if there were any isoform-dependent differences in the degree of change over time. Thus, I calculated a ratio from the data in Figure 4.9: average intensity value at 20 h divided by value at 0 h. When comparing the extent of change of signal intensity between 1N4R and 1N4R-P301S, there was no significant difference (Fig 4.10A).

Similarly, when examining the intensity change for all six tau isoforms, there was no significant difference ($p > 0.05$, one-way ANOVA, followed by Tukey's multiple comparison); one could speculate that both 1N3R and 1N4R have a greater overall increase in signal intensity over time, however given the small effect size, an increased number of biological replicates are needed to establish whether there is a genuine pattern in these data. Furthermore, a larger data set would rule out whether these events are just random occurrences that have been captured within these analyses due to the small numbers.

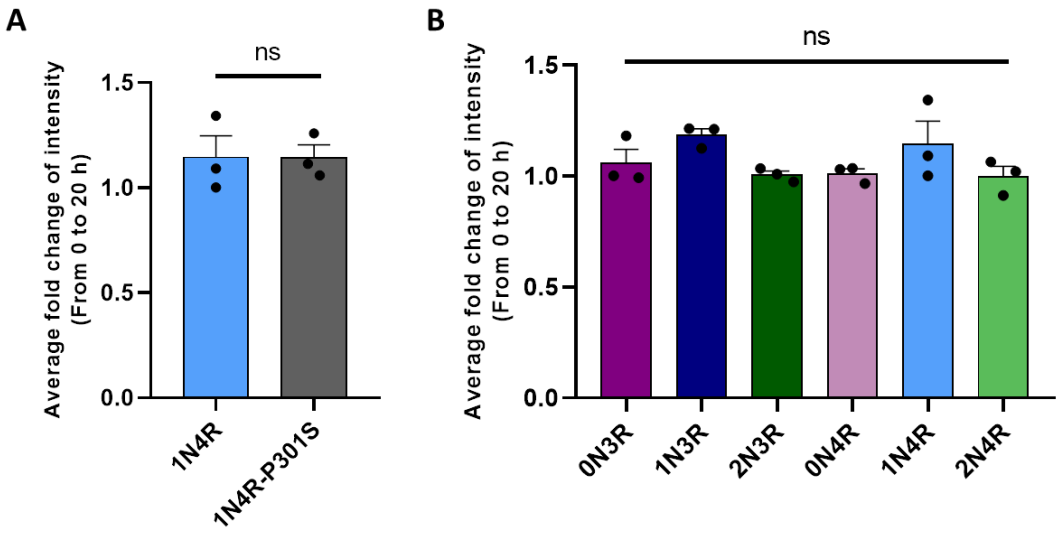

Figure 4.10 – Analysing fold change of reconstituted GFP signal intensity over time of tau. The average intensity value at 20 h was divided by the average intensity value at 0 h for each biological replicate (Intensity values presented in Figure 4.9)

(A) Comparing average fold change of reconstituted GFP signal intensity from 0 to 20 h between 1N4R and 1N4R-P301S tau. No significant different was observed ($p = 0.9938$, unpaired Student's t-test, with Welch's correction).

(B) Comparing average fold change of reconstituted GFP signal intensity from 0 to 20 h between all six isoforms of tau. No significant difference was observed (A one-way ANOVA followed by Tukey's multiple comparisons test was conducted).

Bar and data points represent mean ± SEM (n = 3, biological replicates).

From these data it would seem that initial cytosolic entry of tau occurs primarily at a single time point (within a 4 h period), and then over time either tau levels stabilise with little protein degradation, or an equilibrium is established by a balance between continuous tau entry and tau protein turnover. Alternatively, the GFP1-10 sensor fragment could be saturated therefore cannot detect further tau-GFP11 entry. As previously highlighted, these images were acquired every four hours and so there could be an initial phase of gradual tau entry that is not being captured in these imaging events. Nevertheless, I have been able

to examine the long-term accumulation of tau following cytosolic translocation using the reconstituted GFP signal.

4.2.3 Investigating biological mechanisms mediating cytosolic entry of tau

Thus far, I have confirmed that the split-GFP assay can reliably detect differences in the extent of cytosolic transfer between tau isoforms. Given the evidence within the literature of co-localisation between tau and membrane compartments from the endolysosomal pathway (Ait-Bouziad et al., 2017; Calafate et al., 2016; Chen et al., 2019; Falcon et al., 2018a; Puangmalai et al., 2020; Wu et al., 2013), I wanted to investigate whether manipulation of this endocytic process could be detected in this newly developed assay and moreover, influence the cytosolic translocation of tau.

4.2.3.1 Evaluating the role of pH in cytosolic translocation of tau

To address whether overall functioning of the endolysosomal pathway would directly impact cytosolic transfer of tau I wanted to explore the effect of altering the pH of endosomal and lysosomal compartments. Two agents were chosen, Bafilomycin A1 (BafA1) (Wang et al., 2021) and Concanamycin A (ConA), both specific and very potent inhibitors of the V-ATPase (Dröse and Altendorf, 1997). Both BafA1 and ConA act in the nanomolar range with reported K_i 0.44 and 0.02 nM respectively. One of the physiological roles of the V-ATPase is to maintain the acidic pH of intracellular organelles, by actively pumping protons from the cytosol into the vesicular lumen (Dröse and Altendorf, 1997). By blocking this process, there is an increase of the pH within the vesicles, which alters their physiological function. As such, these V-ATPase inhibitors are typically used to block the activity of lysosomes and late endosomal compartments. To confirm

the activity of both compounds, I used LysoTracker® Red DND-99 (Invitrogen) that can be used to track acidic organelles under live conditions. This probe is made up of a red fluorophore linked to a weak base, when it is present within a neutral environment the base is only partially protonated, thus it will selectively accumulate in acidic environments, enabling detection of lysosomes.

HEK293 cells were first treated with either BafA1 or ConA for five minutes at 5 nM or 10 nM respectively. Cells were washed and 50 nM of LysoTracker® Red DND-99 was applied with a low level of BafA1 or ConA both at 0.5 nM for 30 min. This chronic treatment will give rise to 50 % and > 95 % of V-ATPase inhibition for BafA1 (K_i 0.44 nM) and ConA (K_i 0.02 nM) respectively. As shown in Figure 4.11A, there is a clear reduction in the intensity of the LysoTracker® fluorescence with both BafA1 and ConA, indicating that this short incubation period was enough to alter the intraluminal pH of acidic organelles using both inhibitors. By quantifying the LysoTracker® intensity, it could be seen that both BafA1 and ConA prevented the accumulation of the Lysotracker® probe in the acidic lumen, with ConA evoking the strongest effect compared to DMSO control (Fig 4.11B). Consequently, both compounds were tested in following experiments.

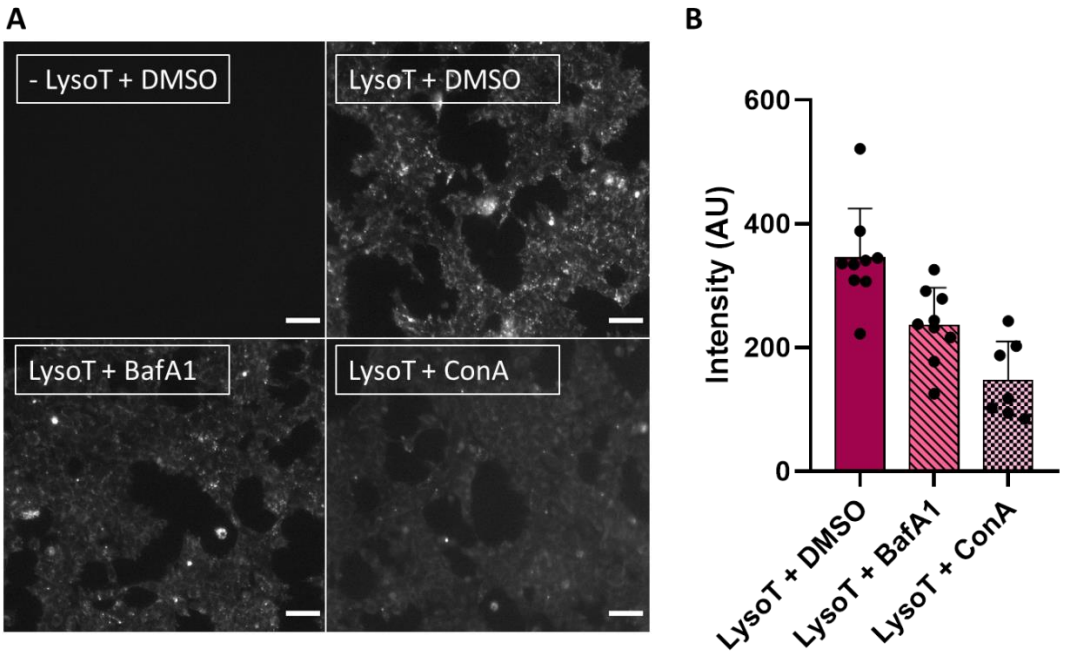

Figure 4.11 – Effect of Bafilmoycin A1 (BafA1) and Concanamycin (ConA) on LysoTracker® Red DND-99 (LysoT) in HEK293 cells.

(A) Live imaging of HEK293 cells:
-LysoT + DMSO; 5 min treatment with DMSO with no LysoT
LysoT + DMSO; 5 min treatment with DMSO followed by 30 min treatment with LysoT with DMSO
LysoT + BafA1; 5 min treatment with 5 nM BafA1, followed by 30 min with LysoT with 0.5 nM BafA1
LysoT + ConA; 5 mins treatment with 10 nM ConA, followed by 30 min with LysoT with 0.5 nM ConA. Scale bar, 100 µm.

(B) Quantification of signal intensity of LysoT treated conditions. Background signal from untreated condition (-LysoT + DMSO) was subtracted from all experimental conditions.

Bar graph represent mean ± standard deviation (n = 1, biological replicate). AU, arbitrary units.

To identify the best time-point during the cytosolic translocation assay to treat with either BafA1 or ConA, I first conducted a time course experiment with 1N4R tau. As described in the previous chapter; 1N4R tau was expressed in HEK293 cells for two days and the cell supernatant incubated with GFP1-10 expressing cells at time 0. After different time periods (5, 15, 30, 60, 120 and 240 min) cells were treated with 5 nM BafA1 or 10 nM ConA for five minutes in tau free media. After the five minute treatment, cells were exposed to the

original tau media in the presence of 0.5 nM BafA1 or 0.5 nM ConA to maintain chronic V-ATPase inhibition throughout the duration of the experiment. I also included a pre-treatment condition whereby the GFP1-10 expressing cells were treated for five minutes with either 5 nM BafA1 or 10 nM ConA, prior to the addition of tau-media containing either 0.5 nM BafA1 or 0.5 nM ConA, noted as time 0, before the final image acquisition at time 60 h (Fig 4.12A).

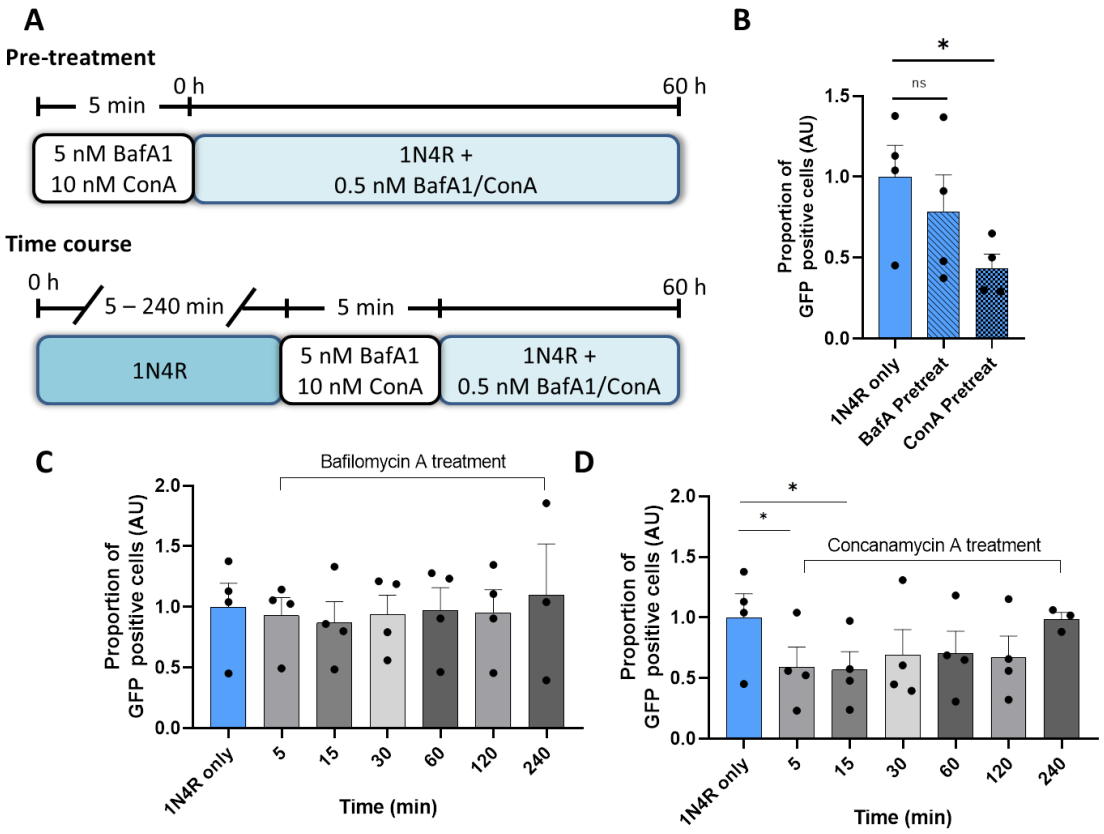

Figure 4.12 – Effect of Bafilomycin A1 and Concanamycin A on efficiency of cytosolic translocation of 1N4R tau. All measurements of the proportion of GFP positive cells were taken after 60 h of tau incubation with GFP1-10 expressing HEK293 cells.

(A) Schematic of experimental set up for pre-treatment or time course experiment with either BafA1 or ConA.

(B) Quantification of proportion of GFP-positive cells, after pre-treatment with either 5 nM BafA1 or 10 nM ConA normalised to 1N4R only. No significant difference was observed between 1N4R only and BafA1 pre-treatment ($p = 0.467$); a significant difference was observed between 1N4R only and ConA pre-treatment (* $p = 0.045$), A one-way ANOVA followed by Dunnett's multiples comparison was conducted.

(C) Time course of 5 nM BafA1 treatment; proportion of GFP positive cells normalised to control 1N4R only condition No significant differences were observed between 1N4R only and treated conditions ($p > 0.05$). A one- way ANOVA followed by Dunnett's multiples comparison was conducted.

(D) Time course of 10 nM ConA treatment; proportion of GFP positive cells normalised to control 1N4R only condition. A significant difference was observed between 1N4R only and ConA treatment at 5 and 15 minutes, * $p = 0.0412$ and * $p = 0.0485$, respectively. All other comparisons between 1N4R only and treated conditions were not significant $p > 0.05$, A one- way ANOVA followed by Dunnett's multiples comparison was conducted.

Bar graphs represent mean ± SEM. (n = 4, biological replicates). AU, arbitrary units.

When comparing the proportion of GFP positive cells in the 1N4R only condition versus pre-treatment with BafA1 there was no significant reduction (Fig 4.12B). In contrast, ConA pre-treatment elicited a significant reduction in the proportion of GFP-positive cells (Fig 4.12B). Similarly, when examining the effect of BafA1 during the time course, there was no significant reduction compared with the 1N4R only control at any time point tested (5 – 240 min) (Fig 4.12C). While ConA treatment, after five or 15 min of tau incubation, led to a significant decrease in proportion of GFP positive cells (Fig 4.12D). After 30, 60 and 120 min there was still reduced level of GFP positive cells, albeit not significant, but by 240 min the levels were comparable with 1N4R only control (Fig 4.12D).

When selecting the agent and experimental condition to test the remaining isoforms, including 1N4R-P301S mutant I selected ConA for a 5 min pre-treatment (10 nM) followed by chronic ConA 0.5 nM treatment with tau, as this had the strongest overall effect. I first wanted to investigate whether ConA treatment was having an effect on endocytosis, before investigating its role in cytosolic translocation for the remaining tau isoforms. To date, there are several theories regarding the internalisation pathway for the different conformers of tau (De La-Rocque et al. 2021). As such I wanted to first examine the effect of raising the endolysosomal pH on CME and bulk/fluid phase endocytosis, with transferrin and dextran respectively.

First, I pre-treated HEK293 cells for five minutes with 10 nM ConA and then incubated with either 50 µg/ml transferrin-Alexa-fluor 488 or 100 µg/ml dextran-Alexa-fluor 647 with 0.5 nM ConA. Three hours post-incubation, cells were fixed and imaged by fluorescent microscopy. With transferrin, there was no significant change in the intensity of the fluorescent signal following the pre-treatment with

ConA (Fig 4.13B). Yet for dextran, while there is an observable change in the dextran florescence following ConA treatment, there was no significant reduction for the signal intensity (p = 0.287, unpaired student's t-test) and this was likely due to high variability in the control condition (Fig 4.13C). As can be seen in the representative images, there is a reduction in the overall intensity of the dextran signal, which is not seen with transferrin (Fig 4.13A).

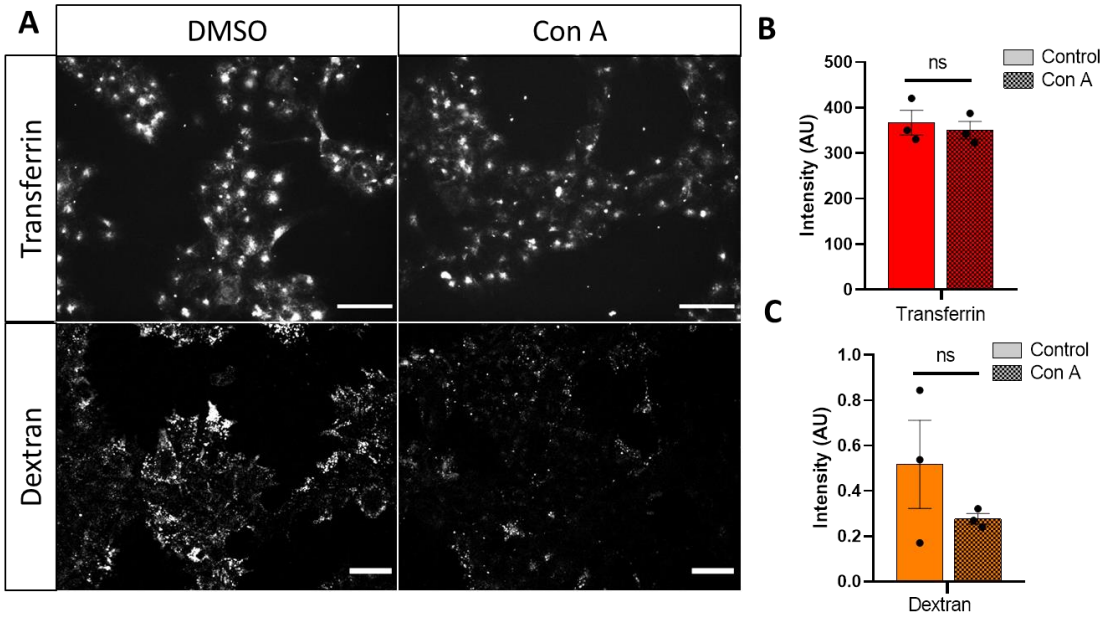

Figure 4.13 – Effect of Concanamycin A on internalisation of endocytic markers transferrin and dextran.

(A) Fluorescence microscopy images of the internalisation in HEK293 cells of 50 µg/ml transferrin-488 and 100 µg/ml dextran-647 with 5 min pre-treatment of either vehicle control DMSO or 10 nM ConA. Images acquired 3 h post-treatment. Scale bar, 50 µm.
(B) Quantification of transferrin-488 internalisation in HEK293 with or without pre-treatment of ConA. No significant difference observed (p = 0.644, unpaired student's t-test).
(C) Quantification of Dextran-647 internalisation in HEK293 with or without pre-treatment of ConA. No significant difference observed (p = 0.287, unpaired student's t-test).

Bar and data points represents mean ± SEM (n = 3 biological replicates). AU, arbitrary units.

While dextran is an established marker for fluid-phase endocytosis, it also labels all endocytic compartments including lysosomes, given its high co-localisation with both LAMP-1 and LysoTracker® (Humphries et al., 2011; Johnson et al., 2016), importantly this is not the case for transferrin which is redirected to recycling endosomes (Mayle et al., 2012). As such, this overall decrease seen with dextran may be due to the reduced lysosomal function caused by the rise in pH. Therefore, I continued the work with ConA to investigate cytosolic translocation of the remaining tau isoforms.

As conducted with 1N4R tau, the GFP1-10 expressing cells were pre-treated for five minutes with 10 nM ConA prior to being incubated with one of six tau isoforms, including the 1N4R-P301S mutant containing 0.5 nM ConA to maintain a chronic V-ATPase inhibition.

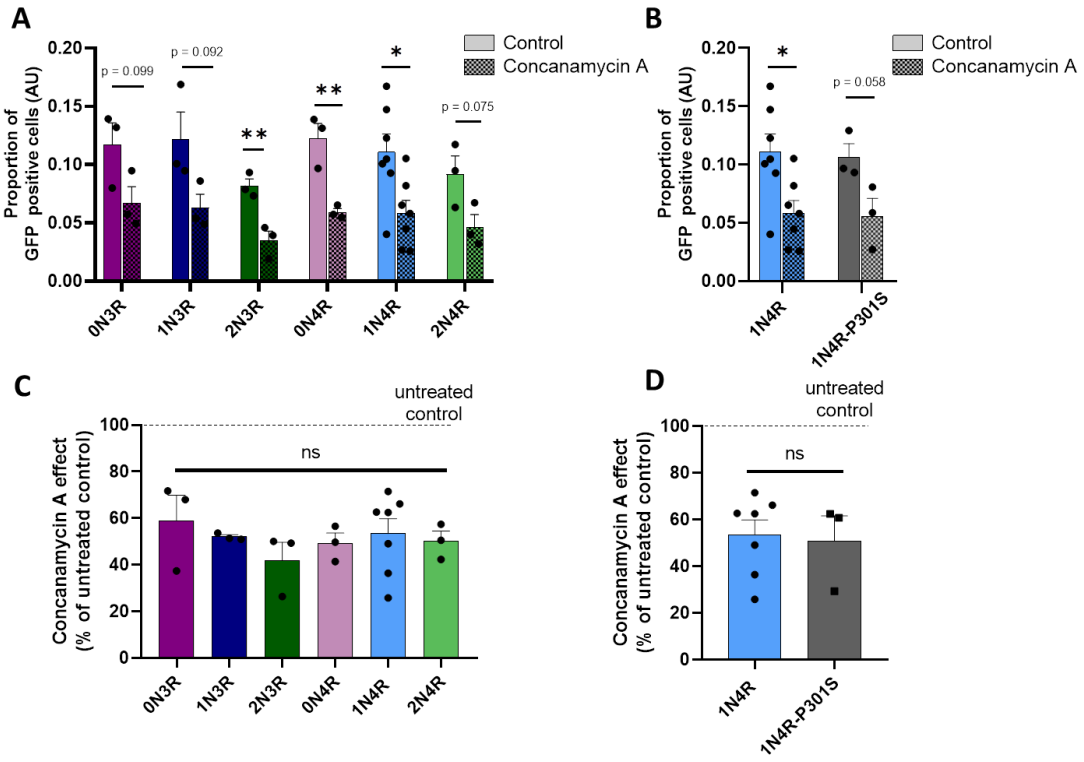

Figure 4.14 – Effect of Concanamycin A on cytosolic entry of tau. All measurements of the proportion of GFP positive cells were calculated from values taken after 60 h of tau incubation with GFP1-10 expressing cells.

(A, B) Proportion of GFP-positive cells under control conditions or following a pre-treatment of 10 nM ConA. ConA pre-treatment evoked a strong effect with all isoforms tested. A significant difference was seen with 2N3R, 0N4R and 1N4R (** p = 0.0094, ** p = 0.0091 and * p = 0.0171 respectively). An unpaired Student's t-test was conducted for each isoform (control and ConA condition). All other comparisons were not significant.

(C, D) Effect of ConA pre-treatment reported as a percentage of the untreated control for each individual tau isoform. Dotted line at 100% represents untreated control for all isoforms. A one-way ANOVA, followed by Tukey's multiple comparison was conducted. No significant difference was identified p > 0.05.

Bar graphs represent mean ± SEM. (n = 3, biological replicates). AU, arbitrary units.

As expected, all tau isoforms tested displayed reduced levels of GFP positive cells when compared to non-treated controls. Although only 2N3R, 0N4R and 1N4R tau were found to be significantly reduced by the ConA pre-treatment, all

other isoforms were close to significance (Fig 4.14A). Similarly, the 1N4R-P301S mutant also displayed reduced levels of cytosolic transfer in the presence of ConA when compared with untreated controls (Fig 4.14B). Furthermore, I wanted to establish if the extent of reduction in the number of GFP positive cells was consistent across all isoforms. Figure 4.14C displays the effect of ConA on the number of GFP-positive cells as a percentage of the untreated control for each isoform; while there was no significant difference identified between the isoforms, 1N4R tau appears overall the most resistant to the effect of ConA, alongside 0N4R and 2N4R tau. Overall, 2N3R tau appears the least resistant to ConA. One could speculate that this resembles the baseline internalisation data presented earlier in this chapter (Fig 4.6C), whereby 4R tau had the most effective internalisation, compared with 3R tau, with the exception of 1N3R. However, the effect of ConA on 0N3R in relation to 1N3R tau does not seem to follow the previous trend, since 0N3R tau appears less affected by ConA compared with 1N3R (Fig 4.14C). It may be argued that since there is high variability in responses per experiment, it is possible that with additional biological replicates a significant effect could be seen.

When comparing the 1N4R WT to P301S mutant, there is no significant difference in the extent of the ConA effect, while the P301S mutation confers a reduced ability for 1N4R-P301S tau to reach the cytosol, in the presence of ConA the P301S mutation is not eliciting any additional effect (Fig 4.14D). However, the high variability seen in these responses may be masking a subtle effect.

From these experiments it is clear that altering the pH of endosomal/lysosomal compartments has a widespread effect across isoforms on tau translocation into the cytosol, irrespective of the isoform. However, there may be subtle differences between isoforms that require additional replicates to establish clear significance. Furthermore, these data have highlighted the necessity for a functional V-ATPase in the efficient translocation of tau into the cytosol, as seen for diphtheria toxin (Umata et al., 1990).

4.2.3.2 Examining the effect of overexpression of Rab mutants on cytosolic translocation of tau

Having seen a clear reduction in cytosolic transfer of tau by disrupting the pH of the endolysosomal pathway, I next wanted to try and decipher where along the pathway this effect could be taking place. To do this, I expressed dominant negative (DN) forms of Rab5 (N33I), Rab7 (T22N), and Rab11 (S25N). With this strategy, I would be able to target different parts of the endocytic pathway, including early endosomes (Rab5), maturing late endosomes into lysosomes (Rab7) and recycling endosomes (Rab11) (Hu et al., 2015).

Briefly, I incubated recipient HEK293 cells co-expressing GFP1-10 and dominant-negative forms of dsRed-Rabs with conditioned media containing tau-GFP11 and monitored over time in the Incucyte®. However, due to the excitation spectrum of dsRed, there was high level of 488 nm excitable background signal that consequently made it difficult to identify cells positive for reconstituted GFP with the Incucyte®. Since the tau construct has a Flag-tag, this was used in immunofluorescence to quantify the number of cells positive for

internalised tau. Given the previous experiments I had conducted, using α-Flag antibody in parallel with reconstituted GFP signal to identify tau positive cells, I was confident that when the Flag signal was diffuse and cytosolic this indicated that tau was present in the cytosol. As such, no tau-containing punctate signal was considered in the quantification for Flag-positive cells.

First, I examined the overall effect of co-expression of dominant-negative Rab GTPases and cellular internalisation of tau. This pilot experiment was conducted with 1N4R tau; from Figure 4.15A it seems that overall the expression of mutant Rab GTPases 5, 7 or 11 triggered a reduction in the average Flag positive cell count, when compared to cells expressing GFP1-10 only. To further analyse the effects of mutant Rab GTPases I quantified the number of cells positive for both tau-Flag and mutant Rab GTPases as a proportion of total cells expressing either DN Rab5, 7 or 11 to determine if there are Rab-GTPase specific effects on tau internalisation. Preliminary data presented in Figure 4.15B demonstrates that the expression of DN Rab7 had the greatest inhibitory effect on cytosolic translocation of 1N4R tau, compared with DN Rab 5 and 11. However, these are just preliminary results that require further biological replicates. Nevertheless, it seems that the expression of mutant Rab GTPases, and in particular Rab7, does impair the ability for tau to reach the cytosol in HEK293 cells.

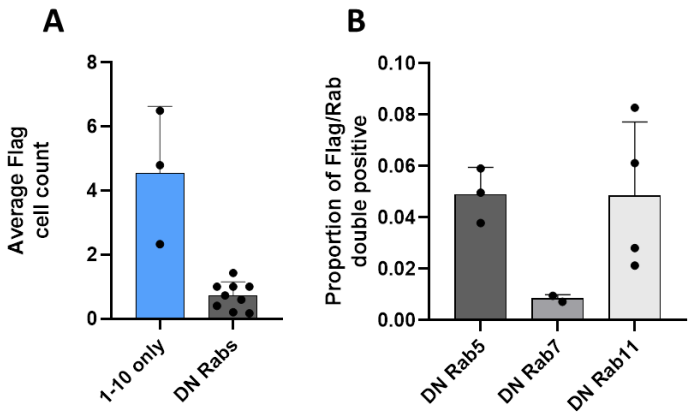

Figure 4.15 – Effect of Rab GTPase mutants on cellular internalisation of tau. There is an overall reduction in the cellular internalisation of tau following expression of dominant-negative Rab GTPases, with DN Rab7 (T22N) exhibiting the most pronounced effect on tau.

(A) Average count of tau-Flag (α-Flag, Mouse) positive cell per field of view in cells expressing either GFP1-10 only or DN Rab GTPase 5, 7 or 11.

(B) Number of cells positive for tau-Flag and DN Rab as a proportion of total number of cells expressing DN Rab5, 7 or 11.

Bar and data points represent mean ± Standard deviation (n = 2 - 4, biological replicates).

4.3 Discussion

4.3.1 Understanding cytosolic translocation properties between isoforms

In this chapter I first compared the baseline cytosolic translocation activity of all six tau isoforms including the 1N4R-P301S mutant. When comparing 1N4R and 1N4R-P301S tau, the mutant consistently had reduced ability to internalise compared to the WT protein. The P301S mutation is present within the R2 region of the MTBR, this P301 position is unique within the MTBR, as the mutation in this position has a strong effect for seeding and/or aggregation compared to mutations in other nearby positions (Strang et al., 2019). However, it is not well understood the role it has with regards to cellular internalisation and/or cytosolic translocation. One might expect that given the role of 1N4R-

P301S in pathology, it would have an enhanced ability for transcellular spread; however in my hands, the P301S mutation appears to confer a reduced ability for internalisation.

A possible reason may be linked with its reduced affinity for microtubules; once 1N4R-P301S has entered the cytosol, it may remain unbound, this may trigger the recruitment of autophagy machinery for degradation, similar to what is seen with 1N4R-P301S aggregates (Falcon et al., 2018a). Alternatively, since 1N4R-P301S has a high propensity for aggregation, it may be that it has undergone a conformational change either from within secreting cells, or within the recipient cells which in turn means that the GFP11-tag is no longer available for GFP reconstitution. Therefore, only the population of non-aggregated 1N4R-P301S may have the GFP11 tag available to reconstitute the GFP. Furthermore, the mutation may trigger cellular cascades that do not allow tau to exit the endolysosomal pathway in the recipient GFP1-10 expressing cell and rather be targeted for lysosomal degradation. While a large part of the literature on the 1N4R-P301S mutant relates to its propensity for aggregation or to seed aggregation, it is important to understand its ability to spread, because this mutation is present from birth in familial FTD cases (Bugiani et al., 1999); therefore tau will likely be spreading throughout the brain during pre-symptomatic stages, prior to aggregation as well as during the symptomatic stage with oligomeric/aggregated tau.

Comparing the cellular properties all six tau isoforms is not routinely conducted, in particular when investigating tau spread. However, very few tauopathies are caused by a single tau isoform mutation/alteration as in familial FTD; in AD

there are no known mutations in the *MAPT* gene and importantly all six tau isoforms are present in pathology, therefore understanding their individual internalisation propensity and mechanism is important for deciphering their contribution to spread in the disease.

Here, I have shown that the 4R isoforms have relative equal ability for cellular internalisation, with a slight trend for 2N4R and 0N4R to be weaker in the group. In contrast, for 3R tau isoforms, 1N3R tau displayed a significantly greater ability to internalise compared with 2N3R and 0N3R tau, furthermore the ability of the 1N3R tau was equal to that of 1N4R tau, whereas 1N4R-P301S mutant appeared more in line with the remaining 3R group (0N3R and 2N3R). A potential interpretation could be the 2N- has an inhibitory effect over the maximal translocation ability, although under this assumption the 0N- and 1N-tau would have either a similar ability to translocate or potentially a graded response with enhanced internalisation of 0N compared with 1N tau. However, this is not the case for either 3R or 4R tau. An interesting additional experiment could be to co-transfect multiple tau isoforms in the secreting tau HEK cells to collect supernatant with more than one isoform and assess the cytosolic translocation. This could be further investigated with isoform-specific tau antibodies to assess if translocation activity is altered when tau isoforms are mixed together as would occur under physiological and pathological conditions.

Interestingly, work conducted by Ait-Bouziad and colleagues demonstrated that the interaction of tau isoforms with lipid bilayers was influenced by the presence of R2 within the MTBR, demonstrating that 4R containing tau had an enhanced ability to bind to liposomes with better stability (Ait-Bouziad et al., 2017). The

presence of the two hexapeptide motifs, PHF6*(^{275}VQIINK^{280}) and PHF6 (^{306}VQIVYK^{311}) may contribute to the enhanced cytosolic translocation seen by 4R tau compared with 3R tau, with the exception of 1N3R. Furthermore, since the mutant 1N4R-P301S tau was more in line with 3R tau cytosolic translocation activity, this may be due to the mutation present at the P301 site that is only 5 residues away from the PHF6 motif; this mutation and potential PTMs may influence the lipid binding abilities, subsequently reducing the cytosolic translocation propensity. Furthermore, while the role of PHF6 and PHF6* in relation to tau aggregation is well established, recent work has also shown that when applying antibodies to recombinant tau targeting these two motifs for immunodepletion it prevents seeded aggregation in HEK293 cells expressing mutant 2N4R-P301S tau (Roberts et al., 2020); this effect may also be a result of preventing uptake, or potentially, preventing the tau/lipid interaction to facilitate the cytosolic translocation of tau.

The aggregation kinetics has been examined between all six WT isoforms and it is known that 4R tau has higher propensity for aggregation when compared with 3R tau and moreover it was found that within the 3R group, the 1N3R had the highest aggregation kinetics (Zhong et al., 2012). Therefore, there may be a connection between aggregation kinetics and the cytosolic translocation data I have obtained; two diverging groups have emerged, 1- 1N3R and all 4R tau, 2- 0N3R, 2N3R and 1N4R-P301S. These findings suggest that the differences seen between tau isoforms are not simply sequence driven, but likely due to tau structure or post-translational differences amongst the isoforms, or by some or all of these factors simultaneously.

A similar difference has also been seen in post-mortem human tissue taken from both Alzheimer's and age-matched controls (Wesseling et al., 2020). With mass spectrometry analysis of sarkosyl-soluble fractions from angular gyrus tissue, the tau isoform composition was determined. Overall, it was found that 1N and 4R isoforms were most dominant in AD and healthy samples, with the 2N- and 0N- isoforms consistently lower (Wesseling et al., 2020), a finding which is remarkably comparable with the results obtained from the cytosolic translocation assay. Figure 4.5D demonstrates that even when data for 2N-, 1N- and 0N- tau isoforms are grouped, there is still a greater ability for cytosolic internalisation of 1N containing tau, compared with 2N and 0N. Since we have obtained corresponding data in cell lines as seen in human tissue, I am confident in the assay and its ability to detect differences in internalisation dynamics between tau isoforms.

On the other hand, *in vivo* work conducted by Dujardin and colleagues demonstrated that following injection of viral vectors expressing human tau (1N4R or 1N3R) in WT rat brains, 4R tau can propagate further in the brain from the injection site compared with 3R tau (Dujardin et al. 2018). These data are comparable with the results presented in this chapter: 4R tau has an enhanced internalisation activity compared to 0N3R and 2N3R, while 1N3R tau appears to be the anomaly in the data set. Crucially, post-mortem rat brain sections revealed that 1N3R tau travelled a significantly smaller distance compared with 1N4R (Dujardin et al. 2018). However, there were no additional comparisons made with the remaining tau isoforms to assess whether the distance travelled by 1N3R was greater than 0N3R or 2N3R. Nevertheless, this work demonstrates that WT tau is also capable of cell-to-cell transmission (Dujardin

et al. 2018). Furthermore, the *in vivo* spread that is being measured in this study does not only take into account cytosolic entry, but will encompass all stages of prion-like tau spreading i.e. secretion levels, stability in the extracellular space and uptake. While there was no difference in the transgene expression between 1N4R and 1N3R (Dujardin et al. 2018), there may have been different secretion rates, and consequently different extracellular levels of tau, which in turn would influence the pattern of spread.

While the overall ability for cytosolic translocation of tau was assessed by quantifying the number of GFP-positive cells, the intensity of the reconstituted GFP signal was also analysed to assess the dynamics of tau entry into the cytosol and the overall accumulation of tau in the cytosol. From the data acquired it seems that tau has an entry modality whereby within four hours, all the tau that is competent for cytosolic entry will enter a cell in a single event, rather than occurring gradually overtime. Given that over approximately 40 h, new GFP-positive cells continue to appear, one can assume that there is still tau in the extracellular media of cells that are already GFP-positive, yet there is no significant increase in the GFP signal intensity. This could be tested by removing extracellular media containing tau after varying time periods (as described in chapter 3, Figure 3.8) and then measuring the GFP signal intensity, to assess whether there is any change in the pattern of signal intensity.

Currently, the stable GFP signal intensity observed may be a result of multiple biological processes, one example is protein turnover; there may be an equilibrium between internalisation and degradation of tau which maintains the

overall GFP intensity stable. In cells where there is an imbalance of these two processes it may give rise to higher or lower GFP signal compared with the initial measured intensity. By applying a blocker of proteasome degradation e.g. MG-132, in the recipient GFP1-10 expressing cells, this could be tested, if tau degradation is blocked and the GFP signal intensity continues to rise, this would support the hypothesis described. Of the tau isoforms tested, only 1N3R tau exhibited a significant increase over time in the GFP intensity, therefore it is clear that the overall equilibrium for tau present in the cytosol has shifted overtime. There have been reports that 3R tau have slower turnover rates compared to 4R tau (Sato et al. 2018). From my data, it would seem that 1N3R tau has the greatest internalisation capacity out of the 3R group, equivalent to 4R tau. As such, if 1N3R tau has the greatest cytosolic translocation with a slower turnover, over time tau is likely to build up. On the other hand, 2N3R and 0N3R tau have slower turnover, but also less effectively taken up, therefore the total amount of cytosolic tau would remain stable. Similarly, for 4R tau, while it has a greater internalisation ability compared to 3R tau, it has a faster turnover, as such the overall intensity will remain relatively stable. Since there is an opposite trend between internalisation efficacy and turnover rates between 3R and 4R, this could explain why the overall change of intensity is similar between both groups.

Interestingly, the half-life of non-transfected tau in SH-SY5Y has been reported to be around 12 – 14 h (David et al. 2002) so this may suggest that while there is one event where the majority of tau enters the cytosol, over time there may still be tau entering the cell, in parallel with tau degradation leading to this equilibrium. Experiments using a proteasome degradation blocker, as described

above, would also address whether the time frame of tau degradation is influencing the GFP signal intensity pattern. Furthermore, one cannot exclude the possibility that upon cytosolic entry there is no continuous degradation of tau, and so following the treatment of MG-132 there would be no change to the GFP signal intensity. However, a lack of change in the GFP signal intensity, following MG-132 treatment, or under non-treated conditions could also be a result of saturating the GFP1-10, which would mean that no further tau entry could be detected within a single cell. One way to address this could be with a photobleaching experiment. First, one could apply tau-GFP11 media to recipient GFP1-10 cells and allow reconstituted GFP signal to develop. This would be followed by photobleaching of the GFP signal and then applying fresh tau-GFP11 media. From this, one could observe whether previously GFP-positive cells are able to recover their GFP signal, suggesting that there is still available unbound GFP1-10 present within the cytosol.

4.3.2 Investigating biological mechanisms mediating the cytosolic entry of tau

4.3.2.1 The pH of the endocytic pathway mediates tau entry into the cytosol

Having confirmed the ability of this assay to reliably detect tau entry I next sought to investigate potential biological mechanisms that could be mediating this process, and assess whether this assay was sensitive enough to detect any changes in the system. To date, there has been evidence within the literature that tau gets localised within the endocytic pathway. As previously discussed,

tau has been shown by multiple groups to co-localise with Rab5 (Calafate et al. 2016; Falcon et al. 2018a; Wu et al. 2013; Puangmalai et al. 2020), EEA1 (Ait-Bouziad et al. 2017), Rab7 (Falcon et al. 2018a; Chen et al. 2019) and LAMP1/2 (Chen et al. 2019; Wu et al. 2013; Puangmalai et al. 2020). Critically, tau has been found to be resistant to proteases (Novak et al., 1993); it is also suspected that tau seeds are resistant to lysosomal degradation, therefore can undergo cytosolic transfer directly from endolysosomal compartments (Polanco et al. 2021). Further evidence comes from treating primary hippocampal neurons with cell-secreted 2N4R-P301L aggregates. By using the galectin-3 assay to detect the change of diffuse to punctate galectin-3 signal, it was suggested that 2N4R-P301L aggregates escaped through holes in the endosomal membranes to reach the cytosol (Falcon et al. 2018).

Furthermore, a change of pH in the endolysosomal vesicles has been shown to affect the ability for tau to efficiently enter the cytosol. Recent work published by Polanco and colleagues revealed that when treating tau biosensor cells with ammonium chloride, an alkalinising agent used to raise the cellular pH, seed competent EVs derived from rTg4510 mice were less able to seed tau aggregation, than under acidic conditions. With an observed 63% reduction in the FRET signal it has been suggested that seed competent tau require fully functioning lysosomes at the physiological pH in order to efficiently escape the endolysosomes to seed aggregation (Polanco et al. 2021). Cytosolic entry has been measured by the seeding ability of tau which is hypothesized to occur via its exit from the endolysosomal compartments in order to reach cytosolic tau (Polanco et al. 2021; Chen et al. 2019; Falcon et al. 2018). However, when changing the cellular pH, the induction of tau aggregation may also be affected,

if this is the case, tau seeds may have entered the cytosol but not triggered aggregation, since seeded tau aggregation is being used as a proxy for cytosolic tau entry, these results would suggest that cytosolic entry of tau has reduced following a change in pH.

In attempts to bypass these problems, I decided to test whether the cytosolic translocation assay could be used to examine if raising the pH would affect cytosolic entry of WT and mutant tau. In this experimental setup the tau under investigation is not seed-competent, therefore one does not have to rely on seeding aggregation, but rather a direct visualisation for when tau has escaped the endocytic compartment and reached the cytosol. First I chose two well established antibiotics that raise the pH within the endolysosomal compartments, BafA1 and ConA and confirmed their ability to increase lysosomal pH. It has been reported that ConA is up to four times more potent that BafA1 (Muroi et al., 1994), therefore it was not surprising that BafA1 had a weaker effect.

As described in Figure 4.12, both a pre-treatment and a time course assay were conducted with BafA1 and ConA. Pre-treating the GFP1-10 expressing cells with either BafA1 or ConA, would alter the endolysosomal pathway prior to the internalisation of tau. On the other hand, the time course assay allowed tau to be applied first to the GFP1-10 expressing cells to enable a certain proportion of tau to be internalised, prior to the drug treatment. In this experimental design I wanted to examine whether there was a critical time point after tau had entered the endocytic vesicle in which changing the pH of either endosomes or lysosomes would impact its ability to reach the cytosol. Previous work has

shown that tau endocytosis is rapid and can occur within five minutes of exposure (Wu et al., 2013) and subsequently co-localises with early and late endosomes / lysosomes within hours (Evans et al., 2018; Falcon et al., 2018a). Therefore, I chose to incubate tau with the GFP1-10 cells over a range of time periods (5, 15, 30, 60, 120 and 240 min) before treating with BafA1 or ConA. In this way I would likely capture tau within different stages of the internalisation pathway. In this experiment there was no significant difference in the proportion of GFP-positive cells observed with either BafA1 pre-treatment or its addition during the time course. While there was a slight reduction seen with the pre-treatment, this effect was not strong enough; therefore I did not continue to use BafA1. It is important to note that BafA1 did effectively raise endolysosomal pH, albeit to a lesser extent than ConA (Fig 4.11), therefore tau appears able to tolerate small changes in the pH throughout the endolysosomal pathway and still translocate to the cytosol.

In contrast, ConA pre-treatment evoked over a 50% reduction in the reconstituted GFP signal count, while ConA treatment after five and 15 min of tau incubation evoked approximately a 40% reduction. It was found that the longer 1N4R tau was incubated with the GFP1-10 cells, the less effect ConA had on tau's ability enter the cytosol. This is likely to be linked to the location and site of translocation of tau within the endolysosomal pathway at the point of drug treatment. In line with this argument, it is likely that after four hours of tau incubation, a large proportion of tau has already entered the cytosol, therefore raising the pH at this stage would have no further impact on its ability to escape the endolysosomes. Nevertheless, what is critical to understand is the site of translocation to assess how the change of pH is affecting cytosolic entry.

Since pre-treatment of ConA gave rise to the strongest inhibitory effect, this experimental setup was chosen to test the remaining tau isoforms. On average, all isoforms including the 1N4R-P301S tau mutant were subject to a 50% reduction in the reconstituted GFP signal count when compared to non-treated control. When comparing the effect of ConA on 1N4R WT and P301S mutant, there appears to be no major difference in the effect of ConA, despite 1N4R-P301S being significantly less effective at internalisation compared to WT. When closely analysing the remaining isoforms specific results, it appears that overall 4R tau was the most resistant to ConA's effect, while 2N3R appeared to be the least resistant. When considering the data from the previous chapter that examined the normalised internalisation rates between the isoforms, one might have expected a similar trend for ConA effects. While 1N3R appears more resistant to pH changes compared with 2N3R tau, 0N3R tau has not followed this trend, and appears more resistant than 1N3R tau. Nevertheless, these data may suggest that there is an isoform specific mechanism, which could be related to the particular tau conformation of a certain isoform, or to PTMs that lends itself to being more or less resistant to changes in pH. It is important to note that at the moment these are only speculations. Additional biological replicates would be needed to decipher whether this is a genuine trend.

These experiments have also demonstrated the involvement of the V-ATPase in the cytosolic translocation of tau. Interestingly, this has also been confirmed for diphtheria toxin, a protein that requires access to the cytosol following endocytosis to exert its cytotoxic effect (Umata et al., 1990). Purified diphtheria toxin applied to Vero cells treated with 10 - 500 nM of BafA1 had a reduced toxic effect as measured by protein synthesis levels; when examining the

cellular binding of diphtheria toxin, there was no difference between control and BafA1 conditions, suggesting that the reduction in toxicity was occurring after internalisation and likely due to the blockade of cytosolic translocation, which is mediated by the V-ATPase (Umata et al., 1990).

4.3.2.2 Modulating pH to assess effect on endocytic markers

When utilising ConA to prevent acidification of the endolysosomal pathway, I also wanted to examine its effect on known makers for endocytosis; I chose transferrin and dextran to address both CME and bulk/fluid phase endocytosis respectively, both pathways that have been associated with tau uptake.

Following the pre-treatment with ConA there was no significant difference between the signal intensity detected for transferrin when compared to vehicle control. There is evidence within the literature, that changes of endolysosomal pH via V-ATPase inhibition with BafA1 does not affect endocytosis of transferrin, but that rather it may slow down the transferrin receptor recycling process to the membrane (Presley et al., 1997). In contrast, ConA elicited a strong albeit not significant reduction in the signal intensity of dextran. Previous work has demonstrated that pre-treatment with BafA1, at concentrations 20 fold higher than used in this work did not inhibit endocytosis of dextran, but did block its accumulation into lysosomes (Baravalle et al., 2005), confirming that inhibition of the V-ATPase does not inhibit endocytosis of dextran. In my experimental setup pre-treatment with 10 nM ConA is likely to have affected dextran's normal trafficking process, as expected, rather than inhibiting its endocytosis. Moreover, a potential reason that we do not see a similar effect with transferrin is likely to be linked to its differential cellular trafficking.

Typically, once transferrin is internalised, it is trafficked to early/late endosomes and then redirected to recycling endosomes before returning to the plasma membrane. Once transferrin has been internalised, it gets enriched in two populations of early endosomes, one that is slower maturing, and another dynamic population that are faster maturing into late endosome (Mayle et al., 2012). It is possible that upon neutralization of the endosomal lumen, a sort of compensation takes place between the reduction of transferrin signal due to the impaired functionality of the late endosomes and a slowing down of recycling endosomes causing an accumulation of transferrin within the early endosomes / recycling endosomes. Although transferrin accumulation would usually be accompanied by a swelling of the endolysosomal compartment, which was not evident in my results (Fig 4.14A) this may be due to impaired function of the endocytic compartments. Nevertheless, to establish the effect of V-ATPase inhibition on endocytosis, applying BafA1 or ConA and probing for both transferrin and dextran over a time course experiment would be beneficial to understand whether endocytosis, in addition to endolysosomal pH, is being affected, to ensure that the results seen with tau are not due to impaired endocytosis.

4.3.2.3 Expression of Rab mutants to investigate cytosolic entry of tau

To better understand the role of the endolysosomal pathway in the cytosolic translocation of tau, I have halted traffic at different stages of endosomal maturation by expression of DN Rab-GTPases, to target the endocytic pathway and gain insight on this biological process. Briefly, DN Rab5 will prevent the delivery of cargo from endocytic vesicle to early endosomes (Bucci et al., 1992), DN Rab7, prevents the maturation between late endosomes to lysosome

(Vanlandingham and Ceresa, 2009) and finally DN Rab11, will prevent the slower recycling of cargoes from sorting endosomes / recycling compartments back to the cell surface (Ren et al., 1998).

Co-expression of GFP1-10 with mutant Rab5, 7 or 11 evoked an overall reduction in the number of cells positive for tau (Fig 4.15). Given how interconnected the progression of the endocytic / endolysosomal pathway is, the effect of over-expressing Rab-GTPase 5, 7, or 11 may not be isolated, therefore this could be having an effect on endocytosis and other parts of the pathway, leading to this overall reduction in tau internalisation. Interestingly, I have found that DN Rab7 appeared to have the greatest inhibitory effect for tau translocation, when compared with the DN Rab 5 and 11. Similar findings have been previously reported by Polanco and colleagues, who found that siRNA silencing of Rab7 reduced the seeding ability of exosomes derived from rTg4510 mice. Moreover, overexpression of Rab7 increased seeded aggregation, therefore confirming the necessity for functioning Rab7 in the process of tau entering the cytosol (Polanco et al., 2021).

On the other hand, other groups have shown that downregulation of Rab7 increased the extent of escape of tau seed to trigger aggregation, as assessed by galectin staining (Falcon et al., 2018a). A complementary assay using split-luciferase has also demonstrated that >90 % siRNA knockdown of Rab5 exhibited no significant difference in cytosolic entry of tau seeds, yet silencing of Rab7 increased the overall reconstituted luciferase signal indicating a greater entry of tau in the cytosol (Tuck et al., 2021). These data have the opposite effect to the published work by Polanco and colleagues (2021) and from the

data in this thesis; to date the differences in these findings are still not understood.

Therefore it is clear that the role of Rab7 is important in the exit of tau from the endolysosomal pathway and it is likely occurring from late endosomes maturing into lysosomes, however the cellular mechanisms still need to be fully determined. One hypothesis for this could be linked with the pH changes that occur within the endolysosomal pathway. The maturation of late endosomes to lysosomes include acidification of the lumen pH; it has been reported that pH changes can trigger polymerisation of tau (Ait-Bouziad et al., 2017), this may be necessary for the escape of tau into the cytosol. Alternatively, the role of Rab7 has been implicated in the secretion of tau and it has been demonstrated that following depletion of Rab7A there is a hypophosphorylation of tau leading to a reduction of tau secretion (Rodriguez et al., 2017). In addition, it has been reported that depletion of Rab7 in Hela cells can affect the recruitment of kinases / phosphatases to organelles of the endolysosomal pathway (Rodriguez et al., 2017). In relation to cytosolic translocation, it may be that the expression of the DN mutant Rab7 is also affecting the recruitment of kinases / phosphatases to the endolysosomal pathway, which in turn alter the PTMs of tau required for its cytosolic entry.

With regards to the efficacy of the split-GFP assay, further optimisation is required to make it compatible with additional fluorophores in the cytosol and still retain the ability to decipher genuine GFP reconstitution versus background noise. In this experiment, due to the high 488 nm excitable signal from the dsRed tag on the mutant Rabs, it was a confounding factor for the detection of

the GFP signal to determine cytosolic tau entry. Therefore, future experiments are required to confirm the results obtained with the α-Flag antibody. One option could be to remove the fluorescent tag from the DN Rab GTPase construct and carry out the same experiment under live imaging and confirm the DN Rab expression via immunofluorescent staining using α-Rab antibodies.

In this chapter I have conducted a comprehensive investigation on the cytosolic translocation of all six tau isoforms including the 1N4R-P301S mutant tau. I have demonstrated the ability for this newly developed assay to detect isoform-dependent differences in the translocation of tau into cytosol. Furthermore, I have investigated cellular mechanisms which may contribute to the cytosolic translocation of tau, presenting data that implicates V-ATPase functionality, pH sensitivity and physiological activity of Rab GTPases in the process of tau internalisation.

Chapter 5: Evaluating the cytosolic translocation assay in primary neuronal cultures

5.1 Introduction

Having optimised the cytosolic assay in HEK293 cells and obtained data regarding the mechanisms mediating translocation of tau in the cytosol, I sought to implement this assay in primary neuronal cultures.

Since tau is widely reported to undergo prion-like trans-synaptic spread (Holmes et al., 2014), it is assumed that neurons will secrete and internalise tau, and this is suggested to occur at the pre- and post-synaptic sites respectively (De La-Rocque et al., 2021; Puangmalai et al., 2020; Sokolow et al., 2015; Wu et al., 2016). In addition, it has been shown that WT neurons are capable of secreting (Pooler et al., 2013) and internalising tau (Wu et al., 2016) and finally, that WT tau (AT8 and/or MC1 positive) is capable of spreading in absence of any *MAPT* mutation *in vivo* (Dujardin et al., 2018). While tau uptake has been widely studied in neurons and extensively described in the introduction, very little is known about the process that mediates the entry of tau into the cytosol.

The timeline of this process has been addressed by some groups; when monitoring the uptake of cell-secreted tau in tau-knockout neurons, lysates were used to measure tau levels by ELISA and were shown to be significantly higher after one hour of incubation compared to control, suggesting that extracellular tau had been internalised (Wu et al., 2016). However, when conducting

immunocytochemistry the anti-tau staining revealed discrete tau-positive puncta after two days of incubation likely representing its presence in vesicular compartments (Wu et al., 2016); only after six days did the signal shift to a diffuse staining suggesting an entry into the cytosol (Wu et al., 2016). This would indicate that following rapid uptake, tau remains enclosed in an ill-defined endosomal compartment for an extended period of time. On the other hand, recent work conducted by the McEwan lab has demonstrated with a novel split luciferase assay, analogous to the split-GFP system, that upon incubation with recombinant tau, only one hour of incubation is required prior to the detection of the reconstituted luciferase signal within the cytosol (Tuck et al., 2021). These conflicting findings confirm that there is still a necessity for further research in this field.

Using the split-GFP tool, I will investigate the cytosolic translocation of multiple forms of tau-GFP11 in primary neuronal cultures, including recombinant purified tau and neuron or HEK293 cell secreted tau. Furthermore, I will explore the use of MFCs as a method to study trans-synaptic spread of tau using cytosolic translocation as a readout for tau spread.

5.2 Results

5.2.1 Confirming the activity of the cytosolic translocation assay in neuronal cell line

While all the experiments discussed in the previous chapter have been conducted in HEK293 cells, I wanted to ensure that this experimental setup

could be applied to other cell lines and importantly within a neuronal system. Neuroblastoma cell lines have routinely been used as a proxy to study neuronal function; to conduct a proof of principle experiment I chose N2a cells to confirm that secreted tau-GFP11 could undergo internalisation and interact with the cytosolic GFP1-10 to reconstitute the GFP fluorophore. To ensure that there was an efficient level of GFP1-10 expression, I co-expressed tau-GFP11 and GFP1-10 in N2a cells. Consequently, I was able to monitor the extent of GFP1-10 expression. As seen in Figure 5.1A there was a high number of GFP1-10 positive cells which were approximately 80 - 90 % GFP positive. Therefore I considered the level of GFP1-10 expression sufficient to carry out the cytosolic translocation assay.

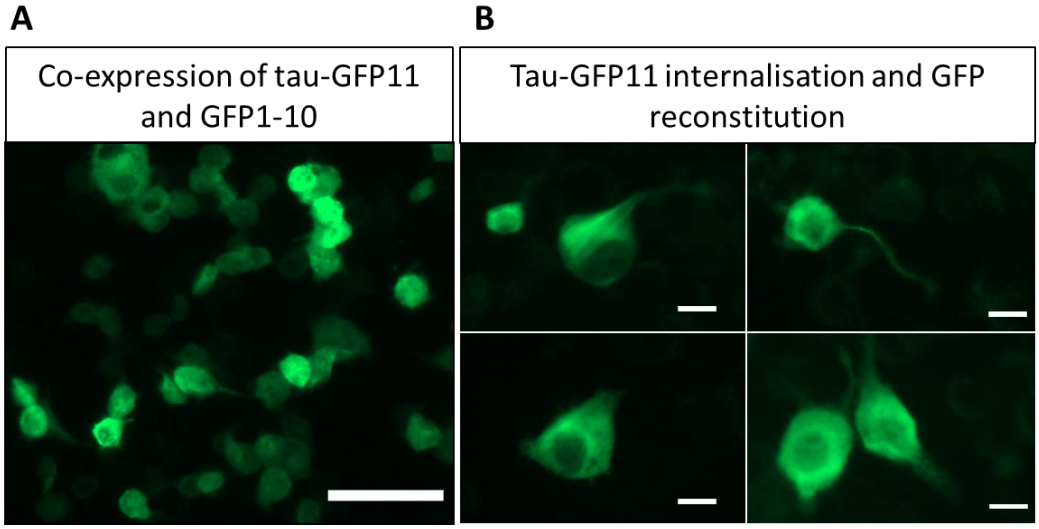

Figure 5. 1– Confirming functionality of tau-GFP11 and GFP1-10 in N2a cells. Imaging conducted on fluorescent microscope with a green LED

(A) Tau-GFP11 and GFP1-10 were co-expressed for 24 h prior to fixation. Representative image confirm high levels of tau-GFP11 and GFP1-10 expression and functionality of the two split-GFP domains. Scale bar, 100 µm.

(B) N2a cells expressing cytosolic GFP1-10 were incubated with HEK293 cell secreted tau-GFP11 for 24 h prior to fixation. Cytosolic translocation of tau-GFP11 was monitored by GFP reconstitution; representative images display individual cells that are positive for tau internalisation. Scale bar, 10 µm.

Experiment repeated with 2 technical replicates, achieving similar results.

To maintain consistency between the HEK293 and N2a cell line experiments, I collected tau-GFP11 from HEK293 cells culture medium, since they were reliably producing high enough levels of tau give rise to reconstitution of GFP signal. Therefore, N2a cells were transiently transfected with GFP1-10 and then incubated with tau-GFP11 containing media. In Figure 5.1B I have displayed representative images of N2a cells with positive GFP reconstitution, confirming successful entry of tau-GFP11 into the cytosol over a 24 h period. This experiment was carried out to confirm that the basic experimental design that was optimised and described in Chapters 2 and 3 was not specific to HEK293 cells, but rather could be applied to other cell systems. Importantly, I wanted to transfer this assay into primary neuronal cultures, therefore trialling the assay in a neuronal cell line was the first step in this direction.

5.2.2 Confirming the functionality of neuron expressed tau-GFP11

Having confirmed the functionality of the split-GFP domains in HEK293 and N2a cell lines, I sought to do this in primary neuronal cultures. The mammalian expression vectors for tau-GFP11 isoforms and GFP1-10 were tested in primary cortical/hippocampal neurons. The GFP1-10 construct was transfected into primary cortical neurons (DIV 5); expression of GFP1-10 can be visualised in Figure 5.2 by an α-GFP antibody. As expected, there was no detectable GFP signal, confirming that this fragment alone is not auto-fluorescent. In parallel, tau-GFP11 isoforms were transfected into primary cortical neurons and their expression detected by α-Flag antibody (Fig 5.2- single isoform shown). Importantly, the transfection of tau tagged with the GFP11 construct did not yield any detectable GFP signal in neurons. Finally, both GFP1-10 and tau-GFP11 constructs were co-transfected in primary cortical neurons to confirm the

ability of the two split-GFP domains to reconstitute GFP signal in neurons (Fig 5.2).

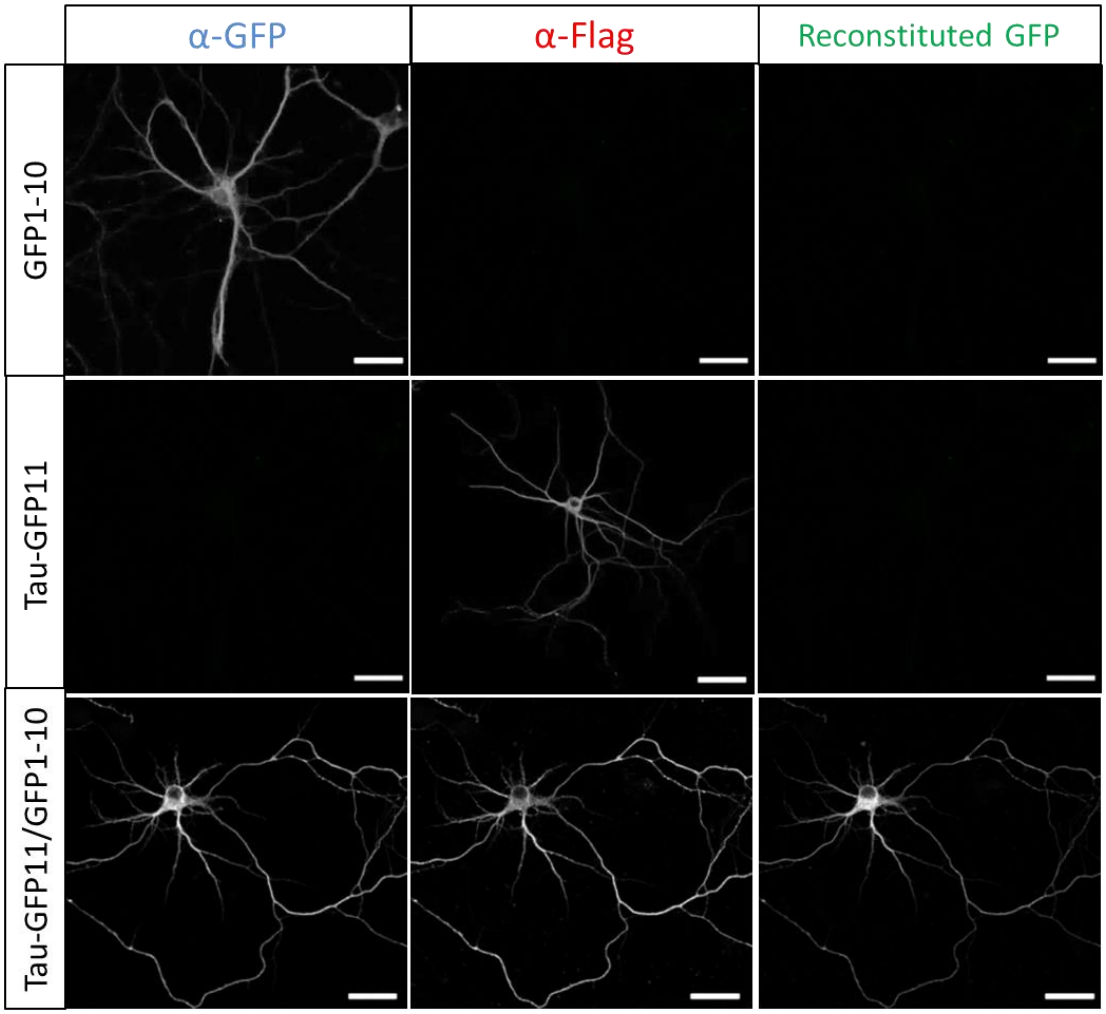

Figure 5.2 – Expression of tau split-GFP constructs in primary cortical neurons. DIV 5 neurons transfected with either GFP1-10 and probed with α-GFP (chicken) (Alexa Fluor 647) or tau-GFP11 and probed with α-Flag (Mouse) (Alexa Fluor 555) or co-transfected with GFP1-10 and tau-GFP11. At DIV 8 there is no detectable signal in the 488 nm channel when split-GFP constructs are expressed in isolation. When GFP1-10 is co-transfected with human tau tagged with GFP11, the reconstituted GFP signal is present. Scale bar, 30 µm. Experiment repeated with 3 biological replicates, achieving similar results.

To improve GFP signal detection I also conducted live imaging for the co-transfection of all six tau isoforms, to avoid any dampening of the GFP signal. Figure 5.3 displays the live imaging of all isoforms in primary hippocampal

neurons, confirming the functionality of the split-GFP domains for all six isoforms of tau.

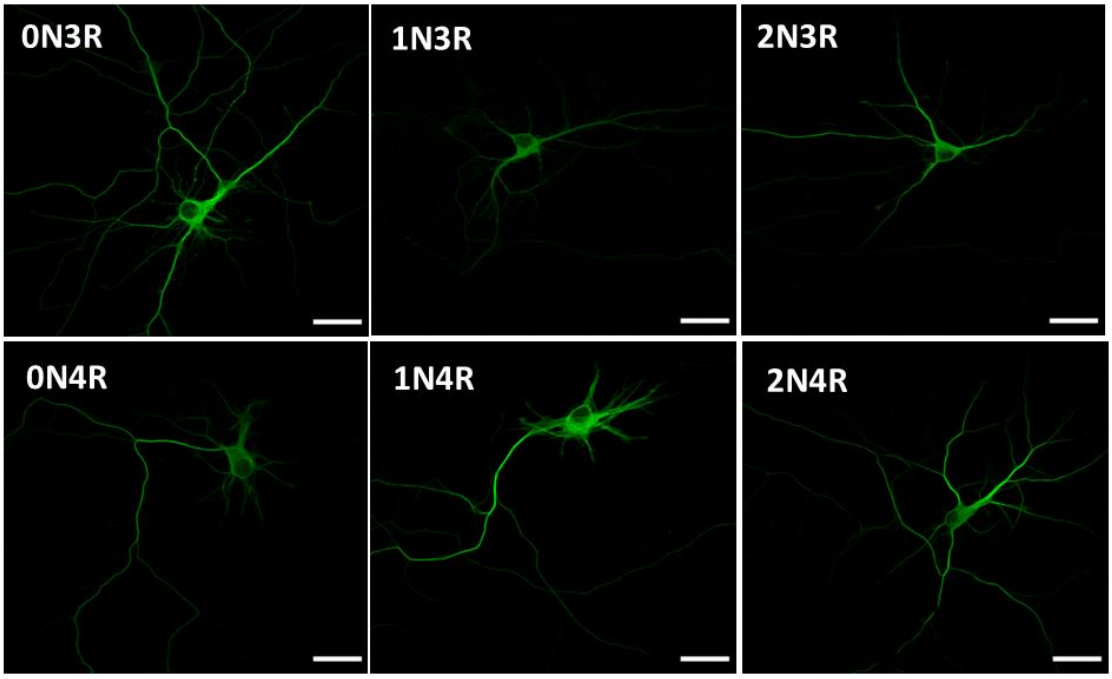

Figure 5.3 – Reconstitution of tau split-GFP constructs in primary hippocampal neurons. DIV 7 neurons co-transfected with GFP1-10 and one of the human tau isoforms tagged with GFP11; the reconstituted GFP signal is present in all conditions tested. Live imaging conducted with LSM 880 confocal microscope. Scale bar, 30 µm. Experiment repeated with 2 biological replicates, achieving similar results.

All transfection experiments were confirmed in primary hippocampal and cortical neurons (data not shown). In HEK293 cells, the reconstituted GFP signal generated by the split-GFP domains can give rise to a distinct signal localisation (Fig 3.5A). This specificity was also seen in primary neuronal cultures; upon co-transfection of 1N4R-GFP11 tau and GFP1-10 I detected a distinct microtubule localisation from the reconstituted GFP signal (Fig 5.4).

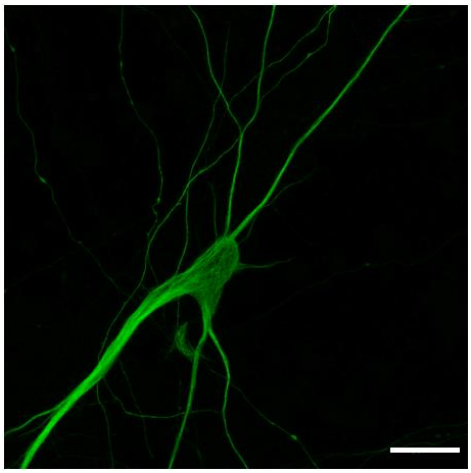

Figure 5.4 - 1N4R split-GFP reconstitution in primary hippocampal neurons. Neurons were co-transfected at DIV 7 with 1N4R-GFP11 and GFP1-10. Image taken at DIV 14 by live imaging with LSM 880 confocal microscope reveal distinct microtuble localisation of the GFP signal. Scale bar, 20 µm. Experiment repeated with 2 biological replicates, achieving similar results.

Lastly, given the low transfection efficiency within primary neuronal cultures, I decided to produce lentiviral particles encoding GFP1-10 to ensure there were a high proportion of neurons expressing GFP1-10 for future tau uptake experiments. Figure 5.5 demonstrates the widespread GFP1-10 expression, upon treatment with lentivirus encoding GFP1-10, confirmed with an α-GFP antibody.

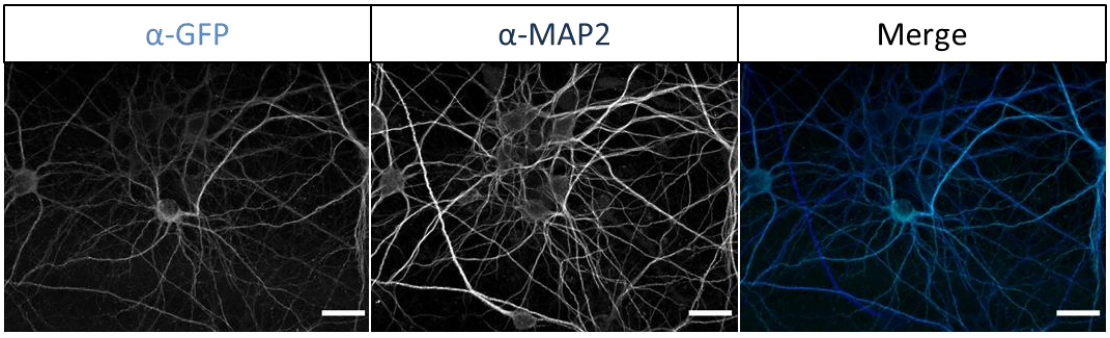

Figure 5.5 – Lentiviral transduction of GFP1-10 in primary cortical neurons. Primary cortical neurons transduced at DIV 6 with GFP1-10. α-GFP chicken antibody (Alexa Fluor 647) confirms widespread expression of GFP1-10 (DIV 18). Neurons also stained with α-MAP2 guinea pig (Alexa Fluor 405). Scale bar, 25 µm. Experiment repeated with 3 biological replicates, achieving similar results.

These proof of principle experiments confirmed that the split-GFP tool can be confidently used in primary neuronal cultures since the GFP reconstitution

occurs reliably when the split-GFP domains are co-expressed. The GFP11 tag has not triggered any overt mis-localisation of tau, retaining a soluble and cytosolic signal pattern as expected for endogenous tau. The GFP1-10 fragment is not auto-fluorescent, and using lentiviral transduction, I can achieve widespread GFP1-10 expression, an essential requirement for reliably observing tau-GFP11 uptake. With this, I sought to examine cytosolic translocation of tau-GFP11 in GFP1-10 expressing neurons.

5.2.3 Investigating recombinant tau-GFP11 in primary neurons

As discussed in Chapter 3, *E. coli* produced recombinant tau-GFP11 did not evoke high levels of GFP reconstitution in the cytosolic translocation assay when tested in HEK293 cells. This observation may have been HEK923-specific and so I wanted to test whether in neurons the internalisation activity would be better.

Given that only high concentrations of recombinant tau-GFP11 gave rise to positive GFP signal in HEK293 cells (Fig 3.10), I decided to trial high concentrations of recombinant tau-GFP11 with a short incubation time to assess whether this would give rise to any detectable GFP signal. Below is a representative image of primary cortical neurons transduced with GFP1-10 and incubated with recombinant tau-GFP11 (DIV 8) for one hour prior to fixation and immunocytochemistry. Neurons display visible puncta of recombinant tau-GFP11 with an α-Flag antibody (Fig 5.6A). I tested three concentrations of recombinant tau-GFP11; 0.5, 1 and 2 μM, plus vehicle control. The levels of Flag signal were quantified demonstrating a dose-dependent increase in the number of puncta detected with an α-flag antibody within α-GFP positive

neurons (Fig 5.6B). In parallel, the intensity of the GFP signal was measured for all conditions. These experiments demonstrated that despite the increase in the tau-GFP11 present within the neuron, there was no appearance of a GFP signal (Fig 5.6C).

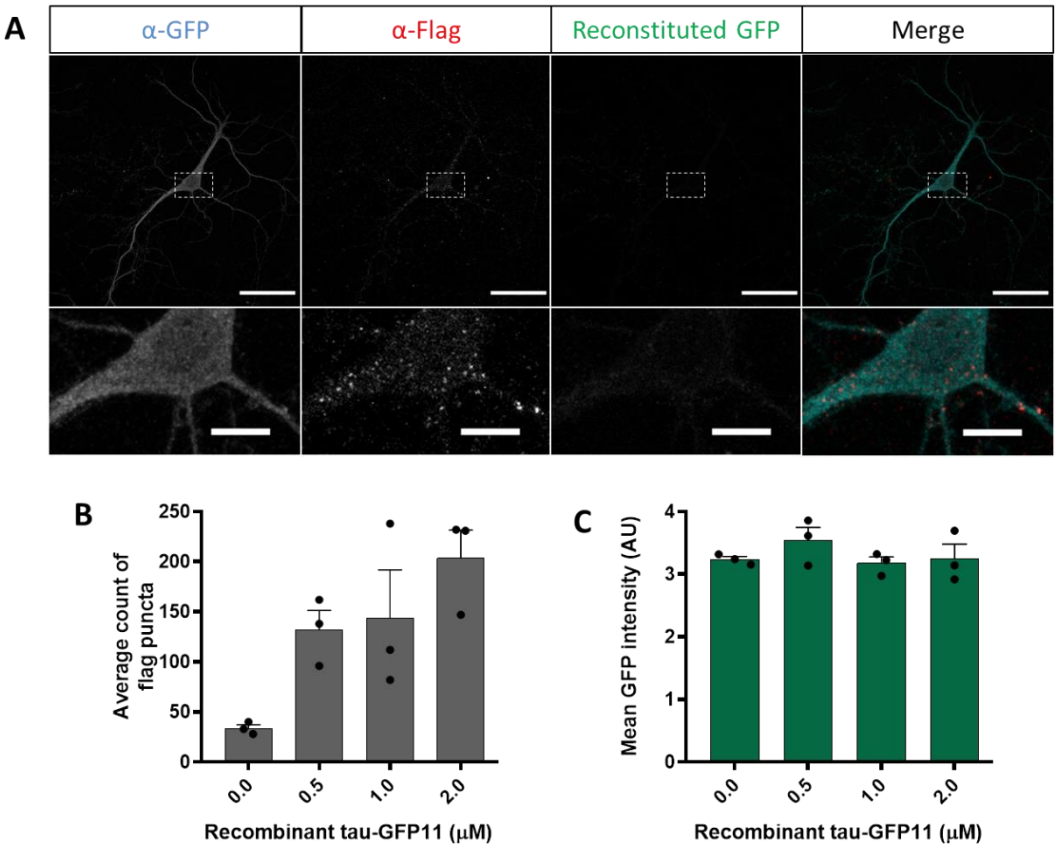

Figure 5.6 – 1 h treatment of cortical neurons with recombinant purified tau-GFP11.

(A) Representative image of neuron transduced at DIV 6 with GFP1-10, and incubated with 2 μM tau-GFP11 (DIV8) for 1 h prior to fixation and immunocytochemistry. α-GFP (chicken) (Alexa Fluor 647) and α-Flag (Mouse) (Alexa Fluor 555) antibodies were used to probe for GFP1-10 and tau-GFP11 respectively. Despite co-localisation between GFP1-10 and tau-GFP11 there is no GFP reconstitution. Scale bar, 50 μm and cropped scale bar, 10 μm.

(B) Quantification of mean count of tau-GFP11 puncta within α-GFP positive neurons for 0, 0.5, 1 and 2 μM of recombinant tau-GFP11.

(C) Quantification of mean GFP signal intensity for neurons positive of α-GFP for all concentrations of recombinant tau-GFP11 tested.

Bar graph represent mean ± S.E.M, (3 technical replicates, n = 2 biological replicates). AU, arbitrary units.

Given the signal localisation of tau-GFP11, it seems likely that the internalised tau remained within a membrane bound compartment and therefore was not able to interact with the cytosolic GFP1-10. To try and overcome this problem I incubated GFP1-10 expressing neurons with 2 µM tau-GFP11 over six days and monitored the reconstituted GFP signal. Throughout this time period there was no convincing GFP reconstitution and by day six of tau incubation there was extensive neuronal death (Fig 5.7). Consequently, in these conditions the neurons were unable to effectively internalise tau-GFP11.

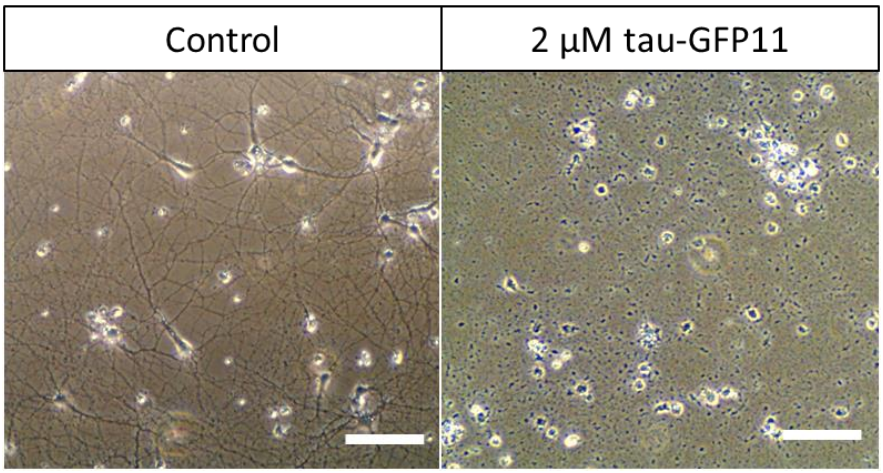

Figure 5.7 – Long term treatment of cortical neurons with recombinant purified tau-GFP11. Representative images of neurons transduced at DIV 6 with GFP1-10, and incubated with 2 µM tau-GFP11 (DIV8) or vehicle control for 6 days. By day 6 there is widespread neuronal death in the presence of 2 µM tau-GFP11. Scale bar 100 µm. Experiment repeated with 2 technical replicates, achieving similar results.

From these data, I decided that bacterially expressed recombinant tau-GFP11 would not be best source of tau for this study therefore I changed the methodology to resemble the work conducted in HEK293 cells.

5.2.4 Testing functionality of neuron-secreted tau-GFP11

Having investigated the internalisation activity of recombinant tau-GFP11, I next wanted to apply the same approach experimented in HEK293 cells, by producing neuron-secreted tau-GFP11 and applying the conditioned media to the primary neuronal cultures.

Due to low transfection efficiency of primary cortical neurons, I sought to produce lentiviral particles encoding tau-GFP11 (1N4R and 1N4R-P301S) in order to have widespread expression of tau throughout the culture. In this way, I would have the greatest chance of collecting the highest amount of neuronally secreted tau-GFP11. In Figure 5.8 I have displayed representative images of primary cortical neurons transduced at DIV 5 with 1N4R-GFP11 tau both via live imaging (Fig 5.8A) and by immunocytochemistry (Fig 5.8B). The widespread expression of both 1N4R and 1N4R-P301S tau in the primary cortical cultures was confirmed via western blotting where an α-Flag antibody was used to probe for tau-GFP11 (Fig 5.8C). Consequently, transduction of tau-GFP11 was used in the following experiments.

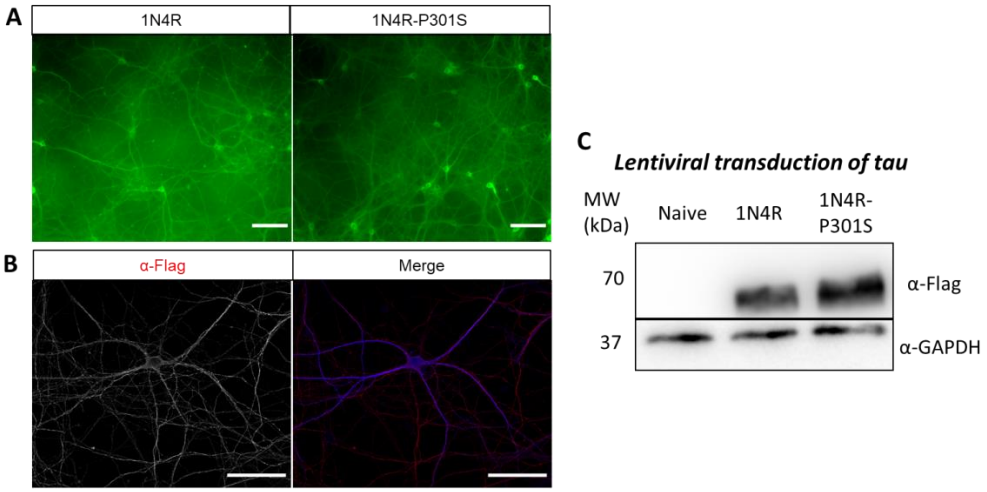

Fig 5.8 – Tau-GFP11 expression in primary cortical neurons. DIV 5 cortical neurons transduced with tau-GFP11 encoding lentivirus.

(A) Co-expression of 1N4R or 1N4R-P301S-GFP11 with GFP1-10. GFP positive neurons detected two days post-transduction. Scale bar, 100 µm. Experiment repeated with 2 biological replicates, achieving similar results.

(B) Expression of tau-GFP11 in DIV 18 neurons, neurons stained with α-Flag antibody (Mouse) (Alexa Fluor 555) to probe for tau-GFP11. Neurons were also stained with α-MAP2 (guinea pig) (Alexa Fluor 405), shown in merge. Scale bar, 50 µm.

(C) Immunoblot confirming transduction of primary cortical neurons (DIV 18) with lentivirus-encoding either 1N4R or 1N4R-P301S tau-GFP11 using α-Flag antibody.

I then adopted the basic experimental set-up optimised in HEK293 / N2a cell lines. Two groups of primary cortical neurons were transduced at DIV 5 with either tau-GFP11 or GFP1-10; 24 h later a 50 % media change was conducted. By DIV 8-10 media containing tau-GFP11 was transferred to GFP1-10 expressing neurons (DIV8-10) and monitored over seven days by live imaging and immunocytochemistry. In Figure 5.9 there is a representative image from live confocal imaging that displays primary cortical neurons positive for GFP. When these neurons were fixed for immunocytochemistry, α-Flag and α-GFP antibodies confirmed the presence of tau-GFP11 and GFP1-10 respectively in GFP positive neurons, suggesting that tau-GFP11 had been internalised (Fig

5.9, top panel). However, given previous experience with potential effect of Lipofectamine 3000 leading to co-expression of the two split-GFP domains in HEK293 cells, I wanted to ensure that a similar phenomenon was not occurring due to lentiviral expression. Since only 50% of the media was swapped post-transduction to promote neuronal viability, there was a risk that residual lentiviral particles were still present in media leading to co-transduction in the GFP1-10 expressing neurons.

As such I conducted the reverse experiment by transferring conditioned media from GFP1-10 expressing neurons and applying to tau-GFP11 expressing neurons. Given that GFP1-10 should not get secreted from neurons, any positive GFP signal would indicate the presence of residual lentiviral particles present in the conditioned media leading to co-transduction. In the bottom panel of Figure 5.9 it can be seen that media taken from GFP1-10 expressing neurons did in fact contain residual lentiviral particles, as the recipient tau-GFP11 expressing neurons are positive for GFP1-10 and display a robust reconstituted GFP signal visible upon 488 nm light excitation.

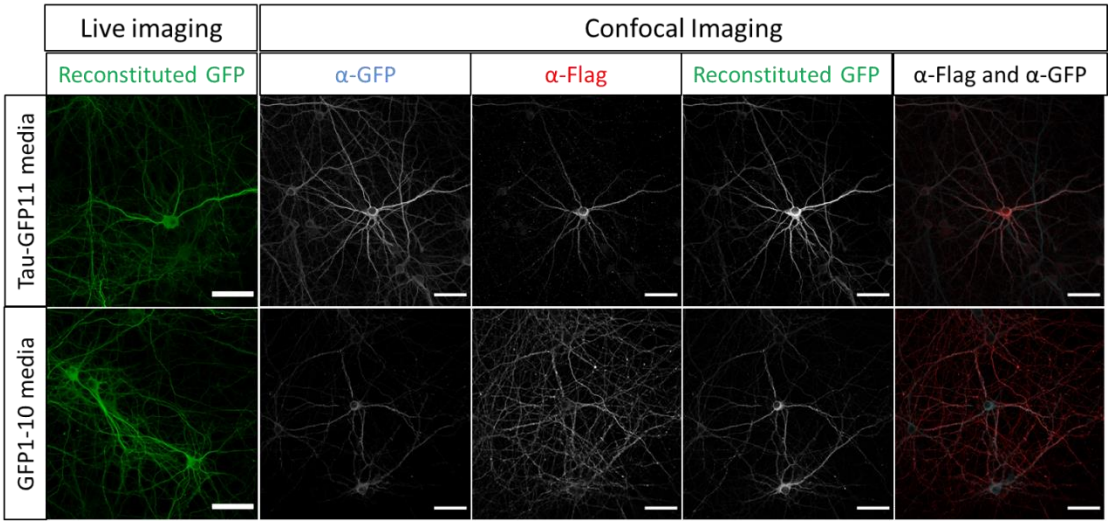

Figure 5.9 – Long-term treatment of cortical neurons with conditioned media from neurons expressing either tau-GFP11 or GFP1-10. Primary cortical neurons (DIV8-10) expressing either GFP1-10 (*top panel*) or tau-GFP11 (*bottom panel*) were incubated with media taken from neurons expressing tau-GFP11 or GFP1-10 respectively for six days. Live imaging with LSM 880 confocal microscope confirms detectable GFP signal in the 488 channel in both conditions. The presence of both tau-GFP11 and GFP1-10 was confirmed using α-Flag (mouse) (Alexa Fluor 555) and α-GFP (chicken) (Alexa Fluor 647) antibodies respectively. Neurons were also stained α-MAP2 (guinea Pig) (Alexa Fluor 405). Scale bar, 50 µm. Experiment repeated with 2 biological replicates, achieving similar results.

An additional control was included whereby DIV 5 neurons were transduced with EGFP. 24 h later 50 % media change was conducted, by DIV 8-10 conditioned media from neurons expressing EGFP was transferred to naïve neurons. This experiment generated high levels of positive GFP signal upon transfer to naïve neurons confirming that conditioned media after transduction contains residual lentiviral particles still capable of efficient transduction (Fig 5.10).

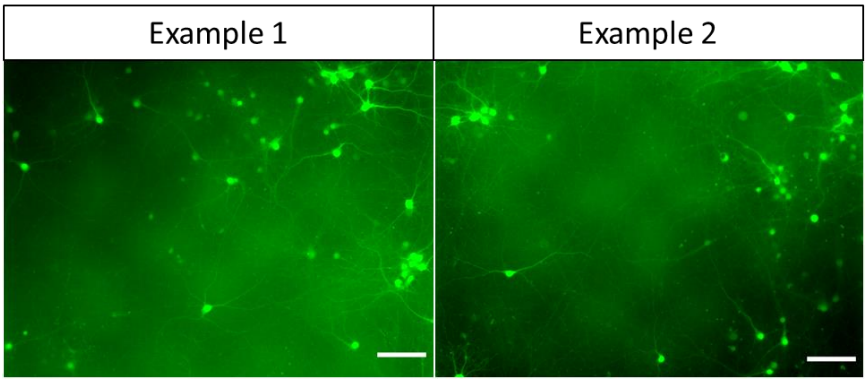

Figure 5.10 – Long-term treatment of cortical neurons with conditioned media from neurons expressing EGFP. Naïve primary cortical neurons (DIV 8-10) were incubated with conditioned media taken from neurons transduced with EGFP and monitored over six days on the Incucyte. Two examples of representative images taken on the 6th day of observation. Scale bar, 100 µm. Experiment repeated with 2 biological replicates, achieving similar results.

Overall, this set of experiments demonstrated that the 50 % media change 24 h post-transduction was not sufficient to eliminate residual lentiviral particles which, in turn were responsible for the co-transduction of the split-GFP domains. Following this test, I changed the protocol to carry out 100 % media change 24 h post-transduction to ensure no live lentiviral particles would remain in the media. Unfortunately, with this revised protocol, I observed no neurons positive for GFP following the incubation with conditioned tau-GFP11 media, despite positive GFP1-10 expression (Fig 5.11).

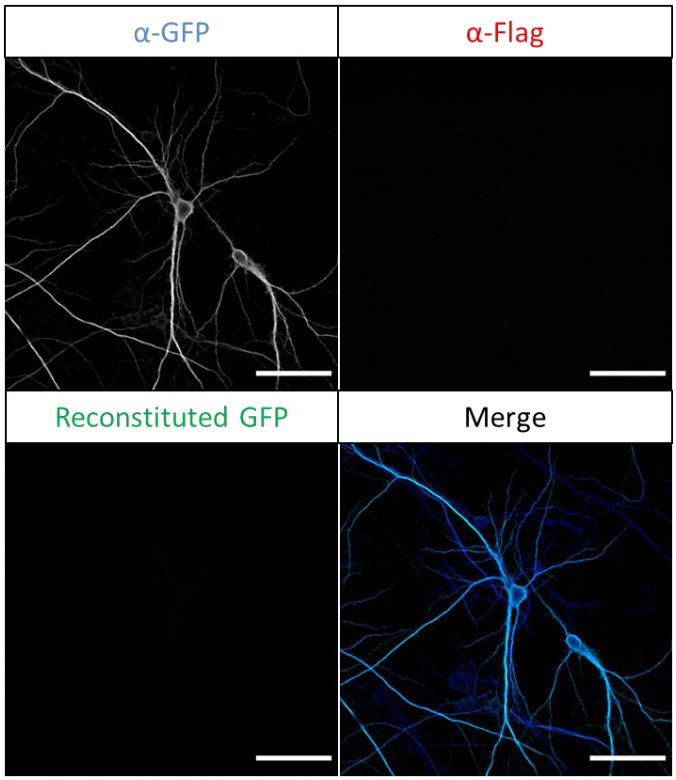

Figure 5.11 – Treatment of GFP1-10 expressing cortical neurons with tau-GFP11 media. Primary cortical neurons (DIV8-10) expressing GFP1-10 were incubated with media taken from neurons expressing tau-GFP11 for six days. Imaging with LSM 880 confocal microscope reveals no tau-GFP11 (probed for with α-Flag mouse antibody, Alexa Fluor 555) and consequently there is no GFP reconstitution signal in the 488 channel. The presence of GFP1-10 was confirmed using α-GFP chicken antibody (Alexa Fluor 647). Neurons were also stained α-MAP2 guinea pig antibody (Alexa Fluor 405). Scale bar, 50 µm. Experiment repeated with 2 biological replicates, achieving similar results.

Moreover, there was no detectable α-Flag signal, which suggested either there was no tau-GFP11 internalised in the neurons (or that tau could not be detected by immunocytochemistry), or low levels of tau-GFP11 in the conditioned media (Fig 5.11). To verify that the conditioned neuronal media contained tau-GFP11 I utilised the ELISA that was successfully optimised for HEK293 culture medium to test whether I could detect tau secreted from primary cortical neuron. Figure 5.12 demonstrates the absorbance values at 450 nm excitation of the recombinant 1N4R tau standard curve, alongside the culture media samples

taken from naïve neurons or neurons expressing either 1N4R or 1N4R-P301S tau.

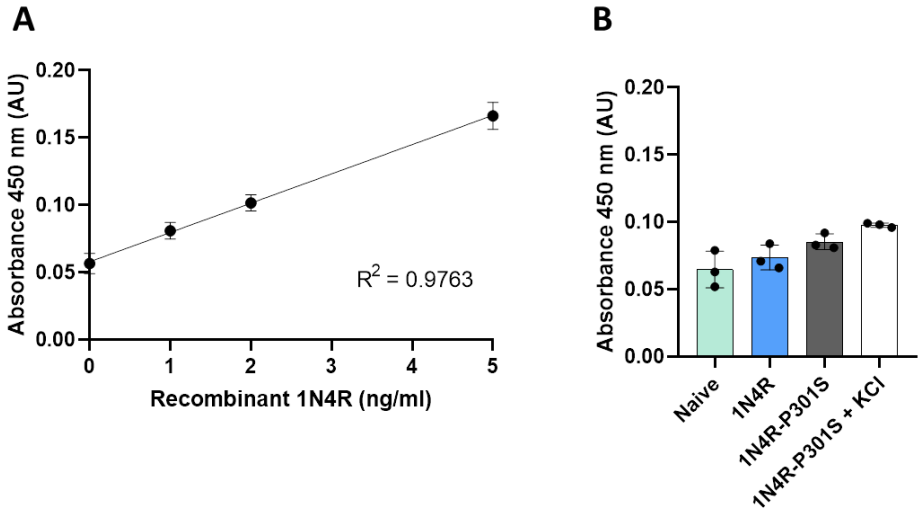

Figure 5.12 – ELISA assay to determine tau concentration secreted from primary cortical neurons.

(A) Scatter plot displaying absorbance values at 405 nm for each known concentration of recombinant 1N4R-tau-GFP11. Values are displayed with the best fitting regression line and the correlation coefficient R^2.

(B) Bar chart displaying absorbance values at 405 nm for culture media samples taken from naïve cortical neurons and neurons expressing 1N4R or 1N4R-P301S (± 30 mM KCl treatment to stimulate tau secretion).

Bar and data points represent mean ± standard deviation. AU, arbitrary units.

This representative bar graph displays how little secreted tau there was in the media compared with control conditions. Furthermore, when quantifying the concentration of tau secreted from HEK293 cells it ranged on average between 50 – 200 ng/ml for all isoforms (Fig 3.9B). However, from primary cortical neurons, the concentration of tau in the media appears 50 – 100 fold lower, falling in the 1 – 2 ng/ml range (Fig 5.12), which corresponds more closely with reported values of human CSF tau levels (Blennow et al., 1995; Olsson et al., 2005).

Since it is widely reported that neuronal stimulation triggers tau secretion (Pooler et al., 2013) I wanted to test whether stimulation by potassium chloride (KCl, 30 mM) would enhance the release of tau. From the data shown in Figure 5.12 it appears that the KCl treatment evoked a small increase in tau release (Fig 5.12) but this increase was not considered big enough to make a considerable difference for the split-GFP cytosolic translocation assay. It may be that in this experimental setup the secreted tau is internalised by the neurons in the same well, therefore the overall levels of tau in the extracellular media will remain relatively stable.

These data suggest that cultures of primary cortical neurons would not supply enough secreted tau to reach the detection limits of the split-GFP assay. Consequently, I decided to change my approach and utilise HEK293 cells as an alternative source of secreted tau, since this had been previously successful in both HEK293 and N2a cells.

5.2.5 Testing functionality of HEK293 cell-secreted tau-GFP11 in primary cortical neurons

First, I decided to trial three different HEK293 culture media containing either 0, 1, or 10% FBS over a 24 h period to test whether neurons could endure this change of conditions over a short time period. From this test, I found that the less FBS present within the media the more resistant the neurons were, however by 24 h all conditions had high level of neuron death (Fig 5.13). Consequently, I did not think collecting tau in HEK293 cell culture media would be the best approach to pursue.

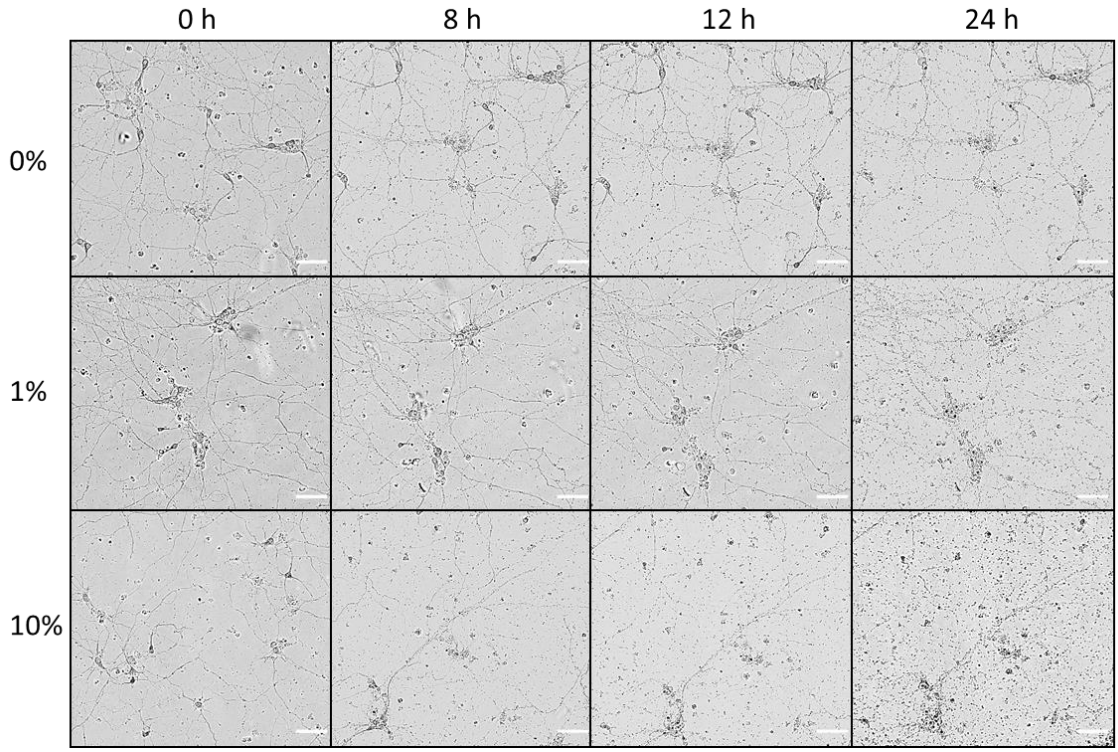

Figure 5.13 – Treatment of primary cortical neurons with HEK293 cell culture media. DIV 6 cortical neurons incubated with HEK293 cell media containing either 0, 1, or 10% fetal bovine serum and monitored over 24 h.
By 24 h all three conditions have resulted in neuronal death. Scale bar 100 µm. Experiment repeated with 2 biological replicates, achieving similar results.

Given that HEK293 cells are in general more resilient than primary cultures, I decided to culture tau-GFP11 expressing HEK293 cells in primary neuronal culture medium. In this way, after the 48 h time period allowed for tau secretion, the media transferred to cortical neurons would be in principle compatible with primary cultured neurons.

I first wanted to check whether the levels of tau secreted from HEK293 cells would be altered in these different culture conditions. To directly compare between primary neuronal media and regular HEK293 cell media, I carried out the ELISA with recombinant 1N4R tau resuspended in both media types alongside both culture media samples, to accurately compare tau levels.

This ELISA demonstrated that the change in media affected the overall absorbance value of the proteins present in the sample. In the neuronal media the same concentration of recombinant 1N4R tau, generated lower absorbance values when compared with HEK293 cell culture media (Fig 5.14A, B). Yet, when calculating the average secreted tau concentration in both culture media samples, they were equivalent for both 1N4R and 1N4R-P301S tau ranging between 100 - 150 ng/ml (Fig 5.14 C, D).

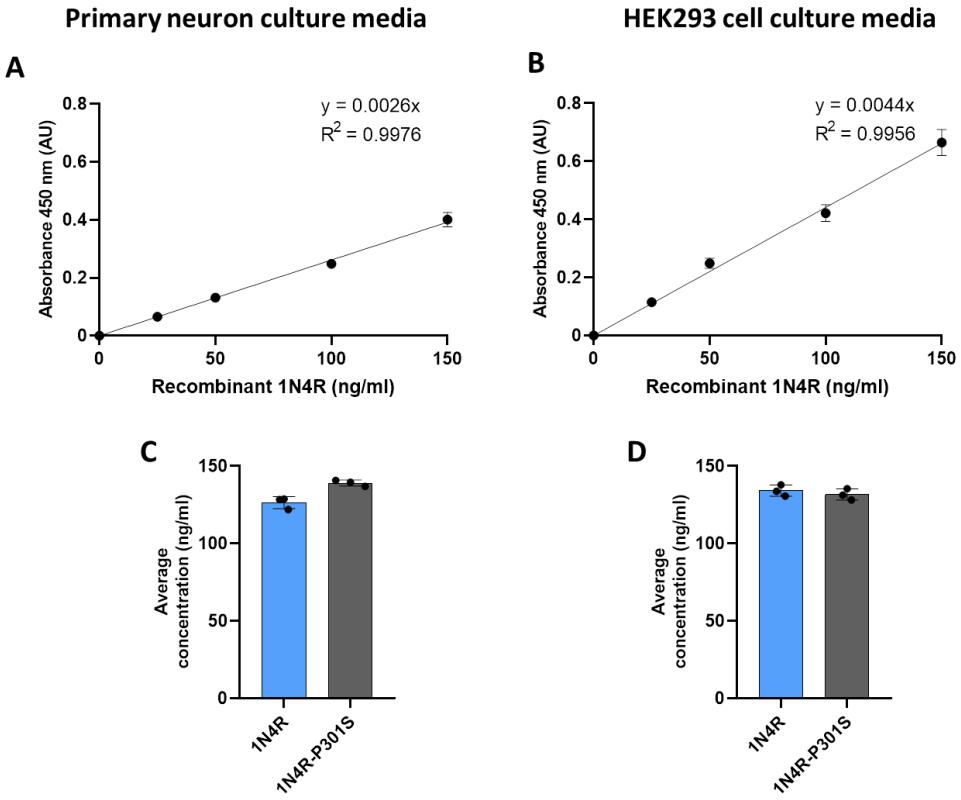

Figure 5.14 – Comparison of tau concentration secreted from HEK293 cells cultured in cell line or primary neuronal media.

(A, B) Scatter plot data displayed with best fitting regression line, equation of line and the correlation coefficient R^2 for each known concentration of recombinant 1N4R-tau-GFP11 resuspended in primary neuronal media (A) or cell line media (B).

(C) Bar chart displaying concentration obtained for 1N4R and 1N4R-P301S using the standard curve shown in A.

(D) Bar chart displaying concentration obtained for 1N4R and 1N4R-P301S using the standard curve shown in B.

Bar and data points represent mean ± standard deviation. AU, arbitrary units.

To ensure that the tau secreted was competent for cytosolic translocation, I transferred the primary neuronal media containing tau-GFP11 from HEK293 cells onto GFP1-10 expressing HEK293 cells. While the overall percentage of HEK293 cells displaying GFP reconstitution appears lower than when this experiment is conducted under normal conditions (Fig 5.15B), the cells which have internalised tau-GFP11 from the neuronal conditioned media displayed a similar intensity and localisation of signal (Fig 5.15A), as previously described in Chapter 3, Figure 3.5.

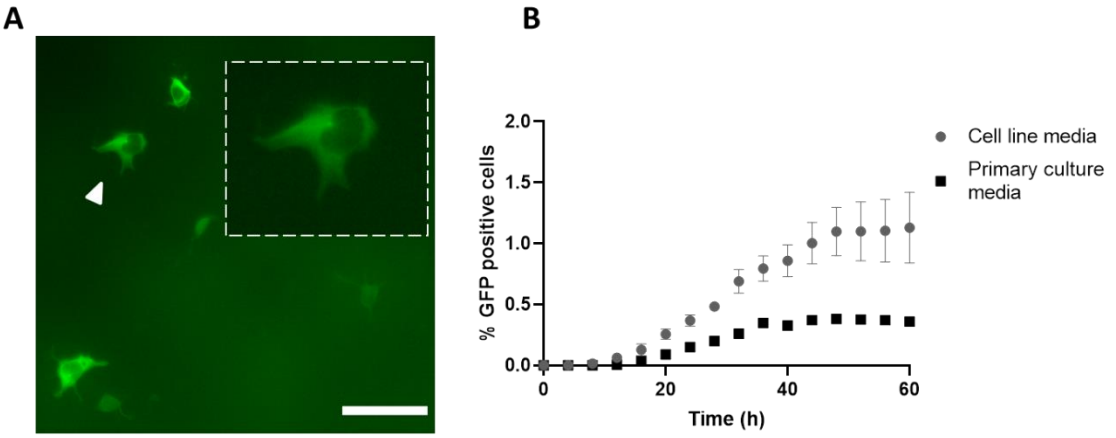

Figure 5.15 – Internalisation of tau-GFP11 secreted from HEK293 cells cultured in primary culture media.

(A) Live imaging of HEK293 cells expressing GFP1-10 incubated with tau-GFP11 media taken from HEK293 cells cultured in primary neuronal culture media; fluorescence monitored in the Incucyte. Scale bar, 50 µm.

(B) Quantification of percentage of GFP positive cells over time between original cell line media (n = 4) versus primary culture media (n = 1, biological replicates). Data points represent mean ± SEM.

I hypothesized that the reason for the lower GFP reconstitution rate in HEK293 cells was due to the foreign culture conditions which in turn may affect the efficiency of tau uptake in HEK293 cells. It is possible that the different culture media will affect the cell cycle which in turn alters endocytosis (Santos and

Boucrot, 2018), resulting in fewer number of cells in the correct “ON” state for tau internalisation. Consequently, I decided to pursue this methodology for primary cortical and hippocampal neurons to test the split-GFP based cytosolic translocation assay.

First, I confirmed that neurons could tolerate the conditioned media from HEK293 cells in the absence of tau-GFP11 with no overt neuronal death after one week of incubation (Fig 5.16). Subsequently, I transferred 1N4R and 1N4R-P301S tau containing media from HEK293 cells to GFP1-10 expressing neurons and incubated over six days. GFP reconstitution was monitored by live imaging with the Incucyte (Fig. 5.16). Over the six days there was no positive GFP reconstitution for either 1N4R or 1N4R-P301S tau.

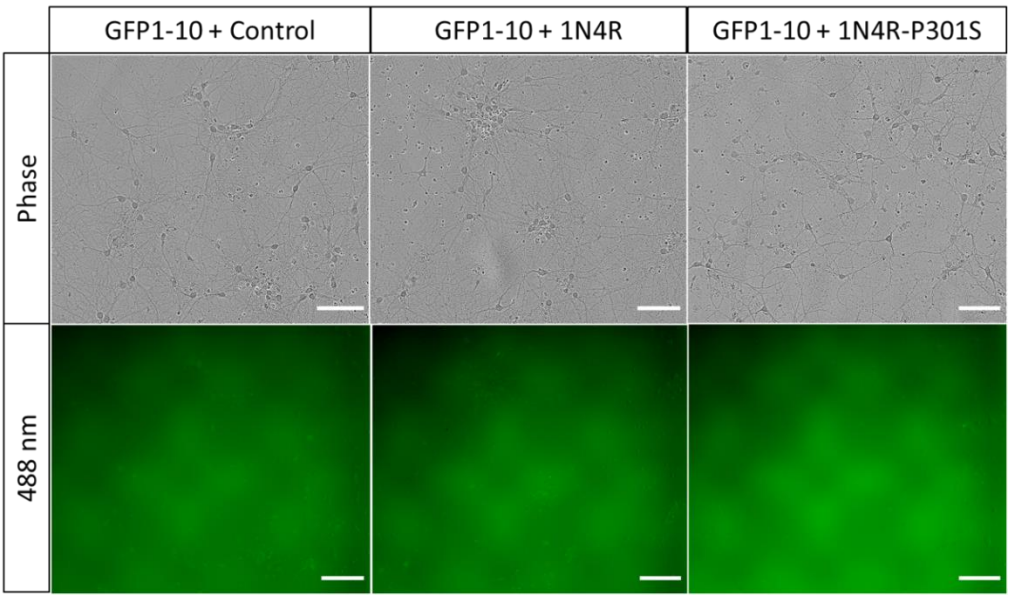

Figure 5.16 – Treatment of primary cortical neurons with tau-GFP11 containing media from HEK293 cells.
Primary cortical neurons (DIV 8-10) expressing GFP1-10 were incubated for six days with conditioned media taken from HEK293 cells cultured in primary neuronal media, expressing either 1N4R or 1N4R-P301S tau-GFP11. Phase-contrast (*top panel*) and 488 nm channel (*bottom panel*) images displayed from the Incucyte. No GFP reconstitution was detected, 488 nm excitation of culture dish has given rise to background pattern. Scale bar, 100 µm. Experiment repeated with 3 biological replicates, achieving similar results.

Since I had previously detected tau uptake with only one hour of treatment, I decided to apply tau-GFP11 media collected from HEK293 cells for one hour and then replace with conditioned neuronal media, to maximise the health of the neurons. However, given that the concentration of secreted tau-GFP11 is much lower than recombinant tau, I decided to stimulate the recipient GFP1-10 expression neurons with bicuculline 50 µM and 4-AP 2.5 mM in the presence of tau-GFP11 in attempts to promote neuronal uptake of tau, as it is reported that tau propagation is promoted by neuronal stimulation (Wu et al., 2016). The media was then swapped with tau-GFP11 containing media or conditioned neuronal media (no tau-GFP11) with no further stimulation.

In the condition where tau-GFP11 containing media returned to the culture, there was no GFP reconstitution and no significant detection of tau-GFP11 (data not shown). However, when swapping back with the conditioned neuronal media, and conducting immunocytochemistry, after six days I detected α-Flag positive puncta within the neurons, but still no GFP reconstitution. Figure 5.17A demonstrates a representative image of a primary cortical neuron with tau-GFP11 puncta detected by an α-Flag antibody. When compared with GFP1-10 neurons stimulated in the absence of tau-GFP11 media, there appeared to be an increase in the percentage of neurons positive for tau-GFP11, albeit not significant. This was seen for both 1N4R (Fig 5.17B) and 1N4R-P301S (Fig 5.17C).

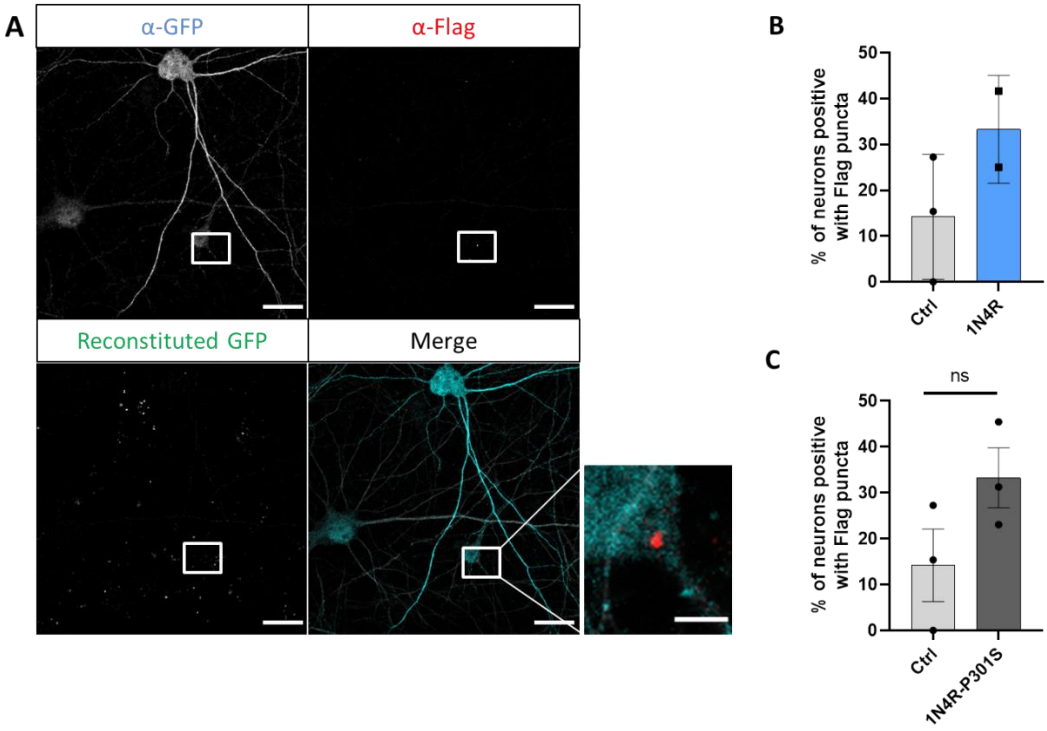

Figure 5.17 – Secreted tau-GFP11 uptake in primary cortical neurons.
GFP1-10 expressing neurons DIV (8-10) were stimulated for 1 h with bicuculline 50 µM and 4-AP 2.5 mM in the presence of tau-GFP11 containing media. After treatment media was swapped to conditioned neuronal media

(A) Representative image of GFP1-10 expressing neuron (GFP1-10 probed with α-GFP chicken antibody, Alexa Fluor 647) with α-Flag (mouse) positive puncta in the soma, indicative of tau-GFP11 uptake (Alexa Fluor 555). No genuine reconstituted GFP was detected, only autofluorescence of debris. Neurons also stained with α-MAP2 (guinea pig (Alexa Fluor 405), shown in the merge image. Scale bar, 20 µm, cropped inset scale bar, 5 µm.

(B) Bar chart of percentage of GFP1-10 neurons positive for α-Flag puncta of 1N4R tau. (n = 2, biological replicates) Bar and data points represent mean ± standard deviation.

(C) Bar chart of percentage of GFP1-10 neurons positive for α-Flag puncta of 1N4R-P301S tau (n = 3, biological replicates). Bar and data points represent mean ± SEM.

Despite detecting tau-GFP11 within neurons expressing GFP1-10, there was no reconstitution of GFP signal. Given that the signal is punctate and not cytosolic, it is likely that tau-GFP11 has remained encapsulated within a membrane-bound organelle and therefore will not come into contact with the GFP1-10. Given the reports that *in vivo* models of AD display hyperactive cortical neurons

(Busche and Konnerth, 2016), I wanted to test whether this excited cortical state would enhance the ability for tau internalisation. In an attempt to drive the system, I decided to test mild chronic stimulation with 4-AP (> 24 h) of primary cortical neurons in the presence of tau-GFP11 containing media. In this experimental set up, the neuronal survival was extremely low, and therefore did not prove a viable method (data not shown).

As an alternative strategy, I tested whether preventing tau protein degradation by inhibiting the proteasome using MG–132 (100 nM) would enable detection of the reconstituted GFP signal. By increasing the cytosolic pool of tau-GFP11 following endocytosis, I hypothesized that this increase in tau levels would surpass the detection limit with GFP1-10, to allow a more efficient reconstitution of the split GFP domains in the cytosol. By using the same experimental setup, recipient GFP1-10 expressing neurons (DIV 8-10) were stimulated with 4-AP (2.5 mM) with or without MG-132 (100 nM) and incubated with tau-GFP11 containing media from HEK293 cells for four hours. Conditioned neuronal media were then returned to the primary cortical cultures expressing GFP1-10, prior to live imaging with the LSM 880 confocal microscope. Unfortunately, neither the neuronal stimulation alone, nor stimulation in the presence of MG-132 improved the conditions for detecting cytosolic translocation of tau with the split-GFP tool (Fig 5.18).

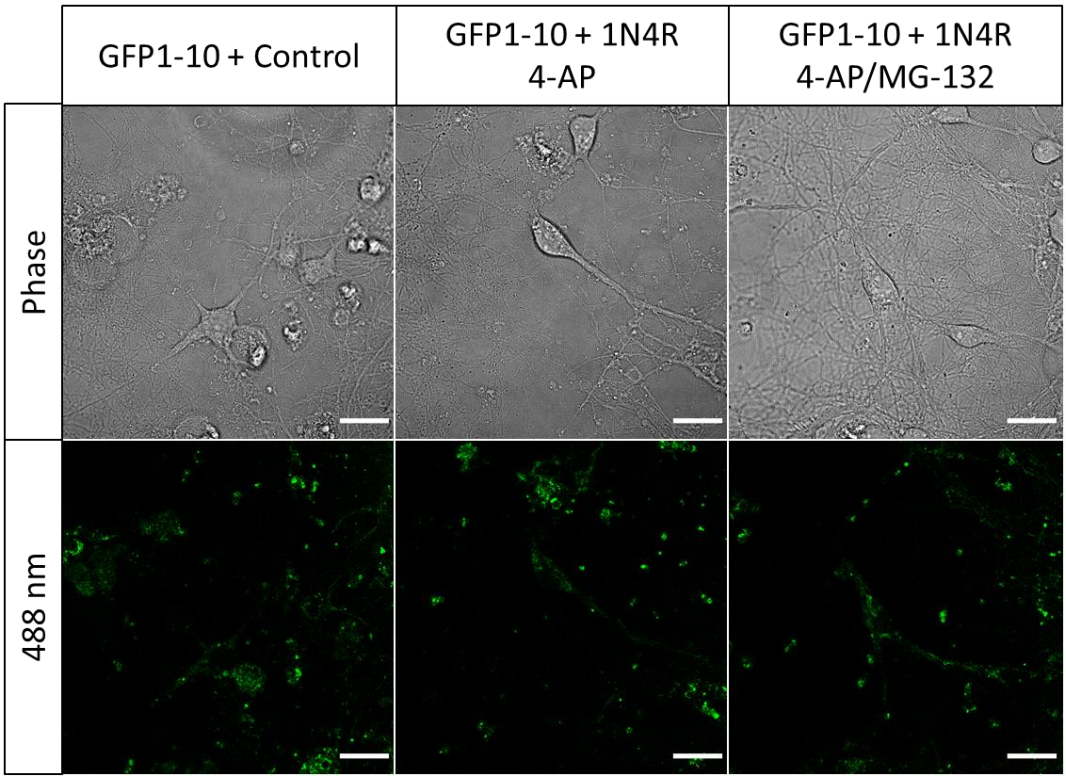

Figure 5.18 – Investigating the effect of neuronal stimulation and proteasomal inhibition on cytosolic translocation of tau. GFP1-10 expressing primary cortical neurons (DIV 8-10) treated for 4 h with 4-AP (2.5 mM) with or without MG-132 (100 nM) in the presence of secreted tau-GFP11 from HEK293 cells. Phase-contrast (*top panel*) and 488 nm channel (*bottom panel*). No GFP reconstitution was detected in the experimental conditions, only autofluorescence of debris and from GFP1-10 expressing neurons. Scale bar 20 µm. Experiment repeated with 2 biological replicates, achieving similar results.

5.2.6 Evaluating the use of microfluidic chambers for studying cytosolic translocation of tau

In parallel to the work investigating tau uptake in primary neurons in mass culture, I was also interested in studying the internalisation of tau at specific neuronal sites and investigating unidirectional transfer of tau. MFCs are a well-established tool used to achieve compartmentalisation of neuronal cultures. MFCs are composed of two chambers typically named “somatic” and “axonal” according to where neurons are plated. These chambers are commonly connected by straight microgrooves, which ensure fluidic isolation between the

two main chambers. In the case of plating two neuronal populations, one in the somatic and one in the axonal compartment, which are connected by straight microgrooves, the axons of neurons plated in the “axonal” compartment will be susceptible to grow back through the microgroove, thus making it difficult to assess unidirectional transfer of tau from one neuronal population to another. In collaboration with Dr. Andrea Serio, The Francis Crick Institute, London UK, we designed a novel microgroove structure adapted from Galdkov et al. (2017) to promote unidirectional growth of axons from the somatic to the axonal compartment (Gladkov et al., 2017).

Figure 5.19A display both microgroove designs, the traditional straight microgrooves and the newly developed triangular “zig-zag” microgrooves. The triangular microgrooves have been designed to have the optimal balance between promoting forward axonal growth whilst preventing back propagation of axons from neurons plated in the axonal compartment; moreover the axons will experience low and high levels of resistance for forward and backward growth respectively. As such, this should provide a useful setup to obtain reliable directional neuronal networks.

Maintaining fluidic isolation between the somatic and axonal compartment is critical to ensure there is no passive diffusion between the compartments, but rather a genuine neuron-to-neuron transmission. Furthermore, the ability to target a single population of neurons in one compartment for protein expression via lentiviral transduction, without affecting the second population is critical for the study of tau transfer. Fluidic isolation in the straight microgroove MFCs was maintained by keeping the difference in volume between somatic and axonal

compartments greater than 50 µl, as previously established by the Schiavo laboratory. When this was tested with the triangular MFCs, 50 µl was not sufficient to maintain fluidic isolation (data not shown). Figure 5.19 demonstrates the test using Coomassie blue R250 as the visual aid for fluid flow. When keeping the volume difference greater than 150 µl, whereby 100 µl of Coomassie blue R250 was counter-balanced with 250 µl of water, there was no flow of Coomassie blue R250 into the neighbouring compartment over 12 h of incubation (Fig 5.19B, C). Importantly, when applying 250 µl of Coomassie blue in the somatic compartment over the same time period, there was clear flow into the water filled compartment, as seen by the presence of Coomassie within the microgrooves and axonal compartment (Fig 5.19D).

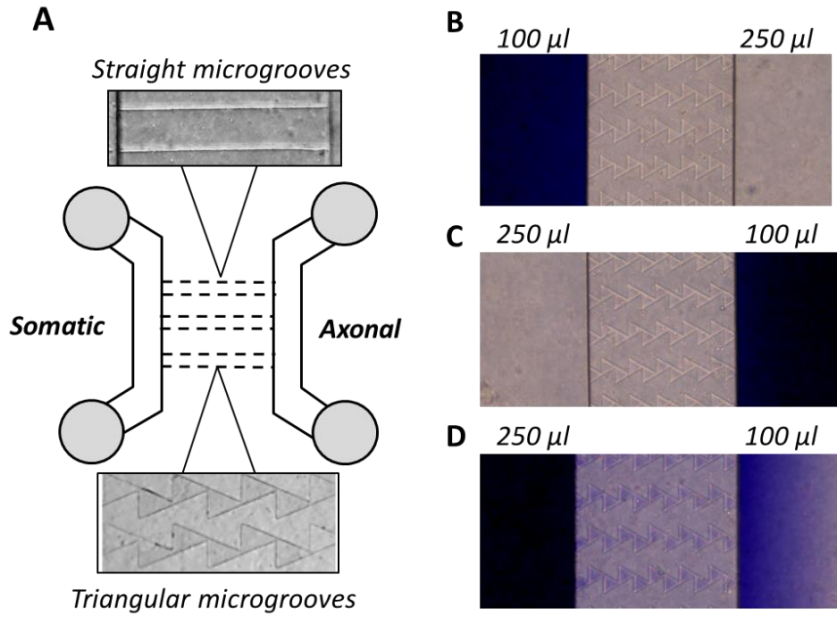

Figure 5.19 – Microfluidic chambers with microgrooves promoting unidirectional axon growth for two neuronal populations.

(A) Schematic of MFCs displaying two microgroove designs, typically one mould has 100 microgrooves and each microgroove is separated by 60 µm: Straight (500 µm in length, 10 µm in width and 3 µm in height) and triangular "zig-zag" (520 µm in length, 50 µm equilateral triangles, and 5 µm in height).

(B,C) Fluidic isolation demonstrated by the addition of Coomassie Blue R250 and water in somatic or axonal compartment. 150 µl volume difference prevents flow of Coomassie Blue from somatic (B) or axonal (C) compartment, after 12 h incubation.

(D) In contrast, clear flow was observed by applying 250 µl of Coomassie Blue in the somatic compartment.

Experiment repeated twice, achieving similar results.

Next, I conducted a trial experiment by plating neurons in either the somatic or axonal compartment expressing EGFP, in this way I could monitor the forward and back axonal growth respectively (Fig 5.20A). This triangular design contains 11 triangles making up each microgroove, therefore I counted how many triangles each axon had crossed within every microgroove in the MFC. In this way I could assess the extent of forward and backward axonal extension. Importantly, it was seen that when neurons were plated in the axonal compartment, no axon reached over halfway (six triangles), with the majority of

axons reaching up to three triangles. In contrast when neurons were plated in the somatic compartment, almost 100% of the axons successfully crossed the channels to reach the axonal compartment (Fig 5.20B). This confirmed that the "zig-zag" triangular design was able to promote unidirectional axonal growth.

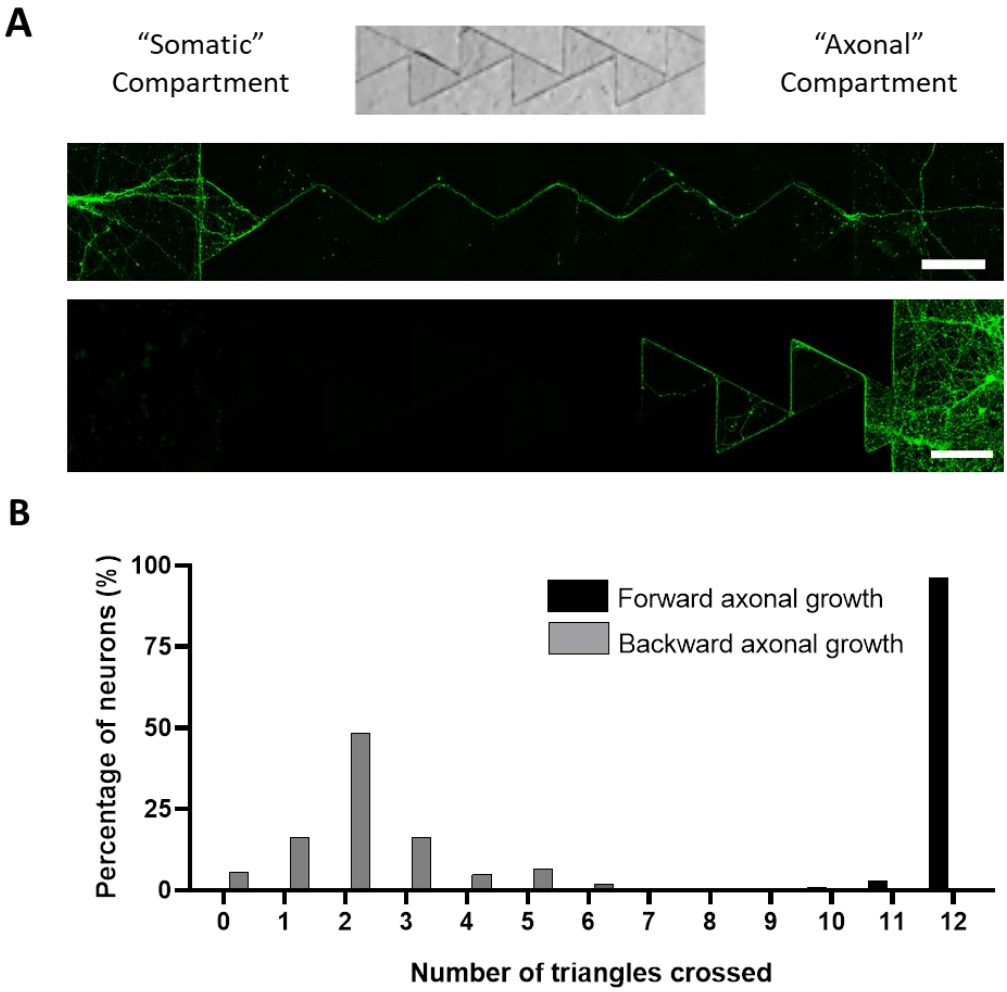

Figure 5.20 – Evaluating the unidirectional axonal growth in MFCs.

(A) Representative images of triangular "zig-zag" MFCs plated with neurons expressing EGFP. (*Top panel*) Axons from neurons plated in somatic compartment have successfully reached the axonal compartment; (*Bottom panel*) axons from neurons plated in axonal compartment do not cross the microgrooves. Scale bar, 50 µm.

(B) Quantification of the percentage of neurons that reach each individual triangle as a measure of axonal extension. Overall, the majority of axons undergoing backward growth will cross three triangles, while during forward axonal growth almost 100% will successfully cross into next compartment. n = 1, biological replicate.

Having confirmed the ability of the triangular MFCs to retain fluidic isolation and to prevent backward growth of axons from neurons plated in the axonal compartment, I next sought to verify the ability to transduce a single population of neurons within the same device. Figure 5.21 demonstrates the expression of GFP1-10 in neurons plated in the somatic side, but absence of expression in neurons plated in the axonal compartment. With these controls confirmed, I was confident I could test the cytosolic translocation assay by applying tau-GFP11 containing media directly to either the soma or the axons and in addition, investigate neuron-to-neuron transmission of tau-GFP11.

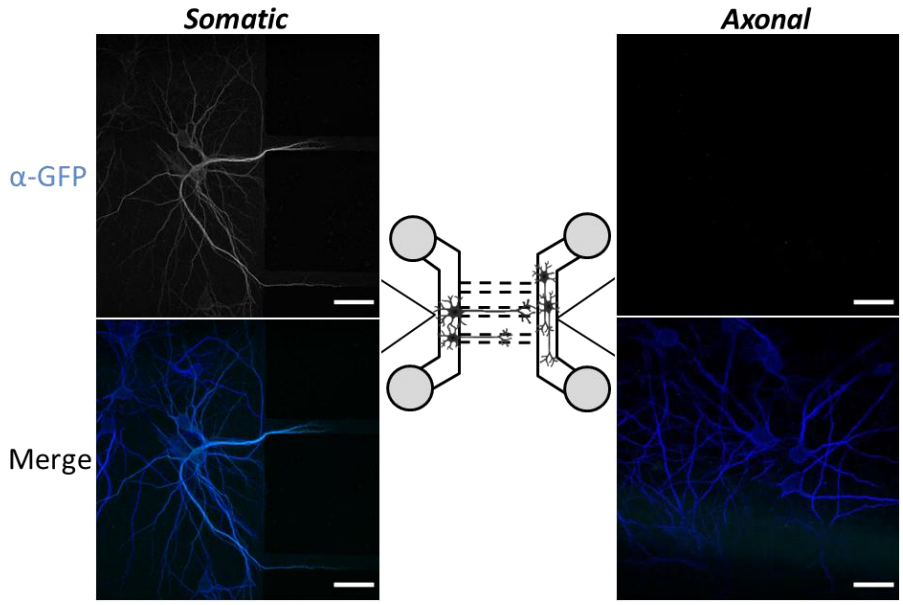

Figure 5.21 – Transduction of single population of neurons between two cultured networks. Representative image of positive GFP1-10 expression (α-GFP chicken antibody, Alexa Fluor 647) in the somatic compartment following lentiviral transduction, confirming fluidically isolated microenvironment; no neurons in the axonal compartment were positive for GFP1-10. Neurons were also stained with α-MAP2 guinea pig antibody (Alexa Fluor 405). Scale bar, 30 µm. Experiment repeated with 3 biological replicates, achieving similar results.

Earlier in this chapter I described how neurons expressing tau-GFP11 secrete low levels of tau-GFP11 into the media. However, I wanted to test whether

having both populations of neurons expressing either tau-GFP11 or GFP1-10 within the same culture dish would heighten the chance for neurons to internalise secreted tau. The theory of trans-synaptic spread of tau predicts that tau-GFP11 is secreted from presynaptic axonal terminals (Holmes and Diamond, 2014). Therefore, in this experimental design neurons plated in the somatic compartment were transduced with tau-GFP11 (DIV 6), and the neurons plated in the axonal compartment were transduced with a lentivirus encoding GFP1-10 (DIV 4). In this setup, the tau-GFP11 could be released from axonal terminals to undergo cytosolic translocation within GFP1-10 expressing neurons. Figure 5.22A shows two populations of neurons (DIV 14-16) expressing either split-GFP domain within the same MFC. I have highlighted the axonal compartment which contains axons expressing tau-GFP11 amongst GFP1-10 expressing neurons. However, no GFP reconstitution was detected in this experimental set-up (Fig 5.22B). This may be due to low levels of tau-GFP11 that are being secreted which are below the detection level of the adopted approach.

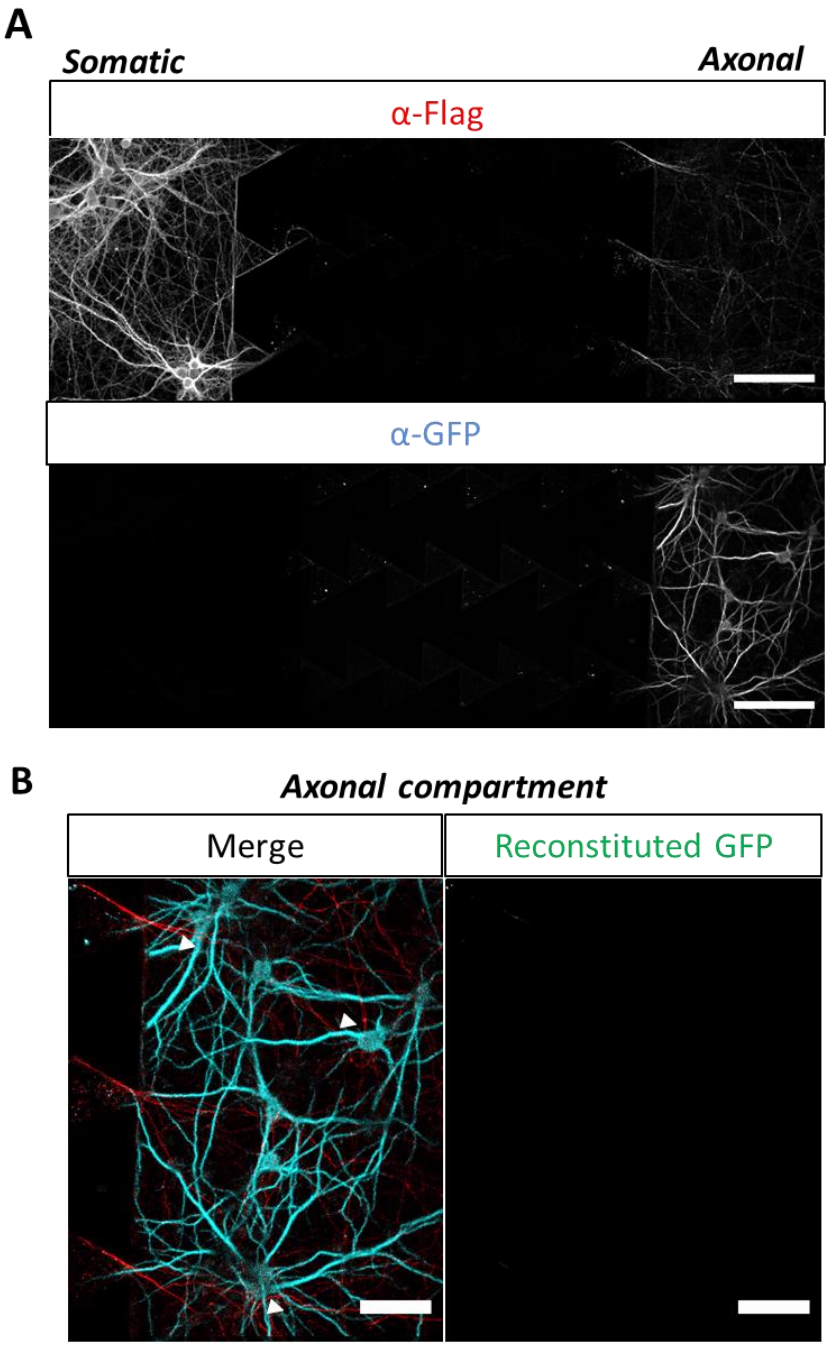

Figure 5.22 – Evaluating unidirectional MFCs for the study of trans-synaptic tau spread. DIV 14-16 primary cortical neurons transduced with GFP1-10 (DIV 4) and tau-GFP11 (DIV 6) in axonal and somatic compartment respectively.

(A) Low magnification image of MFCs with tau-GFP11 probed for with α-Flag mouse antibody (Alexa Fluor 555) and GFP1-10 probed for with α-GFP chicken antibody (Alexa Fluor 647). Neurons plated in the somatic and axonal compartment express tau-GFP11 and GFP1-10 respectively. Scale bar 100 µm.

(B) High magnification image of the axonal compartment with tau-GFP11 expressing axons mixing with GFP1-10 expressing neurons (highlighted by triangles). No GFP reconstitution was detected. Scale bar 50 µm. Experiment repeated with 2 biological replicates, achieving similar results.

To date, there have been reports that tau can be internalised both at the soma or at the axonal terminals, suggesting that tau can undergo both anterograde and retrograde axonal transport (Small and Swanson, 2018; Wu et al., 2013). Therefore, I decided to use MFCs to explore the location of tau uptake, by treating neurons with conditioned media taken from HEK293 cells expressing tau-GFP11 and applying to either the somatic or axonal compartment. Since this was an exploratory experiment I did not simultaneously stimulate the neurons. When directly applying tau-GFP11 containing media to either the somatic (Fig 5.23A) or axonal compartment (data not shown), there was no GFP reconstitution.

Given the unique ability of MFCs to compartmentalise different cell populations, I decided to plate HEK293 cells expressing tau-GFP11 in the axonal compartment in order to have on-going secretion of tau-GFP11 that would come into contact with axons from GFP1-10 expressing neurons. I have shown a representative image demonstrating axons clearly crossing the microgrooves entering the compartment containing HEK293 cells. Since transfection of HEK293 cells could not be easily conducted within the MFCs and could risk the health of the primary cortical neurons, I transfected HEK293 cells and after 48 h I split and plated the transfected HEK293 cells into the axonal compartment of the MFCs, ensuring the direction of fluidity was from the axonal to somatic compartment (Fig 5.23B). While the neurons remained healthy over three to four days, by day six there were high levels of neuronal death. However, within the first four days there was no GFP reconstitution (data not shown). While this result may not be surprising given the reports from Wu and colleagues suggesting that it takes at least six days for internalised tau to reach the cytosol

(Wu et al., 2016), it may also be that axonal terminals are not the primary source of uptake for tau.

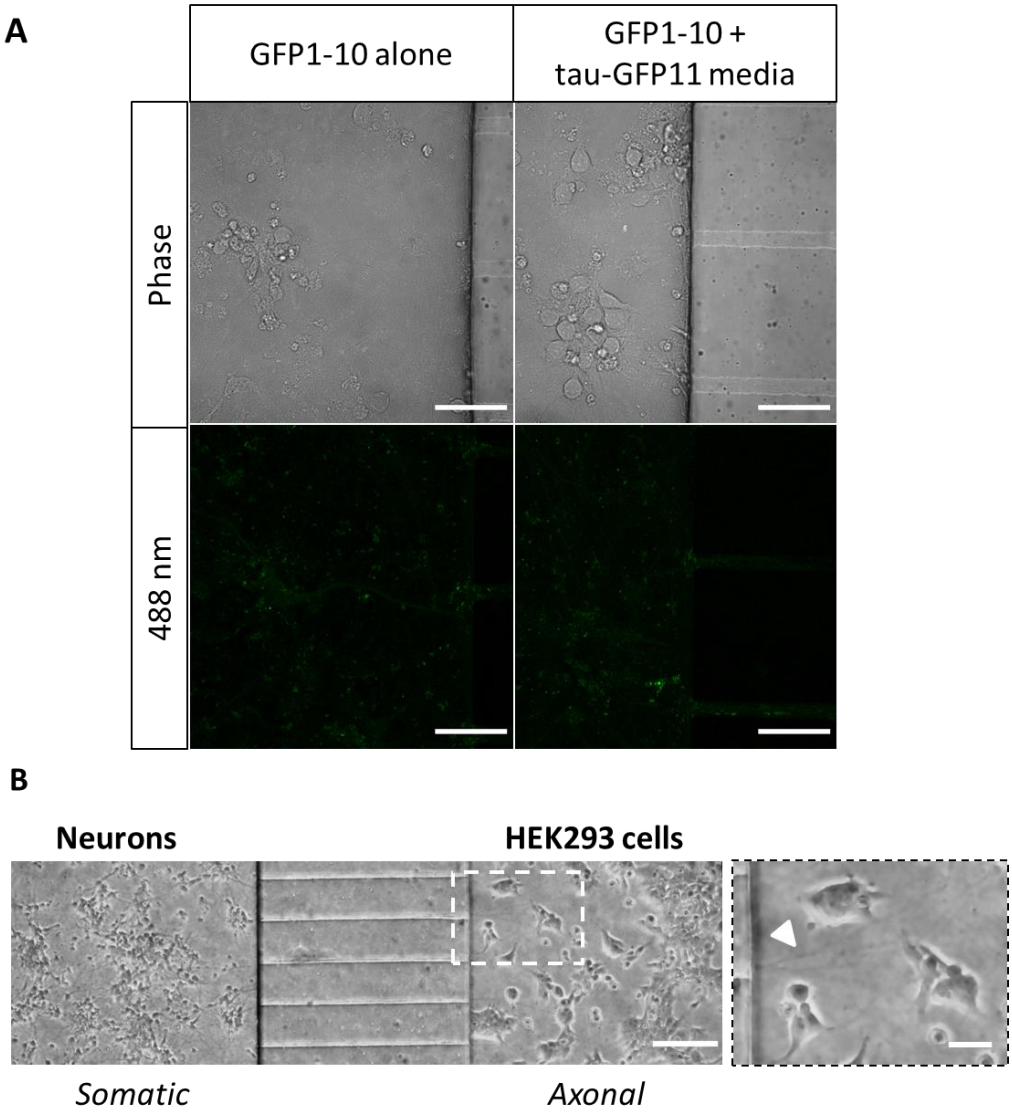

Figure 5.23 – Treatment of cortical neurons with secreted tau-GFP11 in MFCs.

(A) GFP1-10 expressing neurons (DIV 14-16) plated in the somatic compartment of MFCs, incubated in the somatic compartment with conditioned media collected from HEK293 cells expressing tau-GFP11. Live imaging conducted with LSM 880 confocal microscope 6 days post tau-treatment. Scale bar, 50 µm. Experiment repeated with 2 biological replicates, achieving similar results.

(B) Co-culture of GFP1-10 expressing neurons (DIV 14-16) and tau-GFP11 expressing HEK293 cells plated in the somatic and axonal compartment of MFCs respectively. Magnified inset displaying axons crossing into the axonal compartment containing HEK293 cells. Scale bar, 100 µm, magnified inset scale bar, 25 µm. Experiment repeated with 2 technical replicates, achieving similar results.

5.3 Discussion

In this chapter I transferred the cytosolic translocation assay optimised in HEK293 cells into primary neuronal cultures. From the data presented to date, I was unable to visualise cytosolic translocation in neurons with the split-GFP technology.

Given that the bulk of optimisation shown in previous chapters was conducted in HEK293 cells, I chose to test the system in the neuroblastoma cell line, N2a. This test demonstrated that secreted tau-GFP11 was internalised and detected by GFP1-10 expressing N2a cells which displays robust GFP reconstitution (Fig 5.1). This was an encouraging result as it confirmed that the functionality of the assay was not HEK293 specific but could be applied to different cell types.

As conducted with HEK293 cells, I first validated the functionality of the split-GFP domains in primary neuronal cultures by expression of tau-GFP11 and GFP1-10 either in isolation or concurrently. As expected, there was no major auto-fluorescence detected upon GFP11 or GFP1-10 expression. Importantly, the reconstituted GFP signal revealed by tau co-expression was detected and following fixation and immunocytochemistry was confirmed to supersede any background signal elicited by GFP11 or GFP1-10 alone (Fig 5.2). Furthermore, I carried out live imaging of all six WT tau isoforms co-transfected with GFP1-10; the cytosolic and soluble signal confirmed that the GFP11 tag did not induce any mislocalisation of tau, moreover, the reconstituted GFP signal provided discrete microtubule localisation as seen in HEK293 cells (Fig 5.3, 5.4).

To date, there have been conflicting reports regarding the timeline of tau reaching the cytosol following uptake in neurons, with data suggesting a very rapid kinetics, as quickly as one hour (Tuck et al., 2021) or up to six days (Wu et al., 2016); as such, I wanted to test tau uptake within this time range. Having produced the lentivirus for the transduction of GFP1-10 in primary neurons, I decided to first test the activity of bacterially expressed recombinant tau-GFP11. Based on the optimisation experiments conducted with HEK293 cells, I decided to use higher concentrations of recombinant tau than typically used, ranging from 0.5 to 2 µM to maximise the chance of cytosolic translocation; moreover, 2 µM is the reported concentration of tau in mature neurons, (Iqbal et al., 2010), therefore this experiment is still utilising physiologically relevant concentrations of tau. In Figure 5.6 I showed a representative image displaying clear tau-GFP11 positive puncta but no GFP reconstitution after one hour of tau treatment. As described by Wu and colleagues, this punctate signal may indicate that tau is trapped within a membrane-bound compartment (Wu et al., 2016). This could be further investigated by using antibodies targeted against components of the endocytic/endolysosomal pathway e.g. Rab5, Rab7 or Lamp1 to see if there is co-localisation with the tau signal. In parallel I incubated primary neurons with 2 µM recombinant tau-GFP11 over six days. During this time there was no detection of reconstituted GFP and by day six the culture was no longer viable (Fig 5.7). This unexpected toxicity was likely due to the high extracellular concentration of tau that can cause adverse effects in neuronal cells (Gómez-Ramos et al., 2006).

Studying tau uptake using a bacterially expressed form of tau is not a method that closely resembles physiological conditions. Cryo-EM analyses

demonstrated that recombinant tau aggregate structures do not match those obtained from human patients (Falcon et al., 2018b; Fitzpatrick et al., 2017; Zhang et al., 2019). Furthermore, in neurons it has been shown that despite globular aggregates isolated from human samples proving to be effectively internalised, similar sized recombinant aggregates formed *in vitro* were not internalised (Takeda et al., 2015), highlighting the difference between *in vivo* and *in vitro* formation of tau aggregates and the subsequent effect on tau uptake.

These findings prompted me to change approach and utilise cell secreted tau-GFP11 within primary neuronal cultures. First, I sought to transduce neurons with tau-GFP11 (1N4R or 1N4R-P301S) and then collect secreted tau within the extracellular medium and incubate with GFP1-10 expressing neurons. While this method initially gave rise to high levels of reconstituted GFP (Fig 5.9), it was later confirmed that this was due to residual lentiviral particles present within the conditioned media leading to co-transduction of GFP1-10 and tau-GFP11 rather than representing genuine cytosolic translocation. Once eliminating this possibility by conducting a full media change 24 h post transduction there was no GFP reconstitution.

Lentiviral transduction allows a widespread expression of tau-GFP11; however, at the level of the individual neuron the extent of protein expression appears lower when compared with transfection. Previous work has suggested that secretion of endogenous tau produces low levels of extracellular tau (Pooler et al., 2013), therefore it may be that in untreated conditions, i.e. in the absence of stimulation or other neuronal insults, the conditioned media will not contain high

enough levels of tau-GPF11 to give rise to a positive GFP signal upon uptake. Moreover, while it has been reported that neurons secrete full-length tau (Pooler et al., 2013), there is evidence that C-terminal truncated tau is also found in the extracellular space (Cicognola et al., 2019; Kanmert et al., 2015). As such, given the low levels of endogenous tau secretion, if a sub-population of that group has had the C-terminal truncated, the GFP11 tag will have also been eliminated impairing the assay functionality.

As an alternative, I maintained HEK293 cells expressing tau-GFP11 in primary neuronal media in order to avoid neuronal death upon transfer of culture supernatant containing tau to neurons. While this method was sufficient to avoid neuronal death even after six days of incubation with GFP1-10 neurons, there was no intracellular GFP detection. This may be due to the sub-optimal conditions in which the primary neurons are kept therefore preventing efficient protein internalisation. Since I observed that one hour incubation with recombinant tau was sufficient to detect tau-containing puncta within neurons (Fig 5.6A), I sought to try a similar approach with secreted tau-GFP11 in the presence of neuronal stimulation to promote tau propagation (Wu et al., 2016). In the absence of stimulation, there was no tau uptake detected (data not shown), however tau treatment in the presence of bicuculline and 4-AP for one hour gave rise to positive tau puncta six days post treatment (Fig 5.17). Since the α-Flag signal was punctate, it was not surprising that there was no GFP reconstitution, as this signal appearance suggests that tau is still present within a membrane-bound compartment.

I hypothesized that perhaps the turnover of tau within neurons was reducing the cytosolic pool of tau-GFP11 available for GFP reconstitution. As such, I stimulated the neurons and then added the proteasome inhibitor MG-132, to prevent degradation of ubiquitin-conjugated proteins and enhance the chances of tau-GFP11 being freed within the cytosol. From the preliminary experiment conducted I did not see any difference in the GFP signal from GFP1-10 alone or in the presence of secreted tau-GFP11. This would suggest that the lack of GFP signal is likely due to low tau-GFP11 concentration, combined with suboptimal neuronal conditions, rather than the extent of tau degradation.

As established in Chapter 2, the concentration of secreted tau present in conditioned media of HEK293 cells is ~4 nM, much lower when compared with the endogenous neuronal concentration of tau (~2 µM) used for recombinant tau experiments. As such, this may explain the necessity for neuronal stimulation to enhance the uptake of secreted tau-GFP11.

Finally, in this Chapter I discussed the testing of novel “zig-zag” triangular MFCs developed to promote unidirectional growth of axons and to investigate tau dynamics. Currently, tau transfer is typically investigated with multi-chambered MFCs connected with straight microgrooves (Dujardin et al., 2014b; Takeda et al., 2015; Wu et al., 2013). However, in the presence of straight microgrooves the risk of back axonal growth means that neurons have to be plated in sequence to ensure that a sufficient number of axons have crossed to prevent this phenomenon; consequently, the cultured neurons display different DIV differentiation. With these novel triangular MFCs, it is possible to simultaneously

plate multiple groups of neurons without extensive axonal back growth, whilst ensuring that all neurons are of the same DIV.

When applying secreted tau-GFP11 to GFP1-10 expressing neurons or by transducing two populations of neurons with either tau-GFP11 or GFP1-10 I was unable to detect reconstituted GFP. Complementary work conducted by Miss Skye Stuart, a PhD student in the Schiavo laboratory, detected tau positive puncta in recipient neurons plated in the axonal compartment, suggesting that tau is secreted from tau-expressing neurons plated in the somatic compartment. These experiments are highly encouraging since they demonstrate that it is possible to detected translocated tau using a MFC-based approach.

Since it had been established that HEK293 cells secrete high levels of tau-GFP11 and they were capable of growing in primary neuronal media, I decided to use MFCs to co-culture primary neurons and HEK293 cells. Given the small diameter of the microgrooves, HEK293 cells expressing tau-GFP11 would remain confined to the axonal compartment. While this set up was ineffective in displaying reconstituted GFP signal, I think this method should be further explored and optimised, as it is a unique approach for providing a consistent source of tau-GFP11. However, modifications to promote neuronal survival well beyond 4 to 5 days in culture in these conditions should be found and implemented.

Overall, there was limited success in investigating cytosolic translocation of tau within neurons using the split-GFP strategy. This is likely due to a combination of reasons including low levels of cytosolic tau-GFP11 or GFP1-10 expression.

Moreover, the bimolecular fluorescence complementation system appears to have low sensitivity in primary neuronal cultures requiring high levels of tau-GFP11 to be present within the cytosol, which does not seem to occur in the experimental conditions I have tested. The split-luciferase system newly developed by the McEwan lab, has demonstrated a higher sensitivity allowing the detection of low levels of recombinant tau (50 nM) entering the cytosol of primary neurons (Tuck et al., 2021). It would be interesting to assess with the split-luciferase assay whether cell-secreted tau would give rise to similar results seen with recombinant tau.

Chapter 6: Conclusions and future perspectives

The mechanism responsible for the cytosolic translocation of tau has recently become a highly discussed topic within the field of tau pathology research. While many groups have published data supporting diverse mechanisms for uptake, there are still questions regarding the process of how tau enters the cytosol upon uptake (Deinhardt, 2020). To date, few studies have directly addressed this mechanism (Chen et al., 2019; Falcon et al., 2018a; Tuck et al., 2021; Wu et al., 2016). The study presented here sought to develop a novel cell-based assay to provide a complementary strategy for the investigation of cytosolic translocation of tau and its trans-synaptic spread.

Using the split-GFP technology, I was able to detect the cytosolic entry of secreted tau-GFP11 in GFP1-10 expressing HEK293 and N2a cells. While bacterially expressed tau-GFP11 was also tested, I found that secreted tau generated a more robust GFP signal. Using the ELISA assay, I was able to test equivalent concentrations of recombinant and secreted tau-GFP11; here I found that recombinant tau did not give rise to high levels of reconstituted GFP. This was interesting, as it demonstrated that the bacterially expressed tau does not behave in the same way as cell-secreted tau. This observation has been reported previously (Takeda et al., 2015; Zhang et al., 2019) and consequently should encourage validation of current proposed internalisation mechanisms with cell-secreted or tissue extracted tau samples.

By testing all six tau isoforms, including the 1N4R-P301S mutant, I was able to detect isoform-specific differences in the propensity for cytosolic translocation.

Furthermore, I highlighted the importance of pH level dependent mechanisms, specifically via the V-ATPase proton pump, and the role of Rab GTPase activity in the cellular entry of tau. While pH and Rab GTPases have already been implicated in the cytosolic translocation of tau aggregates and vesicles containing tau seeds (Falcon et al., 2018a; Polanco et al., 2021; Tuck et al., 2021), I have now demonstrated their role for all WT isoforms of tau and the 1N4R-P301S mutant tau.

An important consideration that emerged from this work is that the cell-secreted tau-GFP11 used in these studies was not characterised, therefore it is not known whether this is free or membrane-encapsulated tau. In the future, this would be a key experiment to conduct to expand the described results of this thesis. Should tau be within an organelle, it would have to overcome at least two membrane barriers to gain access to the cytosol of the recipient cell, a phenomenon already being investigated (Polanco et al., 2021, 2016). Alternatively, this tau containing vesicle may undergo direct fusion with the plasma membrane or endocytic compartment.

Additionally, the phosphorylation state and/or conformation of secreted tau-GFP11 are currently unknown. There are reports that transient transfection of WT tau (0N3R) in HEK293 cells can lead to aberrant tau phosphorylation, as detected by α-PHF-1 antibody, which recognizes phosphorylation at ser 396 and 404 sites (Houck et al., 2016). Furthermore, by immunoblot analysis of cell lysates expressing 0N3R, tau was shown to aggregate within 24 h of transfection in the absence of seeded aggregation (Houck et al., 2016). The cytosolic translocation experiments presented in Chapters 2 and 3 were

conducted in reduced, but not depleted, serum (1 % FBS). While Houck and colleagues provided evidence to suggest that complete depletion of serum prevents the secretion of tau compared with 10 % FBS media samples, this was assessed via western blot and therefore is unlikely to be sensitive enough to detect low levels of secreted tau. Moreover, when measuring protein levels from cell media with high FBS content this can confound experimental results and affect the findings of the western blot (Houck et al., 2016). Nevertheless, this work has reported that serum depletion increases the levels of tau phosphorylation and aggregation in cell lysates (Houck et al., 2016). If the same changes in phosphorylation or aggregation are occurring in the 1 % FBS experimental setup, this could affect the nature of tau-GFP11 secreted and tested for cytosolic translocation. Furthermore, since the conditioned media is being transferred to recipient GFP1-10 cells, the reduced serum content may alter the internalisation dynamics. However, given that this experimental setup is kept constant across conditions, I believe any detected isoform-specific difference is genuine rather than an experimental artefact; nevertheless, understanding the phosphorylation and aggregation status of secreted tau-GFP11 will improve our understanding of factors that mediate tau internalisation.

This assay was also used to test cytosolic translocation of tau in primary neuronal cultures but unfortunately did not generate usable results. While I could detect positive tau puncta after incubation with both bacterially-expressed and cell-secreted tau-GFP11 conditions, there was no positive GFP reconstitution in spite of multiple experimental conditions tested. Since it was confirmed that cell-secreted tau-GFP11 is competent for cytosolic translocation

in HEK293 and N2a cells, it was surprising that primary neuronal cultures did not yield a positive result. This assay was also tested in MFCs designed to promote unidirectional growth of axons, in attempts to isolate the site of internalisation and test trans-synaptic spread of tau. To date, I have not been successful in detecting reconstituted GFP following tau uptake in MFCs.

However, cytosolic translocation has been detected within primary neuronal cultures; work by the McEwan lab has seen the development of a split-luciferase assay from NanoLuc that has been split into an 18 kDa subunit (LgBiT) expressed in the cytosol and an 11 amino acid peptide (HiBiT) used to tag tau (Tuck et al., 2021). In this setup, recombinant tau-HiBiT was detected in the cytosol after only 1 h of incubation with primary neuronal cultures (Tuck et al., 2021). Interestingly, when comparing the cytosolic entry of recombinant tau-HiBiT in HEK293 and primary neuronal cultures, it appears that neurons overall have a lower propensity for tau internalisation; when examining luciferase reconstitution by the relative light unit (RLU), lower concentrations of recombinant tau-HiBiT, resulted in higher RLU levels in HEK293 cells compared with neurons (Tuck et al., 2021). This may suggest that endocytosis is more tightly regulated in neurons; therefore, given that the split-GFP technology is less sensitive compared with split-luciferase, lower amounts of tau-GFP11 are unlikely to be internalised at the rate required for detectable GFP reconstitution. It is important to note that the expression of the LgBiT sensor may be different in HEK293 cells compared with primary neurons, therefore a higher rate of cytosolic entry in HEK293 cells may be the combination of more efficient endocytosis and higher expression of the LgBiT fragment.

The split-luciferase domains are reported to self-interact with sub nanomolar affinity generating rapid signal (Schwinn et al., 2018; Tuck et al., 2021). However, despite *in vitro* work demonstrating similar sub nanomolar affinity between GFP11 and GFP1-10, the chromophore maturation time is longer (Cabantous et al., 2005), when compared with the generation of the luciferase signal. Overall, these two models could be complementary as the split-GFP has the advantage of allowing precise subcellular visualisation of tau translocation, while the split-luciferase has heightened signal sensitivity.

In primary neuronal cultures, lentiviral-driven transduction of GFP1-10 was used in order to achieve widespread expression. However this method is known to yield low/moderate level of protein overexpression. This factor may contribute to the low relative efficacy of the system in neurons, since a higher concentration of internalised of tau-GFP11 may be needed to generate a robust GFP signal. A potential improvement to the system could be increasing the number of GFP11 repeats tagged to tau. While consideration would be needed on the number of GFP11 repeats and the most suitable spacers, to avoid affecting tau physiology; previous reports have demonstrated a significant increase in the GFP fluorescent signal following the addition of either three or seven GFP11 repeats in tandem (Kamiyama et al., 2016), albeit tandem GFPs are prone to aggregation (Romei and Boxer, 2019). Alternatively the use of other brighter split fluorescent proteins i.e. YFP could boost the cytosolic signal in neurons (Köker et al., 2018). These methods for fluorescence amplification could help improve signal detection within the primary neuronal cultures and boost the sensitivity of the system.

6.1 Future applications

Having developed this assay to monitor cytosolic translocation, future experiments will be aimed to better understand the mechanism mediating the exit of tau from a membrane-bound compartment into the cytosol.

Further work should be conducted targeting Rab GTPases, either via expression of dominant-negative / constitutively-active mutant forms, or with a siRNA-knockdown approach to assess whether alterations of the endolysosomal pathway will change the incidence or intensity of the GFP signal. In addition, as described in the introduction, the ESCRT pathway has also been shown to be involved in the extent of seeded aggregation by recombinant tau fibrils (Chen et al., 2019). As such, it would be interesting to use the cytosolic translocation assay following knockdown of ESCRT components such as, CHMP2, -3 and -6, all shown to trigger membrane damage, thus leaving tau free to seed aggregation in the cytosol (Chen et al., 2019); if this pathway affects soluble tau, one would expect an increase in the frequency or intensity of the reconstituted GFP signal.

Moreover, mutations within the ESCRT pathway have been identified in familial FTD, in particular CHMP2B has been reported to cause a rare form of autosomal dominant FTD linked to chromosome 3 (FTD-3) (Isaacs et al., 2011). In FTD-3, CHMP2B mutation leads to a truncation of the CHMP2B protein which can have subsequent effects on vesicle fusion in the endolysosomal pathway, a process likely to be required for the entry of tau to the cytosol; since cargo progression throughout the endolysosomal pathway includes vesicle fusion i.e. the endocytic vesicle fusing with early endosomes. Interestingly, tau

pathology was detected in FTD-3 patients corresponding with Braak stage IV (Isaacs et al., 2011). Furthermore, CHMP2B mutant expressing cells have been shown to have a deficit in the ability to recruit Rab7 to late endosomes (Isaacs et al., 2011). As such, investigating the ESCRT pathway using the split-GFP cytosolic translocation assay could provide further mechanistic information regarding the role of ESCRT in tau pathology spread; by quantifying the number of GFP positive cells or the intensity of the signal, any increase or decrease will be informative to know if that mutation is impacting tau dynamics.

While the data in this study has examined cytosolic translocation of tau using two independent read out measures of GFP signal (frequency and intensity), the benefit of having a fluorescent signal as a visual readout is that any changes to signal localisation could shed light on the dynamics of tau post-uptake. This aspect of the split-GFP technology should be explored further in relation to cytosolic translocation of tau and pathology. One example of this could be by tagging GFP1-10 to potential interaction partners of tau throughout the endocytic pathway and observe whether there is reconstitution with tau-GFP11. As an example, LRP1, a recently identified receptor for tau (Rauch et al., 2020), could be sub-cloned into a GFP1-10 expressing vector; assuming there is close interaction with tau and LRP1 one would expect there to be GFP reconstitution at the cell surface, given that LRP1 is a membrane-bound protein. This strategy could in turn be used for downstream intracellular binding partners of tau involved in its cytosolic translocation. Furthermore, GFP trap® could potentially be used to pull down the bound tau-GFP11 and GFP1-10 to further elucidate, via immunoprecipitation, the binding partners within the tau/GFP complex. The use of GFP trap® could also be applied to the existing cytosolic

translation assay described in this thesis; following the entry of tau in the cytosol, the tau/GFP complex could be precipitated and be used for proteomic analyses to examine the PTMs present on tau that is competent for cytosolic entry. Importantly, the high affinity between GFP1-10 and GFP11 needs to be considered if investigating binding partners, as this could generate artificial interactions with tau-GFP11, rather than a genuine interaction between tau, LRP1 and other potential interactors. Furthermore, steric constraints may hinder interaction between GFP1-10 and GFP11. Nevertheless, these are potential experiments that could be explored using the split-GFP technology.

Alternatively, in the context of tau aggregation the visual detection of cytosolic translocation of tau could be investigated. While it has been previously reported that aggregates of tau tagged with GFP11 would be unable to reconstitute with GFP1-10 as the GFP11 would be sequestered (Chun et al., 2011), I sought to conduct a single trial experiment with tau seeds. Briefly, tau seeds extracted from rTg4510 mice expressing the 0N4R-P301L mutation, previously reported to seed intracellular tau aggregation (Bennett et al., 2017), were used to seed aggregation of tau-GFP11 that had undergone cytosolic translocation. In this setup, the cytosolic translocation assay optimised in Chapter 3, was slightly adapted, so that upon transfer of the tau-GFP11 conditioned media, secreted tau was mixed with 500 ng/ml of rTg4510 tau seed and incubated with GFP1-10 expressing HEK293 cells to be monitored over 60 h. This experiment was performed with both 1N4R and 1N4R-P301S tau-GFP11. The data presented here have been obtained using 1N4R-P301S tau as WT 1N4R tau did not give rise to any changes in the GFP signal localisation (data not shown).

In Chapter 2, it was discussed that upon uptake of tau-GFP11, tau localised to the microtubules and potentially to the MTOC. Following incubation with the rTg4510 tau seed, an initial observation was the change in structure of the MTOC; over time there appeared to be an accumulation of tau at the MTOC leading to its enlargement, as shown in Figure 6.1A (highlighted by the triangle). This was accompanied by potential fragmentation of the MTOC (highlighted by the arrow, Figure 6.1A). It is important to note, that these conclusions are speculative given there was no immunocytochemistry conducted to stain for tubulin to verify the composition or localisation of these puncta.

Furthermore, when monitoring GFP positive cells following 1N4R-P301S tau-GFP11 uptake I was able to detect the transition of diffuse cytosolic GFP signal into puncta (Fig 6.1B). Lastly, the presence of the rTg4510 tau seed appeared to generate different forms of tau aggregates: punctate and tangle-like, detected by live imaging of the split-GFP reconstitution (Fig 6.1C). Although I cannot confirm whether these are pathological tau aggregates, since I did not probe with antibodies targeted against aggregated or hyperphosphorylated tau e.g. MC1 or AT8 respectively, this signal does represent a discrete accumulation of tau-GFP11 as a result of the co-incubation of the rTg4510 tau seed.

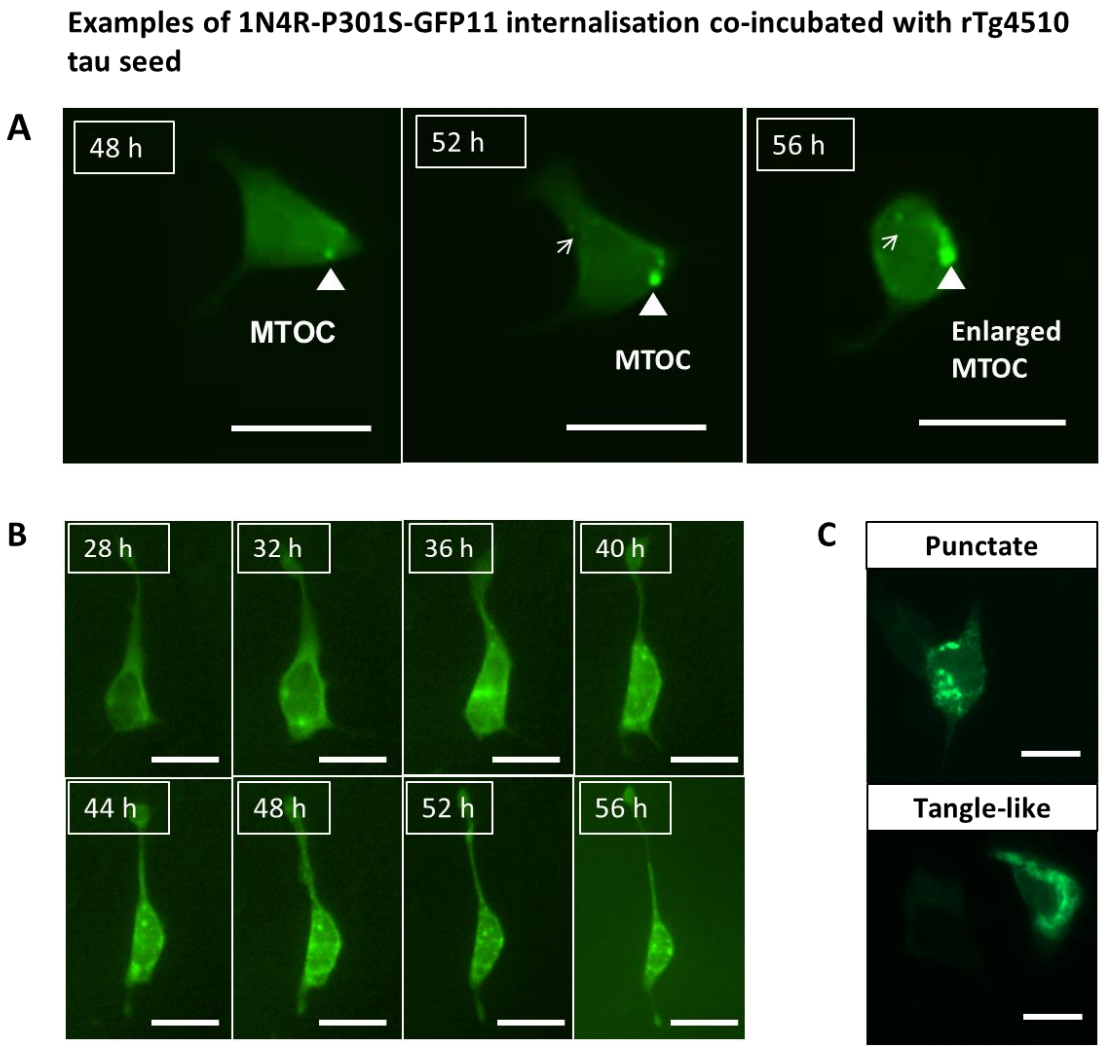

Figure 6.1 – The effect of seeded aggregation on cytosolic translocation of 1N4R-P301S tau-GFP11. HEK293 conditioned media containing secreted 1N4R-P301S tau-GFP11 was collected and incubated with 500 ng/ml of rTg4510 tau seed (0N4R-P301L) to be transferred to GFP1-10 expressing HEK293 cells and monitored live over 60 h.

(A) Effect of rTg4510 tau seed on predicted microtubule organising centre (MTOC) following tau uptake. Triangle, displaying predicted MTOC and arrow, pointing to tau puncta.

(B) Transition from diffuse to punctate GFP reconstitution in a HEK293 cell following 1N4R-P301S tau uptake and rTg4510 tau seed incubation.

(C) Different forms of 1N4R-P301S tau aggregates triggered by rTg4510 tau seed.

Live imaging conducted on Incucyte (A,B) and bench top fluorescent microscope with a green LED (C). Scale bar, 25 µm. Experiment repeated with 2 biological replicates, achieving similar results.

It appears that following GFP reconstitution, aggregate tau structures can be detected. Although they may not represent accurate structural features of tau

aggregates found in tauopathy patients, these different signals could be used as a proxy for understanding the effect of tau seeds and whether they evoke different types of tau aggregates following cytosolic translocation.

This work also sheds light on the conformer of tau that is being secreted; given that the addition of tau seed leads to a change in the reconstituted GFP signal from diffuse to punctate, which is likely a sign of aggregation, it suggests that under control conditions the diffuse GFP signal is representative of monomeric tau (or LMW oligomeric forms). Nevertheless, this requires further characterisation, to address both the form of tau that is being secreted and subsequently internalised and whether the tau puncta are pathological tau aggregates.

Interestingly, Tuck and colleagues reported that following aggregation of recombinant tau-HiBiT, reconstitution with cytosolic LgBiT was still possible, as such it would be interesting to try and seed aggregation of secreted tau-GFP11 prior to incubating with GFP1-10 expressing cells, to assess whether there is robust GFP reconstitution and if the signal localisation is different compared with unseeded secreted tau-GFP11.

Finally, a future application of the cytosolic entry assay using split-GFP could be the use of FACS, followed by mass spectrometry. Cells that have effectively undergone cytosolic translocation will be GFP-positive and therefore can be efficiently isolated by flow cytometry (Kaddoum et al., 2010). It would then be interesting to examine whether there are any differences at the proteomic level

between the cell populations that have internalised tau versus those cells that have not.

6.2 Concluding remarks

The prion-like spread of tau has become a widely studied phenomenon from the discovery that tau protein alone is capable of causing neurodegeneration, as seen in familial FTD. Furthermore, it has been shown that tau spread in AD correlates closely with cognitive decline, therefore understanding the mechanism of tau spread could have wide clinical applications. In this thesis I have developed a cell-based assay using the split-GFP technology to investigate in living cells the cytosolic translocation of tau. To date, the mechanism mediating tau entry into the cytosol remains elusive; the assay optimised in this thesis can provide a complementary strategy to enhance our understanding of this process and aid the identification of novel pharmacological targets to improve therapeutics targeting tau-mediated pathologies.

References

Ait-Bouziad, N., Lv, G., Mahul-Mellier, A.-L., Xiao, S., Zorludemir, G., Eliezer, D., Walz, T., Lashuel, H.A., 2017. Discovery and characterization of stable and toxic Tau/phospholipid oligomeric complexes. Nat. Commun. 8, 1678.

Aman, A.T., Fraser, S., Merritt, E.A., Rodigherio, C., Kenny, M., Ahn, M., Hol, W.G., Williams, N.A., Lencer, W.I., Hirst, T.R., 2001. A mutant cholera toxin B subunit that binds GM1- ganglioside but lacks immunomodulatory or toxic activity. Proc. Natl. Acad. Sci. USA 98, 8536–8541.

Appelbaum, J.S., LaRochelle, J.R., Smith, B.A., Balkin, D.M., Holub, J.M., Schepartz, A., 2012. Arginine topology controls escape of minimally cationic proteins from early endosomes to the cytoplasm. Chem. Biol. 19, 819–830.

Balleza, E., Kim, J.M., Cluzel, P., 2018. Systematic characterization of maturation time of fluorescent proteins in living cells. Nat. Methods 15, 47–51.

Banker, G.A., Cowan, W.M., 1977. Rat hippocampal neurons in dispersed cell culture. Brain Res. 126, 397–342.

Baravalle, G., Schober, D., Huber, M., Bayer, N., Murphy, R.F., Fuchs, R., 2005. Transferrin recycling and dextran transport to lysosomes is differentially affected by bafilomycin, nocodazole, and low temperature. Cell Tissue Res. 320, 99–113.

Barondeau, D.P., Putnam, C.D., Kassmann, C.J., Tainer, J.A., Getzoff, E.D., 2003. Mechanism and energetics of green fluorescent protein chromophore synthesis revealed by trapped intermediate structures. Proc. Natl. Acad. Sci. USA 100, 12111–12116.

Barthélemy, N.R., Li, Y., Joseph-Mathurin, N., Gordon, B.A., Hassenstab, J., Benzinger, T.L.S., Buckles, V., Fagan, A.M., Perrin, R.J., Goate, A.M., Morris, J.C., Karch, C.M., Xiong, C., Allegri, R., Mendez, P.C., Berman, S.B., Ikeuchi, T., Mori, H., Shimada, H., Shoji, M., Suzuki, K., Noble, J., Farlow, M., Chhatwal,

J., Graff-Radford, N.R., Salloway, S., Schofield, P.R., Masters, C.L., Martins, R.N., O'Connor, A., Fox, N.C., Levin, J., Jucker, M., Gabelle, A., Lehmann, S., Sato, C., Bateman, R.J., McDade, E., Dominantly Inherited Alzheimer Network, 2020. A soluble phosphorylated tau signature links tau, amyloid and the evolution of stages of dominantly inherited Alzheimer's disease. Nat. Med. 26, 398–407.

Bennett, R.E., DeVos, S.L., Dujardin, S., Corjuc, B., Gor, R., Gonzalez, J., Roe, A.D., Frosch, M.P., Pitstick, R., Carlson, G.A., Hyman, B.T., 2017. Enhanced tau aggregation in the presence of amyloid β. Am. J. Pathol. 187, 1601–1612.

Binder, L.I., Frankfurter, A., Rebhun, L.I., 1985. The distribution of tau in the mammalian central nervous system. J. Cell Biol. 101, 1371–1378.

Blennow, K., Wallin, A., Agren, H., Spenger, C., Siegfried, J., Vanmechelen, E., 1995. Tau protein in cerebrospinal fluid: a biochemical marker for axonal degeneration in Alzheimer disease? Mol. Chem. Neuropathol. 26, 231–245.

Bolton, D.C., McKinley, M.P., Prusiner, S.B., 1982. Identification of a protein that purifies with the scrapie prion. Science 218, 1309–1311.

Braak, E., Braak, H., Mandelkow, E.M., 1994. A sequence of cytoskeleton changes related to the formation of neurofibrillary tangles and neuropil threads. Acta Neuropathol. 87, 554–567.

Braak, H., Alafuzoff, I., Arzberger, T., Kretzschmar, H., Del Tredici, K., 2006. Staging of Alzheimer disease-associated neurofibrillary pathology using paraffin sections and immunocytochemistry. Acta Neuropathol. 112, 389–404.

Braak, H., Braak, E., 1991. Neuropathological stageing of Alzheimer-related changes. Acta Neuropathol. 82, 239–259.

Briner, A., Götz, J., Polanco, J.C., 2020. Fyn kinase controls tau aggregation in vivo. Cell Rep. 32, 108045.

Bucci, C., Parton, R.G., Mather, I.H., Stunnenberg, H., Simons, K., Hoflack, B., Zerial, M., 1992. The small GTPase rab5 functions as a regulatory factor in the early endocytic pathway. Cell 70, 715–728.

Bugiani, O., Murrell, J.R., Giaccone, G., Hasegawa, M., Ghigo, G., Tabaton, M., Morbin, M., Primavera, A., Carella, F., Solaro, C., Grisoli, M., Savoiardo, M., Spillantini, M.G., Tagliavini, F., Goedert, M., Ghetti, B., 1999. Frontotemporal dementia and corticobasal degeneration in a family with a P301S mutation in tau. J. Neuropathol. Exp. Neurol. 58, 667–677.

Busche, M.A., Konnerth, A., 2016. Impairments of neural circuit function in Alzheimer's disease. Philos. Trans. R. Soc. Lond. B, Biol. Sci. 371.

Cabantous, S., Terwilliger, T.C., Waldo, G.S., 2005. Protein tagging and detection with engineered self-assembling fragments of green fluorescent protein. Nat. Biotechnol. 23, 102–107.

Calafate, S., Buist, A., Miskiewicz, K., Vijayan, V., Daneels, G., de Strooper, B., de Wit, J., Verstreken, P., Moechars, D., 2015. Synaptic Contacts Enhance Cell-to-Cell Tau Pathology Propagation. Cell Rep. 11, 1176–1183.

Calafate, S., Flavin, W., Verstreken, P., Moechars, D., 2016. Loss of bin1 promotes the propagation of tau pathology. Cell Rep. 17, 931–940.

Calì, T., Ottolini, D., Soriano, M.E., Brini, M., 2015. A new split-GFP-based probe reveals DJ-1 translocation into the mitochondrial matrix to sustain ATP synthesis upon nutrient deprivation. Hum. Mol. Genet. 24, 1045–1060.

Chai, X., Dage, J.L., Citron, M., 2012. Constitutive secretion of tau protein by an unconventional mechanism. Neurobiol. Dis. 48, 356–366.

Chen, J.J., Nathaniel, D.L., Raghavan, P., Nelson, M., Tian, R., Tse, E., Hong, J.Y., See, S.K., Mok, S.-A., Hein, M.Y., Southworth, D.R., Grinberg, L.T., Gestwicki, J.E., Leonetti, M.D., Kampmann, M., 2019. Compromised function of the ESCRT pathway promotes endolysosomal escape of tau seeds and propagation of tau aggregation. J. Biol. Chem. 294, 18952–18966.

Chun, W., Waldo, G.S., Johnson, G.V.W., 2007. Split GFP complementation assay: a novel approach to quantitatively measure aggregation of tau in situ: effects of GSK3beta activation and caspase 3 cleavage. J. Neurochem. 103, 2529–2539.

Chun, W., Waldo, G.S., Johnson, G.V.W., 2011. Split GFP complementation assay for quantitative measurement of tau aggregation in situ. Methods Mol. Biol. 670, 109–123.

Cicognola, C., Brinkmalm, G., Wahlgren, J., Portelius, E., Gobom, J., Cullen, N.C., Hansson, O., Parnetti, L., Constantinescu, R., Wildsmith, K., Chen, H.-H., Beach, T.G., Lashley, T., Zetterberg, H., Blennow, K., Höglund, K., 2019. Novel tau fragments in cerebrospinal fluid: relation to tangle pathology and cognitive decline in Alzheimer's disease. Acta Neuropathol. 137, 279–296.

Clavaguera, F., Bolmont, T., Crowther, R.A., Abramowski, D., Frank, S., Probst, A., Fraser, G., Stalder, A.K., Beibel, M., Staufenbiel, M., Jucker, M., Goedert, M., Tolnay, M., 2009. Transmission and spreading of tauopathy in transgenic mouse brain. Nat. Cell Biol. 11, 909–913.

Condomitti, G., de Wit, J., 2018. Heparan sulfate proteoglycans as emerging players in synaptic specificity. Front. Mol. Neurosci. 11, 14.

Crowther, R.A., Olesen, O.F., Jakes, R., Goedert, M., 1992. The microtubule binding repeats of tau protein assemble into filaments like those found in Alzheimer's disease. FEBS Lett. 309, 199–202.

De La-Rocque, S., Moretto, E., Butnaru, I., Schiavo, G., 2021. Knockin' on heaven's door: Molecular mechanisms of neuronal tau uptake. J. Neurochem. 156, 563–588.

de Calignon, A., Polydoro, M., Suárez-Calvet, M., William, C., Adamowicz, D.H., Kopeikina, K.J., Pitstick, R., Sahara, N., Ashe, K.H., Carlson, G.A., Spires-Jones, T.L., Hyman, B.T., 2012. Propagation of tau pathology in a model of early Alzheimer's disease. Neuron 73, 685–697.

Deinhardt, K., 2020. A receptor that lets dementia-associated tau proteins into neurons. Nature 580, 326–327.

DeVos, S.L., Corjuc, B.T., Oakley, D.H., Nobuhara, C.K., Bannon, R.N., Chase, A., Commins, C., Gonzalez, J.A., Dooley, P.M., Frosch, M.P., Hyman, B.T., 2018.

Synaptic tau seeding precedes tau pathology in human alzheimer's disease brain. Front. Neurosci. 12, 267.

Dröse, S., Altendorf, K., 1997. Bafilomycins and concanamycins as inhibitors of V-ATPases and P-ATPases. J. Exp. Biol. 200, 1–8.

Dujardin, S., Bégard, S., Caillierez, R., Lachaud, C., Carrier, S., Lieger, S., Gonzalez, J.A., Deramecourt, V., Déglon, N., Maurage, C.-A., Frosch, M.P., Hyman, B.T., Colin, M., Buée, L., 2018. Different tau species lead to heterogeneous tau pathology propagation and misfolding. Acta Neuropathol. Commun. 6, 132.

Dujardin, S., Bégard, S., Caillierez, R., Lachaud, C., Delattre, L., Carrier, S., Loyens, A., Galas, M.-C., Bousset, L., Melki, R., Aurégan, G., Hantraye, P., Brouillet, E., Buée, L., Colin, M., 2014a. Ectosomes: a new mechanism for non-exosomal secretion of tau protein. PLoS One 9, e100760.

Dujardin, S., Lécolle, K., Caillierez, R., Bégard, S., Zommer, N., Lachaud, C., Carrier, S., Dufour, N., Aurégan, G., Winderickx, J., Hantraye, P., Déglon, N., Colin, M., Buée, L., 2014b. Neuron-to-neuron wild-type Tau protein transfer through a trans-synaptic mechanism: relevance to sporadic tauopathies. Acta Neuropathol. Commun. 2, 14.

Evans, L.D., Wassmer, T., Fraser, G., Smith, J., Perkinton, M., Billinton, A., Livesey, F.J., 2018. Extracellular Monomeric and Aggregated Tau Efficiently Enter Human Neurons through Overlapping but Distinct Pathways. Cell Rep. 22, 3612–3624.

Falcon, B., Cavallini, A., Angers, R., Glover, S., Murray, T.K., Barnham, L., Jackson, S., O'Neill, M.J., Isaacs, A.M., Hutton, M.L., Szekeres, P.G., Goedert, M., Bose, S., 2015. Conformation determines the seeding potencies of native and recombinant Tau aggregates. J. Biol. Chem. 290, 1049–1065.

Falcon, B., Noad, J., McMahon, H., Randow, F., Goedert, M., 2018a. Galectin-8-mediated selective autophagy protects against seeded tau aggregation. J. Biol. Chem. 293, 2438–2451.

Falcon, B., Zhang, W., Murzin, A.G., Murshudov, G., Garringer, H.J., Vidal, R., Crowther, R.A., Ghetti, B., Scheres, S.H.W., Goedert, M., 2018b. Structures of filaments from Pick's disease reveal a novel tau protein fold. Nature 561, 137–140.

Falcon, B., Zhang, W., Schweighauser, M., Murzin, A.G., Vidal, R., Garringer, H.J., Ghetti, B., Scheres, S.H.W., Goedert, M., 2018c. Tau filaments from multiple cases of sporadic and inherited Alzheimer's disease adopt a common fold. Acta Neuropathol. 136, 699–708.

Falcon, B., Zivanov, J., Zhang, W., Murzin, A.G., Garringer, H.J., Vidal, R., Crowther, R.A., Newell, K.L., Ghetti, B., Goedert, M., Scheres, S.H.W., 2019. Novel tau filament fold in chronic traumatic encephalopathy encloses hydrophobic molecules. Nature 568, 420–423.

Fitzpatrick, A.W.P., Falcon, B., He, S., Murzin, A.G., Murshudov, G., Garringer, H.J., Crowther, R.A., Ghetti, B., Goedert, M., Scheres, S.H.W., 2017. Cryo-EM structures of tau filaments from Alzheimer's disease. Nature 547, 185–190.

Flavin, W.P., Bousset, L., Green, Z.C., Chu, Y., Skarpathiotis, S., Chaney, M.J., Kordower, J.H., Melki, R., Campbell, E.M., 2017. Endocytic vesicle rupture is a conserved mechanism of cellular invasion by amyloid proteins. Acta Neuropathol. 134, 629–653.

Foglieni, C., Papin, S., Salvadè, A., Afroz, T., Pinton, S., Pedrioli, G., Ulrich, G., Polymenidou, M., Paganetti, P., 2017. Split GFP technologies to structurally characterize and quantify functional biomolecular interactions of FTD-related proteins. Sci. Rep. 7, 14013.

Frost, B., Jacks, R.L., Diamond, M.I., 2009. Propagation of tau misfolding from the outside to the inside of a cell. J. Biol. Chem. 284, 12845–12852.

Gaston, J., Maestrali, N., Lalle, G., Gagnaire, M., Masiero, A., Dumas, B., Dabdoubi, T., Radošević, K., Berne, P.-F., 2019. Intracellular delivery of therapeutic antibodies into specific cells using antibody-peptide fusions. Sci. Rep. 9, 18688.

Gladkov, A., Pigareva, Y., Kutyina, D., Kolpakov, V., Bukatin, A., Mukhina, I., Kazantsev, V., Pimashkin, A., 2017. Design of Cultured Neuron Networks in vitro with Predefined Connectivity Using Asymmetric Microfluidic Channels. Sci. Rep. 7, 15625.

Goedert, M., Jakes, R., 1990. Expression of separate isoforms of human tau protein: correlation with the tau pattern in brain and effects on tubulin polymerization. EMBO J. 9, 4225–4230.

Goedert, M., Jakes, R., Spillantini, M.G., Hasegawa, M., Smith, M.J., Crowther, R.A., 1996. Assembly of microtubule-associated protein tau into Alzheimer-like filaments induced by sulphated glycosaminoglycans. Nature 383, 550–553.

Goldfarb, L.G., Petersen, R.B., Tabaton, M., Brown, P., LeBlanc, A.C., Montagna, P., Cortelli, P., Julien, J., Vital, C., Pendelbury, W.W., 1992. Fatal familial insomnia and familial Creutzfeldt-Jakob disease: disease phenotype determined by a DNA polymorphism. Science 258, 806–808.

Gómez-Ramos, A., Díaz-Hernández, M., Cuadros, R., Hernández, F., Avila, J., 2006. Extracellular tau is toxic to neuronal cells. FEBS Lett. 580, 4842–4850.

Green, A.J., Harvey, R.J., Thompson, E.J., Rossor, M.N., 1999. Increased tau in the cerebrospinal fluid of patients with frontotemporal dementia and Alzheimer's disease. Neurosci. Lett. 259, 133–135.

Greenwood, J.A., Johnson, G.V., 1995. Localization and in situ phosphorylation state of nuclear tau. Exp. Cell Res. 220, 332–337.

Grundke-Iqbal, I., Iqbal, K., Quinlan, M., Tung, Y.C., Zaidi, M.S., Wisniewski, H.M., 1986. Microtubule-associated protein tau. A component of Alzheimer paired helical filaments. J. Biol. Chem. 261, 6084–6089.

Guix, F.X., Corbett, G.T., Cha, D.J., Mustapic, M., Liu, W., Mengel, D., Chen, Z., Aikawa, E., Young-Pearse, T., Kapogiannis, D., Selkoe, D.J., Walsh, D.M., 2018. Detection of Aggregation-Competent Tau in Neuron-Derived Extracellular Vesicles. Int. J. Mol. Sci. 19.

Hallinan, G.I., Vargas-Caballero, M., West, J., Deinhardt, K., 2019. Tau Misfolding Efficiently Propagates between Individual Intact Hippocampal Neurons. J. Neurosci. 39, 9623–9632.

Hauber, J., Perkins, A., Heimer, E.P., Cullen, B.R., 1987. Trans-activation of human immunodeficiency virus gene expression is mediated by nuclear events. Proc. Natl. Acad. Sci. USA 84, 6364–6368.

Helle, F., Dubuisson, J., 2008. Hepatitis C virus entry into host cells. Cell Mol. Life Sci. 65, 100–112.

Henne, W.M., Buchkovich, N.J., Emr, S.D., 2011. The ESCRT pathway. Dev. Cell 21, 77–91.

Hippius, H., Neundörfer, G., 2003. The discovery of Alzheimer's disease. Dialogues Clin Neurosci 5, 101–108.

Holmes, B.B., DeVos, S.L., Kfoury, N., Li, M., Jacks, R., Yanamandra, K., Ouidja, M.O., Brodsky, F.M., Marasa, J., Bagchi, D.P., Kotzbauer, P.T., Miller, T.M., Papy-Garcia, D., Diamond, M.I., 2013. Heparan sulfate proteoglycans mediate internalization and propagation of specific proteopathic seeds. Proc. Natl. Acad. Sci. USA 110, E3138–47.

Holmes, B.B., Diamond, M.I., 2014. Prion-like properties of Tau protein: the importance of extracellular Tau as a therapeutic target. J. Biol. Chem. 289, 19855–19861.

Holmes, B.B., Furman, J.L., Mahan, T.E., Yamasaki, T.R., Mirbaha, H., Eades, W.C., Belaygorod, L., Cairns, N.J., Holtzman, D.M., Diamond, M.I., 2014. Proteopathic tau seeding predicts tauopathy in vivo. Proc. Natl. Acad. Sci. USA 111, E4376–85.

Houck, A.L., Hernández, F., Ávila, J., 2016. A simple model to study tau pathology. J. Exp. Neurosci. 10, 31–38.

Howitt, J., Hill, A.F., 2016. Exosomes in the pathology of neurodegenerative diseases. J. Biol. Chem. 291, 26589–26597.

Hu, Y.-B., Dammer, E.B., Ren, R.-J., Wang, G., 2015. The endosomal-lysosomal system: from acidification and cargo sorting to neurodegeneration. Transl Neurodegener 4, 18.

Hudák, A., Kusz, E., Domonkos, I., Jósvay, K., Kodamullil, A.T., Szilák, L., Hofmann-Apitius, M., Letoha, T., 2019. Contribution of syndecans to cellular uptake and fibrillation of α-synuclein and tau. Sci. Rep. 9, 16543.

Humphries, W.H., Szymanski, C.J., Payne, C.K., 2011. Endo-lysosomal vesicles positive for Rab7 and LAMP1 are terminal vesicles for the transport of dextran. PLoS One 6, e26626.

Huotari, J., Helenius, A., 2011. Endosome maturation. EMBO J. 30, 3481–3500.

Hutton, M., Lendon, C.L., Rizzu, P., Baker, M., Froelich, S., et al., 1998. Association of missense and 5'-splice-site mutations in tau with the inherited dementia FTDP-17. Nature 393, 702–705.

Iqbal, K., Liu, F., Gong, C.-X., 2016. Tau and neurodegenerative disease: the story so far. Nat. Rev. Neurol. 12, 15–27.

Iqbal, K., Liu, F., Gong, C.X., Grundke-Iqbal, I., 2010. Tau in Alzheimer disease and related tauopathies. Curr Alzheimer Res 7, 656–664.

Isaacs, A.M., Johannsen, P., Holm, I., Nielsen, J.E., FReJA consortium, 2011. Frontotemporal dementia caused by CHMP2B mutations. Curr Alzheimer Res 8, 246–251.

Itagaki, H., 2000. Fluorescence Spectroscopy. In: Experimental methods in polymer science. Elsevier, pp. 155–260.

Jimenez, A.J., Maiuri, P., Lafaurie-Janvore, J., Divoux, S., Piel, M., Perez, F., 2014. ESCRT machinery is required for plasma membrane repair. Science 343, 1247136.

Johnson, D.E., Ostrowski, P., Jaumouillé, V., Grinstein, S., 2016. The position of lysosomes within the cell determines their luminal pH. J. Cell Biol. 212, 677–692.

Jung, N., Haucke, V., 2007. Clathrin-mediated endocytosis at synapses. Traffic 8, 1129–1136.

Kaddoum, L., Magdeleine, E., Waldo, G.S., Joly, E., Cabantous, S., 2010. One-step split GFP staining for sensitive protein detection and localization in mammalian cells. BioTechniques 49, 727–8, 730, 732 passim.

Kakimoto, Y., Tashiro, S., Kojima, R., Morozumi, Y., Endo, T., Tamura, Y., 2018. Visualizing multiple inter-organelle contact sites using the organelle-targeted split-GFP system. Sci. Rep. 8, 6175.

Kamiyama, D., Sekine, S., Barsi-Rhyne, B., Hu, J., Chen, B., Gilbert, L.A., Ishikawa, H., Leonetti, M.D., Marshall, W.F., Weissman, J.S., Huang, B., 2016. Versatile protein tagging in cells with split fluorescent protein. Nat. Commun. 7, 11046.

Kanaan, N.M., Morfini, G., Pigino, G., LaPointe, N.E., Andreadis, A., Song, Y., Leitman, E., Binder, L.I., Brady, S.T., 2012. Phosphorylation in the amino terminus of tau prevents inhibition of anterograde axonal transport. Neurobiol. Aging 33, 826.e15–30.

Kaniyappan, S., Tepper, K., Biernat, J., Chandupatla, R.R., Hübschmann, S., Irsen, S., Bicher, S., Klatt, C., Mandelkow, E.-M., Mandelkow, E., 2020. FRET-based Tau seeding assay does not represent prion-like templated assembly of Tau filaments. Mol. Neurodegener. 15, 39.

Kanmert, D., Cantlon, A., Muratore, C.R., Jin, M., O'Malley, T.T., Lee, G., Young-Pearse, T.L., Selkoe, D.J., Walsh, D.M., 2015. C-Terminally Truncated Forms of Tau, But Not Full-Length Tau or Its C-Terminal Fragments, Are Released from Neurons Independently of Cell Death. J. Neurosci. 35, 10851–10865.

Knauer, M.F., Orlando, R.A., Glabe, C.G., 1996. Cell surface APP751 forms complexes with protease nexin 2 ligands and is internalized via the low density lipoprotein receptor-related protein (LRP). Brain Res. 740, 6–14.

Köker, T., Fernandez, A., Pinaud, F., 2018. Characterization of Split Fluorescent Protein Variants and Quantitative Analyses of Their Self-Assembly Process. Sci. Rep. 8, 5344.

Kounnas, M.Z., Moir, R.D., Rebeck, G.W., Bush, A.I., Argraves, W.S., Tanzi, R.E., Hyman, B.T., Strickland, D.K., 1995. LDL receptor-related protein, a multifunctional ApoE receptor, binds secreted beta-amyloid precursor protein and mediates its degradation. Cell 82, 331–340.

Kowal, J., Arras, G., Colombo, M., Jouve, M., Morath, J.P., Primdal-Bengtson, B., Dingli, F., Loew, D., Tkach, M., Théry, C., 2016. Proteomic comparison defines novel markers to characterize heterogeneous populations of extracellular vesicle subtypes. Proc. Natl. Acad. Sci. USA 113, E968–77.

KrishnaKumar, V.G., Gupta, S., 2017. Simplified method to obtain enhanced expression of tau protein from E. coli and one-step purification by direct boiling. Prep Biochem Biotechnol 47, 530–538.

Lee, G., Cowan, N., Kirschner, M., 1988. The primary structure and heterogeneity of tau protein from mouse brain. Science 239, 285–288.

Lee, G., Neve, R.L., Kosik, K.S., 1989. The microtubule binding domain of tau protein. Neuron 2, 1615–1624.

Lee, S., Mankhong, S., Kang, J.-H., 2019. Extracellular vesicle as a source of alzheimer's biomarkers: opportunities and challenges. Int. J. Mol. Sci. 20.

Leonetti, M.D., Sekine, S., Kamiyama, D., Weissman, J.S., Huang, B., 2016. A scalable strategy for high-throughput GFP tagging of endogenous human proteins. Proc. Natl. Acad. Sci. USA 113, E3501–8.

Levey, A.I., 1996. Muscarinic acetylcholine receptor expression in memory circuits: implications for treatment of Alzheimer disease. Proc. Natl. Acad. Sci. USA 93, 13541–13546.

Li, C., Wen, A., Shen, B., Lu, J., Huang, Y., Chang, Y., 2011. FastCloning: a highly simplified, purification-free, sequence- and ligation-independent PCR cloning method. BMC Biotechnol. 11, 92.

Li, W., Lee, V.M.-Y., 2006. Characterization of two VQIXXK motifs for tau fibrillization in vitro. Biochemistry 45, 15692–15701.

Liu, L., Drouet, V., Wu, J.W., Witter, M.P., Small, S.A., Clelland, C., Duff, K., 2012. Trans-synaptic spread of tau pathology in vivo. PLoS One 7, e31302.

Magliery, T.J., Wilson, C.G.M., Pan, W., Mishler, D., Ghosh, I., Hamilton, A.D., Regan, L., 2005. Detecting protein-protein interactions with a green fluorescent protein fragment reassembly trap: scope and mechanism. J. Am. Chem. Soc. 127, 146–157.

Mayle, K.M., Le, A.M., Kamei, D.T., 2012. The intracellular trafficking pathway of transferrin. Biochim. Biophys. Acta 1820, 264–281.

Mayor, S., Pagano, R.E., 2007. Pathways of clathrin-independent endocytosis. Nat. Rev. Mol. Cell Biol. 8, 603–612.

Méphon-Gaspard, A., Boca, M., Pioche-Durieu, C., Desforges, B., Burgo, A., Hamon, L., Piétrement, O., Pastré, D., 2016. Role of tau in the spatial organization of axonal microtubules: keeping parallel microtubules evenly distributed despite macromolecular crowding. Cell Mol. Life Sci. 73, 3745–3760.

Michel, C.H., Kumar, S., Pinotsi, D., Tunnacliffe, A., St George-Hyslop, P., Mandelkow, E., Mandelkow, E.-M., Kaminski, C.F., Kaminski Schierle, G.S., 2014. Extracellular monomeric tau protein is sufficient to initiate the spread of tau protein pathology. J. Biol. Chem. 289, 956–967.

Milech, N., Longville, B.A.C., Cunningham, P.T., Scobie, M.N., Bogdawa, H.M., Winslow, S., Anastasas, M., Connor, T., Ong, F., Stone, S.R., Kerfoot, M., Heinrich, T., Kroeger, K.M., Tan, Y.-F., Hoffmann, K., Thomas, W.R., Watt, P.M., Hopkins, R.M., 2015. GFP-complementation assay to detect functional CPP and protein delivery into living cells. Sci. Rep. 5, 18329.

Mirbaha, H., Holmes, B.B., Sanders, D.W., Bieschke, J., Diamond, M.I., 2015. Tau trimers are the minimal propagation unit spontaneously internalized to seed intracellular aggregation. J. Biol. Chem. 290, 14893–14903.

Mondragón-Rodríguez, S., Trillaud-Doppia, E., Dudilot, A., Bourgeois, C., Lauzon, M., Leclerc, N., Boehm, J., 2012. Interaction of endogenous tau protein with

synaptic proteins is regulated by N-methyl-D-aspartate receptor-dependent tau phosphorylation. J. Biol. Chem. 287, 32040–32053.

Morell, M., Espargaró, A., Avilés, F.X., Ventura, S., 2007. Detection of transient protein-protein interactions by bimolecular fluorescence complementation: the Abl-SH3 case. Proteomics 7, 1023–1036.

Morozova, V., Cohen, L.S., Makki, A.E.-H., Shur, A., Pilar, G., El Idrissi, A., Alonso, A.D., 2019. Normal and pathological tau uptake mediated by M1/M3 muscarinic receptors promotes opposite neuronal changes. Front. Cell Neurosci. 13, 403.

Muroi, M., Shiragami, N., Nagao, K., Yamasaki, M., Takatsuki, A., 1994. Folimycin (concanamycin A) and Bafilomycin A_1 , Inhibitors Specific for V-ATPase, Exert Similar but Distinct Effects on Intracellular Translocation and Processing of Glycoproteins. Biosci. Biotechnol. Biochem. 58, 425–427.

Neiss, W.F., 1983. The electron density of light and dark lysosomes in the proximal convoluted tubule of the rat kidney. Histochemistry 77, 63–77.

Nizynski, B., Dzwolak, W., Nieznanski, K., 2017. Amyloidogenesis of Tau protein. Protein Sci. 26, 2126–2150.

Nobuhara, C.K., DeVos, S.L., Commins, C., Wegmann, S., Moore, B.D., Roe, A.D., Costantino, I., Frosch, M.P., Pitstick, R., Carlson, G.A., Hock, C., Nitsch, R.M., Montrasio, F., Grimm, J., Cheung, A.E., Dunah, A.W., Wittmann, M., Bussiere, T., Weinreb, P.H., Hyman, B.T., Takeda, S., 2017. Tau Antibody Targeting Pathological Species Blocks Neuronal Uptake and Interneuron Propagation of Tau in Vitro. Am. J. Pathol. 187, 1399–1412.

Novak, M., Kabat, J., Wischik, C.M., 1993. Molecular characterization of the minimal protease resistant tau unit of the Alzheimer's disease paired helical filament. EMBO J. 12, 365–370.

Olsson, A., Vanderstichele, H., Andreasen, N., De Meyer, G., Wallin, A., Holmberg, B., Rosengren, L., Vanmechelen, E., Blennow, K., 2005. Simultaneous measurement of beta-amyloid(1-42), total tau, and phosphorylated tau (Thr181) in cerebrospinal fluid by the xMAP technology. Clin. Chem. 51, 336–345.

Panda, D., Samuel, J.C., Massie, M., Feinstein, S.C., Wilson, L., 2003. Differential regulation of microtubule dynamics by three- and four-repeat tau: implications for the onset of neurodegenerative disease. Proc. Natl. Acad. Sci. USA 100, 9548–9553.

Pérez, M., Cuadros, R., Hernández, F., Avila, J., 2016. Secretion of full-length tau or tau fragments in a cell culture model. Neurosci. Lett. 634, 63–69.

Polanco, J.C., Hand, G.R., Briner, A., Li, C., Götz, J., 2021. Exosomes induce endolysosomal permeabilization as a gateway by which exosomal tau seeds escape into the cytosol. Acta Neuropathol. 141, 235–256.

Polanco, J.C., Li, C., Durisic, N., Sullivan, R., Götz, J., 2018. Exosomes taken up by neurons hijack the endosomal pathway to spread to interconnected neurons. Acta Neuropathol. Commun. 6, 10.

Polanco, J.C., Scicluna, B.J., Hill, A.F., Götz, J., 2016. Extracellular Vesicles Isolated from the Brains of rTg4510 Mice Seed Tau Protein Aggregation in a Threshold-dependent Manner. J. Biol. Chem. 291, 12445–12466.

Pooler, A.M., Phillips, E.C., Lau, D.H.W., Noble, W., Hanger, D.P., 2013. Physiological release of endogenous tau is stimulated by neuronal activity. EMBO Rep. 14, 389–394.

Presley, J.F., Mayor, S., McGraw, T.E., Dunn, K.W., Maxfield, F.R., 1997. Bafilomycin A1 treatment retards transferrin receptor recycling more than bulk membrane recycling. J. Biol. Chem. 272, 13929–13936.

Puangmalai, N., Bhatt, N., Montalbano, M., Sengupta, U., Gaikwad, S., Ventura, F., McAllen, S., Ellsworth, A., Garcia, S., Kayed, R., 2020. Internalization mechanisms of brain-derived tau oligomers from patients with Alzheimer's disease, progressive supranuclear palsy and dementia with Lewy bodies. Cell Death Dis. 11, 314.

Quinn, J.P., Corbett, N.J., Kellett, K.A.B., Hooper, N.M., 2018. Tau proteolysis in the pathogenesis of tauopathies: neurotoxic fragments and novel biomarkers. J. Alzheimers Dis. 63, 13–33.

Ratts, R., Zeng, H., Berg, E.A., Blue, C., McComb, M.E., Costello, C.E., vanderSpek, J.C., Murphy, J.R., 2003. The cytosolic entry of diphtheria toxin catalytic domain requires a host cell cytosolic translocation factor complex. J. Cell Biol. 160, 1139–1150.

Rauch, J.N., Chen, J.J., Sorum, A.W., Miller, G.M., Sharf, T., See, S.K., Hsieh-Wilson, L.C., Kampmann, M., Kosik, K.S., 2018. Tau Internalization is Regulated by 6-O Sulfation on Heparan Sulfate Proteoglycans (HSPGs). Sci. Rep. 8, 6382.

Rauch, J.N., Luna, G., Guzman, E., Audouard, M., Challis, C., Sibih, Y.E., Leshuk, C., Hernandez, I., Wegmann, S., Hyman, B.T., Gradinaru, V., Kampmann, M., Kosik, K.S., 2020. LRP1 is a master regulator of tau uptake and spread. Nature 580, 381–385.

Rebeck, G.W., Reiter, J.S., Strickland, D.K., Hyman, B.T., 1993. Apolipoprotein E in sporadic Alzheimer's disease: allelic variation and receptor interactions. Neuron 11, 575–580.

Ren, M., Xu, G., Zeng, J., De Lemos-Chiarandini, C., Adesnik, M., Sabatini, D.D., 1998. Hydrolysis of GTP on rab11 is required for the direct delivery of transferrin from the pericentriolar recycling compartment to the cell surface but not from sorting endosomes. Proc. Natl. Acad. Sci. USA 95, 6187–6192.

Roberts, M., Sevastou, I., Imaizumi, Y., Mistry, K., Talma, S., Dey, M., Gartlon, J., Ochiai, H., Zhou, Z., Akasofu, S., Tokuhara, N., Ogo, M., Aoyama, M., Aoyagi, H., Strand, K., Sajedi, E., Agarwala, K.L., Spidel, J., Albone, E., Horie, K., Staddon, J.M., de Silva, R., 2020. Pre-clinical characterisation of E2814, a high-affinity antibody targeting the microtubule-binding repeat domain of tau for passive immunotherapy in Alzheimer's disease. Acta Neuropathol. Commun. 8, 13.

Rodriguez, L., Mohamed, N.-V., Desjardins, A., Lippé, R., Fon, E.A., Leclerc, N., 2017. Rab7A regulates tau secretion. J. Neurochem. 141, 592–605.

Romei, M.G., Boxer, S.G., 2019. Split green fluorescent proteins: scope, limitations, and outlook. Annu. Rev. Biophys. 48, 19–44.

Rouse, S.T., Gilmor, M.L., Levey, A.I., 1998. Differential presynaptic and postsynaptic expression of m1-m4 muscarinic acetylcholine receptors at the perforant pathway/granule cell synapse. Neuroscience 86, 221–232.

Rouse, S.T., Levey, A.I., 1997. Muscarinic acetylcholine receptor immunoreactivity after hippocampal commissural/associational pathway lesions: evidence for multiple presynaptic receptor subtypes. J. Comp. Neurol. 380, 382–394.

Ruan, Z., Pathak, D., Venkatesan Kalavai, S., Yoshii-Kitahara, A., Muraoka, S., Bhatt, N., Takamatsu-Yukawa, K., Hu, J., Wang, Y., Hersh, S., Ericsson, M., Gorantla, S., Gendelman, H.E., Kayed, R., Ikezu, S., Luebke, J.I., Ikezu, T., 2021. Alzheimer's disease brain-derived extracellular vesicles spread tau pathology in interneurons. Brain 144, 288–309.

Russell, M.R.G., Nickerson, D.P., Odorizzi, G., 2006. Molecular mechanisms of late endosome morphology, identity and sorting. Curr. Opin. Cell Biol. 18, 422–428.

Sanders, D.W., Kaufman, S.K., DeVos, S.L., Sharma, A.M., Mirbaha, H., Li, A., Barker, S.J., Foley, A.C., Thorpe, J.R., Serpell, L.C., Miller, T.M., Grinberg, L.T., Seeley, W.W., Diamond, M.I., 2014. Distinct tau prion strains propagate in cells and mice and define different tauopathies. Neuron 82, 1271–1288.

Santos, A.J.M., Boucrot, E., 2018. Probing Endocytosis During the Cell Cycle with Minimal Experimental Perturbation. Methods Mol. Biol. 1847, 23–35.

Schweers, O., Mandelkow, E.M., Biernat, J., Mandelkow, E., 1995. Oxidation of cysteine-322 in the repeat domain of microtubule-associated protein tau controls the in vitro assembly of paired helical filaments. Proc. Natl. Acad. Sci. USA 92, 8463–8467.

Schwinn, M.K., Machleidt, T., Zimmerman, K., Eggers, C.T., Dixon, A.S., Hurst, R., Hall, M.P., Encell, L.P., Binkowski, B.F., Wood, K.V., 2018. CRISPR-Mediated Tagging of Endogenous Proteins with a Luminescent Peptide. ACS Chem. Biol. 13, 467–474.

Scott, C.C., Vacca, F., Gruenberg, J., 2014. Endosome maturation, transport and functions. Semin. Cell Dev. Biol. 31, 2–10.

Selkoe, D.J., Hardy, J., 2016. The amyloid hypothesis of Alzheimer's disease at 25 years. EMBO Mol. Med. 8, 595–608.

Shin, R.W., Iwaki, T., Kitamoto, T., Tateishi, J., 1991. Hydrated autoclave pretreatment enhances tau immunoreactivity in formalin-fixed normal and Alzheimer's disease brain tissues. Lab. Invest. 64, 693–702.

Shin, S., Kim, D., Song, J.Y., Jeong, H., Hyeon, S.J., Kowall, N.W., Ryu, H., Pae, A.N., Lim, S., Kim, Y.K., 2020. Visualization of soluble tau oligomers in TauP301L-BiFC transgenic mice demonstrates the progression of tauopathy. Prog. Neurobiol. 101782.

Skowyra, M.L., Schlesinger, P.H., Naismith, T.V., Hanson, P.I., 2018. Triggered recruitment of ESCRT machinery promotes endolysosomal repair. Science 360.

Small, S.A., Swanson, L.W., 2018. A network explanation of alzheimer's regional vulnerability. Cold Spring Harb. Symp. Quant. Biol. 83, 193–200.

Sokolow, S., Henkins, K.M., Bilousova, T., Gonzalez, B., Vinters, H.V., Miller, C.A., Cornwell, L., Poon, W.W., Gylys, K.H., 2015. Pre-synaptic C-terminal truncated tau is released from cortical synapses in Alzheimer's disease. J. Neurochem. 133, 368–379.

Sola, M., Magrin, C., Pedrioli, G., Pinton, S., Salvadè, A., Papin, S., Paganetti, P., 2020. Tau affects P53 function and cell fate during the DNA damage response. Commun. Biol. 3, 245.

Soto, C., Satani, N., 2011. The intricate mechanisms of neurodegeneration in prion diseases. Trends Mol. Med. 17, 14–24.

Stenmark, H., Olkkonen, V.M., 2001. The Rab GTPase family. Genome Biol. 2, REVIEWS3007.

Stillwell, W., 2016. Membrane Transport. In: An introduction to biological membranes. Elsevier, pp. 423–451.

Storrie, B., 1988. Assembly of Lysosomes: Perspectives from Comparative Molecular Cell Biology. In: International review of cytology. Elsevier, pp. 53–105.

Strang, K.H., Golde, T.E., Giasson, B.I., 2019. MAPT mutations, tauopathy, and mechanisms of neurodegeneration. Lab. Invest. 99, 912–928.

Tak, H., Haque, M.M., Kim, M.J., Lee, J.H., Baik, J.-H., Kim, Y., Kim, D.J., Grailhe, R., Kim, Y.K., 2013. Bimolecular fluorescence complementation; lighting-up tau-tau interaction in living cells. PLoS One 8, e81682.

Takeda, S., Commins, C., DeVos, S.L., Nobuhara, C.K., Wegmann, S., Roe, A.D., Costantino, I., Fan, Z., Nicholls, S.B., Sherman, A.E., Trisini Lipsanopoulos, A.T., Scherzer, C.R., Carlson, G.A., Pitstick, R., Peskind, E.R., Raskind, M.A., Li, G., Montine, T.J., Frosch, M.P., Hyman, B.T., 2016. Seed-competent high-molecular-weight tau species accumulates in the cerebrospinal fluid of Alzheimer's disease mouse model and human patients. Ann. Neurol. 80, 355–367.

Takeda, S., Wegmann, S., Cho, H., DeVos, S.L., Commins, C., Roe, A.D., Nicholls, S.B., Carlson, G.A., Pitstick, R., Nobuhara, C.K., Costantino, I., Frosch, M.P., Müller, D.J., Irimia, D., Hyman, B.T., 2015. Neuronal uptake and propagation of a rare phosphorylated high-molecular-weight tau derived from Alzheimer's disease brain. Nat. Commun. 6, 8490.

Théry, C., Witwer, K.W., Aikawa, E., Alcaraz, M.J., Anderson, J.D., et al., 2018. Minimal information for studies of extracellular vesicles 2018 (MISEV2018): a position statement of the International Society for Extracellular Vesicles and update of the MISEV2014 guidelines. J Extracell Vesicles 7, 1535750.

Thurston, T.L.M., Wandel, M.P., von Muhlinen, N., Foeglein, A., Randow, F., 2012. Galectin 8 targets damaged vesicles for autophagy to defend cells against bacterial invasion. Nature 482, 414–418.

Thurston, V.C., Zinkowski, R.P., Binder, L.I., 1996. Tau as a nucleolar protein in human nonneural cells in vitro and in vivo. Chromosoma 105, 20–30.

Triller, A., Choquet, D., 2005. Surface trafficking of receptors between synaptic and extrasynaptic membranes: and yet they do move! Trends Neurosci. 28, 133–139.

Tuck, B.J., Katsinelos, T., Miller, L.V.C., Cheng, S., Vaysburd, M., Knox, C., Tredgett, L., James, L.C., McEwan, W.A., 2021. Tau assemblies enter the cytosol of neurons in a cholesterol sensitive manner. BioRxiv. https://doi.org/10.1101/2021.06.21.449238

Umata, T., Moriyama, Y., Futai, M., Mekada, E., 1990. The cytotoxic action of diphtheria toxin and its degradation in intact Vero cells are inhibited by bafilomycin A1, a specific inhibitor of vacuolar-type H(+)-ATPase. J. Biol. Chem. 265, 21940–21945.

Vanlandingham, P.A., Ceresa, B.P., 2009. Rab7 regulates late endocytic trafficking downstream of multivesicular body biogenesis and cargo sequestration. J. Biol. Chem. 284, 12110–12124.

von Kleist, L., Stahlschmidt, W., Bulut, H., Gromova, K., Puchkov, D., Robertson, M.J., MacGregor, K.A., Tomilin, N., Pechstein, A., Chau, N., Chircop, M., Sakoff, J., von Kries, J.P., Saenger, W., Kräusslich, H.-G., Shupliakov, O., Robinson, P.J., McCluskey, A., Haucke, V., 2011. Role of the clathrin terminal domain in regulating coated pit dynamics revealed by small molecule inhibition. Cell 146, 471–484.

Wagshal, D., Sankaranarayanan, S., Guss, V., Hall, T., Berisha, F., Lobach, I., Karydas, A., Voltarelli, L., Scherling, C., Heuer, H., Tartaglia, M.C., Miller, Z., Coppola, G., Ahlijanian, M., Soares, H., Kramer, J.H., Rabinovici, G.D., Rosen, H.J., Miller, B.L., Meredith, J., Boxer, A.L., 2015. Divergent CSF τ alterations in two common tauopathies: Alzheimer's disease and progressive supranuclear palsy. J. Neurol. Neurosurg. Psychiatry 86, 244–250.

Wang, R., Wang, J., Hassan, A., Lee, C.-H., Xie, X.-S., Li, X., 2021. Molecular basis of V-ATPase inhibition by bafilomycin A1. Nat. Commun. 12, 1782.

Wang, Y., Balaji, V., Kaniyappan, S., Krüger, L., Irsen, S., Tepper, K., Chandupatla, R., Maetzler, W., Schneider, A., Mandelkow, E., Mandelkow, E.-M., 2017. The release and trans-synaptic transmission of Tau via exosomes. Mol. Neurodegener. 12, 5.

Wang, Y., Mandelkow, E., 2016. Tau in physiology and pathology. Nat. Rev. Neurosci. 17, 5–21.

Wegmann, S., Bennett, R.E., Delorme, L., Robbins, A.B., Hu, M., McKenzie, D., Kirk, M.J., Schiantarelli, J., Tunio, N., Amaral, A.C., Fan, Z., Nicholls, S., Hudry, E., Hyman, B.T., 2019. Experimental evidence for the age dependence of tau protein spread in the brain. Sci. Adv. 5, eaaw6404.

Weingarten, M.D., Lockwood, A.H., Hwo, S.Y., Kirschner, M.W., 1975. A protein factor essential for microtubule assembly. Proc. Natl. Acad. Sci. USA 72, 1858–1862.

Wesseling, H., Mair, W., Kumar, M., Schlaffner, C.N., Tang, S., Beerepoot, P., Fatou, B., Guise, A.J., Cheng, L., Takeda, S., Muntel, J., Rotunno, M.S., Dujardin, S., Davies, P., Kosik, K.S., Miller, B.L., Berretta, S., Hedreen, J.C., Grinberg, L.T., Seeley, W.W., Hyman, B.T., Steen, H., Steen, J.A., 2020. Tau PTM profiles identify patient heterogeneity and stages of alzheimer's disease. Cell 183, 1699–1713.e13.

Whitwell, J.L., Jack, C.R., Boeve, B.F., Senjem, M.L., Baker, M., Ivnik, R.J., Knopman, D.S., Wszolek, Z.K., Petersen, R.C., Rademakers, R., Josephs, K.A., 2009. Atrophy patterns in IVS10+16, IVS10+3, N279K, S305N, P301L, and V337M MAPT mutations. Neurology 73, 1058–1065.

Wille, H., Drewes, G., Biernat, J., Mandelkow, E.M., Mandelkow, E., 1992. Alzheimer-like paired helical filaments and antiparallel dimers formed from microtubule-associated protein tau in vitro. J. Cell Biol. 118, 573–584.

Wu, J.W., Herman, M., Liu, L., Simoes, S., Acker, C.M., Figueroa, H., Steinberg, J.I., Margittai, M., Kayed, R., Zurzolo, C., Di Paolo, G., Duff, K.E., 2013. Small misfolded Tau species are internalized via bulk endocytosis and anterogradely and retrogradely transported in neurons. J. Biol. Chem. 288, 1856–1870.

Wu, J.W., Hussaini, S.A., Bastille, I.M., Rodriguez, G.A., Mrejeru, A., Rilett, K., Sanders, D.W., Cook, C., Fu, H., Boonen, R.A.C.M., Herman, M., Nahmani, E., Emrani, S., Figueroa, Y.H., Diamond, M.I., Clelland, C.L., Wray, S., Duff, K.E.,

2016. Neuronal activity enhances tau propagation and tau pathology in vivo. Nat. Neurosci. 19, 1085–1092.

Yamada, K., Cirrito, J.R., Stewart, F.R., Jiang, H., Finn, M.B., Holmes, B.B., Binder, L.I., Mandelkow, E.-M., Diamond, M.I., Lee, V.M.-Y., Holtzman, D.M., 2011. In vivo microdialysis reveals age-dependent decrease of brain interstitial fluid tau levels in P301S human tau transgenic mice. J. Neurosci. 31, 13110–13117.

Yamasaki, M., Matsui, M., Watanabe, M., 2010. Preferential localization of muscarinic M1 receptor on dendritic shaft and spine of cortical pyramidal cells and its anatomical evidence for volume transmission. J. Neurosci. 30, 4408–4418.

Yezid, H., Konate, K., Debaisieux, S., Bonhoure, A., Beaumelle, B., 2009. Mechanism for HIV-1 Tat insertion into the endosome membrane. J. Biol. Chem. 284, 22736–22746.

Zhang, P., Lu, H., Peixoto, R.T., Pines, M.K., Ge, Y., Oku, S., Siddiqui, T.J., Xie, Y., Wu, W., Archer-Hartmann, S., Yoshida, K., Tanaka, K.F., Aricescu, A.R., Azadi, P., Gordon, M.D., Sabatini, B.L., Wong, R.O.L., Craig, A.M., 2018. Heparan Sulfate Organizes Neuronal Synapses through Neurexin Partnerships. Cell 174, 1450–1464.e23.

Zhang, W., Falcon, B., Murzin, A.G., Fan, J., Crowther, R.A., Goedert, M., Scheres, S.H., 2019. Heparin-induced tau filaments are polymorphic and differ from those in Alzheimer’s and Pick's diseases. Elife 8.

Zhong, Q., Congdon, E.E., Nagaraja, H.N., Kuret, J., 2012. Tau isoform composition influences rate and extent of filament formation. J. Biol. Chem. 287, 20711–20719.